

VOLCANOSTRATIGRAPHY AND PETROGENESIS OF SÜPHAN
STRATOVOLCANO

A THESIS SUBMITTED TO
THE GRADUATE SCHOOL OF NATURAL AND APPLIED SCIENCES
OF
MIDDLE EAST TECHNICAL UNIVERSITY

BY

YAVUZ ÖZDEMİR

IN PARTIAL FULFILLMENT OF THE REQUIREMENTS
FOR
THE DEGREE OF DOCTOR OF PHILOSOPHY
IN
GEOLOGICAL ENGINEERING

FEBRUARY 2011

VOLCANOSTRATIGRAPHY AND PETROGENESIS OF SÜPHAN STRATOVOLCANO

submitted by **YAVUZ ÖZDEMİR** in partial fulfillment of the requirements
for the degree of **Doctor of Philosophy in Geological Engineering**
Department, Middle East Technical University by,

Prof. Dr. Canan Özgen _____
Dean, Graduate School of **Natural and Applied Sciences**

Prof. Dr. M. Zeki Çamur _____
Head of Department, **Geological Engineering**

Prof. Dr. Nilgün Güleç _____
Supervisor, **Geological Engineering Dept., METU**

Prof. Dr. A. Ümit Tolluoğlu _____
Co-Supervisor, **Ankara**

Examining Committee Members:

Prof. Dr. M. Cemal Göncüoğlu _____
Geological Engineering Dept., METU

Prof. Dr. Nilgün Güleç _____
Geological Engineering Dept., METU

Prof. Dr. Vedat Toprak

Geological Engineering Dept., METU

Prof. Dr. Abidin Temel

Geological Engineering Dept., Hacettepe University

Assoc. Prof. Dr. Mehmet Keskin

Geological Engineering Dept., İstanbul University

Date: February 15, 2011

I hereby declare that all information in this document has been obtained and presented in accordance with academic rules and ethical conduct. I also declare that, as required by these rules and conduct, I have fully cited and referenced all material and results that are not original to this work.

Name, Last Name : Yavuz ÖZDEMİR

Signature :

ABSTRACT

VOLCANOSTRATIGRAPHY AND PETROGENESIS OF SÜPHAN STRATOVOLCANO

Özdemir, Yavuz

Ph.D., Department of Geological Engineering

Supervisor : Prof. Dr. Nilgün Güleç

Co-Supervisor : Prof. Dr. A. Ümit Tolluoğlu

February 2011, 279 pages

This study is concerned with volcanostratigraphic and petrologic evolution of the Süphan, which is a 4050 m high Quaternary stratovolcano in eastern Anatolia.

The eruptive products of Süphan Stratovolcano, including transitional mildly alkaline to calc-alkaline rocks, are lavas, domes and pyroclastics ranging in composition from basalts to rhyolites. Ar-Ar age data from different levels of the volcanostratigraphic succession yield a range of 0.76-0.06 Ma.

Textural features, wide temperature ranges obtained for intermediate members, and the linear trends of whole-rock geochemistry are strongly suggestive of magma mixing in the evolution of Süphan volcanics. Presence of crystal clots in many lavas suggests that cogenetic plutonic

rocks were also involved in the mixing process. Comparison of whole-rock, melt inclusion and glass chemistry data of Süphan to data from experimental studies reported in literature indicate that the melt inclusions describe true liquid lines of descent from a common hydrous parent at pressures of ~500 MPa.

EC-AFC modeling of trace element and isotopic compositions reveals 2-8% crustal contamination in the differentiated lavas. REE modeling indicates that primitive rocks of Süphan volcanics were products of mixing of melts from spinel and garnet lherzolite sources, with contributions of 60% and 40%, respectively, in the mixture.

A two-stage petrogenetic model is proposed for Suphan stratovolcano. Mantle- derived melts stall and undergo chemical differentiation in a deep hot zone in lower to mid-crust; variably evolved melts ascending from this zone are arrested and mixed at a shallow level where they construct a sub-volcanic magma reservoir beneath Suphan.

Keywords: Eastern Anatolia, Süphan Stratovolcano, volcanostratigraphy, geochemistry, melt inclusion

ÖZ

SÜPHAN STRATOVOLKANININ VOLKANOSTRATİGRAFİSİ VE PETROJENEZİ

Özdemir, Yavuz

Doktora, Jeoloji Mühendisliği Bölümü

Tez Yöneticisi : Prof. Dr. Nilgün Güleç

Ortak Tez Yöneticisi: Prof. Dr. A. Ümit Tolluoğlu

Şubat 2011, 279 sayfa

Bu çalışma, Doğu Anadolu'da yer alan 4050 m yüksekliğindeki Süphan Stratovolkanı'nın volkanostratigrafik ve petrolojik evrimini konu almaktadır.

Süphan volkanizmasının ürünleri bazaltdan riyolite kadar uzanan ortaç alkali ve kalkalkali karakterler arasında geçiş özelliği gösteren, lavlar, domlar ve piroklastiklerden oluşmuştur. Volkanostratigrafik istifin değişik seviyelerinden alınan Ar-Ar yaşları 0.76-0.06 My arasında değişmektedir.

Volkaniklerin petrografik dokuları, ortaç karakterli kayalardan elde edilen geniş sıcaklık aralıkları ve tüm kayaç analizlerinde gözlenen doğrusal yönelimler Süphan volkaniklerinin evriminde magma karışımının varlığına işaret etmektedir. Lavlar içerisinde gözlenen kristal

kümelerinin varlığı, eşkökenli plütonik kayaçların da magma karışımına eşlik ettiğini göstermektedir.

Süphan volkaniklerinin tüm kayaç, ergiyik kapanımları ve cam kimyası analizlerinin literatürden alınan deneysel verilerle karşılaştırılması, ergiyik kapanımlarının, 500 MPa lık basınç koşullarında oluşmuş sulu bir magmadan itibaren gelişen fraksiyonlanma artığını tanımladığını ortaya koymuştur.

İz element ve izotop bileşimleri kullanılarak yapılan EC-AFC modellemesi, evrimleşmiş lavların % 2-8 arasında kabuksal kirlenmeye maruz kaldığını göstermiştir. NTE modellemeleri, Süphan volkanizmasına ait primitif lavların spinel ve granat lerzolitik kaynaklardan türeyen ergiyiklerin karışımından oluştuğuna ve karışımdaki spinel ve granatlı kaynak katkısının, sırasıyla, %60 ve %40 olduğuna işaret etmektedir.

Süphan volkanizması için iki aşamalı bir petrojenetik model öne sürülmüştür. Mantodan türeyen ergiyikler alt-orta kabukta birikerek (derin-sıcak zon) kimyasal farklılaşmaya uğramışlardır. Sıcak zonda evrimleşen ergiyikler daha sonra yükselerek sığ derinliklere yerleşmiş ve magma karışımının da gerçekleştiği sub-volkanik bir magma odasını oluşturmuşlardır.

Anahtar Kelimeler: Doğu Anadolu, Süphan Stratovolkani, volkanostratigrafi, jeokimya, ergiyik kapanımları

To my father and my young brother

ACKNOWLEDGEMENTS

It would not have been possible to write this thesis without the help and support of the kind people around me; it is a pleasure to thank the people who made this thesis possible.

First and foremost I would like to express my deep and sincere gratitude to my PhD thesis supervisor, Prof. Dr. Nilgün Güleç, for her clear guidance, critical vision, encouragements and endless support in every stage of this thesis. I am especially grateful for her monitoring each step of this thesis with a great concern and supporting the progress of the work with her valuable advices. Her wide knowledge and her logical way of thinking have been of great value for me. I really appreciate her dedication and support which gave me the feeling that my work was important all the time. It is a great honor to feel her trust, support and appreciation.

I am indebted to my co-supervisor A. Ümit Tolluoğlu for his invaluable assistance, and encouragements during all my studies. I learned very important things from him. I would also like to thank him for opening my mind and motivating me to attend Middle East Technical University for my PhD studies.

I would like to express my sincere thanks to Prof. Dr. John Blundy for generously sharing his time and knowledge in our cooperative work and also for his invaluable assistance and support during my studies in Bristol University. It was a great chance for me to have had utilized his profound knowledge.

I would like to acknowledge, with grateful thanks, the unique and exceptional support given by Dr Stuart Kearns during the electron microprobe studies in Bristol University.

I would also like to express my sincere gratitude to my examining committee members Prof. Dr. Vedat Toprak, Prof. Dr. Cemal Göncüoğlu, Prof. Dr. Abidin Temel and Assoc. Prof. Dr. Mehmet Keskin for their constructive comments regarding the improvement of my thesis.

I am most grateful to all my friends for their friendships and endless encouragements. In particular, I wish to thank to Harun Aydın, Erkan Yılmaz, Alkım Türközü, Ülker Cem Kaplan and Mehmet Koçak for their helps and encouragements. And my special thanks go to Vural Oyan for scientific discussions and help in the field studies. In addition, I am thankful to all my colleagues, faculty and staff members of Geological Engineering Department at Middle East Technical University for their friendships and motivations. I would also like to thank to Orhan Karaman in the preparation of my thin sections.

My deepest gratitude goes to my family and little daughter for their unflagging love and support throughout my life; this dissertation is simply impossible without them. I am indebted to my father, Yaşar Özdemir, my younger brother, Barış Özdemir, and my father-in-law, Musa Atakul, for their care and love. Although they are no longer with us, they are forever remembered. I am sure they share our joy and happiness. I am grateful to my mom and my brothers for their attentions, encouragements and for making me highly motivated during my education. Words fail me to express my appreciation to my wife Ayşe Özdemir whose dedication, love and persistent confidence in me, has taken the load off my shoulder. Whenever I was discouraged she

motivated me with a wise and affectionate manner and gave me the strength to continue my work. And also I would like to express my deepest gratitude to her for tremendous help at every stage of my PhD. I am also grateful to my little girl, Nehir Özdemir, for her pretty smile and her small pretty fingers tapping on my notebook. Her smile always helped me to concentrate and to work harder than ever. You are one of the best things happened to me in my life. Without the support of my family, this thesis would not have been accomplished.

This thesis has been funded by both Middle East Technical University Scientific Research Project Foundation (ÖYP Project) and TÜBİTAK, the Scientific and Technical Research Council of Turkey (Project No. YDABAG 104Y372). I also would like to thank TÜBİTAK for a scholarship which allowed me to spend 10 months at Bristol, UK in 2009.

Finally, I would like to acknowledge everybody who was important to the successful realization of thesis, as well as expressing my apology that I could not mention personally one by one.

TABLE OF CONTENTS

ABSTRACT	iv
ÖZ.....	vi
ACKNOWLEDGEMENTS	ix
TABLE OF CONTENTS	xii
LIST OF TABLES	xv
LIST OF FIGURES.....	xvii
CHAPTERS	
1. INTRODUCTION.....	1
1.1 Purpose and Scope	1
1.2 Geographic Setting.....	4
1.3 Methods of Study.....	5
1.4 Structure of Thesis.....	7
2. GEOLOGICAL SETTING	9
2.1 Regional Geology and Lithospheric Structure of the Region	9
2.2 History of Post Collisional Volcanism in Eastern Anatolia.....	13
3. GEOLOGY.....	19
3.1 Sedimentary Rocks.....	19
3.1.1 Miocene Sedimentary Units	19
3.1.2 Pliocene-Pleistocene Sedimentary Units.....	22
3.2 Volcanostratigraphy of the Süphan Stratovolcano	23
3.2.1 <i>Debris Avalanche and Phase I. Pyroclastic Rocks</i>	24

3.2.2 Rhyolitic Obsidian Domes and Lava Flows (1)	30
3.2.3 Basalt (2)	35
3.2.4 Basaltic Trachyandesitic Lava Flows (3)	35
3.2.5 Basaltic Trachyandesitic/ Trachyandesitic Lava Series (4)	37
3.2.6 Trachyandesitic Lava Flows (5)	39
3.2.7 Phase II, III, IV Pyroclastic Rocks (6)	40
3.2.8 Trachytic lava flows (7,8,9)	44
3.2.9 Dacitic and Rhyolitic Domes (10)	45
3.2.10 Maar Deposits (11)	52
3.2.11 Travertine	54
4. GEOCHRONOLOGY	56
4.1 Basalt (2)	58
4.2 Basaltic Trachyandesitic/ Trachyandesitic Lava Series (4)	58
4.3 Trachyandesitic Lava Flows (5)	72
4.4 Trachytic lava flow (9)	75
4.5 Dacitic and Rhyolitic Domes (10)	75
5. MINERALOGY AND PETROGRAPHY	82
5.1 Basalt (2)	84
5.2 Basaltic-Trachyandesitic lava flows (3,4)	85
5.3 Trachyandesitic lava flows (4, 5)	86
5.4 Trachytic Lava Flows (7,8,9)	89
5.5 Dacitic Rocks (10)	91
5.6 Rhyolitic Rocks (1,10,6)	92
5.7 Enclaves	94
6. GEOCHEMISTRY	95
6.1 Major Element Geochemistry	95
6.2 Trace and RE Element Geochemistry	108
6.3 Major, Trace and RE Element Geochemistry of Enclaves	116

6.4 Isotope Geochemistry	123
7. MINERAL CHEMISTRY	128
7.1 Chemistry of Melt Inclusions and Glasses	142
7.2 Intensive Parameters: Temperature and Pressure	147
7.3 Oxygen Fugacity	152
8. DISCUSSION	153
8.1 Comparison to the Experimental Data.....	153
8.2 Magma mixing.....	159
8.3 Fractional crystallization	163
8.4 Crustal Contamination	165
8.5 Mantle Source.....	171
8.5.1 Partial Melting	171
8.5.2 Subduction Components.....	174
8.6 Magmatic Plumbing Beneath Süphan	176
8.7 Magmato-Tectonic History and Role of Lithospheric Mantle.....	180
9. CONCLUSIONS	189
REFERENCES	194
APPENDICES	
A UTM coordinates of samples.....	215
B Compositions of minerals from Süphan Volcano.....	217
C Electron microprobe analyses of melt inclusions and matrix glasses	255
D Compositons of experimental glasses (Luhr, 1990).....	271
E Compositons of experimental glasses (Freise et al, 2009).....	273
CURRICULUM VITAE.....	276

LIST OF TABLES

TABLES

Table 4.1 Ar-Ar age dating results of Süphan volcanics.	57
Table 4.2 Ar-Ar age results of sample 2006 99.	60
Table 4.3 Ar-Ar results of the sample 2006 3.	62
Table 4.4 Ar-Ar results of the sample 2007 22.	65
Table 4.5 Ar-Ar results of the sample 2007 24.	67
Table 4.6 Ar-Ar results of the sample 2006 116.	70
Table 4.7 Ar-Ar results of the sample 2006 8.	73
Table 4.8 Ar-Ar results of the sample 2006 59.	77
Table 4.9 Ar-Ar results of the sample 2006 110.	78
Table 4.10 Ar-Ar results of the sample 2007 5.	80
Table 6.1 Major and trace element contents of Süphan volcanics.	96
Table 6.2 Isotope compositions of the selected Süphan Volcanics....	125
Table 7.1 Representative olivine compositions.....	131
Table 7.2 Representative pyroxene compositions	132
Table 7.3 Representative feldspar compositions	138

Table 7.4 Representative amphibole and biotite compositions.	140
Table 7.5 Representative Fe-Ti oxide compositions.....	141
Table 7.6 Representative compositions of melt inclusions and matrix glasses.	143
Table 7.7 Temperatures estimated for Süphan magma using different methods.....	151
Table 8.1 Major element compositions of starting materials.....	154
Table 8.2 Table Least-Square mixing results for selected Süphan volcanics (H ₂ O free).....	161
Table 8.3 EC-AFC (Spera and Bohrsen, 2001) parameters for Süphan volcanics and potential contaminants (lower and upper crust).	170
Table 8.4 Partition coefficients of elements used for EC-AFC modelling	171
Table 8.5 Representative major and trace element data from eastern Anatolian volcanics.....	182
Table A.1 UTM Coordinates of samples.....	215
Table B.1 Compositions of minerals from Süphan Volcano.....	217
Table C.1 Electron microprobe analyses of melt inclusions and matrix glasses.....	255
Table D. 1 Compositons of experimental glasses for trachyandesite (A) and basalt (B) (Luhr, 1990).....	271
Table E.1 Compositons of experimental glasses for alkali basalt (OB93-190) and tholeiitic basalt (35R2) (Freise et al, 2009).....	273

LIST OF FIGURES

FIGURES

Figure 1.1 Tectonic setting of the Süphan Stratovolcano.	2
Figure 1.2 Geographic setting of Süphan Stratovolcano.	5
Figure 2.1 Major tectonic blocks of the Eastern Anatolia region.....	12
Figure 2.2 Simplified geological map of the Eastern Anatolia region showing tectonic units, collision-related volcanic products and volcanic centres.....	14
Figure 3.1 Geological map of the Süphan Stratovolcano.	20
Figure 3.2 Stratigraphic columnar section of the Süphan Stratovolcano.	21
Figure 3.3 Contact of the Miocene Sedimentary units and volcanic products of Süphan Stratovolcano.	22
Figure 3.4. The trachytic lava flow on the Pliocene-Pleistocene sedimentary rocks	23
Figure 3.5 Distribution on the topographic map, of the debris avalanche hummocks at the northeastern part of the volcano. Black areas represent the distribution of hummocks at north of the Süphan Volcano.	26
Figure 3.6 Block facies of the debris avalanche.	27
Figure 3.7 Matrix facies of the debris avalanche.	28
Figure 3.8 Phase I pyroclastic deposits of Süphan stratovolcano.	30
Figure 3.9 Correlation of the stratigraphic columnar sections of Süphan pyroclastics.....	32

Figure 3.10 Idealised stratigraphic section of th"e Süphan pyroclastics.	33
Figure 3.11 Rhyolitic obsidian lava flows at the southern parts of the volcano.	34
Figure 3.12 Basaltic trachyandesitic lava flows on the hummock at the northern flanks of Süphan.	35
Figure 3.13 Basaltic trachyandesitic lava flow on debris avalanche.....	36
Figure 3.14 Basaltic trachyandesitic flows between Süphan and Malazgirt village.....	38
Figure 3.15 Trachyandesitic lava flows of secondary eruption centers at the western flanks of the volcano.....	39
Figure 3.16 Trachyandesitic lava flows at the southern parts of the Süphan	40
Figure 3.17 a) Fractured pumice blocks in P3, b) ash fall deposits of Phase II.	41
Figure 3.18 a) Block and ash flow under the trachytic lava flows, b) radially fractured blocks in block and ash flow.....	43
Figure 3.19 Ash fall deposits of Phase III and pumice fall deposits of Phase IV (P5)	44
Figure 3.20 Three different trachytic lava flows of Süphan Stratovolcano. a) west of Aşağı Süphan, b) north of Aydınlar, c) Ahürük mountain.....	47
Figure 3.21 Dacitic domes of the Süphan Stratovolcano a) Kızdağı hill, Aptalkız hill, Dergekız hill, Salkız hill doms, b) Keftardağı hill dacitic dome, c) İmamdağı hill dacitic dome, d) Yukarıkafir kalesi dacitic dome, e) Büyükkale hill dacitic dome	50
Figure 3.22 Rhyolitic domes of the Süphan volcanism a) Nernek mountain, b) Mustafa hill, c) rhyolitic dome at the summit of the volcano.	51
Figure 3.23 Aygır maar at the southern part of the Süphan Stratovolcano.....	52
Figure 3.24 Dune structures in the maar deposits.....	54

Figure 3.25 Planar flows in the maar deposits	55
Figure 4.1 Plateau age of the sample 2006 99.	61
Figure 4.2 Isochron age of the sample 2006 99.	61
Figure 4.3 Plateau age of the sample 2006 3.	63
Figure 4.4 Isochron age of the sample 2006 3.	63
Figure 4.5 Plateau age of the sample 2007 22.	66
Figure 4.6 Isochron age of the sample 2007 22.	66
Figure 4.7 Plateau age of the sample 2007 24.	68
Figure 4.8 Isochron age of the sample 2007 24.	68
Figure 4.9 Plateau age of the sample 2006 116.	71
Figure 4.10 Isochron age of the sample 2006 116.	71
Figure 4.11 Plateau age of the sample 2006 8.	74
Figure 4.12 Isochron age of the sample 2006 8.	74
Figure 4.13 Isochron age of the sample 2006 110.	79
Figure 4.14 Plateau age of the sample 2007 5.	81
Figure 4.15 Isochron age of the sample 2007 5.	81
Figure 5.1 The distribution of the minerals in different rock groups of the Süphan Volcano.	83
Figure 5.2 a) Subophitic texture in basalt, b) Iddingsitized olivine phenocrysts	85
Figure 5.3 Petrographic features of basaltic trachyandesites a) Oscillatory zoned plagioclase in basaltic trachyandesites, b) Sieve textured plagioclase in basaltic trachyandesites, c) Iddingsitized olivine phenocryst in basaltic trachyandesites, d) An orthopyroxene phenocryst rimmed by clinopyroxene.	86

Figure 5.4 A crystal clot from trachyandesitic lava flows, includes; orthopyroxene, clinopyroxene, plagioclase and Fe-Ti oxides.....	87
Figure 5.5 Petrographic features of trachyandesites, a) apatite inclusions in plagioclase, b) glass inclusions in orthopyroxene, c) an orthopyroxene phenocryst mantled by clinopyroxene, d) an opacitized olivine phenocryst.....	89
Figure 5.6 a) Zircon inclusions in plagioclase, b) amphibole phenocryst replaced by Fe-Ti oxides along their rims	91
Figure 5.7 a) Euhedral and subhedral orthopyroxenes in dacitic rocks, b) biotite and amphibole phenocrysts in dacitic lavas.....	92
Figure 5.8 Petrographic features of rhyolitic rocks. a) sanidine phenocrysts, b) rounded quartz mineral, c) blade shaped biotites, d) perlitic texture in obsidian flows, e) flow texture in obsidian flows.	93
Figure 6.1 TAS diagram of the Süphan volcanics.....	105
Figure 6.2 AFM diagram of Süphan volcanics.	106
Figure 6.3 K ₂ O-SiO ₂ diagram of Süphan Volcanics	107
Figure 6.4 K ₂ O-Na ₂ O diagram of Süphan Volcanics.....	108
Figure 6.5 Major oxide variation diagrams of Süphan Volcanics.....	110
Figure 6.6 Trace element variation diagrams of Süphan Volcanics. ...	111
Figure 6.7 Sc-Th diagram for Süphan volcanics.....	112
Figure 6.8 MORB normalized multi-element patterns of the Süphan volcanics.....	114
Figure 6.9 Chondrite normalized REE patterns of Süphan volcanics.	115
Figure 6.10 TAS diagram of the Süphan enclaves	116
Figure 6.11 AFM diagram of Süphan enclaves.....	117
Figure 6.12 K ₂ O-SiO ₂ diagram of Süphan enclaves	118
Figure 6.13 K ₂ O-Na ₂ O diagram of Süphan enclaves.....	118
Figure 6.14 Major oxide variation diagrams of the Süphan enclaves.	120

Figure 6.15 Trace element variation diagrams of Süphan enclaves...	121
Figure 6.16 MORB normalized multi-element patterns of the Süphan enclaves	122
Figure 6.17 Chondrite normalized REE patterns of Süphan enclaves.	123
Figure 6.18 $^{143}\text{Nd}/^{144}\text{Nd}$ versus $^{87}\text{Sr}/^{86}\text{Sr}$ diagram of the Süphan volcanics.....	126
Figure 6.19 a) $^{143}\text{Nd}/^{144}\text{Nd}$ - $^{206}\text{Pb}/^{204}\text{Pb}$ b) $^{87}\text{Sr}/^{86}\text{Sr}$ - $^{206}\text{Pb}/^{204}\text{Pb}$ c) $^{207}\text{Pb}/^{204}\text{Pb}$ - $^{206}\text{Pb}/^{204}\text{Pb}$ isotop correlation diagrams of the Süphan volcanics.....	127
Figure 7.1 Frequency distribution diagrams for core, rim and microlite compositions of olivine..	130
Figure 7.2 Frequency distribution diagrams for core, rim and microlite compositions of clinopyroxene	133
Figure 7.3 Frequency distribution diagrams for core, rim and microlite compositions of orthopyroxene.	135
Figure 7.4 Frequency distribution diagrams for core, rim and microlite compositions of plagioclase.	136
Figure 7.5 Melt inclusions (MIs) in Süphan volcanics a) BSE (Back-scattered Electron) image of MIs in orthopyroxene, MIs are randomly distributed from core to rim. b) BSE image of MIs in plagioclase, some of them contain some daughter crystals including Fe-Ti oxides.	143
Figure 7.6 Major element variation diagrams for melt inclusions, matrix glasses and whole rocks of Süphan volcanics.....	144
Figure 7.7 Calculated temperature versus SiO_2 plot for selected Süphan volcanics.....	150
Figure 7.8 Temperature vs. oxygen fugacity, estimated from Fe-Ti equilibria in Süphan volcanics using the ILMAT program (Lepage 2003). Oxides were recalculated using Stormer (1983).....	152
Figure 8.1 TAS diagram of the Süphan volcanics and starting compositions of different experimental studies.....	154

Figure 8.2 Comparison of chemical variation in melt inclusions, matrix glasses and whole rocks of Süphan volcanics with experimentally originated melts of two volcanic rocks from Trans-Mexican Volcanic Belt	157
Figure 8.3 Comparison of chemical variation in melt inclusions, matrix glasses and whole rocks of Süphan volcanics with experimentally originated melts of two volcanic rocks from Kerguelen Large Igneous Province.....	158
Figure 8.4 a) $^{87}\text{Sr}/^{86}\text{Sr}$ vs SiO_2 and b) $^{143}\text{Nd}/^{144}\text{Nd}$ vs SiO_2 diagrams of the Süphan volcanics	166
Figure 8.5 Mixing trajectories between sample 2006 122 & sample 2005 69, and between sample 2006 112 & Upper crust.....	167
Figure 8.6 $^{87}\text{Sr}/^{86}\text{Sr}$ vs Sr (ppm) (a) and $^{143}\text{Nd}/^{144}\text{Nd}$ vs $^{87}\text{Sr}/^{86}\text{Sr}$ (b) with model EC-AFC curves calculated using the model of Spera and Bohrson (2001).....	169
Figure 8.7 (a-b). Calculated partial melting curves assuming non-modal batch melting of garnet (Gt) and spinel (Sp) lherzolite sources for Süphan Volcanics.....	173
Figure 8.8 a) Ba/Th vs $^{87}\text{Sr}/^{86}\text{Sr}$, b) Ba/La vs Th/Yb, diagrams of Süphan volcanics.	175
Figure 8.9 $^{143}\text{Nd}/^{144}\text{Nd}$ vs $^{206}\text{Pb}/^{204}\text{Pb}$ and $^{207}\text{Pb}/^{204}\text{Pb}$ vs $^{206}\text{Pb}/^{204}\text{Pb}$ diagrams of the Süphan volcanics.	176
Figure 8.10 Schematic representation of intracrustal magma plumbing system beneath Süphan Stratovolcano	179
Figure 8.11 Calculated partial melting curves assuming non-modal batch melting of garnet (Gt) and spinel (Sp) lherzolite sources for eastern Anatolian volcanics.....	188

CHAPTER 1

INTRODUCTION

1.1 Purpose and Scope

The Eastern Anatolian plateau has formed as part of a Turkic-type orogenic system through the convergence between the Arabian and Anatolian (Eurasian) plates (Figure 1.1). The collision between the two plates caused intense seismic activity, strike-slip fault zones (dextral North Anatolian Fault Zone and sinistral East Anatolian Fault Zone), westward escape of Anatolian plate and widespread Late Cenozoic volcanism. Nature of the tectonism in the region reveal a transition from N-S directed compressional-contractional regime (post-collisional convergence) in Middle Miocene-Early Pliocene to compressional-extensional regime (tectonic escape) in Early Pliocene-Recent time interval (Koçyiğit et al., 2001; Bozkurt, 2001). Shallow and diffuse seismicity in the region indicate that the eastern Anatolian lithosphere is still being actively deformed as a result of ongoing collision and crustal escape tectonics.

Subsequent to the collision, a widespread volcanism affected almost two third of the region (Yılmaz et al., 1987, 1998; Pearce et al., 1990; Notsu et al., 1995; Keskin et al., 1998; Keskin, 2003, 2007; Aydar et al., 2003; Şen et al., 2004, Özdemir et al., 2006). Therefore eastern Anatolia offers an excellent natural laboratory for studying connections between tectonism and volcanism in an active collision zone.

Collision-related volcanic rocks in eastern Anatolia extend from the Erzurum-Kars Plateau in the northern part of the region to the Arabian foreland in the south (Figure 1.1). A series of large shield and stratovolcanoes is present in eastern Anatolia, including Ağrı, Süphan, Nemrut, Tendürek, Etrüsk and many secondary eruption centers.

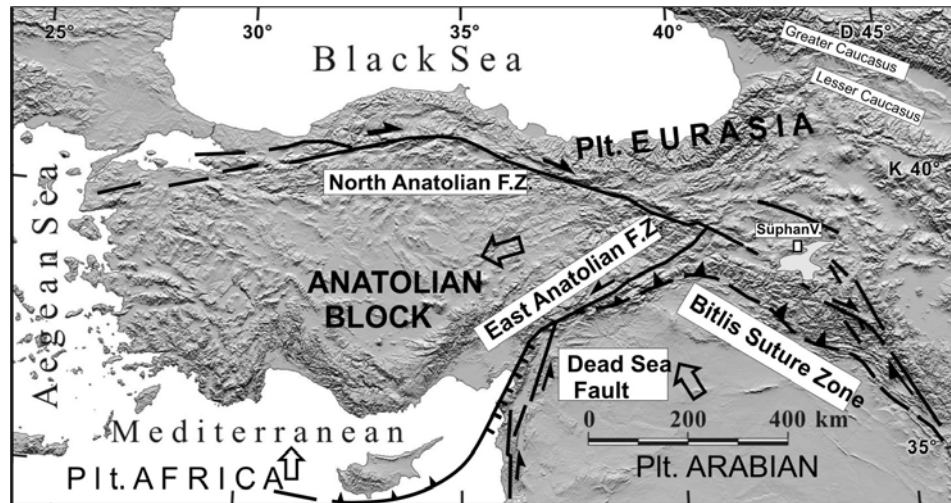


Figure 1.1 Tectonic setting of the Süphan Stratovolcano.

The origin and time-space distribution of the collision related volcanics still remain as a matter of debate. Many models have been put forward to explain the origin of the volcanics. These petrogenetic models can be divided into two main groups; in the first group, these volcanics are considered to have originated by melting in lithospheric mantle (e.g Pearce et al., 1990; Yılmaz et al., 1998, Şen et al., 2004). In the second group, source region of the volcanism is regarded as asthenosphere related to the steepening and breakoff of a northward subducting slab belonging to the northern branch of the Neo-Tethyan ocean (e.g. Şengör, et al., 2003, 2008; Keskin, 2003, 2007).

Testing the validity of these proposed geodynamic models requires detailed volcanological, geochemical and geochronological investigation of products from each volcanic center in the region. With the exception of a few systematic study of individual volcanoes (Özpeker, 1973; Arslan, 1994; Yılmaz et al., 1998; Keskin et al., 1998; Karaoğlu et al., 2005; Özdemir et al., 2006), previous works on the eastern Anatolian volcanics are geochemically oriented most of which are concerned with overall evaluation of the collision-related volcanism based on the insufficient data from the region.

This study aims to reconstruct volcanostratigraphy and model the petrogenesis of the Süphan Stratovolcano which is one of the least known Quaternary volcanoes in eastern Anatolia. The reasons for choosing the Süphan Stratovolcano are as follows; i) the volcanological and petrological evolution of the stratovolcano has not been precisely established yet, ii) it has a critical importance testing the validity of the proposed geodynamic models in eastern Anatolia because of its transitional geochemical character which is quite different from the surrounding volcanic centers (e.g. alkaline Nemrut and Meydan volcanoes).

In order to achieve the aims of the study, geological mapping - accompanied by remote sensing studies- was conducted in the field with detailed investigations on types of pyroclastics and lavas, and paying particular attention to sample collection for age determination which is of critical importance in the construction of volcanostratigraphic succession. Petrographical and geochemical analyses, covering the major and trace elements and isotopic investigations, were undertaken to understand magma genesis at Süphan. A combination of whole-rock, mineral, melt inclusion and glass chemistry was used to interpret the chemical variations of the Süphan volcanics in terms of fractional

crystallization and magma mixing. Isotopic composition of the rocks was utilized to put constraints on the magma sources and/or contamination processes. Thermobarometric and melt inclusion data were also used to gain insights into the magma plumbing system under the Süphan Stratovolcano.

1.2 Geographic Setting

Süphan Stratovolcano (lat. 38° 55'N, long. 42° 59'E) is located in north of Lake Van, among three major towns of the region: Adilcevaz (Bitlis) to the south, Patnos (Ağrı) to the north, Malazgirt (Muş) to the northwest (Figure 1.2). Adilcevaz is the closest town to the main cone. There are approximately 50 villages around the volcano.

Volcanic products of Süphan cover an area of approximately 2000 km² which is included in the Van-K49 a2, b1, b2, b3, b4, Karaköse-J49 c3, c4, d3 quadrangles of 1:25.000 scale topographic maps of Turkey. Süphan stratovolcano, representing the second highest Quaternary volcano in eastern Anatolia, reaches a summit elevation of 4050 m. It is a favorite trekking place for tourists due to its well preserved volcanic nature. The summit is accessible from southern and eastern flanks.

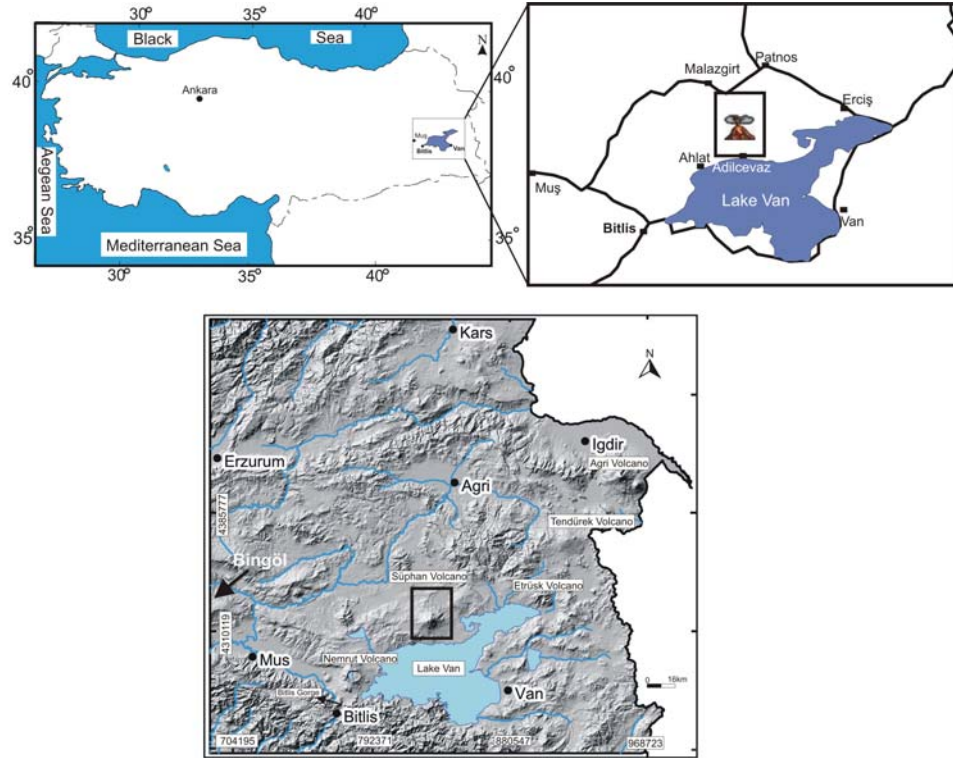


Figure 1.2 Geographic setting of Süphan Stratovolcano.

1.3 Methods of Study

The methods that are utilized in the thesis study are shortly summarized as follows:

i. Fieldwork

Fieldwork was accomplished during the summers of 2005, 2006, 2007 and 2008. Geological map of an area of approximately 1100km² was prepared using 1:25.000 topographic maps. 150 volcanic samples were collected for mineralogical-petrographical, geochemical and geochronical studies.

Aerial photographs (at a scale of 1:35000) and Digital Elevation Models (DEM, at a scale of 1:25000) were utilized both in the field, particularly to help distinguish boundaries of different lava flows, identify secondary eruption centers and structural features.

ii. Analytical Techniques

Thin sections of 140 samples including basalt, basaltic-trachyandesites, trachyandesites, trachytes, dacites and rhyolites were prepared at the laboratories of Middle East Technical University. All thin sections were examined both texturally and mineralogically.

Minerals and glasses within samples, ranging from basalt to rhyolite, were analysed by electron microprobe (EMPA) at the University of Bristol using a CAMECA SX-100 five-spectrometer (WDS) instrument. Minerals were analyzed using a 20 kV accelerating voltage, 10 nA beam current and a 5 μ m beam diameter. Groundmass glasses and melt inclusions were analysed using a 15 kV accelerating voltage, 2-4 nA beam current and a 15 μ m beam diameter to minimize alkali migration (Humphreys et al. 2006). Calibration was carried out on a variety of natural and synthetic minerals and glasses. Data reduction used the PAP routine.

Based on the petrographic studies, a total of 67 of the freshest samples (including 58 lava samples, 2 pyroclastic samples and 7 enclave samples) were selected for major and trace element analysis. Whole rock major element compositions were determined by ICP-Emission Spectrometry following a lithium metaborate/ tetraborate fusion and dilute nitric acid digestion at ACME (Canada) analytical laboratories. Trace element contents were determined in the same laboratory by ICP

Mass Spectrometry following a lithium metaborate/tetraborate fusion and nitric acid digestion.

Rb-Sr (22 samples), Nd-Sm (21 samples) and for Pb (18 samples) isotopic analysis of selected Süphan volcanics were performed at the laboratories of Earth and Ocean Sciences of University of British Columbia (PCIGR) by using Thermal Ionization Mass Spectrometer (TIMS).

The Ar-Ar age dating of 9 samples was performed at the Isotope and Geochronology Laboratories of University of Nevada. All samples were run as conventional furnace step heating analyses. All data are reported at the 1σ uncertainty level.

1.4 Structure of Thesis

This thesis is divided into 9 chapters.

Following this introductory chapter,

Chapter 2 deals with the regional geology of, and the volcanism related previous studies in, eastern Anadolıa.

Chapter 3 presents the geology of the study area.

Chapter 4 presents the Ar-Ar age determinations of samples from different levels of volcanostratigraphic succession.

Chapter 5 is about the mineralogical and petrographical features of the volcanic products.

Chapter 6 is dealing with the major, trace, Rare Earth (RE) element and isotope geochemistry of volcanism.

Chapter 7 is concerned with the mineral, melt and glass chemistry of volcanic rocks.

Chapter 8 discusses geochemical evolution of the volcanism in terms of magma mixing, fractional crystallization, crustal contamination and mantle source characteristics.

Chapter 9 gives the overall conclusions of the thesis.

Chapter 7 and a part of Chapter 8 are published as a paper entitled **“The importance of fractional crystallization and magma mixing in controlling chemical differentiation at Süphan Stratovolcano, Eastern Anatolia, Turkey”** in *Contributions to Mineralogy and Petrology*. The co-authors on this publication are: John Blundy, Department of Earth Sciences, University of Bristol, Wills Memorial Building, Bristol BS8 1 RJ, UK and Nilgün Güleç, Department of Geological Engineering, Middle East Technical University, 06531 Ankara, Turkey.

CHAPTER 2

GEOLOGICAL SETTING

2.1 Regional Geology and Lithospheric Structure of the Region

The basement of the Anatolian-Iranian plateau is consisting of several microcontinents (Şengör, 1990). These microcontinents are separated from each other by ophiolite belts and accretionary complexes. Five different tectonic blocks are recognized in eastern Anatolia, namely; *i)* The Eastern Rhodope-Pontide fragment, *ii)* the Northwest Iranian fragment, *iii)* the eastern Anatolian Accretionary Complex, *iv)* the Bitlis-Pötürge Massif and *v)* autochthonous units of the Arabian continent or foreland (Keskin, 2007 and the references therein) (Figure 2.1). The Eastern Rhodope-Pontide fragment is situated in the northern part of the region (I in Figure 2.1). Granulite facies rocks of Metamorphic Pulur complex formed the basement of Eastern Rhodope-Pontide fragment (Topuz et al., 2004). A thick volcano-sedimentary arc sequence overlies Pulur complex. This sequence is regarded as a south-facing magmatic arc, formed by north-dipping subduction under the Eurasian continental margin (Yilmaz et al., 1997) in a period between the Albian and Oligocene (Şengör et al., 2003). The units of the Northwest Iranian fragment (II in Figure 2.1) is covered by collision related volcanic units in Eastern Anatolia. It is exposed in Armenia (Karapetian et al., 2001) and composed of trondhjemitic, phyllitic, albite-plagiogranitic, and plagiogranite and granite-migmatitic lithologies (Karapetian et al., 2001; Keskin 2007). The Eastern Anatolian Accretionary Complex (EAAC, III

in Figure 2.1) forms a 150 to 180-km-wide, northwest-southeast-extending belt in the middle of the region. It can be regarded as remnant of a large subduction accretion complex formed between the Pontides and the Bitlis-Pötürge Massif (Şengör et al., 2003). EAAC consists of an ophiolitic melange of Late Cretaceous age and Paleocene to Late Oligocene flysch sequences. The Bitlis-Pötürge Massif (IV in Figure 2.1) is exposed in a northwest southeast-extending belt along the Eastern Taurus mountain range. It is regarded as the easternmost extremity of the Menderes- Taurus block (Şengör et al., 2003). The metamorphic rocks are subdivided into a Neoproterozoic basement of amphibolite, paragneiss/schist, eclogite and metagranitoid and a Paleozoic-Mesozoic cover of metapelites and metacarbonates (e.g. Tollluoğlu, 1982; Şengün, 1984; Göncüoğlu and Turhan, 1984; Oyan et al., 2004; Oberhänsli et al., 2009; Okay et al., 2010). The Arabian foreland (V in Figure 2.1) is composed of a continuous stratigraphic sequence of mainly shelf sediments of Early Paleozoic to Miocene age resting on a Precambrian basement (Pearce et al., 1990; Dolmaz et al., 2008). These tectonic units are overlain unconformably by shallow marine deposits of Oligocene to Middle Miocene age in the region. Collision-related volcanic units, on the other hand, unconformably overlie both these five tectonic blocks.

The age of the initial contact between Arabia and Eurasia has not yet been concluded accurately. The reported ages for the collision range from Late Cretaceous (Hall, 1976; Berberian and King, 1981; Alavi, 1994), through Late Eocene-Oligocene (35-25 Ma; Jolivet and Faccenna, 2000; Agard et al., 2005; Allen and Armstrong, 2008), to Miocene (Şengör et al., 1985, 2008; Dewey et al., 1986; Yılmaz, 1993; Robertson et al., 2007). Recently Okay et al. (2010) pointed out that the last oceanic lithosphere between Arabian and Eurasian plates was consumed by the Early Miocene (~20 Ma) by using the apatite fission

track ages of metamorphic rocks and Eocene sandstones from Bitlis-Zagros thrust zone. They also suggested that uplift of the Anatolian plateau occurred between 18–13 Ma and this uplift showed a rapid increase at ~12 Ma.

Regarding the debate about the time of collision event in the region, Keskin (2003) stated that the slab, whose subduction was generating the Pontide arc in the north, was not attached to the Arabia plate but possibly to the Bitlis-Pötürge Massif. According to Şengör et al. (2003), the oceanic realm between the Pontides and the Bitlis-Pötürge Massif was completely closed in the Oligocene, while the oceanic realm between the Bitlis-Pötürge Massif and the Arabian plate occurred much earlier (i.e., in the Late Eocene).

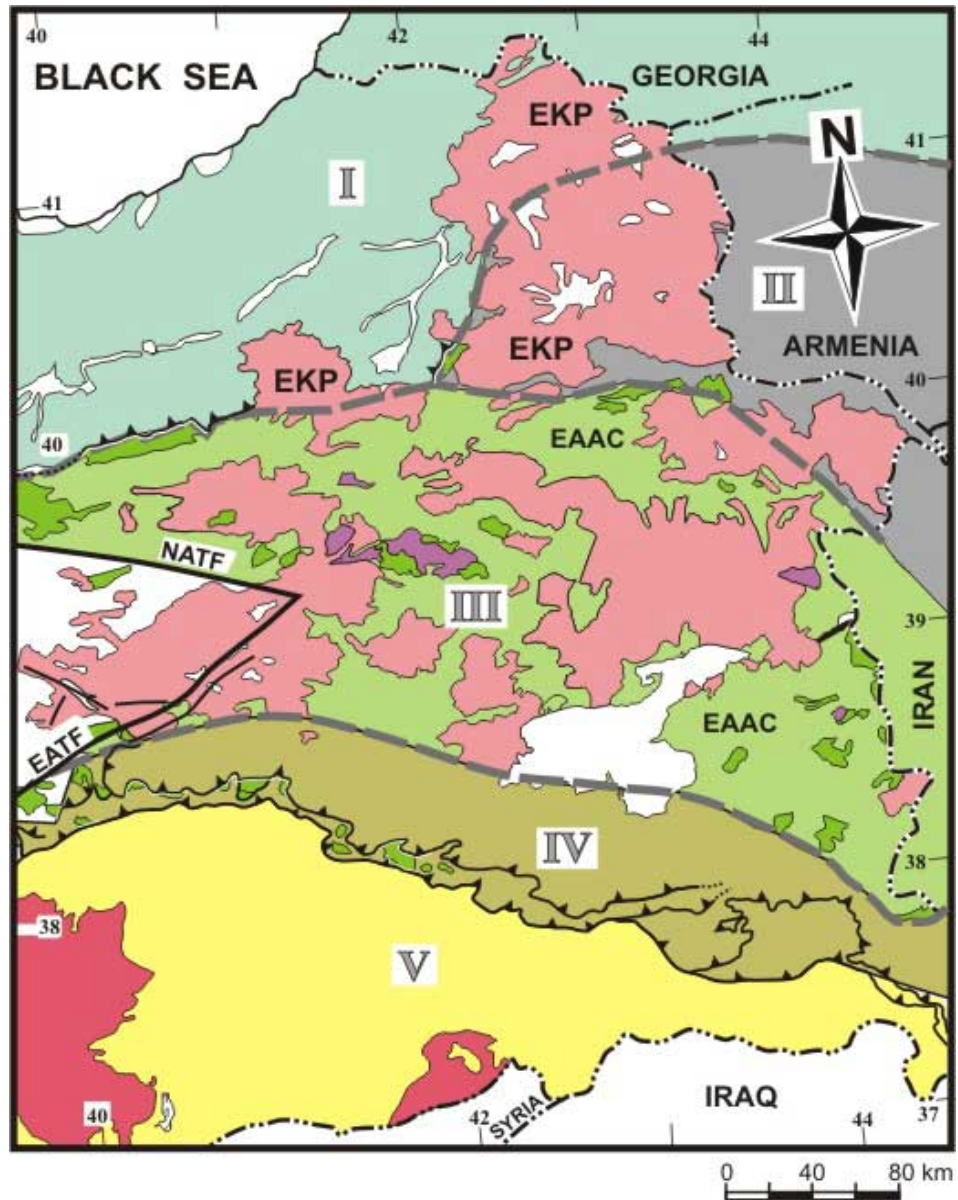


Figure 2.1 Major tectonic blocks of the Eastern Anatolia region (Keskin, 2007; Fig 1B). I: Rhodope-Pontide fragment, II: Northwest Iranian fragment, III: Eastern Anatolian Accretionary Complex (EAAC), IV: Bitlis-Poturge Massif, V: Arabian foreland. Dark green areas: outcrops of ophiolitic melange, Pink and red areas: collision-related volcanic units, white areas: undifferentiated units or young cover formations. EKP: the Erzurum-Kars Plateau in the north.

Results from geophysical studies in eastern Anatolia indicate that the mantle lithosphere is thin (Angus et al. 2006; Özacar et al. 2008) or absent (i.e. Al-Lazki et al., 2003; Sandvol et al. 2003a, b; Şengör et al. 2003; Zor et al. 2003; Gok et al., 2000; 2003;2007) across a considerable portion of the region (Şengör et al., 2003; Keskin, 2003;2007).

The crustal thickness in the region has an average of ~45 km (e.g. Çakır et al., 2000, Zor, et al., 2003) and varies from about 38 km in the Arabian foreland in southern Turkey to 50 km in the north beneath the Pontides mountain range (Zor et al., 2003). Tomographic images of the upper mantle (e.g Piromallo & Morelli 2003; Hafkenscheid et al. 2006; Lei and Zhao 2007; Zor, 2008) indicate slab-like fast-velocity anomalies that are interrupted from above by a widespread slow-velocity anomaly beneath the EAAC, and suggest slab detachment and concomitant emplacement hot asthenosphere at subcrustal depths.

2.2 History of Post Collisional Volcanism in Eastern Anatolia

Volcanic history of the Süphan stratovolcano has been considered, by several researchers, within the overall framework of the evolution of the collision related volcanics in eastern Anatolia (e.g. Innocenti et al.,1976, 1982 a,b; Ercan et al.,1990; Pearce et al.,1990; Notsu et al.,1995; Yılmaz et al.,1998; Keskin, 2003;2007; Şengör et al.,2008). Reported ages of the Süphan volcanism range between 0.1-0.7 Ma (Innocenti et al., 1976; Ogata et al., 1990; Ercan et al., 1990; Pearce et al., 1990; Notsu et al., 1995; Yılmaz et al., 1998). “Collision-related volcanics in eastern Anatolia are exposed in a broad zone across the Arabian-Anatolian collision zone, from the Kars Plateau and Lesser Caucasus in the northeast to the Arabian Foreland in the southwest” (Keskin, 2003) (Figures 1.1, 2.2).

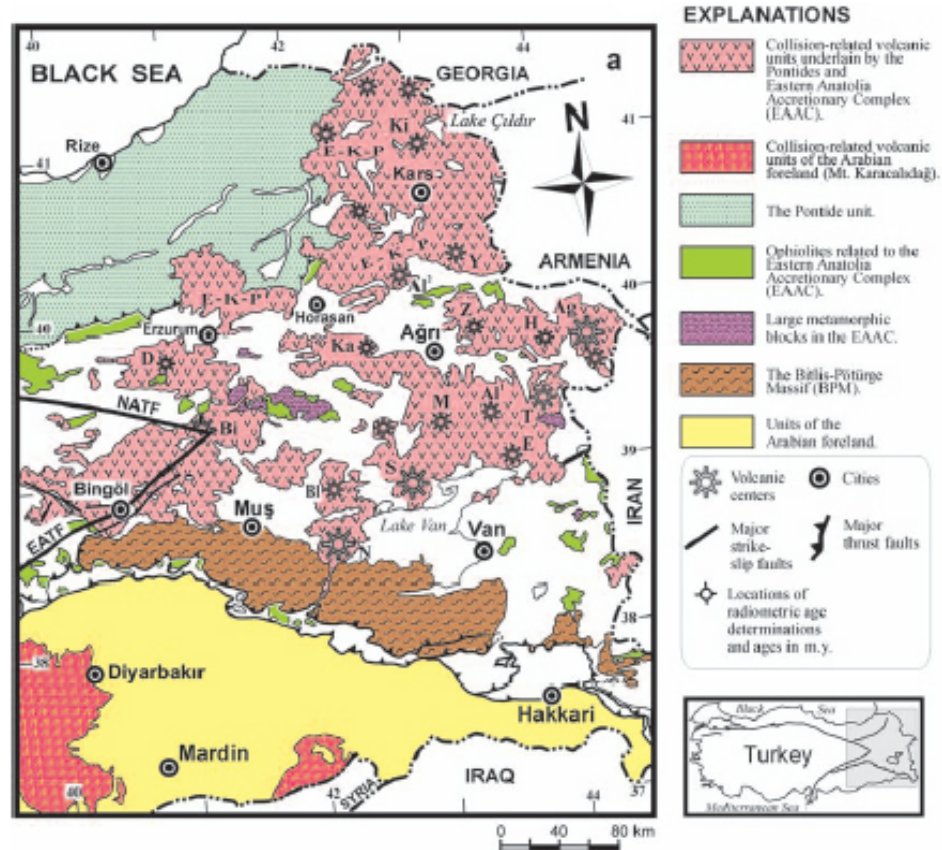


Figure 2.2 Simplified geological map of the Eastern Anatolia region showing tectonic units, collision-related volcanic products and volcanic centres (from Keskin, 2007; Figure 1A). E-K-P: the Erzurum-Kars Plateau; NATF and EATF: North and East Anatolian Transform Faults. Volcanic centers: Ag: Mt. Ağrı (Ararat), Al¹: Mt. Aladağ (SE of Ağrı), Al²: Mt. Aladağ (NW of Horasan), Bi: Mt. Bingöl, Bl: Mt. Bilicandagi, D: Mt. Dumanlıdag, E: Mt. Etrusk, H: Mt. Hamadağ, K: Mt. Karatepe, Ki: Mt. Kisirdağ, M: Mt. Meydandağ, N: Mt. Nemrut, S: Mt. Süphan, T: Mt. Tendürek, Y: Mt. Yağlicadağ, Z: Mt. Ziyaretdağ.

Before the recent seismological investigations including mantle tomographic studies, several geodynamic models were proposed for the genesis of collision-related magmatism in eastern Anatolia (e.g. Innocenti et al., 1982a,b; Dewey et al., 1986; Yılmaz et al., 1987; Ercan et al., 1990; Pearce et al., 1990; Keskin et al., 1998; Buket and Temel, 1998; Yılmaz et al., 1998).

Among these models, the one proposed by Innocenti et al. (1982 a,b) was concerned with slab-break off in eastern Anatolia. The authors claimed that the slab that subducted under the Pontides was broken after the continental collision. According to their model, the detached slab moved northward while it was sinking in the asthenosphere. They suggested that the volcanism becomes younger from south to north. Calcalkaline magmas that formed the Plio-Quaternary volcanic belt in the north were generated above the subducting slab, while the alkaline magmas representing the Miocene volcanic belt in the south were derived from the asthenospheric upwelling through the gap (i.e., slab window) behind the detached subducting slab.

Pearce et al., 1990 (refined by Keskin 1998) proposed the delamination of the lower lithosphere as the triggering mechanism for the widespread volcanism in eastern Anatolia, since asthenosphere is brought into close contact with the thickened layer of metasomatised lithosphere. When delamination occurs, it causes a perturbation in what is left of the mantle lithosphere, raising some parts of it above its solidus. While sinking into the asthenosphere, the delaminated block of the mantle lithosphere may release water that also promotes melting. These two mechanisms play an important role in the generation of extensive partial melting in the mantle, and can produce widespread volcanism in the region (Keskin, 2007).

Yılmaz et al.(1998) studied both the volcanostratigraphy and geochemistry of the major volcanic centers in eastern Anatolia (Nemrut, Süphan,Tendürek, Ağrı). In this study, the volcanologic evolution of Süphan was divided into three major phases: pre-cone phase, cone-building phase and flank eruption phase. According to the authors, the first volcanic activity started with the Plinian-Subplinian eruptions through N-S and NW-SE faults in pre-cone phase. In the cone-building phase, the activity continued with andesitic and dacitic lava flows and associated pyroclastic products, alternated with mobile basalt flows from the central vent until a large dome was built at the top of the cone during the late stage of the cone building phase. The flank eruption phase is the last stage and responsible for formation of the acidic domes, cinder cones and a large maar. Based on the trace element and isotope systematics, Yılmaz et al. (1998) suggested that heterogeneous subduction-modified lithospheric mantle is the source of Süphan volcanics, which have also undergone varying degrees of crustal contamination on the way to surface.

Following the recent seismic studies, (since 2003) concerned with the lithospheric structure in eastern Anatolia (ETSE, Eastern Turkey Seismic Experiment), geochemical data relevant to eastern Anatolian volcanics have been investigated in the light of the new geophysical findings. Keskin (2003, 2007) and Şengör et al. (2008) pointed out that there is a significant variation in lava chemistry in the N-S direction between the Erzurum Kars Plateau (EKP) in the north and the Mus-Nemrut-Tendurek volcanoes in the south (Figure 2.2). Lavas of the Bingol and Suphan volcanoes display transitional chemical characteristics (Pearce et al., 1990). Volcanic products in the north around the EKP and Mt. Ağrı are calc-alkaline in character and appear to have been derived from an enriched mantle source containing a distinct subduction signature (Keskin, 2003). Keskin (2003, 2007) and

Şengör et al. (2008) state that subduction signature decreases to the south and diminishes around Mus-Nemrut-Tendurek volcanoes, where the lavas are alkaline and display within-plate signature. The available radiometric age data point to the commencement of volcanism in about the Middle-Late Miocene on the thickened crust of northern side of the plate boundary (11 Ma Erzurum-Kars volcanics: Keskin et al., 1998). The volcanism appears to have migrated southward in the Plio-Quaternary (Keskin, 2003; Keskin, 2007), forming large volcanic centers and covering almost two thirds of the region, reaching over 1 km in thickness in some localities (Keskin et al., 1998; Keskin 2007). However, the most recent radiometric age data from southern parts of eastern Anatolia (i.e., 11.9-12.6 Ma aged Sarıçimen quartz monzodiorites, Çolakoğlu and Arehart, 2010; ~15 Ma aged Aladağ andezites, Lebedev et al. 2010) are not in support of the suggestion that the volcanism initiated at northern parts of the region and migrated towards the south.

Based on the variations in magma genesis, coupled with the uplift history and new geophysical findings, same authors (Şengör et al., 2003; Keskin, 2003; 2007) proposed a new geodynamic model namely “*Slab Steepening and break – off*”. This model involves a northward subducting slab beneath a large subduction-accretion complex, namely the Eastern Anatolian Accretionary Complex (EAAC), followed by break off around 10-11 Ma ago.

Şengör et al. (2003) suggested that the steepening and breakoff of this slab allowed hot, partially molten asthenospheric material to be emplaced near the base of the crust beneath the region. Emplacement of the asthenospheric mantle with a subduction component at shallow depths beneath the Eastern Anatolian Accretionary Complex would have generated extensive adiabatic decompressional melting in the

mantle wedge (Keskin, 2003). It also probably generated regional block uplift, producing the regional dome like structure (Şengör et al., 2003, 2008; Keskin 2007). In their more recent studies, Keskin (2007) and Şengör et al. (2008) proposed the source of the volcanics in the Eastern Anatolia to be a combination of both undepleted asthenosphere, and subduction-modified upper mantle wedge. Recently, Kheirkhah et al. (2009) suggested that most of the volcanics are derived from a lithospheric source after the partial loss of lower lithosphere, either via mechanical delamination or slab breakoff, or a combination of the two.

CHAPTER 3

GEOLOGY

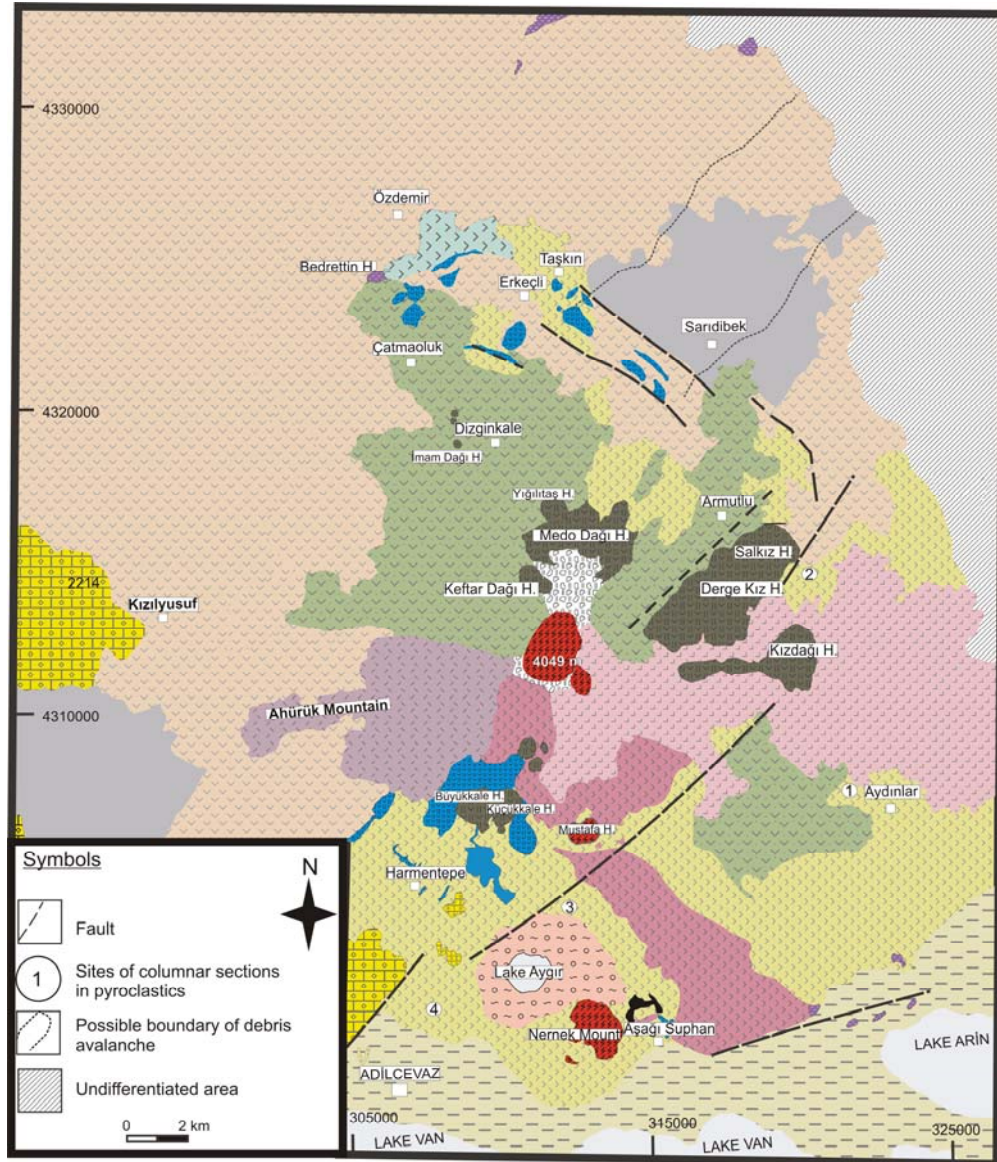
Volcanic products of the Süphan stratovolcano were emplaced over the Miocene and Pliocene-Pleistocene sedimentary units in the region. This section first introduces the general field aspects of the sedimentary rocks over which the volcanic products were emplaced, followed by the description of the volcanostratigraphic succession.

3.1 Sedimentary Rocks

Two groups of sedimentary rock were differentiated during the field studies, Miocene and Pliocene-Pleistocene sedimentary units (Figure 3.1, 3.2)

3.1.1 Miocene Sedimentary Units

Volcanic products of the Süphan Stratovolcano covered the Miocene marine sedimentary rocks at the southern and western parts of the study area (Figure 3.3). Sedimentary rocks are composed of shallow marine and dolomitized limestones (Adilcevaz Limestone) at the southern part, and alternation of sandstones and marls at the western part of the study area (Demirtaşlı and Pissoni, 1965; Yeşilova and Yakupoğlu, 2007).



EXPLANATIONS

	Alluvium debris fall		Trachyte(8)		Basaltic Trachyandesite(3)
	Travertine		Trachyte (7)		Basalt (2)
	Maar Deposits(11)		Pyroclastic Units(6)		Rhyolitic obsidian (1)
	Dacite/Rhyolite (10)		Trachyandesite(5)		Pliocene-Pleistocene Sedimentary Units
	Trachyte(9)		Basaltic Trachyandesite / trachyandesite(4)		Miocene Sedimentary Units

Figure 3.1 Geological map of the Süphan Stratovolcano.












LITHOLOGY	EXPLANATION	AGE
	Alluvium/Debris Fall	
	Travertine	
	Maar Deposits(11)	
	Rhyolite /Dacite(10)	64±14 ka (b) 110±30 ka (b)
	Trachyte(9)	120 ka (b)*
	Trachyte(8)	
	Trachyte(7)	
	Pyroclastic Units(6) Phase II,III,IV	
	Trachyandesite(5)	150±110 ka (b)
	Basaltic Trachyandesite/ Trachyandesite(4)	132±11 ka (b) 219±41 ka (b) 225±29 ka (b) 299±2.5 ka (b)
	Basaltic Trachyandesite (3)	
	Basalt (2)	428±40 ka (b)
	Rhyolitic Obsidian(1)	760±0.56 ka (a)
	Phase I Pyroclastic Units	
	Debris Avalanche	
	Fluvial and Lacustrine Sediments	Pliocene-Pleistocene
	Shallow Marine Sediments	Miocene

Figure 3.2 Stratigraphic columnar section of the Süphan Stratovolcano. Data Source; (a) Ogata et al., (1998), (b); Isochron ages of this study, (c); total gas age of this study.

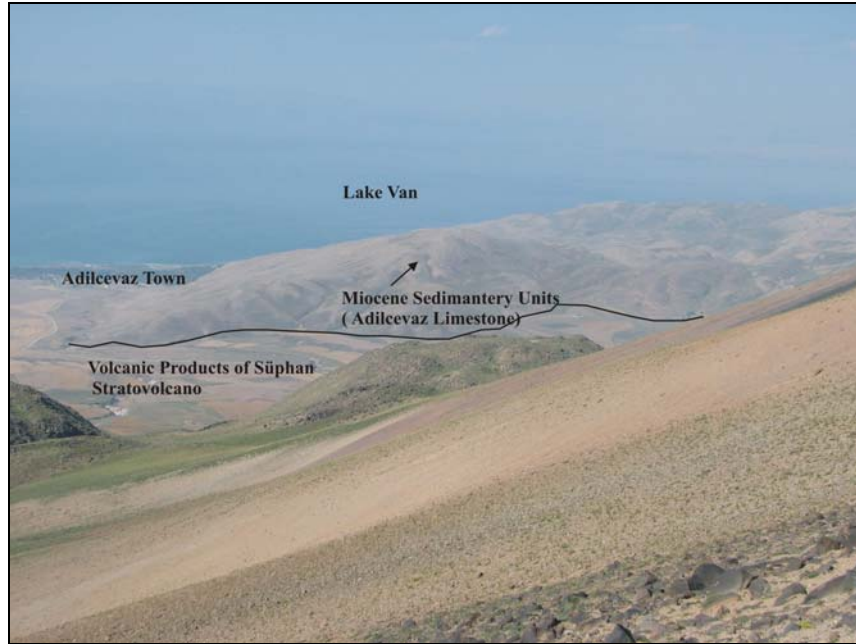


Figure 3.3 Contact of the Miocene Sedimentary units and volcanic products of Süphan Stratovolcano (north of Adilcevaz town).

3.1.2 Pliocene-Pleistocene Sedimentary Units

These group of sedimentary rocks are exposed between Adilcevaz town and Arin lake and are composed of alternating of lacustrine and fluvial sediments. Fluvial and lacustrine sediments contain loose gravel, sand, clay, silt and conglomerate. Volcanic products of the Süphan stratovolcano overlie these units at the southern parts of the volcano (Figure 3.4). Most of the fluvial sediments are exposed at vicinity of the Aşağı Süphan village. Lacustrine sediments are commonly seen at the shoreline of the Lake Van. Lacustrine and fluvial sediments alternate with thin plinian pumice and ash fall layers which are the possible initial products of the volcanism, suggesting that a shallow lake basin had occupied the entire region when volcanic activity began (Yılmaz et al, 1998).



Figure 3.4. The trachytic lava flow on the Pliocene-Pleistocene sedimentary rocks (northeast of Aşağı Süphan village).

3.2 Volcanostratigraphy of the Süphan Stratovolcano

Süphan is a steep sided stratovolcano and raises about 4050 m above the sea level. Its base diameter is approximately 40 km. Products of the Süphan volcanism extend over an area of about 2000 km² between Malazgirt, Patnos and Adilcevaz towns. 1100 km² of the whole area have been mapped during this study (Figure 3.1). 13 different volcanic products have been differentiated based on the field, mineralogical-petrographical and geochemical studies (Figure 3.1, 3.2). Field studies, Ar-Ar age datings and previous studies have been used in building the volcanostratigraphy of the Süphan volcano. Except main cone, 25 monogenetic structures including maar and domes have been identified around the volcano.

1:25 000 scaled Digital Elevation Models (DEM) and 1:35 000 scaled aerial photographs of the Süphan volcano are used to make an approach to the structural lineations that affect the volcanism. Structural lineations that are generated from aerial photographs and DEM are shown on the geological map of the Süphan stratovolcano (Figure 3.1). It is apparent from the figure that the lineations are trending in NE-SW, SW-NE directions. Some of the domes at northeastern parts and a maar occurrence at southern parts of the Süphan volcano are located on these lineations. Yılmaz et al., (1998) suggest that the volcanic center of the Süphan volcano is located at the intersection of two major fault zones, trending NE–SW and NW–SE, however Dhont and Chorowicz (2006) claimed that volcano is rooted in a transtensional zone that opened in a left stepping offset of the Süphan fault.

Field aspects of the units differentiated in the field are given in the following sections; the section headings bear the names of the units along with the number (in parenthesis) that represent the stratigraphic position of the lavas in geological map (Figure 3.1) and stratigraphic columnar section (Figure 3.2).

3.2.1 Debris Avalanche and Phase I. Pyroclastic Rocks

Products of debris avalanche and phase I pyroclastic rocks are covered by later units of Süphan volcanism. They exposed only limited areas that could not mapped in 1/25 000 scaled topographic maps. Based on the distribution of hummocky topography, possible boundary of debris avalanche deposits are shown in Figure 3.1:

Debris avalanche is the product of a large-scale collapse of a sector of a volcanic edifice under water undersaturated conditions. The deposit is characterized by two depositional facies, “block” and “matrix” (Uj, 1989;

Sigurdsson et al. 2000). Debris avalanche block is a fractured and deformed piece of the source volcano included within a debris avalanche deposit. The sizes of single blocks are variable, more than several hundred meters across as a maximum and less than a meter across as minimum. Debris avalanche matrix is a mixture of small volcanic clasts derived from various parts of the source volcano. This facies is massive, poorly sorted, and made up of fragments of volcanoclastic formations and occasionally of fragments of paleosols and plants (Sigurdsson et al. 2000). An amphitheater at source and hummocky topography on the surface of the deposit are characteristic topographic features of a debris avalanche. Hummocky topography is composed of numerous hills and longitudinal and transverse ridges (Glicken 1982; Siebert 1984). Products of the Süphan Debris Avalanche are exposed at the north and northeastern parts of the volcano.

Most characteristic feature of the deposits is their hummocky topography. Hummocky topography of debris avalanche characterizes block facies and displays elipsoidal-circular hills and longitudinal-transverse ridges (Figure 3.5). Blocks of the debris avalanche is composed of rhyolitic obsidian and perlite fragments (Figure 3.6).



Figure 3.5 Distribution on the topographic map, of the debris avalanche hummocks at the northeastern part of the volcano. Black areas represent the distribution of hummocks at north of the Süphan Volcano.

Sizes of the blocks in block facies reach up to 1.5 - 2 m at the vicinity of the Taşkın and Erkeçli villages. Most of the blocks are angular, the size and the number of the big blocks decrease with increasing distance from the source. Siebert (1984) described the decreasing size of the blocks in debris avalanche towards the end of the flow as a result of progressive fracturing of megablocks when they move downvalley.



Figure 3.6 Block facies of the debris avalanche (north of Erkeçli).

Matrix facies of debris avalanche consist of mixture of rhyolitic obsidian, perlite and some exotic material such as clay, fluvial gravel and basement rocks (Figure 3.7). Exotic materials were eroded and mixed with the debris avalanche matrix material during flowage. Matrix facies display grey, yellow and brown colors and are mostly represented by flat topography.



Figure 3.7 Matrix facies of the debris avalanche.

Süphan debris avalanche appears to have traveled approximately 25 km away from the source at the northern parts of the volcanic edifice. Owing to the fact that younger lavas and pyroclastic rocks of the Süphan stratovolcano have covered the debris avalanche products, the true thickness and the areal extent of the debris avalanche could not be determined in the study area. However, apparent thickness of the debris avalanche is approximately measured as 20-25 m from small exposures.

The processes that form the debris avalanches are variable. Three types of debris avalanches have been proposed: *Bezymianny*, *Bandai*, and *Unzen* types (Sigurdsson et al. 2000). *Bezymianny* type debris avalanches are associated with magmatic eruptions, as in the case of Mount St. Helens in 1980. Pyroclastic flows and falls occur and extend over wide areas during or after the debris avalanches (Siebert, 1984;

Siebert et al., 1987). The *Bandai* type is associated with a phreatic eruption, as in the case of Bandai, Japan, in 1988. No juvenile material is included within this type of deposit. The *Unzen* type is not directly related to volcanic activity, but triggered by an earthquake.

In the Süphan stratovolcano, the source area of the debris avalanche is obscured by later volcanic units and post avalanche erosion, and hence avalanche scar could not be determined on the volcanic edifice. This makes it rather difficult to speculate on the possible triggering mechanisms for the Süphan debris avalanche. According to Glicken (1996), in an active volcanic area, the triggering cause of a debris avalanche could be magmatic, phreatomagmatic or seismic, and the first two causes are normally associated with dome-growth deformation and explosive eruptions. In Süphan, dacitic and rhyolitic domes are present at the summit and the flanks of the volcano. However there is no syn-eruptive pyroclastic deposits accompanying the debris avalanche in the area. Only a few thin pyroclastic layers were determined after the debris avalanche emplacement. It is difficult, therefore, to suggest a triggering cause with the available data. Given, however, that tectonic structures have an important role in the evolution of the Süphan volcanism and that there are dacitic and rhyolitic domes at the flanks and summit of the volcano, a combination of magmatic and tectonic processes can be responsible for the debris avalanche at Süphan.

Debris avalanche is overlain by Phase I pyroclastic rocks of the Süphan Stratovolcano (Figure 3.2, 3.8). The first unit of this phase is a plinian pumice fall deposit (P1), observed mainly at the northern parts and also as small exposures at the southern parts under the basaltic trachyandesitic lava flows (4). P1 display white and grey colors and has a maximum pumice size of 3 cm. P1 is overlain by an ash fall deposit

and a scoria fall deposit (Figure 3.9, 3.10) with a maximum scoria size of 4 cm. Ash fall deposit and a scoria fall deposit have a thickness of approximately 50 cm. The scoria fall deposit is probably related to the basaltic trachyandesitic lava flows which extend over wide areas around the volcano. Phase I pyroclastics have culminated by a brown colored paleosoil.



Figure 3.8 Phase I pyroclastic deposits of Süphan stratovolcano (north of Erkeçli).

3.2.2 Rhyolitic Obsidian Domes and Lava Flows (1)

They are situated at the northern parts of the study area as domes and at the southwestern parts as lava flows (Figure 3.1). They have brown and black colors and contain macroscopic feldspar phenocrysts up to 1

cm in size. These lavas have covered an area of approximately 2 km². Obsidian lava flows at southern parts of the volcano are exposed under the trachytic and basaltic trachyandesitic lava flows (Figure 3.11). Ogata et al., (1989) reported the K-Ar age of the obsidians as 0.76±0.56 Ma.

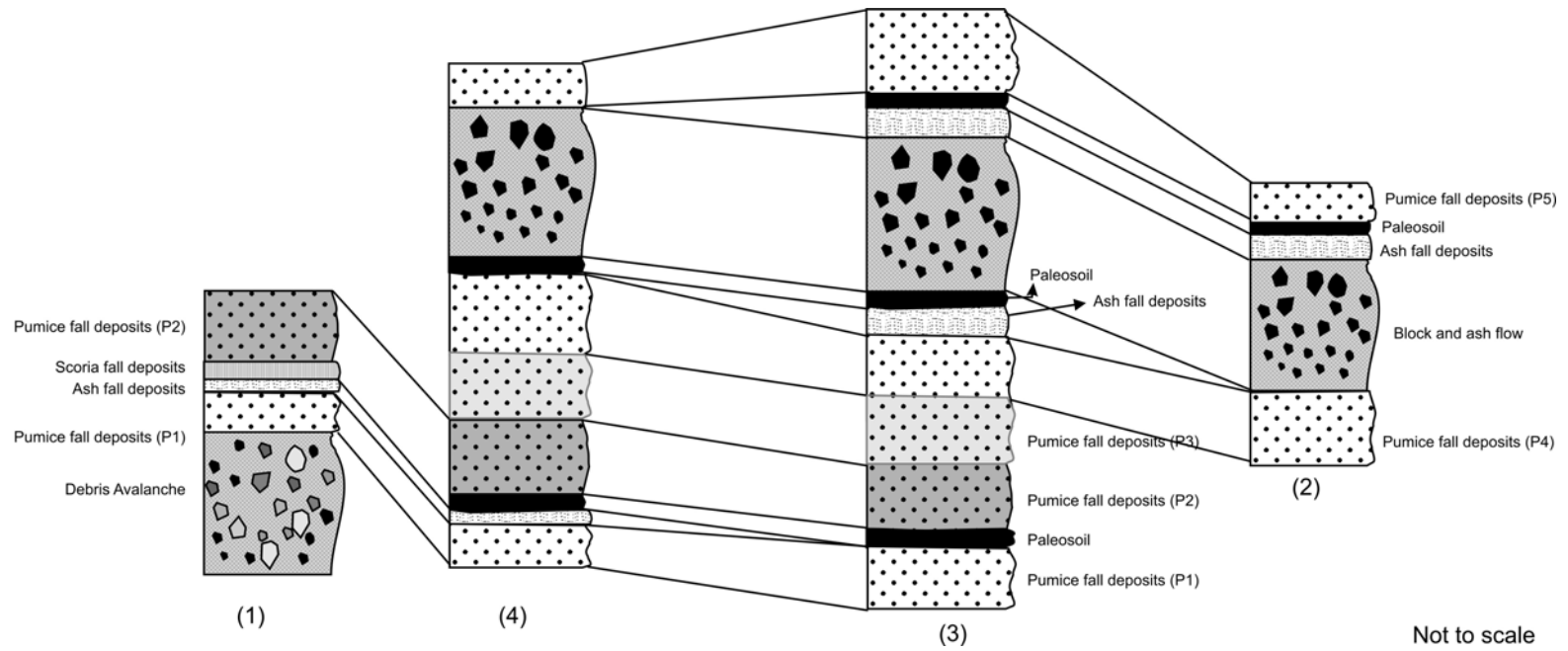
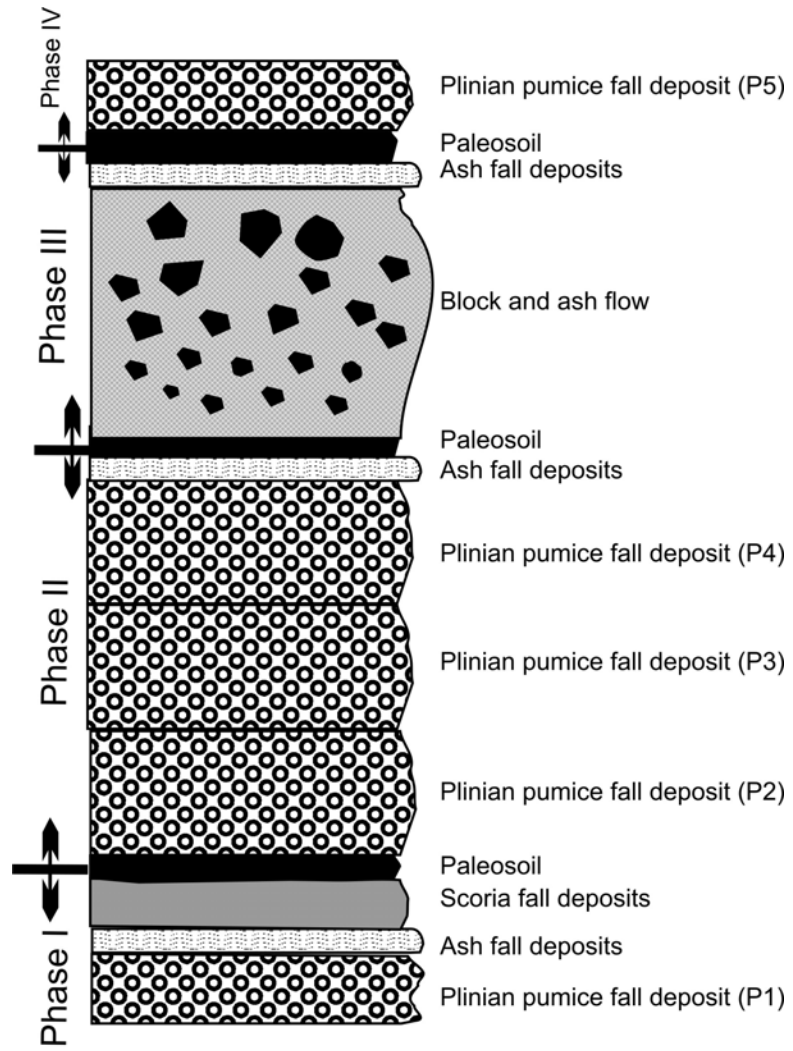


Figure 3.9 Correlation of the stratigraphic columnar sections of Süphan pyroclastics (The sites of columnar sections are indicated by numbers in parenthesis and are shown in Figure 3.1)



Not to scale

Figure 3.10 Idealised stratigraphic section of the Süphan pyroclastics.



Figure 3.11 Rhyolitic obsidian lava flows at the southern parts of the volcano.

Rhyolitic obsidians which are exposed in the northern part of the volcano are circular-elipsoidal in shape, and aligned in NW-SE direction. They display dome like morphology, however a detailed investigation and a closed up view of the dome like morphology reveal that upper parts of these units include obsidian blocks, lower parts contain perlite, rhyolitic obsidian fragments and volcanic ash. These elipsoidal and circular morphologies are partly covered by basalts (2) and basaltic trachyandesites (3,4), and are best seen at the vicinity of Erkeçli village (Figure 3.12).



Figure 3.12 Basaltic trachyandesitic lava flows on the hummock at the northern flanks of Süphan.

3.2.3 Basalt (2)

Basaltic lava flow is only determined at the northern parts of the volcano between Erkeçli and Özdemir villages. This unit flows over debris avalanche deposits and covers an area of approximately 4 km². It is represented by pink color and mostly covered by basaltic trachyandesitic lava flows (3,4). Basalts contain mm-cm sized plagioclase, pyroxene and olivine minerals which can even be seen macroscopically.

3.2.4 Basaltic Trachyandesitic Lava Flows (3)

Basaltic trachyandesitic lava flows are identified in limited areas at the southern and northern parts of the study area. In the southern part, they

exposed are at the north of the Lake Arin. In the northern parts, these lava flows are observed in the vicinity of Bedrettin Hill and around the Kuşkaya villages. Most of the lavas are covered by basaltic trachyandesitic/trachyandesitic lava series (4). They display black and grey colors and contain mm-cm sized plagioclase minerals. Upper parts of the lavas contain numerous gas bubbles, however lower parts are massive. They extent over an area of approximately 4 km². They are mostly exposed in flat areas around the volcano and sometimes observed on hummocky topography of debris avalanches (Figure 3.13).



Figure 3.13 Basaltic trachyandesitic lava flow on debris avalanche (northeast of Taşkın).

3.2.5 Basaltic Trachyandesitic/ Trachyandesitic Lava Series (4)

This unit comprises two different lava flows, namely, basaltic trachyandesitic and trachyandesitic lavas. These lava flows are mapped as a single lava unit (Figure 3.1) as their boundary relationship is not well defined in the field. These are the most widespread lava flows in the study area and extend over an area of approximately 150 km² at the western, northern and northeastern parts of the volcano. They covered most of the hummocky topographies of debris avalanches.

Owing to their low viscosity and high effusion rate basaltic trachyandesitic lavas appear to have flowed a great distance (~30 km) from the volcano and reached the Malazgirt town (Figure 3.14). They are black in color and display porphyritic and vesicular textures and are mostly exposed at flat areas at the northern and western parts of the volcano.



Figure 3.14 Basaltic trachyandesitic flows between Süphan and Malazgirt village.

Basaltic trachyandesitic and trachyandesitic lava flows are well differentiated only at the western parts of the volcano. Trachyandesites at the western parts of the volcano appear to have formed as a result of secondary eruption centers (Figure 3.15) and flowed down to the eastern parts of the Kızılyusuf Village. Small cinder cones exist near the eruption centers.



Figure 3.15 Trachyandesitic lava flows of secondary eruption centers at the western flanks of the volcano.

Trachyandesitic lavas of this series have black and grey colors and display microcrystalline textures and flow over the basaltic trachyandesites. They could not flow great distances from the Süphan main cone as in the case of basaltic trachyandesites.

3.2.6 Trachyandesitic Lava Flows (5)

Trachyandesitic lava flows constitute one of those units responsible for the recent morphology of the stratovolcano and covered an area of approximately 52 km². They are exposed at the southern parts (vicinity of Aydınlar village), northeastern parts (vicinity of Armutlu village), and at the northern parts (vicinity of Güvercinli and Çatmoluk villages) of the volcano. Younger pyroclastic deposits of Süphan partly covered these lavas at the southern parts of the volcano. They are generally dark grey

in color and glassy, and contain large plagioclase minerals ranging up to 2 cm in size. They occupy high topographies and overlie basaltic trachyandesitic and trachyandesitic lava series (4) at the northern parts (Figure 3.16).



Figure 3.16 Trachyandesitic lava flows at the southern parts of the Süphan (west of İmamdağı hill) .

3.2.7 Phase II, III, IV Pyroclastic Rocks (6)

Various pyroclastic units have been differentiated on the basis of the results of field studies. These pyroclastic units occurred at different time periods during the evolution of the volcanism. Stratigraphic sections of pyroclastic units are depicted in Figure 3.9. Pyroclastic units of Süphan are grouped into 4 different phases, each phase being separated by a paleosol level from the other (Figures 3.9, 3.10).

Pyroclastic units of Phase I. have been mentioned previously in section 3.2.1 (Debris Avalanche and Phase I. Pyroclastic rocks).

Phase II pyroclastic rocks start with green colored plinian pumice fall deposit (P2). The maximum pumice size reaches up to 2 cm within this unit. P2 unit is lithic poor and extends radially around the volcano. P2 is overlain by a lithic rich white colored plinian pumice fall deposit (P3, Figures 3.9, 3.10). Sizes of pumice and lithic fragments reach up to 0.5 and 0.2 cm, respectively, within this unit. A plinian pumice fall deposit (P4) with a maximum pumice size of 10 cm overlies the P3 unit. It contains large fractured pumice blocks. The broken pieces of pumice blocks are intact, suggesting that they were deposited before they fractured. Post deposition fractures indicate that the blocks were still hot when emplaced, then cracked upon cooling (Figure 3.17a). Size of the lithic fragments range up to 3 cm. Phase II pyroclastics are terminated by a thin plinian ash fall (Figure 3.17b).



Figure 3.17 a) Fractured pumice blocks in P3, b) ash fall deposits of Phase II.

Phase III started with a block and ash flow (Figures 3.9, 3.10, 3.18a). Block and ash flows can form, in general, by collapse of vulcanian eruption column but most historic examples (Mount Unzen 1991, Mount Merapi 1984, 1994 , 1997-1998 etc.) were generated by partial to total collapse of viscous lava domes as they oversteepen at their fronts during growth. Dome collapse can be gravitational, explosive or both. This kind of pyroclastic flows commonly extend up to 10 km from their source at speeds up to 100 km/h and are accompanied by ash cloud surges. Block and ash flows are commonly described as monolithologic and have usually basaltic-andesite, andesite, dacite and rhyolite compositions (Sigurdsson et al. 2000).

The block and ash flow of Süphan is one of the most common pyroclastic deposit in the study area. Size of the blocks reaches up to 1.5 m at the vicinity of the main cone and it gradually decreases away from the volcano. Block and ash flow contains radially fractured blocks (Figure 3.18b) and bread-crust bombs, and displays reverse grading. The white colored ash fills the spaces between blocks of the flow. Blocks of the unit are mostly rhyolitic and rarely contain fragments of the older products of the volcanism. Block and ash flow is exposed heavily at southern parts but also observed at eastern and northeastern parts of the volcano. This unit seems to have flowed approximately 10 km away from the Süphan cone at the southern parts. Block and ash flow deposit is overlain by a thin plinian ash fall deposit (Figures 3.9, 3.10).



Figure 3.18 a) Block and ash flow under the trachytic lava flows, **b)** radially fractured blocks in block and ash flow.

Süphan block and ash flow deposits possibly formed as a result of collapse of a growing rhyolitic dome at the summit of the volcano. There is a remnant of an old rhyolitic dome at the southeastern part of the summit. This older dome has the same geological, mineralogical and geochemical properties with the blocks in block and ash flow deposits.

Last phase of pyroclastic rocks (Phase IV) contains a white colored plinian pumice fall deposit (P5) and is characterized by pumice and lithic fragments with maximum sizes of 4 cm and 2 cm, respectively (Figure 3.19).



Figure 3.19 Ash fall deposits of Phase III and pumice fall deposits of Phase IV (P5).

3.2.8 Trachytic lava flows (7,8,9)

Based on the field, mineralogical-petrographical and geochemical studies, three different trachytic lava flows are determined on the southern, eastern and western flanks of the volcano.

Vitrophyre Trachyte (7): Vitrophyre trachyte seems to have flowed from southern flank towards the Adilcevaz – Erciş main road (Figure 3.20a). The pyroclastic deposits of the Aygır maar have partly covered vitrophyre trachytic lavas at the southern flanks of the volcano. The lavas display an essentially vitrophyric texture, has large (0.5-2 cm) plagioclase and amphibole minerals, and cover an area of approximately 25 km². The lower parts of the lavas look grey in color, while upper parts display black color and glassy texture due to the rapid cooling.

Trachyte (8): Another trachytic lava flow covers an area of approximately 75 km² on the eastern flanks of the volcano (Figure 3.20b). It has black-grey color and glassy texture, and contain large plagioclase phenocrysts and enclavas, ranging up to 2 cm and 7 cm in size. In contrast to trachyte (7) it has no amphibole crystals.

Trachyte (9); Last trachytic lava flow of Süphan is observed at the western flanks of the volcano. It has flowed from the eastern flanks towards Ahürük mountain. Lava flow displays grey color, is less glassy than the other trachytic flows, and has microcrystalline texture. It covers the basaltic trachy andesitic lava flows at western parts of the volcano (Figure 3.20c).

3.2.9 Dacitic and Rhyolitic Domes (10)

Dacitic and rhyolitic domes were developed after the lavas and pyroclastics of the main cone. They are situated on the summit and on the flanks of the volcano. Rhyolitic and dacitic lavas of domes contain basaltic, doleritic, granitic enclaves.

Dacitic domes are exposed at the southern, northern and northeastern parts of the volcano. Derge Kız , Salkız , Abdal Kız, Kızdağı, Kale, Medodağı, Keftar Dağı, Yiğiltaş, İmamdağı, Büyük Kale, Küçük Kale, Keçel Dağı and Yukarı Kafir Kalesi hills are all dacitic in character.

Salkız, Dergekız, Abdal Kız domes (Figure 3.21a) are situated at the northeastern flanks of the volcano, on a northeast-southwest trending fault system. Five eruption centers have been determined to be related to these domes. Eruption centers are separated by small valleys between them. These domes are elliptical in shape. They extend over an area of approximately 10 km². The long axis of domes reaches up to

5.5 km, whereas the short axis has a length of 2.1 km. The highest and the lowest point of the domes are 3096 m and 200 m respectively. These domes have endogenic character and uplifted the older products of the volcanism. They have grey and whitish grey color and are perlitic, with minor crystals of macroscopic feldspar and pyroxene minerals set in a glassy matrix. They contain cm-dm sized enclaves.

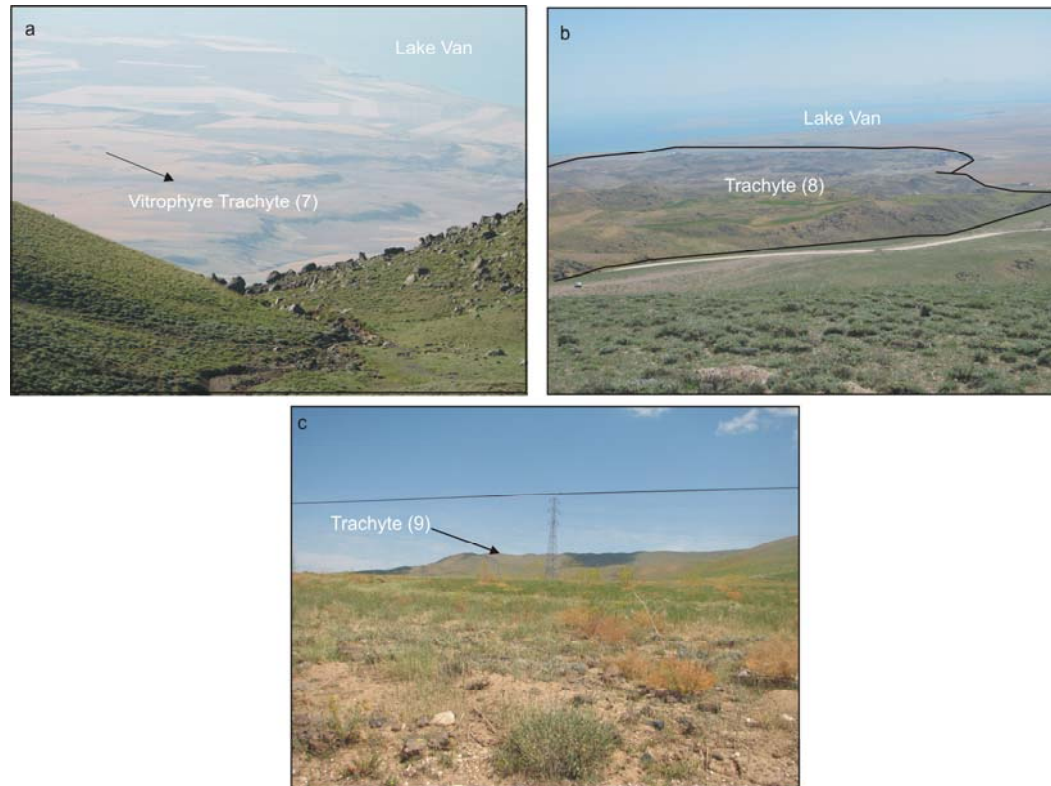


Figure 3.20 Three different trachytic lava flows of Süphan Stratovolcano. a) west of Aşağı Süphan, b) north of Aydınlar, c) Ahürük mountain

Kale hill dacitic dome is situated at the southern parts of, and possibly occurred at the same time with, the Salkız, Abdal Kız and Derge Kız domes. It covers an area of 0.25 km² . The height of the dome from base to top is approximately 110 m.

Kızdağı dacitic dome is situated at the eastern flanks of the stratovolcano and covers an area of 4 km². Its height is 300 m.

Keftar dağı, Yiğilitaş, İmamdağı and Medodağı dacitic domes are situated at the northern parts of the volcano. Medodağı dacitic dome is the biggest among these domes. Its height, from base to top, is 600 m and covers an area of 6km². It is an endogen dome and its top is covered by debris fall.

Yiğilitaş, Keftar dağı and İmamdağı dacitic domes are exogene domes and have circular shapes. Yiğilitaş dome cuts the Medodağı dome and is situated at its northern flank. It covers an area of 0.7 km² and has an height of 150 m from base to top. The bread crust volcanic bombs were found around the eruption center suggest possible eruption of pyroclastic rocks before or during the growth of Yiğilitaş volcanic dome.

Keftar dağı dome has two eruption centers (Figure 3.21b) and covers an area of 0.5 km². It displays similar characteristics with Yiğilitaş dome and has a height of 150 m. It seems to have started its growth possibly with a pyroclastic eruption. There are a few more (secondary) eruption centers near its flanks of this dome.

İmamdağı dacitic domes are situated at the north and south of the Dizgin Kale Village as three different eruption centers (Figure 3.21c). The domes cover an area of 0.3 km², with heights reaching up to 70 m. .Yukarı Kafir kalesi hill, Büyük Kale hill, Küçük Kale hill ve Keçel Dağı

hill dacitic domes are situated at the southern parts of the volcano. Yukarı Kafır Kalesi doms (Figure 3.21d) have several eruption centers, only 3 of them can be depicted in the 1/25000 scaled geological map. These domes cut and uplifted the obsidian (1) and trachytic lava flow (7) units of the stratovolcano. They cover an area of 0.5 km² with a height of 200 m.

Büyük Kale hill (Figure 3.21e), Küçük Kale hill ve Keçel Dağı hill dacitic domes are located at the southern flanks of the volcano as 3 different eruption centers. They cover an area of 2 km². Pyroclastic deposits of these domes could not be determined during the field studies.

Most of the dacitic domes of the Süphan Stratovolcano have similar macroscopic and microscopic properties. Medo dağı dacitic dome is possibly older than the other domes.

Rhyolitic domes of Süphan stratovolcano are Nernek mountain, Mustafa hill and the dome at the summit of the volcano.

Nernek dome has a height of 250 m from base to top (Figure 3.22a) and covers an area of 4 km². It is situated 10 km south of the Süphan main cone, and displays an expanding morphology towards south. Lavas of the dome have whitish grey color and contain macroscopically visible mica, amphibole, and feldspar minerals. A thin pyroclastic deposit of Aygır maar partly covers the Nernek dome.

Mustafa hill rhyolitic dome (Figure 3.22b) is a circular shaped dome covering an area of 0.8 km² and having a height of 250 m. It has similar properties with Nernek dome and cuts the units around it.



Figure 3.21 Dacitic domes of the Süphan Stratovolcano a) Kızdağı hill, Aptalkız hill, Dergekız hill, Salkız hill doms, b) Keftardağı hill dacitic dome, c) İmamdağı hill dacitic dome, d) Yukarıkafir kalesi dacitic dome, e) Büyükkale hill dacitic dome.

The other and possibly the youngest rhyolitic dome seems to have developed on the summit crater of the volcano (Figure 3.22c). It is an exogene dom, has a diameter of 1 km and a height of 150 m. It has grey-white colors and contain feldspar and mica crystals and display

glassy texture. This dome possible plugs the main conduit of Süphan volcano.

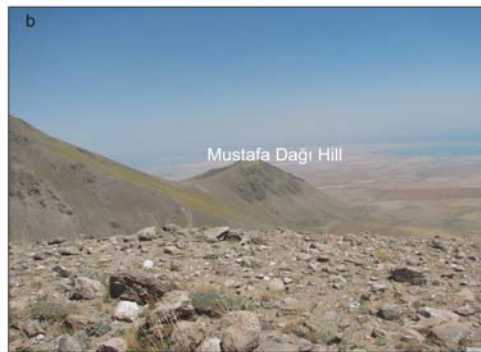


Figure 3.22 Rhyolitic domes of the Süphan volcanism a) Nerek mountain, b) Mustafa hill, c) rhyolitic dome at the summit of the volcano.

3.2.10 Maar Deposits (11)

The most recent product of Süphan volcanism is phreatomagmatic in character and includes a maar occurrence (Aygır Maar) at the southern part of the volcano (Figure 3.23).



Figure 3.23 Aygır maar at the southern part of the Süphan Stratovolcano.

Maars result from phreatomagmatic eruptions due to interaction of ascending magma with ground water or surface water. Deposits are composed of juvenile pyroclasts, derived from erupting magma, accessory clasts of comagmatic volcanic rocks from earlier eruptions, and accidental clasts, derived from subvolcanic basement. Maar craters have a diameter of up to 3 km and depth of 200-300 m (or 500 m??-see the below paragraph). Hydroclastic volcanoes can be subdivided into three different morphological and structural types: (1) maars, (2) tuff rings and (3) tuff cones (Cas and Wright, 1987, Sigurdson et al, 2000). Tuff rings have craters that lie on, or above the preeruption surface. Deposits of tuff rings consist of a mixture of juvenile and accidental clasts, the former comprising the main constituent of the well stratified deposits. Tuff cones differ from tuff rings by having smaller craters and higher profiles than tuff rings and maars and steeper external slopes. Their crater floors are generally above the land surface. Deposits are

mainly composed of juvenile clasts and subordinate amounts of accidental clasts.

Aygir maar have an circular crater with a diameter of 1.5 km. Deposits of the maar extend ~2.5 km away from the crater and show radial distribution. Base surge deposits of Aygir maar display dune, antidune and cross bedding structures. Surge deposits are fine grained and poorly sorted. The thickness of the maar deposits at the crater rims reach up to 40 m, and decreases away from the source.

Aygir maar deposits are located over a lahar which contains fragments of limestone, clay and older volcanic rock fragments. Lower parts of the deposits mostly include accessory clasts and large dune and antidune structures (Figure 3.24). Size of the dune and antidune structures decreases, while their amount increases, towards the upper parts of the deposits. The flow becomes planar at the upper parts (Figure 3.25) and enriched in ash content. The deposits contain i) ash and grey and white pumice fragments as juvenil fragments, ii) perlite and obsidian fragments as accessory clasts, and iii) sedimentary fragments as accidental clasts.

The well known maars are reported in the literature as being formed by interaction of basaltic magma with ground water. In the Aygir maar, however, juvenile fragments are completely acidic (rhyolitic) in composition and suggests that the maar possibly occurred by interaction of a rhyolitic magma with groundwater.

3.2.11 Travertine

The travertine deposits are exposed at vicinity of the Aşağı Süphan village at the southern part of the volcano. The deposition of the recent travertine is still active in the region.



Figure 3.24 Dune structures in the maar deposits.



Figure 3.25 Planar flows in the maar deposits. Lower parts of the flow are enriched in dune and antidune structures, whereas at the upper parts the flow became planar.

CHAPTER 4

GEOCHRONOLOGY

The Ar-Ar age dating analyses were performed at the Isotope and Geochronology Laboratories of University of Nevada. The results given below, and the relevant discussions that follow, are based on the report provided by Dr. Terry Spell from the lab in charge of analyses.

All samples were run as conventional furnace step heating analyses. All data are reported at the 1σ uncertainty level. Furnace step heating analyses produce what is referred to as an apparent age spectrum. The "apparent" derives from the fact that ages on an age spectrum plot are calculated assuming that the non-radiogenic argon (often referred to as trapped, or initial argon) is atmospheric in isotopic composition ($^{40}\text{Ar}/^{36}\text{Ar} = 295.5$). If there is excess argon in the sample ($^{40}\text{Ar}/^{36}\text{Ar} > 295.5$) then these ages will be older than the actual age of the sample. U-shaped age spectra are commonly associated with excess argon (the first few and final few steps often have lower radiogenic yields, thus apparent ages calculated for these steps are affected more by any excess argon present), and this is often verified by isochron analysis, which utilizes the analytical data generated during the step heating run, but makes no assumption regarding the composition of the non-radiogenic argon. Thus, isochrons can verify (or rule out) excess argon, and isochron ages are usually preferred if a statistically valid regression is obtained. If such a sample yields no reliable isochron, the best estimate of the age is that the minimum on the age spectrum is a

maximum age for the sample (it could be affected by excess argon, the extent depending on the radiogenic yield). $^{40}\text{Ar}/^{39}\text{Ar}$ total gas ages are equivalent to K/Ar ages. Plateau ages are sometimes found, these are simply a segment of the age spectrum which consists of 3 or more steps, comprising >50% of the total gas released. Such ages are preferred to total gas or maximum ages if obtained. However, in general an isochron age is the best estimate of the age of a sample, even if a plateau age is obtained. Most of the Süphan samples are very young and are low-K materials. Thus, there were not large quantities of radiogenic argon ($\%^{40}\text{Ar}^*$) to measure during analysis. These types of samples typically yield ages which are of low precision, since large corrections on the measured ^{40}Ar must be made.

The obtained Ar-Ar age dating results of the Süphan volcanics (Table 4.1) summarized below. The number in parenthesis represents the position of the rock group in the volcanostratigraphy (Figures 3.1, 3.2).

Table 4.1 Ar-Ar age dating results of Süphan volcanics.

Sample	Plateau Age (ka)	Isochron Age (ka)	Total Gas Age (ka)
2006 99 (2)	415±103	428±40	
2006 3 (4)	405±60	387±47	
2007 22 (4)	313±37	225±29	
2007 24 (4)	195±26	219±41	
2006 116 (4)	162±11	132±11	
2006 8 (5)	381±56	150±110	
2006 59 (9)			120
2006 110 (10)		110±30	
2007 5 (10)	122±19	64±14	

4.1 Basalt (2)

Sample 2006-99 Plagioclase

Basaltic sample produced a discordant age spectrum, with high initial step ages, followed by decreasing ages, and then increasing ages with the final steps (Table 4.2). The form of the age spectrum is U-shaped, suggesting the presence of excess argon. The total gas age is 934 ± 91 ka. Steps 4-7 (53% of the total gas released) define a plateau age of 415 ± 103 ka (Figure 4.1). Steps 4-7 also define an indistinguishable isochron age of 428 ± 40 ka (Figure 4.2), and do not indicate excess argon is present (initial $^{40}\text{Ar}/^{36}\text{Ar}$ within uncertainty of the atmospheric value of 295.5). The measured ^{36}Ar is low, suggesting that this sample is unaltered.

4.2 Basaltic Trachyandesitic/ Trachyandesitic Lava Series (4)

Ar-Ar ages of 4 different lava flows of this series are summarized below.

Sample 2006-3 Groundmass

This sample produced a discordant age spectrum, with a negative first step age followed by increasing, decreasing and finally increasing ages with the last steps (Table 4.3). Overall the sample exhibited low radiogenic yields ($\%^{40}\text{Ar}^*$) and very high amounts of non-radiogenic argon (indicated by the very large ^{36}Ar measurements). This suggests alteration of the fine grained groundmass minerals. Another indication of alteration is that the first low temperature step released an anomalously large amount of the total ^{39}Ar . The total gas age is 172 ± 38 ka, and steps 2-5 (47% of the total gas released) define a plateau age of 405 ± 60 ka (Figure 4.3). Steps 2-5 (47% of the total gas released) define an isochron age of 387 ± 47 ka (Figure 4.4) , and suggest that a small amount of excess argon may be present (initial

$^{40}\text{Ar}/^{36}\text{Ar} = 299.6 \pm 2.5$), although it should be noted that at 2σ this is indistinguishable from the atmospheric value of 295.5. The isochron age should be considered the most reliable for this sample.

Table 4.2 Ar-Ar age results of sample 2006 99.

step	T (C)	t		% 39Ar							Age			
		(min.)	36Ar	37Ar	38Ar	39Ar	40Ar	%40Ar*	rIsd	Ca/K	40Ar*/39ArK	(ka)	1s.d.	
1	500	12	0.136	0.196	0.031	0.475	37.893	26.3	1.2	29.6679494	28600.39913	4745	893	
2	560	12	0.101	0.425	0.037	1.026	27.122	-533.6	2.5	29.78385851	4603.277088	2025	481	
3	720	12	1.483	4.123	0.484	9.637	418.031	4.6	23.4	30.77037227	2971.450233	1532	330	
4	820	12	0.222	4.709	0.175	10.249	54.385	23.4	24.9	33.06679194	619.811721	444	94	
5	920	12	0.191	2.835	0.123	5.899	49.017	22.3	14.3	34.60262878	566.770172	410	91	
6	1020	12	0.213	1.101	0.080	2.85	57.885	6.1	6.9	27.76078815	532.978024	388	106	
7	1120	12	0.259	1.211	0.088	2.908	70.893	4.1	7.1	29.94393779	562.137851	407	137	
8	1220	12	0.362	1.764	0.102	2.779	101.796	7.9	6.8	45.84901753	3017.707941	1548	274	
9	1400	12	0.378	3.824	0.140	5.33	103.936	12.4	13.0	51.91055065	1829.606142	1084	116	
			Cumulative				%39Ar	rIsd =	100.0			Total gas age	934	91
note: isotope beams in mV, rIsd = released, error in age includes J error, all errors 1 sigma											Plateau age		415	103
(36Ar through 40Ar are measured beam intensities, corrected for decay for the age calculations)											(steps 4-7)			
											Isochron age		428	40
											(steps 4-7)			
4 amu discrimination = 1.0648 ± 0.96%, 40/39K = 0.0002 ± 150.0%, 36/37Ca = 0.000257 ± 8.59%, 39/37Ca = 0.00066 ± 13.80%														

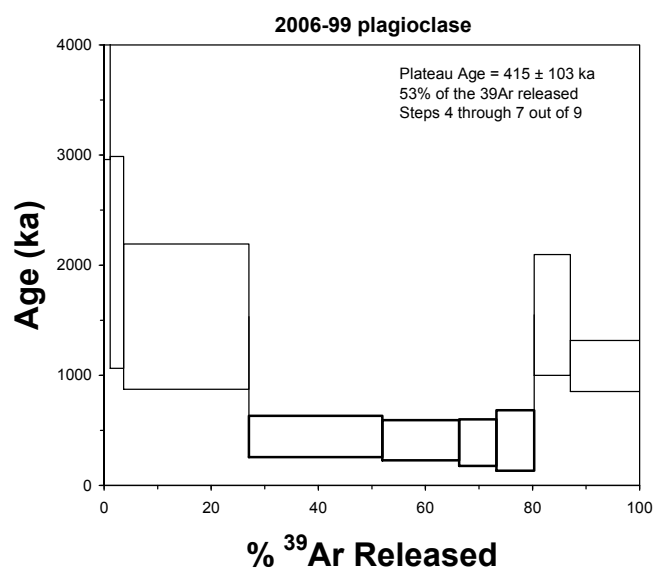


Figure 4.1 Plateau age of the sample 2006 99.

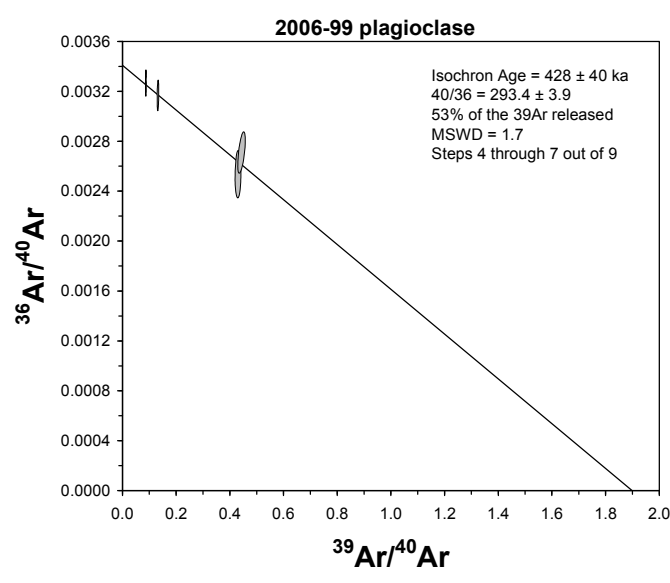


Figure 4.2 Isochron age of the sample 2006 99.

Table 4.3 Ar-Ar results of the sample 2006 3.

step	T (C)	t (min.)	% 39Ar							Age			
			36Ar	37Ar	38Ar	39Ar	40Ar	%40Ar*	rlsd	Ca/K	40Ar*/39ArK	(ka)	1s.d.
1	600	12	50.3	2.595	14.619	384.44	13681.13	-2.0	27.1	0.489554033	-613.782847	-574	-278
2	650	12	17.438	2.563	6.214	214.447	4986.23	3.1	15.1	0.866896973	859.193893	583	181
3	700	12	11.393	3.523	4.675	182.147	3311.52	4.8	12.9	1.403124736	1082.422392	708	142
4	750	12	5.158	4.966	3.274	173.397	1510.54	6.1	12.2	2.078044604	599.867574	426	68
5	800	12	1.436	3.599	1.572	100.036	444.004	10.8	7.1	2.610848149	520.369120	375	35
6	870	12	1.274	4.090	1.455	93.637	366.171	6.3	6.6	3.170308797	252.917046	192	32
7	970	12	1.986	3.984	1.576	91.725	573.045	5.6	6.5	3.152500331	375.230125	278	48
8	1130	12	3.467	5.419	2.053	106.457	983.437	3.5	7.5	3.695183618	347.703474	259	74
9	1400	12	3.011	15.659	1.536	69.949	835.212	4.3	4.9	16.30951915	566.860522	405	99
						Cumulative	%39Ar	rlsd =	100.0	Total gas age		172	38
note: isotope beams in mV, rlsd = released, error in age includes J error, all errors 1 sigma										Plateau age		405	60
(36Ar through 40Ar are measured beam intensities, corrected for decay for the age calculations)										(steps 2-5)			
										Isochron age		387	47
										(steps 2-5)			
4 amu discrimination = 1.0648 ± 0.96%, 40/39K = 0.0002 ± 150.0%, 36/37Ca = 0.000257 ± 8.59%, 39/37Ca = 0.00066 ± 13.80%													

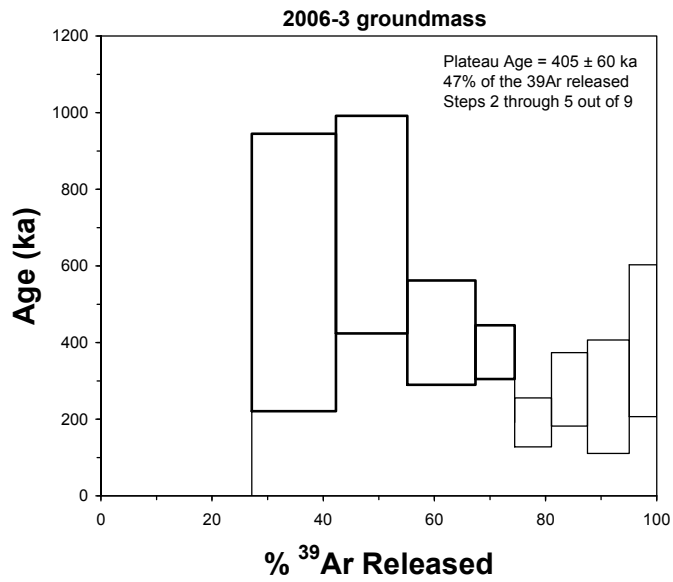


Figure 4.3 Plateau age of the sample 2006 3.

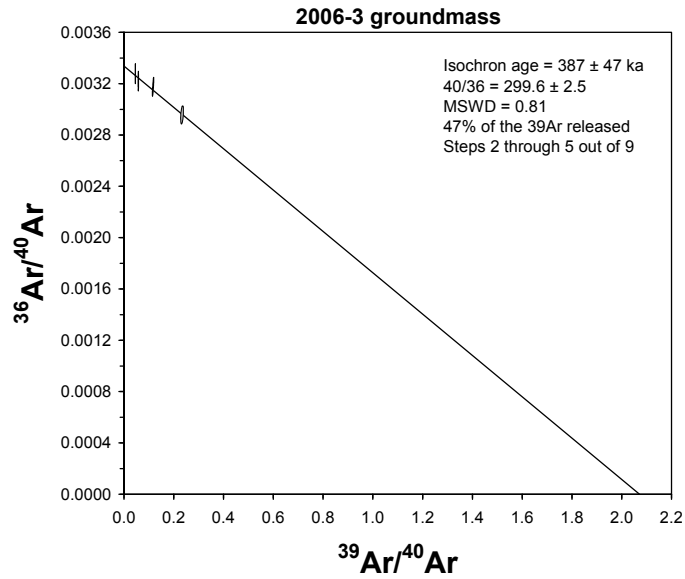


Figure 4.4 Isochron age of the sample 2006 3.

2007-22 Groundmass

This sample produced a generally concordant age spectrum, with slightly older ages in the initial ~20% gas released, followed by ages which overlap at ~300 ka (Table 4.4). The overall form of the age spectrum is distinctly U-shaped, suggesting that excess argon is present. The total gas age for this sample is 430 ± 36 ka. Steps 7-14 (78% of the total gas released) define a younger plateau age of 313 ± 37 ka (Figure 4.5). All steps, 100% of the gas released, define an isochron, which gives an age of 225 ± 29 ka (Figure 4.6), and indicates that a small amount of excess argon is present (initial $^{40}\text{Ar}/^{36}\text{Ar} = 304 \pm 2$). The isochron verifies excess argon, as suggested by the form of the age spectrum. Thus, both the total gas and plateau ages are anomalously old, and the isochron age is accurate and the most reliable.

2007-24 Groundmass

This sample produced a generally concordant age spectrum, with the exception of younger ages in the later gas released (last 4 steps). Individual step ages have large uncertainties due to the young age and low radiogenic yields (Table 4.5). The total gas age for this sample is 159 ± 23 ka. Steps 1-10 (89% of the total gas released) define a slightly older plateau age of 195 ± 26 ka (Figure 4.7), although at the 2σ uncertainty level these ages overlap. Steps 1-10 also define an isochron, which yields an age of 219 ± 41 ka (Figure 4.8) and does not indicate that excess argon is present, with initial $^{40}\text{Ar}/^{36}\text{Ar}$ indistinguishable from the atmospheric ratio. Note that all these ages overlap at 2σ uncertainty, due to the young age of the sample, and the resulting relatively large uncertainties. Thus, in this case one could effectively use any of these calculated ages. However, if a valid isochron is obtained it is generally considered the most reliable.

Table 4.4 Ar-Ar results of the sample 2007 22.

step	t		% 39Ar							Age				
	T (C)	(min.)	36Ar	37Ar	38Ar	39Ar	40Ar	%40Ar*	rlsd	Ca/K	40Ar*/39ArK	(ka)	1s.d.	
1	500	12	4.985	0.306	1.416	31.577	1439.22	2.9	3.1	1.095955261	1773.496130	1037	475	
2	530	12	3.679	0.338	1.140	29.426	1056.2	2.4	2.9	1.299131305	1039.660645	677	375	
3	560	12	3.261	0.442	1.061	31.062	926.805	1.5	3.1	1.609530086	478.083658	343	310	
4	590	12	2.984	0.654	1.106	36.248	869.296	1.2	3.6	2.041050235	1194.173898	759	252	
5	620	12	3.261	0.930	1.251	45.192	962.758	4.1	4.5	2.328183154	1485.193459	904	223	
6	650	12	2.245	1.008	1.055	47.512	662.171	5.5	4.7	2.400280266	916.748609	609	144	
7	690	12	1.987	1.065	1.137	56.918	585.446	5.8	5.7	2.116749176	648.428488	451	105	
8	730	12	1.393	0.899	1.054	58.435	421.299	8.3	5.8	1.740240094	637.075884	444	72	
9	770	12	0.773	0.678	0.877	53.501	237.888	10.8	5.3	1.433349478	464.343218	334	42	
10	820	12	0.999	0.999	1.296	83.008	308.585	11.0	8.3	1.361196577	408.569418	297	36	
11	880	12	1.345	1.428	1.727	107.37	406.017	8.7	10.7	1.504313638	329.195524	243	38	
12	970	12	2.749	2.365	2.643	157.418	819.29	7.0	15.7	1.699394443	384.803041	281	54	
13	1100	12	4.175	3.706	3.113	168.939	1247.13	7.2	16.8	2.481934977	588.917716	414	77	
14	1400	12	3.407	17.201	1.977	97.236	940.866	5.1	9.7	20.1155533	536.860527	381	109	
			Cumulative				%39Ar	rlsd =	100.0		Total gas age		430	36
note: isotope beams in mV, rlsd = released, error in age includes J error, all errors 1 sigma										Plateau age =		(steps 7-14)	313	37
(36Ar through 40Ar are measured beam intensities, corrected for decay for the age calculations)										Isochron age		(steps 1-14)	225	29
4 amu discrimination = 1.0525 ± 1.33%, 40/39K = 0.0002 ± 150.0%, 36/37Ca = 0.000257 ± 8.59%, 39/37Ca = 0.00066 ± 13.80%														

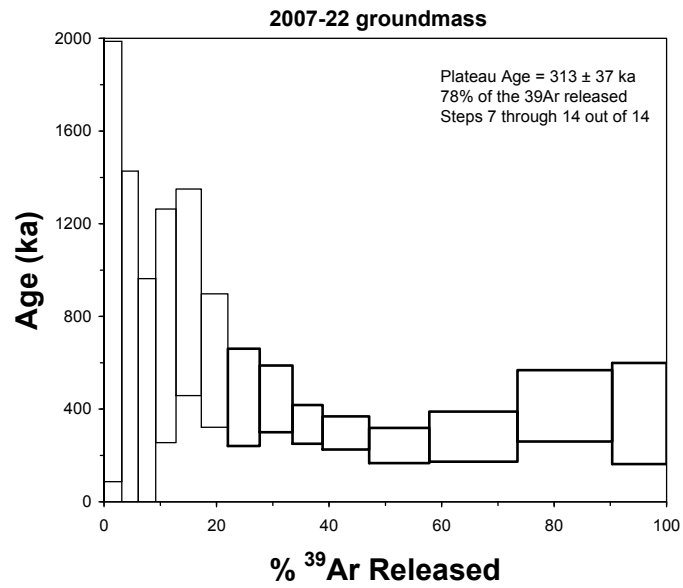


Figure 4.5 Plateau age of the sample 2007 22.

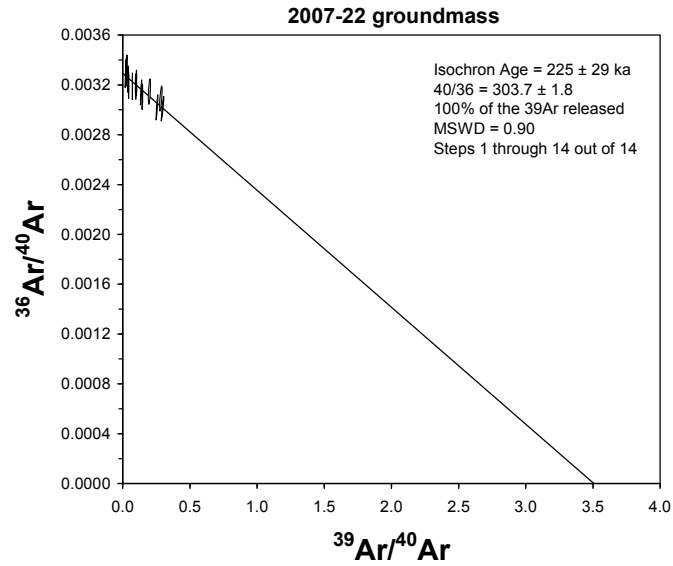


Figure 4.6 Isochron age of the sample 2007 22.

Table 4.5 Ar-Ar results of the sample 2007 24.

step	T (C)	t (min.)	36Ar	37Ar	38Ar	39Ar	40Ar	%40Ar*	r1sd	Ca/K	40Ar*/39ArK	Age (ka)	1s.d.
1	500	12	2.36	0.654	1.902	109.415	685.116	3.9	15.2	0.688557113	248.040609	180	62
2	530	12	1.83	0.616	1.520	87.052	521.571	2.2	12.1	0.815186205	127.824158	95	59
3	560	12	1.590	0.670	1.376	79.531	460.03	3.9	11.0	0.970538076	223.542073	163	57
4	590	12	1.451	0.790	1.302	75.783	415.973	3.2	10.5	1.201042108	169.608254	125	54
5	620	12	1.352	1.027	1.287	76.862	396.409	5.8	10.7	1.539585714	299.211553	215	49
6	650	12	1.049	1.115	1.047	63.317	305.698	5.8	8.8	2.029367285	271.309895	196	46
7	690	12	0.859	1.497	0.931	58.365	250.053	6.9	8.1	2.956588604	280.089220	202	40
8	730	12	0.550	1.648	0.681	42.491	163.22	10.5	5.9	4.472708416	358.921243	255	34
9	770	12	0.340	1.672	0.453	28.211	98.422	12.1	3.9	6.839472384	318.472178	228	31
10	820	12	0.280	1.859	0.390	23.158	77.499	10.4	3.2	9.270120212	227.848586	166	30
11	880	12	0.247	1.598	0.277	16.013	65.881	4.6	2.2	11.53166721	107.191231	80	36
12	970	12	0.255	1.432	0.284	14.915	66.769	-0.0	2.1	11.0931098	-1.310039	-1	-47
13	1100	12	0.297	2.613	0.454	19.804	74.971	1.9	2.7	15.26292406	43.641186	33	50
14	1400	12	0.407	3.909	0.560	26.143	102.138	1.4	3.6	17.30673009	34.317141	26	47
						Cumulative	%39Ar	r1sd =	100.0	Total gas age		159	23
										Plateau age			
note: isotope beams in mV, r1sd = released, error in age includes J error, all errors 1 sigma										=	(steps 1-10)	195	26
(36Ar through 40Ar are measured beam intensities, corrected for decay for the age calculations)													
										Isochron age	(steps 1-10)	219	41
4 amu discrimination = 1.0525 ± 1.33%, 40/39K = 0.0002 ± 150.0%, 36/37Ca = 0.000257 ± 8.59%, 39/37Ca = 0.00066 ± 13.80%													

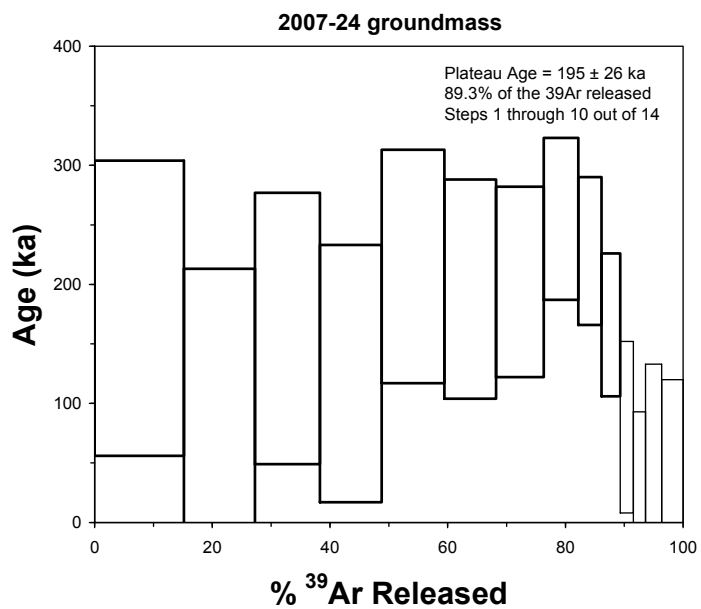


Figure 4.7 Plateau age of the sample 2007 24.

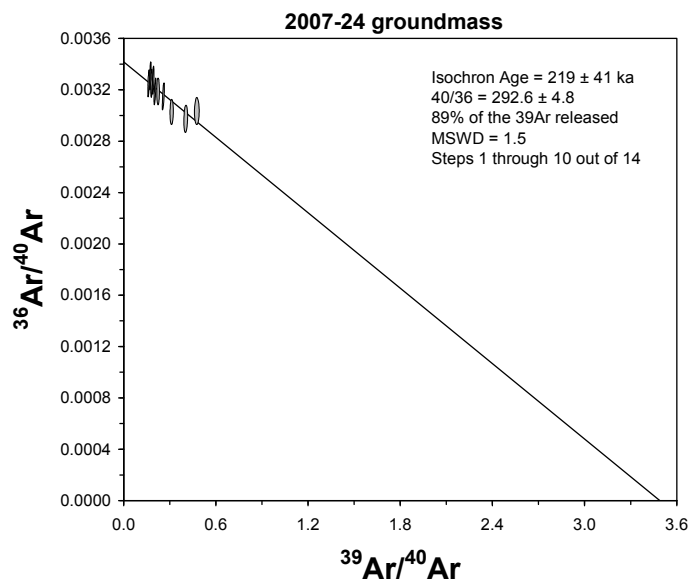


Figure 4.8 Isochron age of the sample 2007 24.

2006-116 Groundmass

This sample produced results very similar to those of 2007-22 described above, and interpretations are identical. The age spectrum is generally concordant, with slightly older ages in the initial ~20% gas released, followed by ages which overlap at ~160 ka. The overall form of the age spectrum is distinctly U-shaped, again suggesting that excess argon is present. The total gas age for this sample is 205 ± 10 ka (Table 4.6). Steps 5-14 (77% of the total gas released) define a younger plateau age of 162 ± 11 ka (Figure 4.9). Steps 2-14, 94% of the gas released, define an isochron, which gives an age of 132 ± 11 ka (Figure 4.10), and indicates that a small amount of excess argon is present (initial $^{40}\text{Ar}/^{36}\text{Ar} = 306 \pm 3$). The isochron thus verifies excess argon, as suggested by the form of the age spectrum. Thus, both the total gas and plateau ages are anomalously old, and the isochron age is accurate and the most reliable.

Table 4.6 Ar-Ar results of the sample 2006 116.

step	T (C)	t		% 39Ar						Age			
		(min.)	36Ar	37Ar	38Ar	39Ar	40Ar	%40Ar*	rIsd	Ca/K	40Ar*/39ArK	(ka)	1s.d.
1	500	12	1.878	0.298	1.106	51.24	533.419	1.6	6.0	0.647961981	159.948987	120	104
2	530	12	1.072	0.283	0.805	41.377	322.159	12.1	4.9	0.762050992	1053.379620	674	76
3	560	12	0.940	0.350	0.816	44.715	281.442	7.7	5.3	0.872137825	486.978238	343	62
4	590	12	0.845	0.464	0.883	52.499	252.636	8.0	6.2	0.984807393	369.460825	266	45
5	620	12	0.770	0.628	1.064	66.048	229.564	8.2	7.8	1.059482107	265.456612	195	32
6	650	12	0.596	0.687	1.045	70.586	181.391	11.3	8.3	1.084513439	262.585778	193	23
7	690	12	0.498	0.884	1.200	85.802	154.962	15.1	10.1	1.148046666	236.890996	175	16
8	730	12	0.368	0.879	1.168	85.212	118.393	21.2	10.0	1.149457663	238.311768	176	12
9	770	12	0.290	0.779	0.988	72.582	93.622	22.1	8.5	1.195966967	204.429655	152	10
10	820	12	0.320	0.870	1.024	71.617	101.303	19.1	8.4	1.353734323	201.626438	150	12
11	880	12	0.339	0.671	0.741	50.441	103.932	13.8	5.9	1.4824675	215.673647	160	18
12	970	12	0.490	0.629	0.629	50.399	143.656	6.8	5.9	1.390796712	161.327098	121	26
13	1100	12	0.775	1.359	0.786	45.452	222.474	4.8	5.3	3.333829396	212.857973	158	45
14	1400	12	0.880	5.203	1.029	61.599	244.685	7.0	7.3	9.434436523	251.134219	185	42
				Cumulative		%39Ar	rIsd =	100.0			Total gas age =	205	10
note: isotope beams in mV, rIsd = released, error in age includes J error, all errors 1 sigma										Plateau age =	(steps 5-14)	162	11
(36Ar through 40Ar are measured beam intensities, corrected for decay for the age calculations)										Isochron age =	(steps 2-14)	132	11
4 amu discrimination = 1.0525 ± 1.33%, 40/39K = 0.0002 ± 150.0%, 36/37Ca = 0.000257 ± 8.59%, 39/37Ca = 0.00066 ± 13.80%													

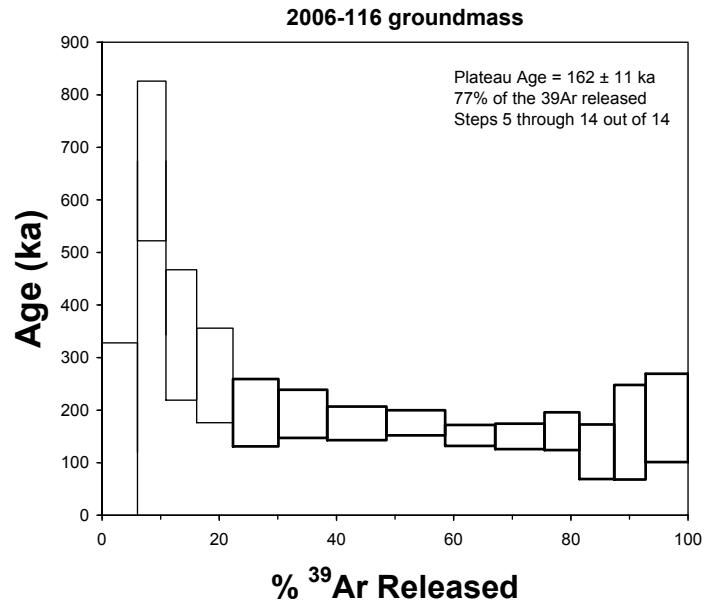


Figure 4.9 Plateau age of the sample 2006 116.

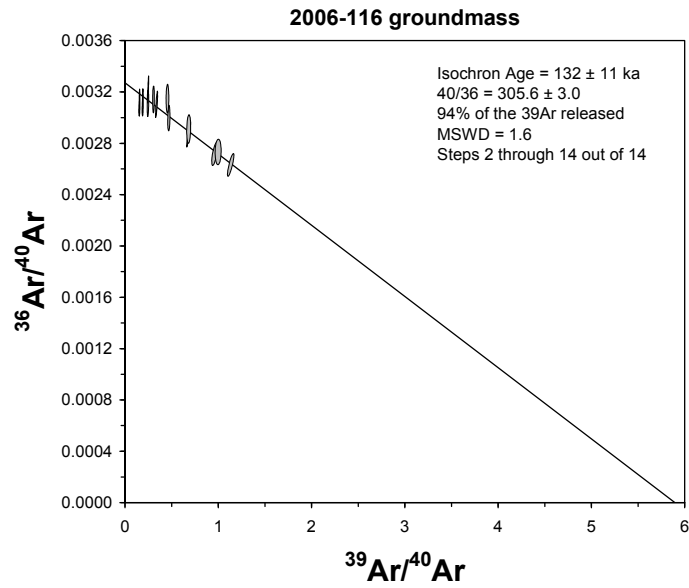


Figure 4.10 Isochron age of the sample 2006 116.

4.3 Trachyandesitic Lava Flows (5)

Only one age is obtained from trachyandesitic lava flows.

2006-8 Groundmass

This sample produced a generally concordant age spectrum, with the exception of older ages in the final 7 steps (Table 4.7). Note that this sample, as for 2006-3 above, also yields large amounts of non-radiogenic argon (high ^{36}Ar measurements) and a large amount of gas released in the initial, low temperature step (high % ^{39}Ar released). This suggests some alteration of the fine grained groundmass minerals. For this sample, the total gas age is 424 ± 23 ka, and steps 1-9 (96% of the total gas released) define a plateau age of 381 ± 56 ka (Figure 4.11). Steps 1-11 (98% of the total gas released) define an isochron age of 150 ± 110 ka (Figure 4.12), and importantly, indicate excess argon is present (initial $^{40}\text{Ar}/^{36}\text{Ar} = 304.5 \pm 3.7$). This isochron defines the initial argon composition well, but the age relatively poorly, due to the low radiogenic yields and the resultant clustering of the data near the y-axis. Since excess argon is clearly identified, the apparent ages from the age spectrum should be considered to be anomalously old. Despite the low precision, the isochron age is the most accurate and should be used for this sample.

Table 4.7 Ar-Ar results of the sample 2006 8.

step	T (C)	t	36Ar	37Ar	38Ar	39Ar	40Ar	%40Ar*	% 39Ar	Ca/K	40Ar*/39ArK	Age	1s.d.
1	550	12	41.135	1.188	14.520	500.755	11637.79	2.0	29.5	0.173147638	507.899144	359	177
2	580	12	9.256	0.509	4.182	177.92	2637.32	2.7	10.5	0.208796339	437.037624	313	113
3	610	12	8.745	0.686	4.187	180.905	2532.45	4.3	10.6	0.276765456	689.839186	472	108
4	640	12	7.345	0.938	3.646	163.909	2112.09	3.6	9.6	0.417691787	521.975942	368	99
5	680	12	7.217	1.108	3.610	162.187	2103.02	4.9	9.5	0.498642976	743.466668	504	99
6	720	12	5.721	1.766	3.546	180.182	1668.49	5.2	10.6	0.71543848	532.973217	375	70
7	760	12	3.539	1.878	2.450	130.989	1031.38	5.3	7.7	1.046634448	455.349402	325	59
8	810	12	2.619	2.150	1.763	92.909	761.203	5.3	5.5	1.689643338	472.242535	336	61
9	860	12	1.907	1.588	0.922	42.316	554.498	5.4	2.5	2.740887323	811.852618	544	101
10	920	12	1.516	1.106	0.590	20.936	443.521	6.0	1.2	3.859632904	1629.366946	964	155
11	980	12	1.087	0.863	0.398	12.983	312.292	4.3	0.8	4.85785523	1235.903904	774	173
12	1040	12	0.807	0.862	0.303	9.956	237.224	7.0	0.6	6.330155765	2229.484859	1220	169
13	1100	12	0.764	0.719	0.246	6.035	222.062	5.8	0.4	8.716464881	3121.911147	1544	289
14	1160	12	0.875	0.952	0.248	5.322	255.995	6.4	0.3	13.10375912	5762.175752	2259	35
15	1220	12	0.583	0.727	0.172	4.092	167.741	4.9	0.2	13.01432069	2769.747391	1423	317
16	1400	12	1.382	1.249	0.394	8.829	412.342	7.7	0.5	10.3548381	7922.611860	2687	358
						Cumulative	%39Ar	rlsd =	100.0		Total gas age	424	42
											Plateau age	381	56
											(steps 1-9)		
											Isochron age	150	110
											(steps 1-11)		
4 amu discrimination = 1.0648 ± 0.96%, 40/39K = 0.0002 ± 150.0%, 36/37Ca = 0.000257 ± 8.59%, 39/37Ca = 0.00066 ± 13.80%													

73

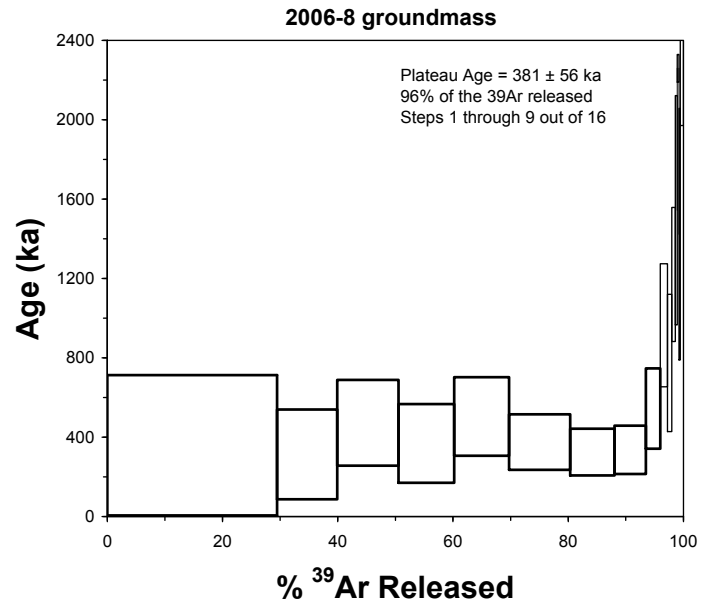


Figure 4.11 Plateau age of the sample 2006 8.

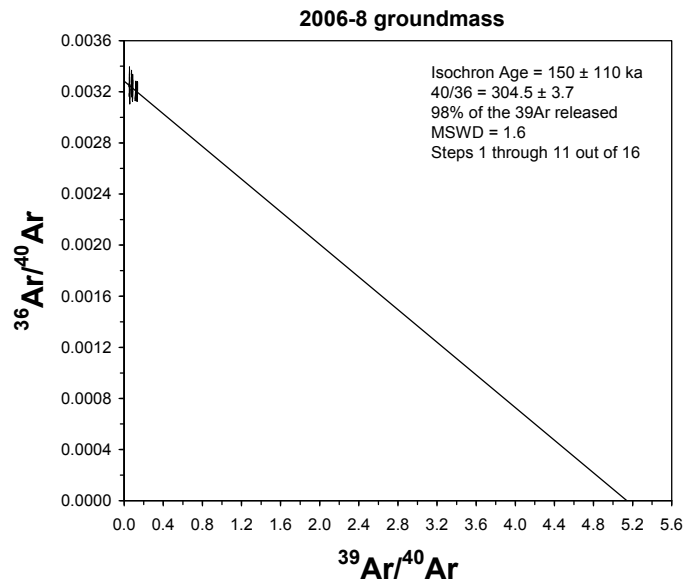


Figure 4.12 Isochron age of the sample 2006 8.

4.4 Trachytic lava flow (9)

Sample 2006 59 is represents the trachytic lava flow at the western flanks of the volcano.

2006-59 Plagioclase

This sample produced a very discordant age spectrum, with ages which vary in an unsystematic way between ~4 Ma and 0.1 Ma. The total gas age is 1.17 ± 0.09 Ma, and these data do not define a plateau or isochron age. The radiogenic yields are quite low, likely due to the combination of young age and low K-contents. The ^{36}Ar measurements are moderately high, which may indicate some alteration. Feldspars, due to their anhydrous nature, typically contain low amounts of non-radiogenic argon, and thus low ^{36}Ar . The discordance of the age spectrum could simply be due to the low radiogenic yields, and difficulty in measuring any radiogenic argon, or alternatively, it could indicate the presence of excess argon. The most conservative approach is to assume excess argon is present, and thus the youngest age on the age spectrum (step 7, 120 ka) is a maximum age for the sample (Table 4.8).

4.5 Dacitic and Rhyolitic Domes (10)

Two Ar-Ar ages are obtained from dacitic and rhyolitic domes, one of which is from Keftar Dağı dacitic dome (Sample 2006 110) and the other (Sample 2007 5) is from rhyolitic dome at the summit of the volcano.

2006-110 Amphibole

This sample produced a discordant age spectrum, with high initial step ages, followed by decreasing ages, and then increasing ages with the final steps (Table 4.9). The form of the age spectrum is U-shaped,

which suggests the presence of excess argon. The total gas age is 1.41 ± 0.08 Ma. There is no plateau age for this sample. Steps 3-7 (62% of the total gas released) define an isochron age of 110 ± 30 ka (Figure 4.13), and indicate excess argon is present (initial $^{40}\text{Ar}/^{36}\text{Ar} = 310.4 \pm 1.5$). The ages from the age spectrum should thus be considered to be too old, and the isochron age should be considered the most reliable for this sample.

2007-5 Biotite

This sample produced a generally discordant age spectrum, with older ages in the initial steps, ages decreasing to a plateau segment, and older and younger ages in the final steps (Table 4.10). The discordance and older initial ages may be an indication of excess argon. The total gas age is 310 ± 12 ka. Steps 9-11 (58% of the total gas released) define a younger plateau age of 122 ± 19 ka (Figure 4.14). Steps 1-12 (98% of the total gas released) define an isochron age of 64 ± 14 ka (Figure 4.15), and do indicate that a small amount of excess argon is present (initial $^{40}\text{Ar}/^{36}\text{Ar} = 306 \pm 2$, greater than the atmospheric value of 295.5). Note that for young samples such as this, which have low radiogenic yields ($\%^{40}\text{Ar}^*$), even a small amount of excess argon has a significant effect on the ages. Thus, the total gas and plateau ages are anomalously old, and the isochron age is accurate, as it effectively takes into account the excess argon when calculating an age. The isochron age is the most reliable for this sample.

Table 4.8 Ar-Ar results of the sample 2006 59.

step	T (C)	t (min.)								% 39Ar		Age	
			36Ar	37Ar	38Ar	39Ar	40Ar	%40Ar*	rlsd	Ca/K	40Ar*/39ArK	(Ma)	1s.d.
1	600	12	5.993	0.118	1.338	15.302	1697.14	2.2	6.6	0.583165415	2.428845	1.98	0.92
2	675	12	2.128	0.126	0.564	11.219	604.138	2.8	4.9	0.849390733	1.452332	1.19	0.41
3	750	12	1.455	0.155	0.410	10.725	417.466	4.2	4.7	1.093089898	1.531956	1.25	0.29
4	800	12	1.860	0.452	0.588	17.917	522.633	2.0	7.8	1.908517746	0.549717	0.45	0.22
5	820	12	7.759	1.048	1.818	23.39	2262.53	5.1	10.1	3.391085539	4.960966	4.05	0.77
6	840	12	1.808	1.913	0.707	26.359	518.64	4.6	11.4	5.496113923	0.869325	0.71	0.16
7	865	12	1.352	2.238	0.561	21.98	371.945	0.9	9.5	7.715750509	0.148128	0.12	0.13
8	890	12	1.175	2.533	0.468	19.321	329.362	3.5	8.4	9.940952149	0.550941	0.45	0.13
9	920	12	1.195	2.731	0.451	17.694	339.879	4.9	7.7	11.70948487	0.852180	0.70	0.15
10	960	12	1.152	2.736	0.435	16.27	326.443	4.6	7.1	12.76148747	0.833811	0.68	0.15
11	1010	12	1.589	2.118	0.455	12.026	459.738	5.7	5.2	13.36757919	2.034267	1.66	0.29
12	1060	12	1.038	1.457	0.298	7.86	297.051	4.8	3.4	14.07254109	1.609133	1.31	0.29
13	1110	12	0.966	1.107	0.252	5.794	280.748	6.1	2.5	14.50636141	2.606551	2.13	0.35
14	1160	12	0.431	0.932	0.153	4.828	121.294	4.0	2.1	14.65739386	0.710127	0.58	0.17
15	1240	12	0.371	0.969	0.135	4.716	106.778	8.0	2.0	15.60542945	1.208577	0.99	0.17
16	1400	12	1.001	3.097	0.390	15.102	279.519	3.3	6.6	15.57502351	0.515432	0.42	0.13
Cumulative							%39Ar	rlsd =	100.0	Total gas age		1.17	0.09
note: isotope beams in mV, rlsd = released, error in age includes J error, all errors 1 sigma										No plateau			
(36Ar through 40Ar are measured beam intensities, corrected for decay for the age calculations)										No isochron			
4 amu discrimination = 1.0648 ± 0.96%, 40/39K = 0.0002 ± 150.0%, 36/37Ca = 0.000257 ± 8.59%, 39/37Ca = 0.00066 ± 13.80%													

Table 4.9 Ar-Ar results of the sample 2006 110.

step	T (C)	t (min.)								% 39Ar		Age		
			36Ar	37Ar	38Ar	39Ar	40Ar	%40Ar*	rIsd	Ca/K	40Ar*/39ArK	(Ma)	1s.d.	
1	750	12	25.333	0.424	5.876	76.644	7201.37	3.1	31.1	0.442137604	2.993936	2.42	0.64	
2	790	12	3.008	0.151	0.794	15.099	886.203	6.7	6.1	0.79936114	3.914237	3.16	0.37	
3	850	12	1.817	0.151	0.465	9.087	518.561	3.7	3.7	1.328423661	2.069056	1.67	0.37	
4	950	12	1.521	0.272	0.381	7.318	441.585	5.4	3.0	2.972771168	3.229557	2.61	0.28	
5	1050	12	2.227	3.156	0.791	19.782	644.172	6.2	8.0	12.79597015	1.999644	1.61	0.22	
6	1150	12	1.739	22.375	2.354	110.206	457.9	8.3	44.8	16.3004333	0.339343	0.27	0.05	
7	1220	12	0.685	3.021	0.266	6.341	191.02	5.6	2.6	38.49270527	1.600563	1.29	0.24	
8	1400	12	0.420	1.530	0.109	1.668	123.209	11.1	0.7	74.87598168	7.217782	5.82	0.62	
											Total gas			
Cumulative									%39Ar	rIsd =	100.0	age =	1.41	0.08
note: isotope beams in mV, rIsd = released, error in age includes J error, all errors 1 sigma											No plateau			
											110			
(36Ar through 40Ar are measured beam intensities, corrected for decay for the age calculations)											Isochron age	(ka)	30	
											(steps 3-7)			
4 amu discrimination = 1.0729 ± 0.78%, 40/39K = 0.0002 ± 150.0%, 36/37Ca = 0.000257 ± 8.59%, 39/37Ca = 0.00066 ± 13.80%														

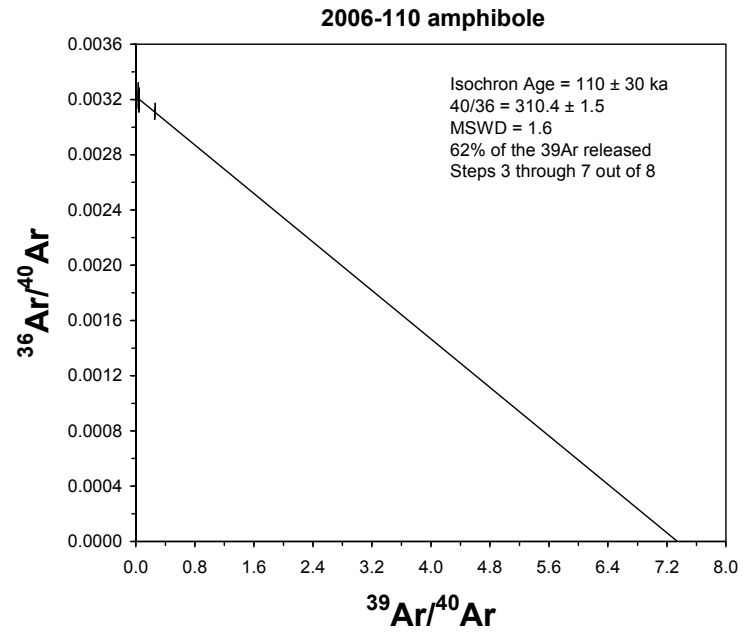


Figure 4.13 Isochron age of the sample 2006 110.

Table 4.10 Ar-Ar results of the sample 2007 5.

step	T (C)	t (min.)								% 39Ar		Age		
			36Ar	37Ar	38Ar	39Ar	40Ar	%40Ar*	rlsd	Ca/K	40Ar*/39ArK	(ka)	1s.d.	
1	550	12	16.769	0.077	3.710	34.733	4847.87	2.9	2.3	0.27157315	11235.27588	3229	1498	
2	580	12	3.279	0.040	0.766	9.62	939.625	2.2	0.6	0.50939299	3365.723522	1649	1027	
3	650	12	7.624	0.051	1.751	20.611	2221.7	3.7	1.4	0.3031192	10917.60289	3186	1144	
4	725	12	5.253	0.055	1.486	34.931	1507.45	2.2	2.3	0.19287692	1187.556644	764	458	
5	790	12	1.67	0.057	0.960	46.988	486.718	3.7	3.1	0.14859732	395.699233	292	105	
6	850	12	2.210	0.069	1.475	75.7	650.109	4.6	5.0	0.11165333	417.807407	307	89	
7	905	12	2.363	0.072	2.108	118.136	701.372	5.6	7.8	0.07465589	343.383600	256	61	
8	960	12	4.638	0.111	3.458	183.507	1382.24	5.9	12.1	0.07409419	482.212508	350	79	
9	1015	12	2.114	0.223	4.277	277.01	637.169	7.2	18.3	0.09861121	164.263707	127	24	
10	1050	12	1.839	0.261	5.483	367.779	566.528	9.4	24.3	0.08692986	142.926866	111	16	
11	1085	12	1.051	0.338	3.375	227.896	330.536	12.0	15.1	0.18168003	165.603553	128	14	
12	1125	12	0.374	0.294	1.161	77.92	111.101	8.0	5.2	0.46223258	83.921673	66	11	
13	1170	12	0.173	0.417	0.348	22.07	52.237	22.2	1.5	2.31593737	212.969137	163	12	
14	1220	12	0.170	0.169	0.112	5.718	48.898	5.7	0.4	3.62408629	173.658245	134	34	
15	1400	12	0.273	0.173	0.188	10.048	80.691	6.7	0.7	2.11025019	307.662650	231	57	
			Cumulative				%39Ar	rlsd =	100.0			Total gas age	310	12
note: isotope beams in mV, rlsd = released, error in age includes J error, all errors 1 sigma											Plateau age		122	19
(36Ar through 40Ar are measured beam intensities, corrected for decay for the age calculations)											(steps 9-11)			
											Isochron age		64	14
											(steps 1-12)			
4 amu discrimination = 1.0525 ± 1.33%, 40/39K = 0.0002 ± 150.0%, 36/37Ca = 0.000257 ± 8.59%, 39/37Ca = 0.00066 ± 13.80%														

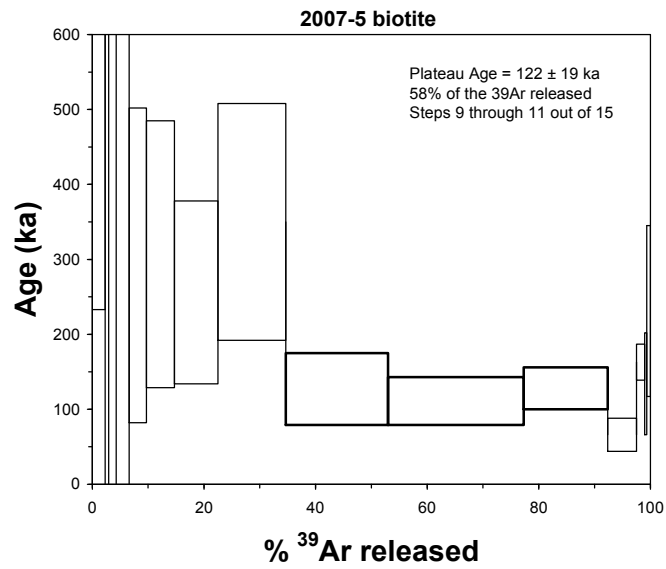


Figure 4.14 Plateau age of the sample 2007 5.

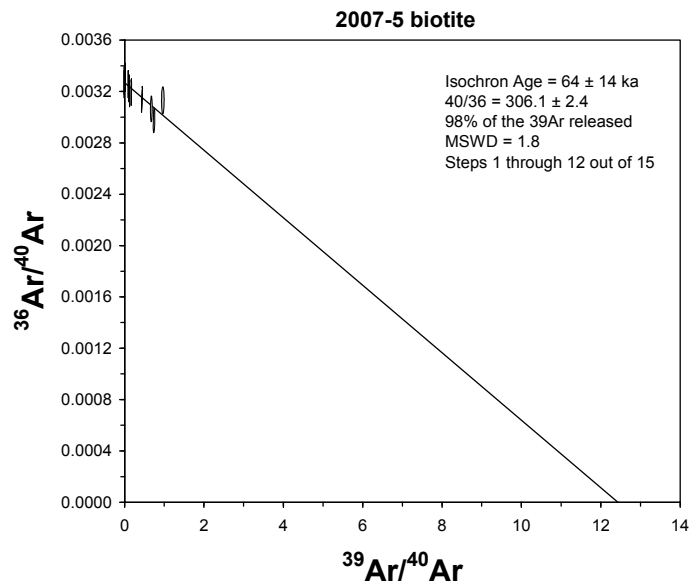


Figure 4.15 Isochron age of the sample 2007 5.

CHAPTER 5

MINERALOGY AND PETROGRAPHY

For the determination of the mineralogical and petrographical features, a total of 140 thin-sections are examined under polarizing microscope. All samples are typically crystal-rich and porphyritic with hyalopilitic groundmass, although only the basaltic sample and the some of the enclaves are entirely crystalline. Most of the phenocrysts contain glass and microcrystal inclusions, and display zoned and reaction rimmed textures.

The groundmass is dark brown to black in mafic (basalt, basaltic trachyandesites), light brown in intermediate (trachyandesites, trachytes) and colourless in felsic rocks (trachytes, dacites, rhyolites) displaying vesicular, microlitic, intersertal, sub-ophitic, seriate, glomeroporphyritic, poikilitic, hyalopilitic, vitrophyric and trachytic textures. Apatite and zircons are found as secondary minerals. Iddingsitization of olivines, and opacitization of the amphiboles and pyroxenes are the major alterations observed in some of the lavas.

The distribution of the minerals in different rock groups is shown in Figure 5.1. Olivine phenocrysts are common in basaltic, basaltic trachyandesitic, and trachyandesitic rocks. Orthopyroxenes are found in almost all rocks from basaltic trachyandesites to rhyolites. Clinopyroxenes are observed in basalts, basaltic trachyandesites, trachyandesites, trachytes and dacites. Amphibole is the common

mineral phase in dacites and also found in trachytes and rhyolites. Biotite occurs as the main mineral phase of the rhyolites and is also found in dacites. Quartz is found as embayed phenocrysts in rhyolitic obsidians and rhyolites. Fe-Ti oxides are present in all of the Süphan lavas.

Given below are the mineralogical-petrographical features of the lava flows/domes. Italic numbers in parenthesis represent the stratigraphic position of the lavas in geological map (Figure 3.1) and stratigraphic columnar section (Figure 3.2).

	Ox	Ol	Plag	Cpx	Opx	Amp	Bio	KF	Q
Basalt	—		—	—					
Bas.Trac and	—		—	—	—				
Trachyand	—	---	—	—	—				
Trachyte	—		—	—	—	---			
Dacite	—		—	---	—	---	---		
Rhyolite	—		—		---	---	—		

Figure 5.1 The distribution of the minerals in different rock groups of the Süphan Volcano.

5.1 Basalt (2)

Regarding the basaltic lava flow, there is only a single exposure at the northern part of the volcano between Erkeçli and Özdemir villages (Sample No: 2006 99). This rock contains euhedral and subhedral mm-sized *plagioclase + clinopyroxene + olivine* phenocrysts in a holocrystalline groundmass consisting of plagioclase, clinopyroxene, olivine and Fe-Ti oxide microcrysts. Pyroxene and plagioclase minerals display typically glomeroporphyritic and subophitic textures (Figure 5.2a).

Plagioclase crystals are subhedral, anhedral and embayed, and contain clinopyroxene and olivine inclusions. Some of them show well developed oscillatory zoning.

Clinopyroxene phenocrysts are subhedral and rounded. They show simple twinning and internal cracks, and may form aggregates of microphenocrysts.

Basaltic lavas are the units having the highest amount of olivine crystals among all the other units in the Suphan volcanics. They are euhedral, subhedral and rounded phenocrysts and are partly or completely converted to iddingsite (Figure 5.2b).

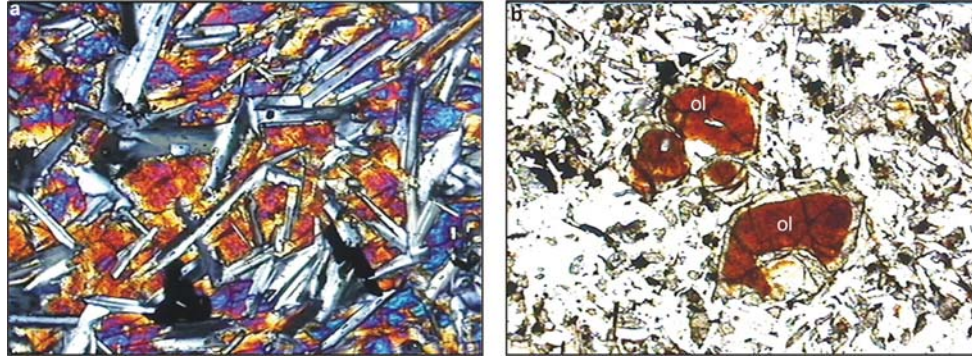


Figure 5.2 a) Subophitic texture in basalt (10xXPL), **b)** Iddingsitized olivine phenocrysts (4xPPL).

5.2 Basaltic-Trachyandesitic lava flows (3,4)

Basaltic trachyandesitic lavas consist of *plagioclase + olivine + clinopyroxene ± orthopyroxene* phenocrysts. The groundmass of these rocks contain plagioclase, pyroxene, olivine and opaque microlites and groundmass glass. These lavas are characterized by glomeroporphyritic, intersertal, ophitic, poikilitic, hypocrystalline and vesicular textures.

Plagioclase phenocrysts observed in these rocks are unzoned or have slight oscillatory zoning, and display patchy and sieve texture. The unzoned or slightly zoned plagioclases (Figure 5.3a) range up to 1 cm in size. Plagioclases with sieve textured rims have small melt inclusions (Figure 5.3b). Patchy textured crystals have an irregular corroded core with abundant large melt and mineral inclusions (pyroxene and Fe-Ti oxides). The amount of olivine is less than that in basalts. Some olivines are replaced by clinopyroxene and iddingsitized either totally (Figure 5.3c) or along their rims. Orthopyroxenes are rare and replaced or rimmed by clinopyroxenes (Figure 5.3d). Olivines, orthopyroxenes and

clinopyroxenes all have melt inclusions. Accessory apatite is found as inclusions in plagioclases.

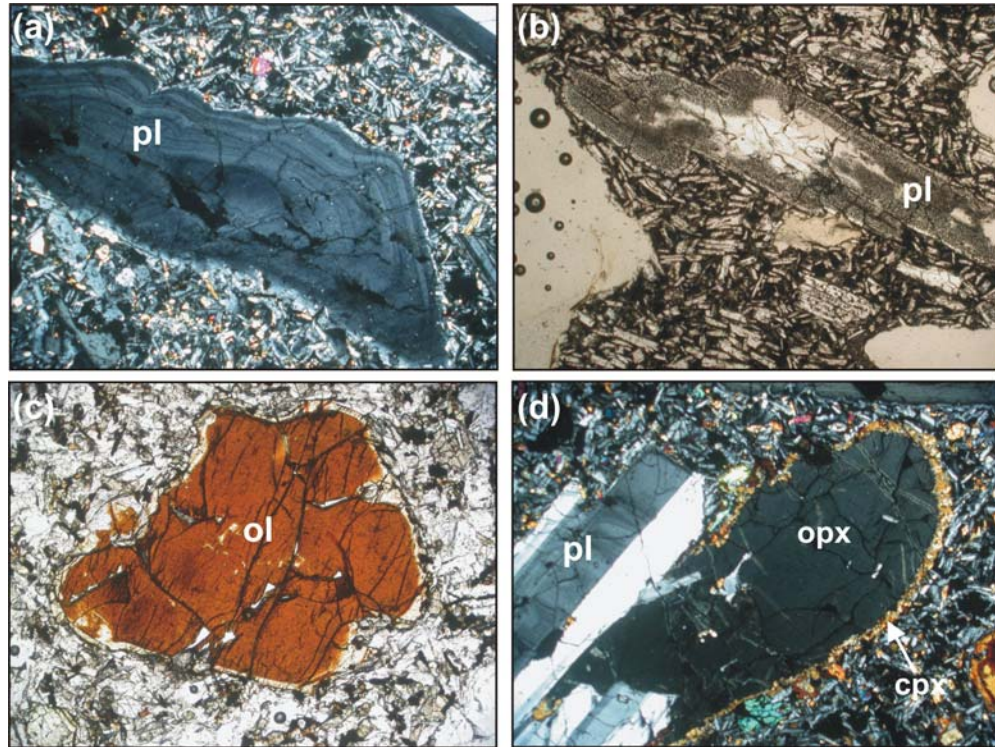


Figure 5.3 Petrographic features of basaltic trachyandesites a) Oscillatory zoned plagioclase in basaltic trachyandesites (4xXPL), b) Sieve textured plagioclase in basaltic trachyandesites (4xPPL), c) Iddingsitized olivine phenocryst in basaltic trachyandesites (10xPPL), d) An orthopyroxene phenocryst rimmed by clinopyroxene (4xXPL). cpx: clinopyroxene, pl: plagioclase, ol: olivine, opx: orthopyroxene.

5.3 Trachyandesitic lava flows (4, 5)

Trachyandesitic lavas consist of *plagioclase + clinopyroxene + orthopyroxene* (4) and *plagioclase + olivine + clinopyroxene + orthopyroxene* (5) paragenesis, with a groundmass of plagioclase,

pyroxene, opaque microlites and glass. These lavas include crystal clots which are made of orthopyroxene, clinopyroxene plagioclase and opaque minerals (Figure 5.4). Most plagioclases, clinopyroxenes, orthopyroxenes and olivines contain melt inclusions. Trachyandesitic lava flows are characterized by trachytic, intersertal, glomeroporphyritic, poikilitic, seriate and microlitic textures.

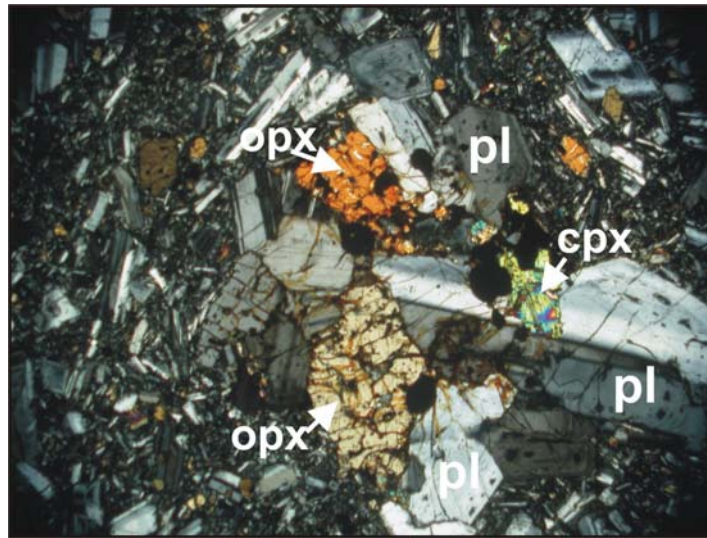


Figure 5.4 A crystal clot from trachyandesitic lava flows, includes; orthopyroxene, clinopyroxene, plagioclase and Fe-Ti oxides. cpx: clinopyroxene, pl: plagioclase, opx: orthopyroxene (4xXPL).

Plagioclases are the most abundant mineral phase in these lavas and appear as large and small subhedral phenocrysts. They contain abundant inclusions of glass and clinopyroxene and rarely accessory apatite (Figure 5.5a). Some of large crystals have sieve texture, patchy textures and corroded rims.

Subhedral clinopyroxenes generally show simple twinning. They contain apatite, opaque mineral and melt inclusions and are sometimes corroded along their rims.

The amount of the orthopyroxenes increases in trachyandesites relative to the basalts and basaltic trachyandesites. Subhedral and euhedral orthopyroxene phenocrysts are the most common mafic minerals in these lava flows. Melt inclusions are very common (Figure 5.5b). Some of them are mantled by clinopyroxenes along their rims (Figure 5.5c).

Olivine phenocrysts are commonly subhedral, sometimes euhedral, and are rarely found in trachyandesitic lavas. Their irregular cracks are typical and show alteration to iddingsite (Figure 5.5d).

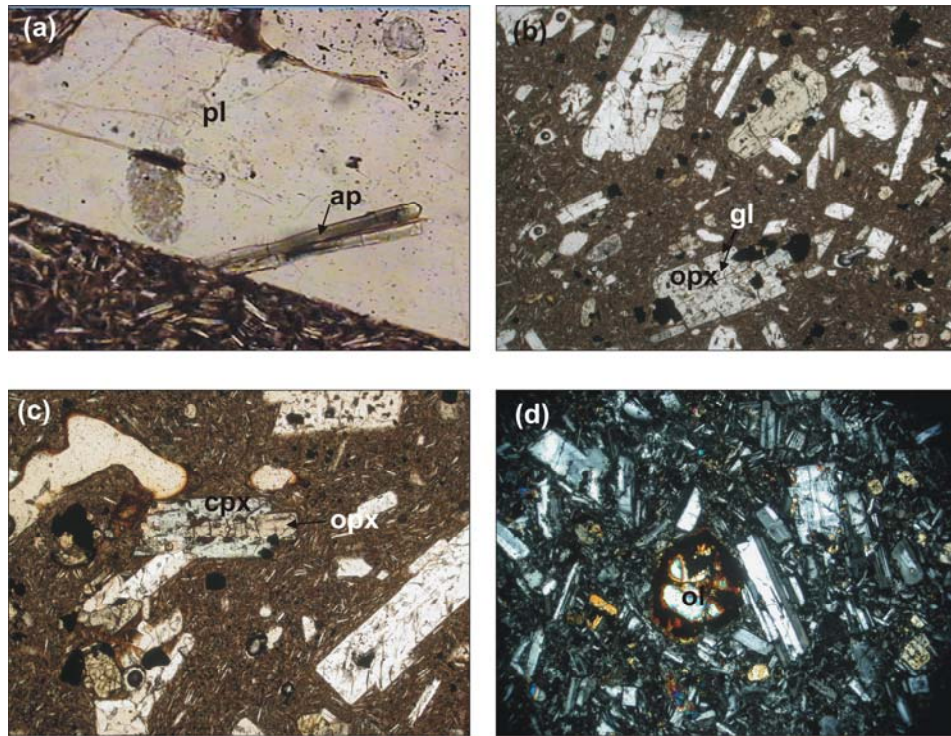


Figure 5.5 Petrographic features of trachyandesites, a) apatite inclusions in plagioclase (10xPPL), b) glass inclusions in orthopyroxene (4xPPL), c) an orthopyroxene phenocryst mantled by clinopyroxene (4xPPL), d) an opacitized olivine phenocryst (4xXPL). ap: apatite, cpx: clinopyroxene, gl: glass, pl: plagioclase, ol: olivine, opx: orthopyroxene.

5.4 Trachytic Lava Flows (7,8,9)

Three different trachytic lava flows exposed at the southern (7), eastern (8), and western (9) parts of the volcano display different mineralogical and petrographical properties. The lavas at the southern and western parts have amphibole phenocrysts, however trachytes at the eastern parts are lacking these minerals. Lavas at the western flanks display microcrystalline texture.

Trachytic lava flows have 2 different mineral paragenesis, including, *Plagioclase + clinopyroxene + orthopyroxene + Fe-Ti oxide (8)* and *plagioclase + clinopyroxene + orthopyroxene + amphibole + Fe-Ti oxide (7,9)* minerals. The groundmass of the lavas consists of plagioclase, clinopyroxene, amphibole, Fe-Ti oxides and glass. These lavas are characterized by vesicular, intersertal and trachytic textures. Most of the phenocryst phases have melt inclusions. Crystal clots of plagioclase, clinopyroxene, orthopyroxene and Fe-Ti oxides are common.

Plagioclases are the most abundant mineral phase in these lavas and appear as large and small subhedral phenocrysts. They contain abundant inclusions of glass, clinopyroxene and rarely accessory zircon (Figure 5.6a). Some of the large crystals have sieve texture and corroded rims. Plagioclase phenocrysts together with clinopyroxene and opaque oxides occur as crystal clots in some lavas. Subhedral clinopyroxenes display simple twinning and sometimes opacitized along their rims. They contain glass, apatite and opaque inclusions. Orthopyroxene is more abundant than clinopyroxene, some of which are opacitized along their rims and mantled by clinopyroxenes.

Trachytes mark the first occurrence of amphiboles, which are characteristically reddish and completely replaced or rimmed by Fe-Ti oxides (Figure 5.6b).

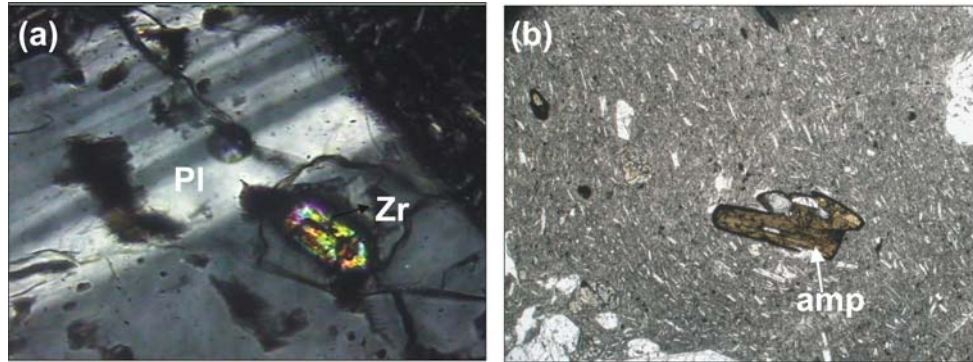


Figure 5.6 a) Zircon inclusions in plagioclase (10xXPL), b) amphibole phenocryst replaced by Fe-Ti oxides along their rims (4xPPL). amp: amphibole, pl: plagioclase, zr: zircon.

5.5 Dacitic Rocks (10)

Dacitic rocks occur as domes only. They consist of *plagioclase* ± *clinopyroxene* + *orthopyroxene* + *amphibole* ± *biotite* + *Fe-Ti oxides* and clear glass. They contain lesser amounts of clinopyroxene in comparison with those of the mafic and intermediate lavas: amphibole is the most abundant mafic mineral. Most phenocrysts have melt inclusions. Plagioclases have sieve texture. Orthopyroxenes are found as euhedral and subhedral phenocrysts (Figure 5.7a). Biotites are rarely found (Figure 5.7b) and partly or completely replaced by Fe-Ti oxides. Zircon and the apatite are found as accessory phases.

The groundmass varies between glassy and fine grained and is composed of plagioclase, clinopyroxene, amphibole micrograins and glass. Seriate and poikilitic textures are common in dacitic lavas.

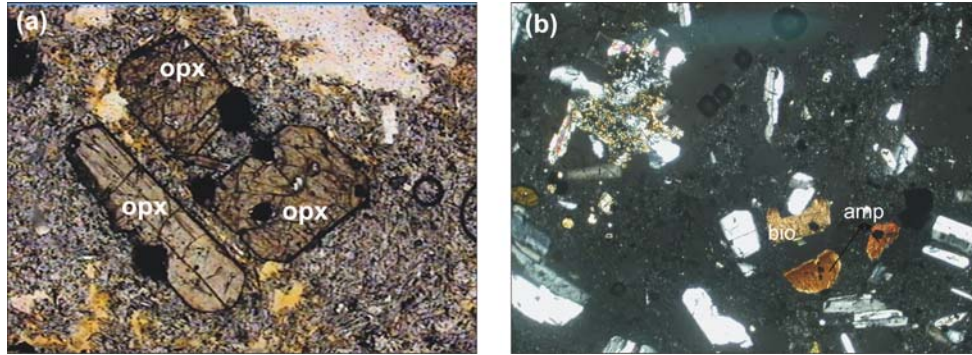


Figure 5.7 a) Euhedral and subhedral orthopyroxenes in dacitic rocks (4xPPL), b) biotite and amphibole phenocrysts in dacitic lavas (4xXPL). amp: amphibole, bio: biotite, opx: orthopyroxene.

5.6 Rhyolitic Rocks (1,10,6)

Rhyolitic rocks are characterized by obsidian flows, rhyolitic domes, blocks of ash and block flow and pyroclastic pumice falls. Rhyolitic lavas are mainly composed of *plagioclase* ± *orthopyroxene* ± *amphibole* + *biotite* + *quartz* + *K-feldspar* + *Fe-Ti oxides*. The groundmass of the lavas consists of feldspar, biotites and glass. Plagioclase phenocrysts are subhedral, anhedral, cracked, embayed and have clinopyroxene and biotite inclusions. Sanidine phenocrysts are subhedral and show Carlsbad twinning (Figure 5.8a), whereas quartz phenocrysts are anhedral, rounded and fragmented (Figure 5.8b). Orthopyroxenes are rare and found only in the older rhyolitic obsidian flows. Amphiboles are partly opacitized along their rims. Biotite phenocrysts are common minerals, especially in rhyolitic domes. They are elongated, blade shaped (Figure 5.8c) and subhedral, and are chloritized from their rims. Obsidian lava flows and domes have perlitic (Figure 5.8d), holohyaline and flow textures (Figure 5.8e), whereas rhyolitic domes mainly have seriate texture. Zircon and apatites are found as accessory phases.

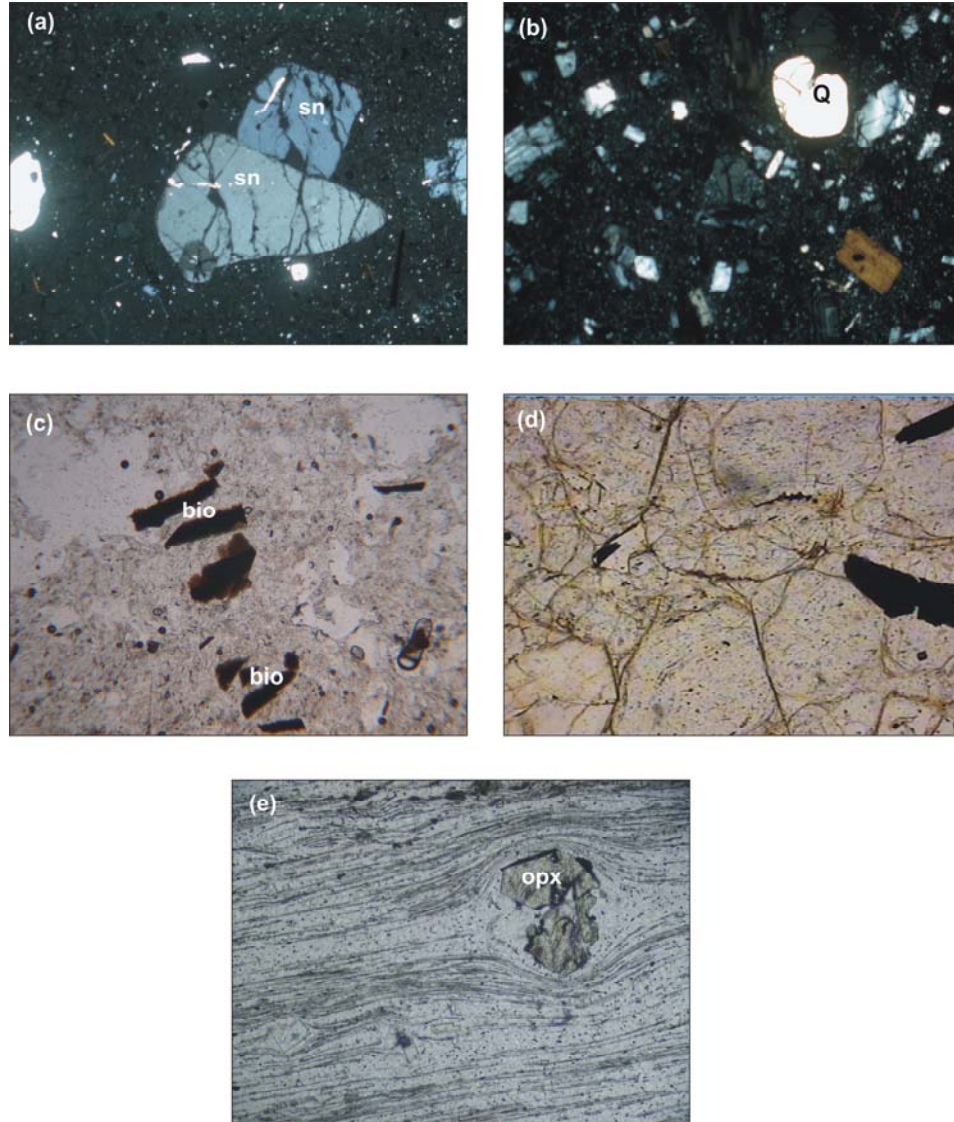


Figure 5.8 Petrographic features of rhyolitic rocks. a) sanidine phenocrysts (4xXPL), b) rounded quartz mineral (4xXPL), c) blade shaped biotites (4xPPL), d) perlitic texture in obsidian flows, e) flow texture in obsidian flows(4xXPL).

5.7 Enclaves

Enclaves from the Suphan Stratovolcano are collected from dacitic - rhyolitic domes and trachytic lava flows. They are coarse and fine grained gabbros, dolerites and microdiorites. Their contact with their host rocks are commonly sharp.

Coarse and fine grained gabbros consist of *plagioclase* + *orthopyroxene* + *amphibole* minerals, whereas dolerites and microdiorites include *plagioclase* + *orthopyroxene* + *clinopyroxene* + *amphibole* .

Coarse and fine grained gabbros and dolerites have holocrystalline texture, but microdiorites contain glass in their groundmass.

CHAPTER 6

GEOCHEMISTRY

Based on the petrographic studies, a total of 67 of the freshest samples (including 58 lava samples, 2 pyroclastic samples and 7 enclave samples) were selected for major and trace element analysis, 22 samples for Rb-Sr, 21 samples Nd-Sm and 18 samples for Pb isotopic analysis. Whole rock major element compositions were determined by ICP-Emission Spectrometry following a lithium metaborate/ tetraborate fusion and dilute nitric acid digestion at ACME (Canada) analytical laboratories. Trace element contents were determined in the same laboratory by ICP Mass Spectrometry following a lithium metaborate/tetraborate fusion and nitric acid digestion. Isotopic analyses were performed at the laboratories of Earth and Ocean Sciences of University of British Columbia (PCIGR) by using Thermal Ionization Mass Spectrometer (TIMS).

6.1 Major Element Geochemistry

A total of 60 samples were analyzed for their whole rock compositions (Table 6.1, sample locations and corresponding units in volcanostratigraphic columnar section are given in Appendix A). The major element compositions of the volcanics are recalculated on an anhydrous base before they are plotted on various digrams. Volcanic products of Süphan Stratovolcano cover a broad compositional spectrum from basalt to rhyolite, with SiO₂ ranging from 51.5 to 74.8 wt% (anhydrous).

Table 6.1 Major and trace element contents of Süphan volcanics.

Sample	2006 99	2006 112	2006 114	2006 76	2006 1	2006 130	2007 23	2005 61
Rock Type	Basalt	Basaltic Trachyandesite						
SiO ₂ (%)	51.47	52.09	54.13	54.70	54.97	54.33	54.22	54.89
TiO ₂	1.92	2.02	2.13	1.89	1.96	2.28	2.09	1.97
Al ₂ O ₃	17.44	16.95	15.96	16.64	17.01	15.93	16.15	16.32
Fe ₂ O ₃	10.98	9.97	11.17	10.37	9.98	11.12	11.01	10.03
MgO	7.15	4.42	3.01	3.53	3.39	2.94	3.10	3.17
CaO	9.19	7.47	6.34	6.46	6.07	6.30	6.21	6.29
Na ₂ O	4.01	4.35	3.86	4.09	4.00	3.76	3.80	3.76
K ₂ O	0.90	1.67	2.17	1.87	2.00	2.12	2.15	2.35
P ₂ O ₅	0.36	0.44	0.41	0.39	0.36	0.44	0.39	0.36
MnO	0.17	0.14	0.18	0.17	0.17	0.18	0.17	0.17
LOI	0.00	0.20	0.40	-0.10	0.10	0.60	0.40	0.60
Total	103.63	99.75	99.75	100.01	100.01	100.00	99.69	99.91
CIPW Norm								
Quartz	-	-	4.52	3.78	4.69	5.73	4.90	5.17
Orthoclase	5.18	9.99	13.02	11.13	11.92	12.71	12.91	14.09
Albite	32.88	37.27	33.15	34.85	34.13	32.28	32.66	32.28
Anorthite	26.23	22.07	20.12	21.67	22.75	20.63	20.98	21.02
Nepheline	0.09	-	-	-	-	-	-	-
Diopside	12.95	10.23	7.57	6.63	4.33	6.79	6.40	6.83
Hypersthene	-	7.43	12.62	13.81	14.09	12.52	13.32	12.43
Olivine	15.94	4.59	-	-	-	-	-	-
Magnetite	2.37	3.51	3.94	3.63	3.50	3.92	3.88	3.53
Ilmenite	3.55	3.88	4.11	3.61	3.76	4.39	4.03	3.80
Apatite	0.81	1.04	0.96	0.91	0.84	1.03	0.92	0.85
Mg#	60.35	53.59	41.25	47.00	46.94	40.78	42.32	45.16
Sr (ppm)	355.70	342.30	272.60	296.90	269.20	272.20	274.20	263.60
Rb	19.40	41.00	65.40	58.10	58.60	63.70	63.40	58.70
Ba	150.00	272.00	389.00	333.80	312.10	419.10	404.00	355.40
Ni	59.50	34.80	4.30	5.40	5.10	4.70	4.10	3.90
Sc	29.00	21.00	24.00	21.00	22.00	22.00	23.00	22.00
Co	42.30	32.10	28.10	36.10	31.40	31.60	31.40	31.80
Cs	0.10	0.50	2.10	2.00	1.90	2.00	2.00	2.00
Ga	18.20	19.30	21.60	20.80	20.40	22.70	22.50	20.40
Th	2.60	6.00	9.00	9.30	9.40	10.00	9.90	9.70
Ta	0.60	0.90	1.20	1.20	1.10	1.20	1.20	1.10
Nb	9.30	15.70	17.60	15.50	14.80	17.50	17.90	15.10
U	0.80	1.70	2.60	2.40	2.50	2.60	2.50	2.30
Zr	191.70	268.80	309.10	293.10	274.20	315.30	302.20	263.70
Hf	4.80	6.40	7.70	7.50	6.90	8.10	7.40	6.80
Y	32.80	38.30	48.50	45.30	42.30	48.90	43.90	41.70
Ce	36.10	58.20	71.60	68.50	64.40	74.60	69.60	65.10
Nd	22.90	33.20	41.20	35.40	32.00	37.70	38.20	31.70
Sm	5.18	6.73	8.62	7.90	7.40	8.90	8.07	7.40
Eu	1.62	1.91	2.29	2.05	1.88	2.22	2.34	1.80
Gd	5.73	6.95	8.77	8.02	7.49	8.41	8.26	7.11
Tb	0.98	1.19	1.48	1.51	1.35	1.66	1.43	1.35
Dy	5.53	6.69	8.22	8.08	7.30	8.60	8.52	7.33
Ho	1.23	1.40	1.74	1.50	1.54	1.61	1.69	1.49
Er	3.42	3.94	4.91	4.78	4.60	5.12	4.85	4.37
Tm	0.51	0.59	0.75	0.70	0.66	0.75	0.73	0.64
Pr	5.11	7.75	9.40	8.93	8.11	9.61	9.50	8.17
Yb	3.15	3.48	4.61	4.08	3.89	4.65	4.47	3.82
La	16.20	27.40	33.00	29.50	29.10	33.30	34.30	29.50
Lu	0.47	0.53	0.67	0.65	0.62	0.69	0.67	0.57
Pb	1.2	2.1	1	0.8	0.7	1	0.9	1

Table 6.1 Continued

Sample	2005 62	2005 68	2006 79	2006 86	2006 89	2006 95	2006 102	2006 118
Rock Type	Trachyandesite							
SiO2 (%)	52.38	54.31	58.90	58.86	57.23	58.62	60.41	58.32
TiO2	2.08	2.35	1.15	1.68	1.74	1.19	1.04	1.59
Al2O3	17.28	15.77	16.33	15.81	15.08	15.76	15.98	16.26
Fe2O3	9.24	11.27	6.77	8.30	8.62	7.32	8.25	8.34
MgO	3.95	3.05	2.88	2.36	2.37	2.41	1.58	2.49
CaO	7.98	6.22	6.05	4.99	5.97	5.73	4.34	5.43
Na2O	4.23	3.99	3.88	4.54	4.24	4.33	4.59	4.37
K2O	1.61	2.07	2.36	2.44	2.45	2.51	2.84	2.01
P2O5	0.43	0.41	0.23	0.28	0.28	0.30	0.50	0.28
MnO	0.13	0.18	0.12	0.13	0.13	0.13	0.15	0.13
LOI	0.60	0.30	1.10	0.40	1.70	1.50	0.10	0.60
Total	99.91	99.92	99.73	99.81	99.80	99.81	99.80	99.82
CIPW Norm								
Quartz	-	4.68	10.18	8.78	7.93	8.69	10.39	9.44
Orthoclase	9.65	12.39	14.21	14.60	14.85	15.18	16.94	12.04
Albite	36.30	34.19	33.45	38.89	36.81	37.48	39.20	37.50
Anorthite	23.74	19.24	20.55	15.75	15.27	16.53	14.75	19.08
Nepheline	-	-	-	-	-	-	-	-
Diopside	11.08	7.71	6.95	6.16	10.96	8.73	3.12	5.28
Hyperstene	10.21	12.35	9.49	8.71	6.73	7.52	9.24	9.69
Olivine	0.76	-	-	-	-	-	-	-
Magnetite	3.25	3.96	2.40	3.22	3.39	2.87	3.20	3.24
Ilmenite	4.01	4.52	2.23	3.23	3.39	2.31	1.99	3.06
Apatite	1.01	0.96	0.55	0.66	0.67	0.70	1.16	0.66
Mg#	52.69	41.35	52.56	43.37	42.55	47.00	34.04	44.58
Sr (ppm)	375.20	257.00	260.70	219.80	225.60	232.10	212.60	239.20
Rb	41.30	61.20	63.40	80.30	77.10	69.90	92.80	55.30
Ba	291.30	368.50	307.00	308.00	293.00	315.00	456.00	311.00
Ni	31.50	4.80	4.70	4.70	5.00	4.20	1.20	1.80
Sc	19.00	23.00	15.00	17.00	17.00	17.00	17.00	16.00
Co	34.10	32.00	22.70	25.10	25.40	16.70	13.10	22.00
Cs	1.20	2.00	2.20	2.80	2.80	2.80	2.10	2.20
Ga	20.60	21.90	18.20	19.70	19.70	18.60	22.10	18.80
Th	6.30	10.40	8.00	8.40	8.30	9.40	12.10	7.30
Ta	1.00	1.20	0.80	0.80	0.70	0.90	1.20	0.80
Nb	15.90	17.70	10.90	9.50	9.30	11.70	18.60	9.60
U	1.70	2.50	2.70	3.40	3.40	3.00	3.40	2.80
Zr	265.80	302.90	215.40	303.80	299.50	278.30	357.70	228.30
Hf	6.50	7.50	5.50	7.60	7.50	6.80	9.40	5.90
Y	38.40	45.90	31.60	45.80	44.00	41.90	55.90	36.00
Ce	59.10	69.40	43.80	49.30	49.30	54.90	82.20	43.90
Nd	30.10	37.50	23.60	30.50	30.20	30.70	47.30	25.50
Sm	6.20	8.10	5.27	6.88	6.77	6.71	10.09	5.88
Eu	1.82	2.19	1.40	1.85	1.80	1.77	2.52	1.62
Gd	6.79	8.31	5.38	7.48	7.27	7.01	10.22	6.14
Tb	1.21	1.49	0.94	1.27	1.26	1.23	1.71	1.07
Dy	6.65	8.09	5.33	7.45	7.21	7.27	9.59	6.15
Ho	1.31	1.65	1.15	1.63	1.59	1.53	2.07	1.30
Er	3.97	4.78	3.40	4.64	4.67	4.50	5.66	3.78
Tm	0.56	0.68	0.50	0.71	0.70	0.68	0.88	0.56
Pr	7.46	8.79	5.64	6.73	6.65	7.17	10.74	5.82
Yb	3.29	4.20	3.13	4.45	4.32	4.16	5.42	3.55
La	27.40	31.50	20.80	22.00	21.30	24.80	36.90	20.30
Lu	0.50	0.66	0.47	0.67	0.65	0.64	0.81	0.52
Pb	1.8	0.8	0.4	0.4	0.4	1.1	1.3	0.6

Table 6.1 Continued

Sample	2006 131	2007 19A	2005 59	2006 6	2006 72	2006 74	2006 77	2006 81
Rock Type								
SiO2 (%)	56.94	55.75	58.52	60.31	57.64	57.65	60.44	58.94
TiO2	1.70	1.82	1.17	1.29	1.54	1.30	0.99	1.52
Al2O3	16.13	15.90	16.12	16.53	16.42	16.18	16.09	16.17
Fe2O3	8.89	9.83	8.92	7.18	8.40	9.73	8.36	8.35
MgO	2.67	2.79	1.91	2.40	2.36	1.96	1.37	2.36
CaO	5.99	5.44	4.70	5.11	5.34	5.12	4.47	5.31
Na2O	4.28	4.64	4.38	4.45	4.16	3.88	4.26	4.20
K2O	1.89	2.30	2.68	2.19	2.20	2.84	3.06	2.23
P2O5	0.29	0.69	0.61	0.26	0.39	0.51	0.46	0.28
MnO	0.14	0.16	0.16	0.12	0.14	0.16	0.14	0.13
LOI	0.90	0.40	0.30	0.10	1.30	0.70	0.40	0.40
Total	99.78	99.71	99.47	99.94	99.89	100.03	100.04	99.89
CIPW Norm								
Quartz	7.94	4.37	9.05	11.01	9.52	9.12	11.31	10.49
Orthoclase	11.36	13.79	16.07	13.03	13.27	17.02	18.26	13.33
Albite	36.85	39.82	37.62	37.92	35.93	33.29	36.40	35.95
Anorthite	19.56	15.99	16.66	18.79	20.04	18.61	15.90	18.89
Nepheline	-	-	-	-	-	-	-	-
Diopside	7.22	5.65	2.49	4.14	3.65	3.17	2.94	4.88
Hyperstene	9.62	11.43	10.94	9.26	10.40	11.31	8.98	9.64
Olivine	-	-	-	-	-	-	-	-
Magnetite	3.47	3.83	3.47	2.77	3.29	3.79	3.24	3.24
Ilmenite	3.29	3.51	2.26	2.47	2.99	2.50	1.90	2.92
Apatite	0.69	1.62	1.43	0.61	0.92	1.20	1.08	0.66
Mg#	44.72	43.33	36.59	47.39	43.08	35.19	30.64	43.23
Sr (ppm)	250.40	282.50	230.50	230.10	270.60	258.90	245.50	242.30
Rb	53.60	70.80	80.30	64.90	56.20	85.00	100.90	61.90
Ba	297.00	376.00	419.70	319.60	422.30	515.00	547.90	336.70
Ni	2.50	3.60	0.90	3.60	3.30	1.70	0.80	1.70
Sc	17.00	18.00	15.00	16.00	15.00	18.00	15.00	15.00
Co	23.20	23.70	22.50	23.90	24.50	27.00	20.30	26.40
Cs	2.10	2.10	2.70	1.60	2.20	3.00	3.40	2.40
Ga	19.60	22.60	22.30	17.80	21.30	23.90	23.70	19.30
Th	8.20	10.70	10.50	8.10	7.90	12.50	13.40	7.60
Ta	0.80	1.20	1.50	0.90	1.00	1.50	1.50	0.90
Nb	10.10	19.50	17.50	9.20	11.90	19.80	20.10	10.30
U	2.70	3.30	3.30	2.70	3.10	3.10	3.90	2.70
Zr	238.50	416.90	341.40	236.10	283.30	355.80	395.40	256.10
Hf	5.90	10.00	9.00	6.20	7.60	9.40	10.10	7.00
Y	38.10	57.40	54.10	34.10	50.90	53.30	58.90	39.30
Ce	44.20	83.70	77.70	47.40	56.60	91.60	96.30	49.30
Nd	25.60	49.40	42.60	24.40	33.10	47.40	49.30	25.70
Sm	5.85	10.43	9.40	5.40	7.60	9.70	10.50	6.20
Eu	1.68	2.83	2.44	1.44	1.95	2.44	2.40	1.71
Gd	6.38	11.41	9.47	5.80	8.20	9.51	9.70	6.33
Tb	1.14	1.90	1.73	1.06	1.56	1.89	1.87	1.26
Dy	6.43	10.85	9.57	5.97	8.24	9.84	9.88	6.56
Ho	1.34	2.15	1.89	1.25	1.60	1.75	1.80	1.21
Er	3.89	6.17	5.34	3.68	5.30	5.85	5.81	4.01
Tm	0.59	0.93	0.80	0.52	0.86	0.86	0.87	0.62
Pr	5.96	11.73	9.97	5.88	7.93	11.66	12.10	6.37
Yb	3.65	5.89	4.76	3.32	4.63	4.86	4.93	3.69
La	19.50	39.80	34.50	21.00	27.00	40.80	42.80	21.50
Lu	0.55	0.88	0.76	0.53	0.76	0.76	0.76	0.57
Pb	1.1	0.9	0.3	1.4	1.9	1	1	0.7

Table 6.1 Continued

Sample	2006 105	2005 60	2006 8	2005 10	2005 25	2005 38	2005 51	2005 55
Rock Type	Trachyte							
SiO2 (%)	60.63	61.31	61.49	62.77	63.80	63.45	62.48	66.94
TiO2	0.97	1.15	0.86	0.92	0.86	0.89	1.02	0.66
Al2O3	15.95	15.79	15.80	15.56	16.06	15.91	15.71	15.58
Fe2O3	7.96	7.20	8.15	6.16	5.42	5.65	6.42	4.27
MgO	1.53	2.10	1.17	1.47	1.27	1.64	1.82	0.97
CaO	4.25	4.46	3.80	4.32	3.63	3.90	4.19	2.92
Na2O	4.30	4.44	4.34	4.83	4.82	4.36	4.47	4.85
K2O	3.04	2.65	3.13	2.48	2.71	2.82	2.88	2.92
P2O5	0.47	0.31	0.40	0.30	0.27	0.22	0.25	0.20
MnO	0.15	0.13	0.16	0.11	0.10	0.10	0.11	0.08
LOI	0.80	0.40	0.60	1.00	1.00	1.00	0.60	0.40
Total	100.05	99.94	99.90	99.92	99.94	99.94	99.95	99.79
CIPW Norm								
Quartz	11.67	12.17	12.89	14.22	15.54	16.18	13.77	19.53
Orthoclase	18.21	15.81	18.74	14.88	16.25	16.91	17.21	17.42
Albite	36.88	37.94	37.21	41.50	41.38	37.43	38.24	41.41
Anorthite	15.45	15.48	14.58	13.66	14.39	15.74	14.46	12.23
Nepheline	-	-	-	-	-	-	-	-
Diopside	2.37	4.00	1.60	5.08	1.74	2.01	4.05	0.89
Hypersthene	9.36	8.87	9.23	5.38	5.95	6.91	6.82	4.85
Olivine	-	-	-	-	-	-	-	-
Magnetite	3.10	2.79	3.17	2.81	2.47	2.58	2.92	1.94
Ilmenite	1.87	2.21	1.65	1.77	1.66	1.72	1.96	1.27
Apatite	1.10	0.73	0.94	0.70	0.64	0.52	0.59	0.47
Mg#	34.12	44.00	27.88	40.66	40.22	45.46	44.88	39.49
Sr (ppm)	221.10	188.90	188.20	193.30	190.50	183.40	195.30	151.40
Rb	91.00	78.20	93.90	69.90	72.20	85.80	87.00	84.70
Ba	489.80	326.20	445.50	320.90	336.80	371.60	340.10	373.90
Ni	0.90	3.00	0.50	0.50	0.90	2.50	2.10	0.70
Sc	15.00	16.00	17.00	11.00	10.00	11.00	14.00	8.00
Co	18.50	20.50	13.60	16.90	15.20	14.60	19.70	16.80
Cs	3.10	3.10	3.20	2.50	2.60	3.50	3.50	2.30
Ga	23.10	19.40	21.60	20.30	19.70	18.90	18.70	19.60
Th	12.10	11.20	11.80	10.10	8.60	11.40	10.70	11.70
Ta	1.50	1.00	1.40	0.90	0.90	0.80	1.00	0.80
Nb	18.20	12.20	18.30	10.10	9.70	10.20	12.00	8.40
U	3.50	3.40	3.50	3.40	3.50	3.60	3.50	4.00
Zr	385.40	304.40	385.40	298.20	304.70	248.30	308.50	307.80
Hf	9.70	8.20	9.80	7.40	7.80	6.60	8.30	7.90
Y	56.10	42.30	56.00	39.50	38.70	34.60	40.60	37.00
Ce	86.00	56.00	83.20	53.60	53.80	50.70	57.00	53.10
Nd	45.00	29.00	44.50	28.00	27.70	23.90	28.90	25.90
Sm	9.90	6.40	9.50	6.30	5.90	5.50	6.40	5.60
Eu	2.57	1.64	2.39	1.73	1.60	1.31	1.61	1.38
Gd	9.86	6.76	9.88	6.67	6.50	5.61	6.42	5.81
Tb	1.89	1.30	1.77	1.29	1.18	1.07	1.28	1.12
Dy	9.74	7.11	9.65	7.15	6.92	6.05	6.95	6.46
Ho	1.85	1.37	2.00	1.37	1.43	1.15	1.32	1.31
Er	6.12	4.18	5.91	4.10	4.06	3.40	3.93	3.68
Tm	0.93	0.65	0.90	0.62	0.62	0.50	0.61	0.60
Pr	11.06	7.00	10.73	6.81	6.81	6.17	7.06	6.51
Yb	5.20	3.99	5.26	3.86	3.76	3.33	3.88	3.75
La	37.40	25.80	36.90	24.10	24.00	23.80	26.30	24.30
Lu	0.81	0.61	0.84	0.59	0.58	0.50	0.59	0.58
Pb	0.8	0.6	0.5	0.7	0.7	0.6	0.9	0.8

Table 6.1 Continued

Sample	2008 4	2006 14	2006 27	2006 59	2006 85	2006 109	2006 128	2006 117
Rock Type								
SiO2 (%)	64.11	63.93	63.19	65.49	63.27	63.21	67.07	63.07
TiO2	0.87	0.84	0.98	0.68	1.07	0.88	0.66	0.99
Al2O3	15.70	16.03	16.22	15.73	15.24	16.62	15.78	16.19
Fe2O3	5.73	5.53	6.41	5.02	6.67	5.64	3.62	5.71
MgO	1.38	1.25	1.49	0.96	1.38	0.92	0.63	1.65
CaO	3.60	3.43	3.90	2.95	3.47	3.73	2.14	4.20
Na2O	4.72	4.80	4.88	3.67	4.74	5.03	4.35	4.48
K2O	2.61	2.72	2.47	2.13	3.18	3.20	4.63	2.73
P2O5	0.27	0.27	0.31	0.23	0.26	0.28	0.29	0.23
MnO	0.11	0.10	0.12	0.10	0.11	0.10	0.05	0.10
LOI	0.70	1.00	-0.20	0.80	0.40	0.20	0.60	0.50
Total	99.80	99.90	99.77	97.76	99.79	99.82	99.80	99.83
CIPW Norm								
Quartz	16.60	15.94	14.26	27.99	13.94	12.27	18.53	14.99
Orthoclase	15.63	16.32	14.67	13.03	18.99	19.06	27.65	16.31
Albite	40.46	41.23	41.49	32.15	40.54	42.89	37.19	38.31
Anorthite	14.13	14.37	15.13	13.60	11.04	13.43	8.84	16.17
Nepheline	-	-	-	-	-	-	-	-
Diopside	1.81	0.93	1.89	-	3.88	2.82	-	2.79
Hyperstene	6.46	6.44	7.07	6.68	5.91	4.63	3.81	6.41
Olivine	-	-	-	-	-	-	-	-
Magnetite	2.61	2.53	2.90	2.00	3.03	2.56	1.65	2.60
Ilmenite	1.67	1.62	1.87	1.34	2.06	1.69	1.27	1.90
Apatite	0.64	0.64	0.72	0.55	0.61	0.66	0.67	0.53
Mg#	40.89	39.37	40.03	34.00	37.28	31.90	33.31	45.35
Sr (ppm)	188.90	186.50	210.90	169.90	172.60	190.70	177.90	219.40
Rb	80.80	77.60	73.40	96.90	105.50	102.30	188.40	90.30
Ba	344.70	355.00	345.10	429.80	367.00	367.00	432.00	388.00
Ni	0.60	0.70	0.60	0.60	1.40	0.60	3.00	1.10
Sc	10.00	10.00	11.00	8.00	12.00	10.00	7.00	12.00
Co	17.30	16.40	17.50	15.40	16.60	11.10	10.80	14.80
Cs	2.90	2.80	2.60	3.80	4.00	3.00	5.50	3.20
Ga	19.90	19.00	20.30	19.50	19.80	20.20	18.20	17.90
Th	11.00	10.70	10.40	12.60	12.10	12.40	27.40	11.20
Ta	0.90	1.00	0.90	1.10	1.00	0.90	1.70	0.80
Nb	9.40	9.90	10.50	11.90	12.30	11.40	21.40	10.90
U	3.60	3.20	3.20	4.40	4.30	4.20	8.40	3.60
Zr	320.20	331.00	317.00	355.60	426.10	402.60	376.40	268.20
Hf	8.60	8.70	8.10	9.00	10.90	10.30	9.50	6.80
Y	40.20	41.20	42.90	44.60	51.10	52.00	35.00	36.90
Ce	53.80	57.50	56.40	62.10	63.40	62.80	79.00	55.10
Nd	27.50	29.80	29.00	31.30	38.20	37.70	31.30	27.60
Sm	6.30	6.70	6.80	6.60	8.16	8.29	5.82	5.76
Eu	1.55	1.76	1.78	1.65	1.82	1.94	1.17	1.42
Gd	6.45	6.76	7.18	7.09	8.68	8.52	5.24	6.14
Tb	1.22	1.21	1.27	1.29	1.50	1.47	0.92	1.09
Dy	7.07	7.34	7.12	7.50	8.59	8.77	5.46	6.07
Ho	1.42	1.45	1.44	1.53	1.91	1.83	1.17	1.29
Er	4.18	4.54	4.43	4.88	5.34	5.29	3.64	3.73
Tm	0.61	0.57	0.64	0.72	0.84	0.82	0.59	0.60
Pr	6.81	7.28	7.29	7.86	8.44	8.46	9.13	6.85
Yb	3.97	4.00	4.01	4.27	5.22	5.13	3.83	3.63
La	24.10	25.60	24.70	28.00	28.40	28.40	41.80	25.50
Lu	0.62	0.66	0.65	0.72	0.78	0.77	0.58	0.54
Pb	0.4	0.5	1.6	0.3	0.4	1.5	1.9	0.2

Table 6.1 Continued

Sample	2007 2	2005 1	2005 3	2005 28	2006 43	2006 47	2006 101	2006 108
Rock Type	Dacite							
SiO2 (%)	64.06	63.02	65.78	65.11	65.26	66.46	64.80	65.75
TiO2	0.72	0.97	0.72	0.82	0.67	0.68	0.79	0.71
Al2O3	15.36	15.75	14.96	15.28	15.28	15.02	15.35	15.53
Fe2O3	4.58	5.47	4.70	5.16	4.86	4.39	5.07	4.78
MgO	1.09	1.87	1.15	1.29	1.17	1.15	1.32	1.18
CaO	2.92	4.19	3.60	3.50	3.50	3.33	3.59	3.40
Na2O	4.48	4.32	4.12	4.29	4.34	4.09	4.22	4.54
K2O	3.02	2.58	2.89	2.96	2.81	2.99	2.98	2.90
P2O5	0.19	0.21	0.32	0.24	0.29	0.20	0.23	0.27
MnO	0.09	0.10	0.09	0.09	0.10	0.08	0.09	0.10
LOI	3.30	1.20	1.60	1.20	1.50	1.40	1.40	0.70
Total	99.79	99.68	99.93	99.94	99.83	99.76	99.81	99.84
CIPW Norm								
Quartz	18.50	16.06	21.42	19.05	19.80	22.12	18.89	18.83
Orthoclase	18.56	15.54	17.43	17.78	16.96	18.02	17.96	17.35
Albite	39.41	37.27	35.58	36.91	37.50	35.29	36.41	38.88
Anorthite	13.39	16.28	14.08	13.92	14.21	14.06	14.42	13.59
Nepheline	-	-	-	-	-	-	-	-
Diopside	0.34	2.90	1.69	1.78	1.31	1.21	1.82	1.41
Hypersthene	5.80	7.43	5.82	6.40	6.32	5.79	6.44	6.09
Olivine	-	-	-	-	-	-	-	-
Magnetite	2.14	2.14	1.84	2.01	1.91	1.72	1.98	1.86
Ilmenite	1.42	1.88	1.40	1.58	1.30	1.32	1.53	1.36
Apatite	0.45	0.50	0.76	0.57	0.69	0.47	0.55	0.64
Mg#	40.60	47.95	39.74	40.26	39.34	41.38	41.22	39.94
Sr (ppm)	150.90	195.70	188.00	188.00	211.60	196.60	189.60	197.80
Rb	91.00	83.70	82.60	93.80	82.80	100.40	96.50	85.60
Ba	347.00	364.20	468.80	446.40	436.00	493.00	471.00	438.00
Ni	1.90	2.20	1.40	1.30	1.30	1.80	1.90	0.70
Sc	9.00	12.00	9.00	10.00	9.00	9.00	10.00	9.00
Co	32.70	19.40	15.40	15.80	9.80	10.40	12.70	9.80
Cs	3.30	3.50	2.60	2.90	2.60	3.00	2.70	2.60
Ga	19.00	19.20	18.70	19.50	18.10	18.80	18.30	17.40
Th	11.50	10.60	11.10	11.90	11.60	14.10	12.80	12.90
Ta	0.80	0.90	1.50	1.40	1.40	1.30	1.30	1.40
Nb	8.90	10.00	17.20	16.50	17.20	17.30	16.30	16.90
U	4.00	3.50	3.90	4.20	4.30	4.20	4.00	4.60
Zr	315.60	241.60	288.60	292.10	321.70	287.10	275.20	290.00
Hf	8.50	6.40	7.90	8.10	7.90	7.30	7.50	7.00
Y	39.30	34.20	39.70	41.10	39.10	41.10	40.80	38.30
Ce	54.60	49.50	66.70	66.90	61.80	68.60	67.50	61.20
Nd	28.70	23.80	31.90	33.20	32.20	34.30	35.10	32.40
Sm	6.12	5.30	6.70	6.60	6.64	6.79	6.87	6.32
Eu	1.38	1.28	1.66	1.52	1.70	1.66	1.55	1.71
Gd	6.43	5.63	6.68	6.85	6.67	6.79	6.90	6.40
Tb	1.11	1.07	1.25	1.28	1.16	1.14	1.17	1.09
Dy	6.54	6.15	7.09	7.00	6.20	6.67	6.68	6.20
Ho	1.38	1.19	1.39	1.38	1.42	1.47	1.47	1.36
Er	4.17	3.43	3.97	4.10	4.10	4.27	4.24	3.91
Tm	0.67	0.50	0.57	0.61	0.59	0.64	0.66	0.61
Pr	7.21	5.95	7.97	8.23	7.71	8.26	8.31	7.68
Yb	4.13	3.31	3.91	3.91	3.86	4.08	4.03	3.80
La	24.60	22.90	32.00	32.60	30.30	33.30	32.30	29.60
Lu	0.64	0.52	0.61	0.61	0.58	0.61	0.62	0.59
Pb	0.7	0.5	2	1.1	0.4	0.4	0.3	0.2

Table 6.1 Continued

Sample	2006 110	2006 111	2007 4	2005 52	2005 63	2005 69
Rock Type	Rhyolite					
SiO2 (%)	64.97	63.31	65.06	72.79	72.01	74.81
TiO2	0.77	0.88	0.78	0.15	0.19	0.08
Al2O3	15.40	15.31	15.08	13.71	13.86	13.52
Fe2O3	5.18	5.97	5.00	1.40	1.67	1.41
MgO	1.25	1.52	1.40	0.30	0.35	0.04
CaO	3.43	4.00	3.88	1.29	1.41	0.54
Na2O	4.46	4.39	4.13	3.75	4.02	4.25
K2O	2.89	2.67	2.91	4.44	4.34	4.91
P2O5	0.28	0.46	0.24	0.06	0.07	0.03
MnO	0.10	0.11	0.09	0.06	0.06	0.03
LOI	1.10	1.20	1.30	1.80	1.90	0.20
Total	99.84	99.82	99.82	99.75	99.88	99.82
CIPW Norm						
Quartz	18.37	16.76	19.56	31.11	28.70	29.78
Orthoclase	17.36	16.07	17.51	26.81	26.21	29.16
Albite	38.37	37.83	35.59	32.43	34.76	36.13
Anorthite	13.69	14.45	14.27	6.14	6.68	2.49
Nepheline	-	-	-	-	-	-
Diopside	1.44	2.25	3.10	-	-	-
Hyperstene	6.59	7.52	5.94	1.89	2.19	1.27
Olivine	-	-	-	-	-	-
Magnetite	2.02	2.33	1.95	0.64	0.77	0.64
Ilmenite	1.49	1.70	1.51	0.29	0.37	0.15
Apatite	0.67	1.08	0.57	0.14	0.17	0.07
Mg#	39.40	40.68	43.00	38.05	37.60	7.50
Sr (ppm)	198.20	215.20	192.90	83.80	97.80	16.50
Rb	84.20	81.60	94.40	105.00	108.60	132.90
Ba	440.00	398.00	458.00	1017.50	892.40	440.80
Ni	1.20	1.30	1.80	1.60	1.80	0.20
Sc	9.00	10.00	10.00	4.00	4.00	3.00
Co	11.40	13.40	12.60	6.50	9.90	15.00
Cs	2.50	2.60	2.70	2.50	2.60	4.90
Ga	17.90	18.30	17.70	15.30	15.20	15.90
Th	12.20	11.10	12.80	20.30	17.90	15.90
Ta	1.40	1.20	1.20	2.30	2.40	1.20
Nb	17.90	15.70	16.70	26.30	23.60	8.00
U	4.50	4.10	4.10	7.30	7.10	4.60
Zr	309.20	262.80	290.40	109.80	127.60	106.50
Hf	7.60	6.40	7.80	4.10	4.40	4.00
Y	40.50	38.90	41.80	37.00	37.20	26.00
Ce	61.80	60.40	69.30	72.70	69.00	58.40
Nd	32.80	32.50	32.90	29.30	28.90	23.20
Sm	6.67	6.73	6.86	5.80	5.80	4.60
Eu	1.70	1.66	1.61	1.20	1.24	0.45
Gd	6.78	6.99	6.90	5.81	5.89	4.32
Tb	1.17	1.16	1.22	1.13	1.10	0.83
Dy	6.53	6.69	7.12	6.34	6.17	4.50
Ho	1.46	1.39	1.45	1.19	1.27	0.89
Er	4.16	4.03	4.27	3.72	3.65	2.64
Tm	0.63	0.60	0.64	0.58	0.56	0.38
Pr	7.71	7.63	8.55	8.17	7.93	6.54
Yb	3.99	3.72	4.30	3.67	3.61	2.62
La	29.90	28.90	32.70	37.30	34.50	28.00
Lu	0.61	0.56	0.64	0.55	0.59	0.41
Pb	0.3	0.3	0.3	1	0.5	0.3

Table 6.1 Continued

Sample	2005 75	2006 120	2006 135	2006 137	2007 5	2007 14
Rock Type						
SiO2 (%)	73.63	70.15	73.20	71.81	72.91	71.10
TiO2	0.02	0.29	0.18	0.18	0.18	0.15
Al2O3	13.74	14.95	13.77	13.93	13.92	13.49
Fe2O3	0.93	3.10	1.71	1.57	1.58	1.47
MgO	0.02	0.32	0.34	0.35	0.27	0.32
CaO	0.49	1.64	1.30	1.26	1.21	1.18
Na2O	4.23	4.78	4.00	3.85	4.05	3.68
K2O	4.49	4.06	4.34	4.35	4.23	4.34
P2O5	0.03	0.09	0.06	0.05	0.05	0.05
MnO	0.07	0.07	0.06	0.06	0.06	0.06
LOI	2.40	0.40	0.90	2.40	1.30	3.90
Total	100.05	99.84	99.82	99.84	99.80	99.76
CIPW Norm						
Quartz	31.18	22.20	29.95	29.93	30.27	31.01
Orthoclase	27.19	24.18	25.95	26.42	25.42	26.79
Albite	36.68	40.76	34.24	33.48	34.85	32.53
Anorthite	2.29	7.40	6.11	6.12	5.74	5.79
Nepheline	-	-	-	-	-	-
Diopside	-	0.16	-	-	-	-
Hyperstene	0.99	3.13	2.20	2.13	1.91	2.05
Olivine	-	-	-	-	-	-
Magnetite	0.43	1.41	0.78	0.73	0.72	0.69
Ilmenite	0.04	0.55	0.35	0.35	0.35	0.30
Apatite	0.07	0.22	0.15	0.11	0.13	0.12
Mg#	5.69	22.84	36.34	39.06	32.88	38.45
Sr (ppm)	3.70	93.40	89.90	84.70	87.00	88.70
Rb	213.80	141.00	111.80	111.60	106.70	117.30
Ba	34.70	507.00	877.00	881.00	925.00	864.00
Ni	1.00	0.50	1.00	1.30	1.00	1.70
Sc	4.00	7.00	4.00	4.00	4.00	4.00
Co	9.10	5.10	4.90	7.50	27.10	11.80
Cs	11.30	4.10	2.60	2.50	2.50	2.60
Ga	17.10	19.20	15.40	14.90	15.00	16.10
Th	15.40	17.70	18.90	19.80	21.80	21.90
Ta	2.40	1.10	2.40	2.30	2.40	2.50
Nb	15.90	13.70	26.70	26.00	26.50	27.70
U	10.10	4.60	7.50	7.40	7.40	7.80
Zr	60.70	325.00	121.20	113.10	147.30	112.00
Hf	3.30	8.70	4.40	4.20	5.10	4.30
Y	44.30	46.60	39.40	37.80	40.50	39.00
Ce	30.60	81.70	69.50	68.30	96.60	71.40
Nd	14.70	39.10	30.90	29.00	39.40	32.00
Sm	4.30	7.55	6.22	5.95	7.14	6.19
Eu	0.10	1.24	1.16	1.15	1.39	1.20
Gd	5.17	7.46	6.09	5.98	6.84	6.42
Tb	1.16	1.31	1.09	1.07	1.18	1.12
Dy	6.96	7.56	6.15	6.18	6.69	6.58
Ho	1.38	1.62	1.33	1.28	1.42	1.35
Er	4.28	4.79	3.85	3.83	4.24	4.02
Tm	0.64	0.73	0.63	0.60	0.65	0.63
Pr	3.79	10.00	8.12	7.97	10.95	8.57
Yb	4.15	4.69	3.98	3.80	4.11	4.12
La	12.40	39.70	34.60	34.60	49.40	37.50
Lu	0.64	0.72	0.59	0.59	0.60	0.61
Pb	1	0.5	0.3	0.4	0.2	0.5

Table 6.1 Continued

Sample	2005 4A	2005 4B	2005 29	2005 34	2005 41	2005 77	2007 6
Rock Type	Enclave						
SiO2 (%)	50.23	60.77	58.43	60.86	50.97	51.38	52.13
TiO2	2.28	1.18	1.54	1.23	0.79	2.32	1.55
Al2O3	16.02	15.6	15.62	15.77	18.97	16.19	18.68
Fe2O3	11.79	6.86	8.52	6.96	9.22	11.86	11.42
MgO	5.31	2.29	3.04	1.8	7.33	5.42	2.61
CaO	7.96	4.7	5.52	4.77	8.38	7.38	6.77
Na2O	3.91	4.31	4.3	4.02	3.13	4.1	4.87
K2O	1.04	2.41	1.84	2.46	0.25	0.67	0.86
P2O5	0.33	0.37	0.28	0.53	0.13	0.32	0.567
MnO	0.16	0.12	0.15	0.12	0.14	0.18	0.18
LOI	0.9	1.3	0.7	1.4	0.5	0.1	0.1
Total	99.93	99.91	99.94	99.92	99.81	99.92	99.73
CIPW Norm							
Quartz	-	13.00	9.52	14.96	-	-	-
Orthoclase	6.26	14.51	11.03	14.83	1.50	4.01	5.15
Albite	33.73	37.17	36.90	34.71	26.88	35.11	41.73
Anorthite	23.53	16.41	18.14	18.09	37.53	24.08	26.90
Nepheline	-	-	-	-	-	-	-
Diopside	11.90	4.03	6.41	2.11	3.10	8.94	2.82
Hyperstene	10.34	9.03	11.37	9.20	25.00	17.23	14.90
Olivine	5.33	-	-	-	2.10	2.78	0.19
Magnetite	3.70	2.68	3.00	2.47	2.07	2.65	4.01
Ilmenite	4.41	2.29	2.97	2.38	1.52	4.46	2.98
Apatite	0.78	0.87	0.66	1.25	0.31	0.75	1.33
Mg#	53.12	47.35	48.17	40.26	65.02	51.65	37.31
Sr (ppm)	284.6	217.6	235.6	233.9	491	291	349.5
Rb	25.5	63.1	51.8	72.1	2.5	8.1	15.2
Ba	179.6	424.7	369.8	394.5	217.5	274.5	324
Ni	23.9	3.4	5.4	1.6	11.6	8	2
Sc	23	14	18	14	35	24	24
Co	40.7	30.9	29.6	25.2	34	42.7	18.3
Cs	0.6	1.3	1.5	2.1	0.1	0.2	0.2
Ga	20.8	19.8	19.2	19.3	19	19.8	22.9
Th	3.5	10.1	8.3	10.3	1.8	3.9	1.5
Ta	0.7	1.6	1.2	1.4	0.2	0.7	0.8
Nb	8.1	18.7	15.6	17.6	1.9	8.2	17
U	1.1	3.2	2.7	3.2	0.6	1.2	0.9
Zr	206.4	292.6	257.2	248.9	58	223	517.3
Hf	5.5	7.9	7.1	6.7	1.9	5.6	11.3
Y	36.5	47.9	45.7	40	18.4	38	44.3
Ce	40.3	68.3	60.3	63	19.5	41.3	58.4
Nd	24.7	34.4	32	33.3	11.4	24.8	38.4
Sm	6	7.7	7.1	6.5	2.4	6	8.91
Eu	1.8	1.98	1.85	1.75	0.83	2.06	3.09
Gd	6.52	7.94	7.27	7.16	2.84	6.74	9.49
Tb	1.2	1.52	1.47	1.34	0.59	1.25	1.52
Dy	6.47	8.2	7.99	7.11	3.28	7.05	8.37
Ho	1.28	1.61	1.6	1.43	0.67	1.42	1.66
Er	3.69	4.84	4.4	4.02	2.11	4.29	4.6
Tm	0.56	0.74	0.71	0.61	0.31	0.62	0.68
Pr	5.48	8.74	7.8	7.75	2.61	5.69	8.48
Yb	3.4	4.54	4.31	3.72	1.99	3.61	4.01
La	17.1	31.7	27.2	29.1	9.9	16.6	24.9
Lu	0.51	0.7	0.63	0.58	0.31	0.57	0.6
Pb	0.8	1.2	0.7	0.8	1.1	1	0.5

MgO contents range between 7.15 and 0.02 wt%, with mg# between 60 and 5.6. On the basis of total alkali vs. silica contents (TAS, Le Bas et al., 1986; Figure 6.1) Süphan volcanic rocks straddle the transition between subalkaline and alkaline fields. The majority of volcanics plot on the subalkaline field of Miyashiro (1978) and Irvine and Baragar (1971), however some of them plot on the alkaline-subalkaline division line of Miyashiro (1978) and a few of them within the alkaline field. The lavas which have the mildly alkaline character are the older lavas of the volcano and overall the character of the volcanism seems to have turned into transitional and subalkaline with time.

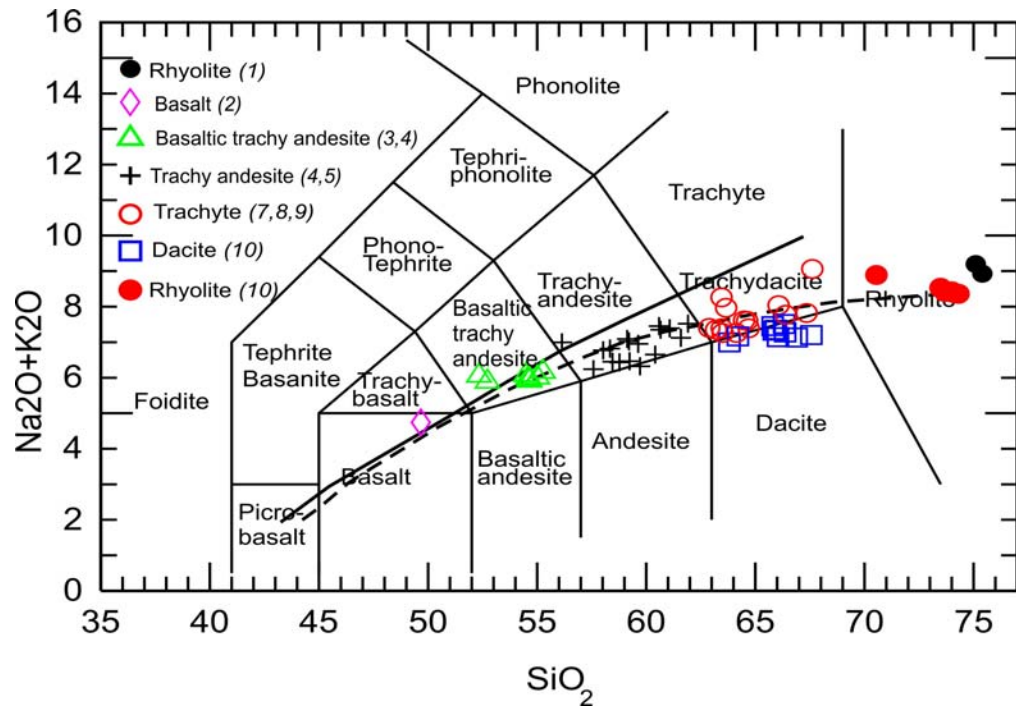


Figure 6.1 TAS diagram of the Süphan volcanics (Le Bas et al., 1986). Subalkaline-alkaline divisions are from Miyashiro (1978) (dashed line) and Irvin&Baragar (1971) (solid line). Number in parenthesis in the legend correspond to the units in Figure 3.2.

Subalkaline Süphan lavas appear to be transitional between calcalkaline and tholeiitic fields (Figure 6.2). On $\text{SiO}_2\text{-K}_2\text{O}$ plot (Figure 6.3) all the volcanics are in the calcalkaline to high K – calcalkaline fields, whereas $\text{Na}_2\text{O-K}_2\text{O}$ diagram suggests a general transition in the nature of volcanics from sodic in the mafic, to potassic in the felsic members (Figure 6.4).

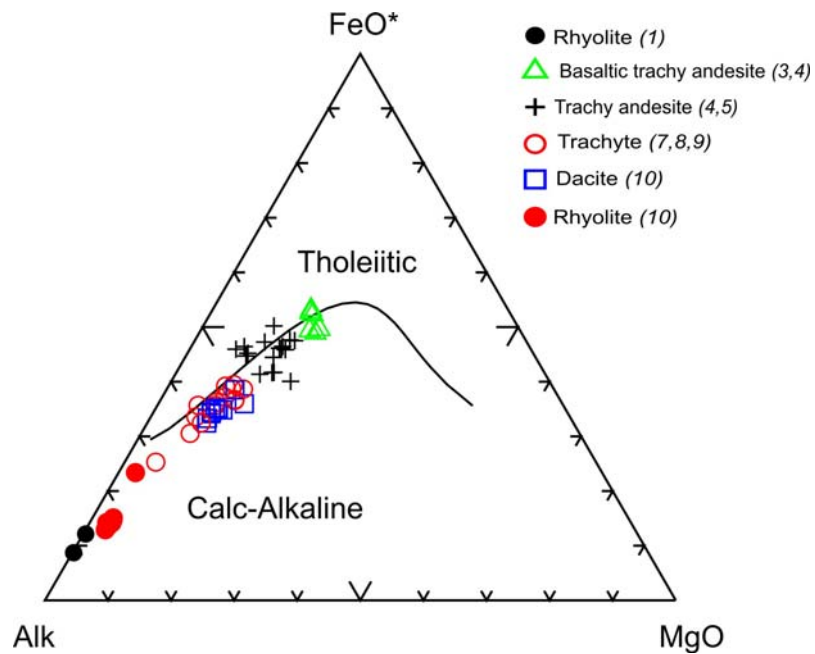


Figure 6.2 AFM diagram (Irvine&Baragar, 1971) of Süphan volcanics FeO^* ; FeO , Alk ; $\text{Na}_2\text{O} + \text{K}_2\text{O}$. Number in parenthesis in the legend correspond to the units in Figure 3.2.

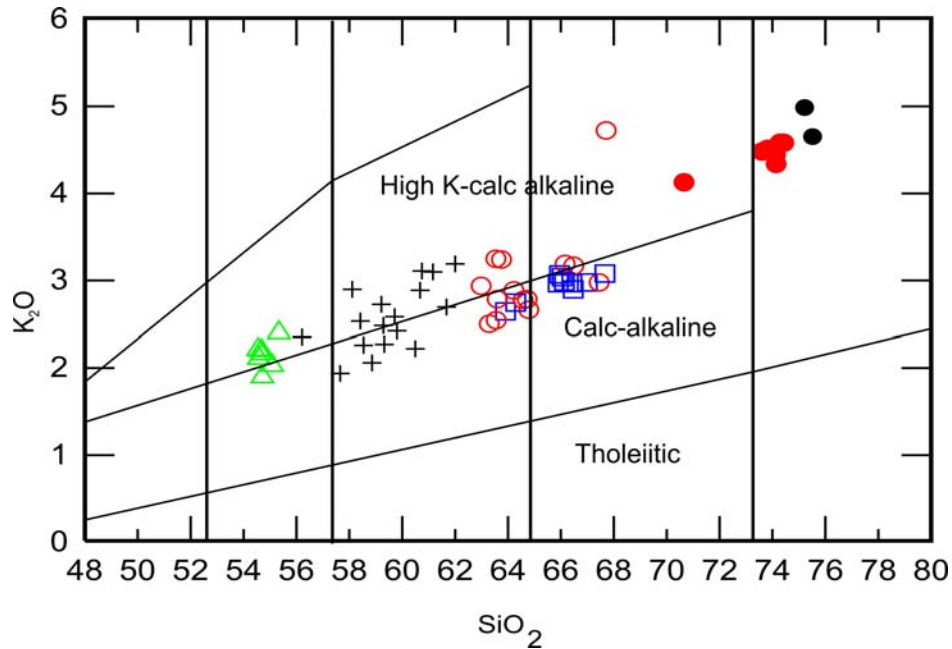


Figure 6.3 K₂O-SiO₂ diagram of Süphan Volcanics (Peccerillo ve Taylor, 1976) (Symbols same as Figure 5.2).

Major element variation diagrams are illustrated in Figure 6.5. As can be seen from the figure, Fe₂O₃, CaO, TiO₂, MgO, MnO, Al₂O₃ display well defined negative, whereas K₂O display positive correlation with SiO₂. Na₂O vs. SiO₂ plot does not yield a distinct trend. The negative trends yielded by Fe₂O₃, CaO, TiO₂, MgO vs. SiO₂ plots seem to be compatible with fractional crystallization (governed by olivine + clinopyroxene + plagioclase + Fe-Ti oxides) and/or magma mixing.

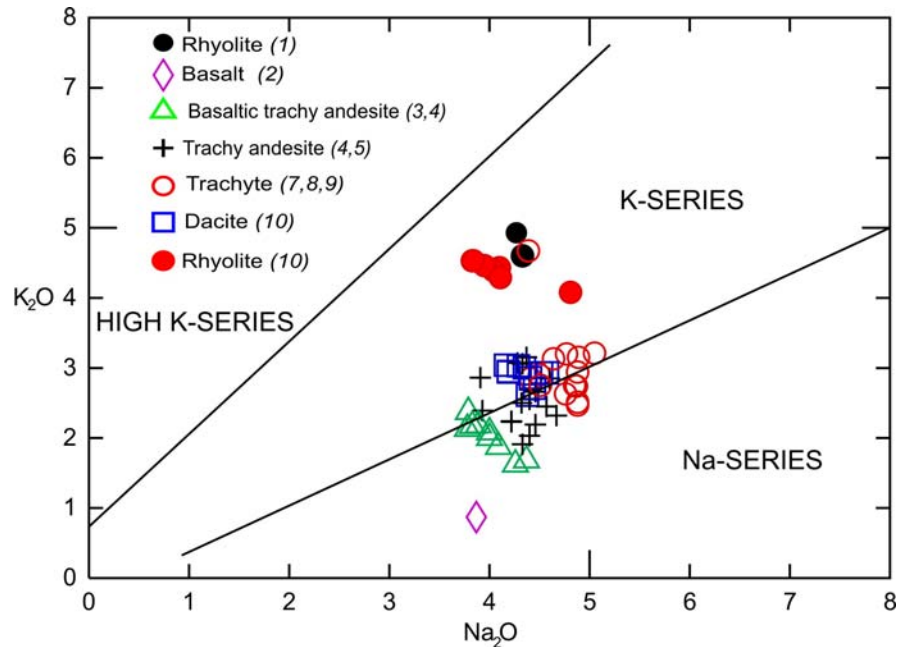


Figure 6.4 K₂O-Na₂O diagram of Süphan Volcanics (Middlemost 1975). Number in parenthesis in the legend correspond to the units in Figure 3.2.

6.2 Trace and RE Element Geochemistry

Trace element variation diagrams are shown in Figure 6.6. According to these diagrams, Co, Sc, Ni and Sr, show well defined negative, and Rb, Th and U show positive correlation with SiO₂. The negative correlation of Ni, Co, Sc and Sr can be attributed to the fractionation of the olivine + pyroxene + plagioclase + minerals, whereas the positive correlation of the incompatible elements such as Ba and Rb can reflect K-feldspar, biotite fractionation. It is striking that most trends in both major and trace element variation diagrams are linear, except at <55 wt% SiO₂, where there is some evidence of curvature in Al₂O₃, FeO and TiO₂. Likewise on a bivariate graph on which highly incompatible-compatible elements are plotted can be useful to differentiate a fractional crystallization process from magma mixing processes. On a such

diagram magmas related to each other by mixing processes display trace element abundances that lie on straight lines. In contrast magmas evolved by fractionation processes have trace element contents that follow a curve. Th and Sc can be used for this purpose (Figure 6.7). Th is a highly incompatible element, whereas Sc is compatible for most of the ferromagnesian minerals, except olivine. It is apparent from the figure most of the Süphan volcanics lie on the straight lines and display linear trends. These are important observations in establishing the extent to which the observed trends are the products of fractional crystallization, as opposed to magma mixing or crustal assimilation, and it will be discussed in detail in chapter 8.

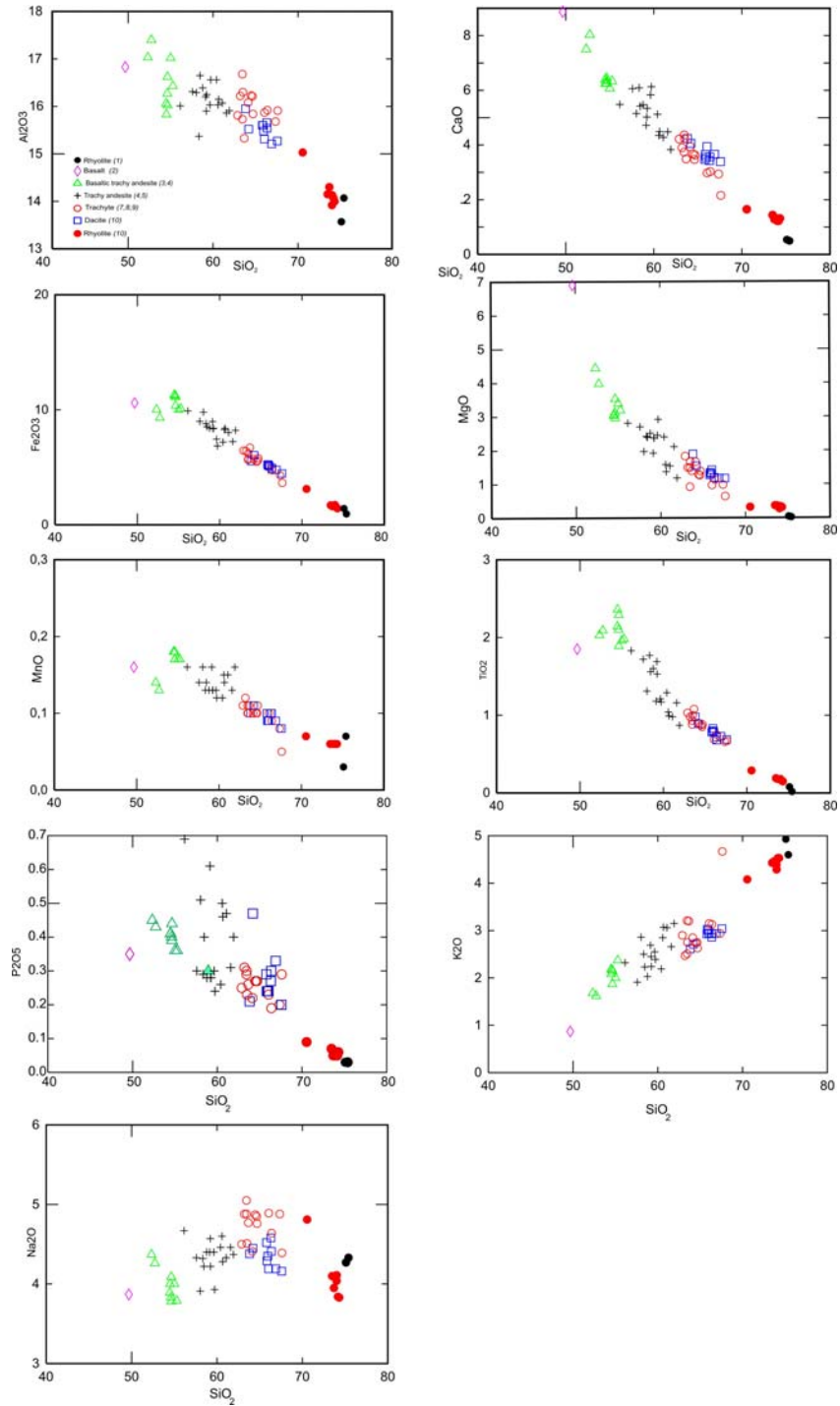


Figure 6.5 Major oxide variation diagrams of Süphan Volcanics. Number in parenthesis in the legend correspond to the units in Figure 3.2.

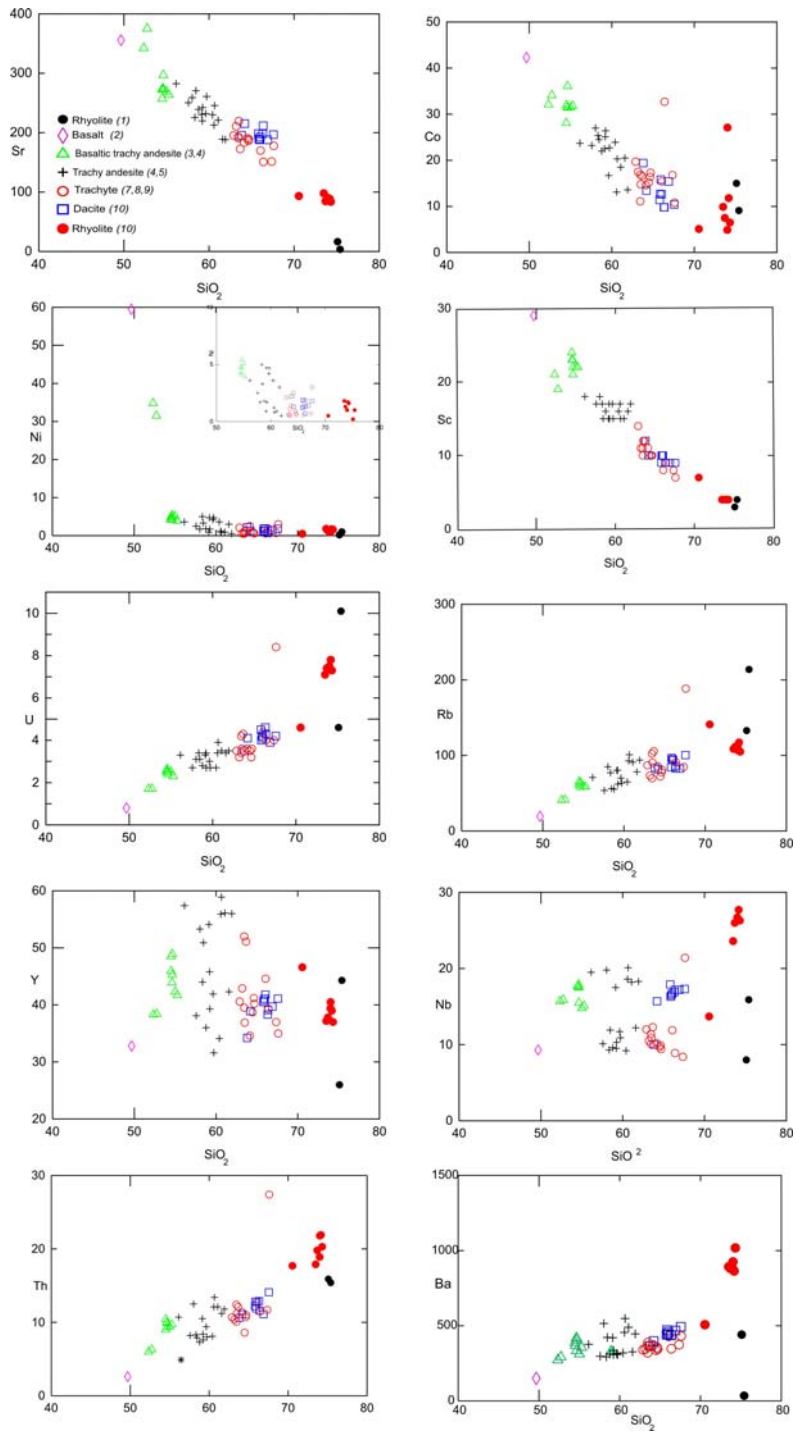


Figure 6.6 Trace element variation diagrams of Süphan Volcanics. Number in parenthesis in the legend correspond to the units in Figure 3.2.

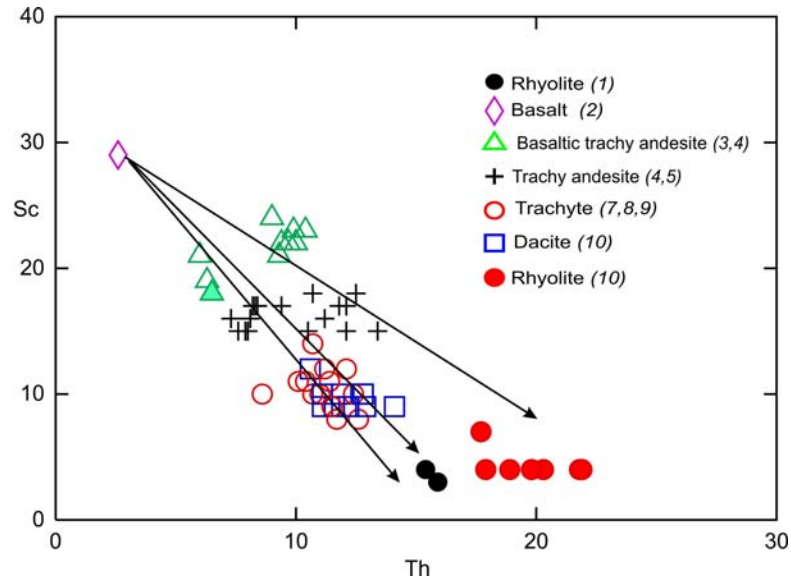


Figure 6.7 Sc-Th diagram for Süphan volcanics. Number in parenthesis in the legend correspond to the units in Figure 3.2.

MORB- normalized trace element and chondrite-normalised REE patterns of Süphan volcanics are shown in Figures 6.8 and 6.9, respectively. All samples show similar MORB-normalized trace element patterns (Figure 6.8) characterized by enrichment (relative to MORB) of both large-ion lithophile (LIL) and high field-strength (HFS) elements, although the former are more pronounced than the latter. Sr, Ba, P and Ti in the intermediate-felsic members have distinctive negative anomalies compared to mafic members. The depletion of Nb and Ta point to the presence of an inherited subduction component in the mantle source and/or crustal contamination. The chondrite-normalized REE patterns (Figure 6.9) reveal enrichment of Light Rare Earth Elements (LREE) over Heavy Rare Earth Elements (HREE). $(La/Yb)_N$ ratio is 3.4 for basaltic rocks and increases slightly with increasing SiO_2 : 4.8-5.3 for basaltic trachyandesites, 3.3-5.8 for trachyandesites, 3.6-4.7

for trachytes, 4.6-5.6 for dacites and 5.7-8.0 for rhyolites. The magnitude of negative Eu anomaly increases with increasing SiO₂.

MORB and REE patterns of the Süphan volcanics display similarities with each other, but there is a slight difference in trachyandesites and rhyolites (Figure 6.8). The younger trachyandesites (number 5 in Figures 3.2 and 3.1) are more enriched in LILE and HFSE compared to the older ones (number 4 in Figures 3.2 and 3.1) and also have the highest REE contents among all the volcanics including the high and low SiO₂ end-members. Younger rhyolites are more enriched in REE contents compared to the older ones.

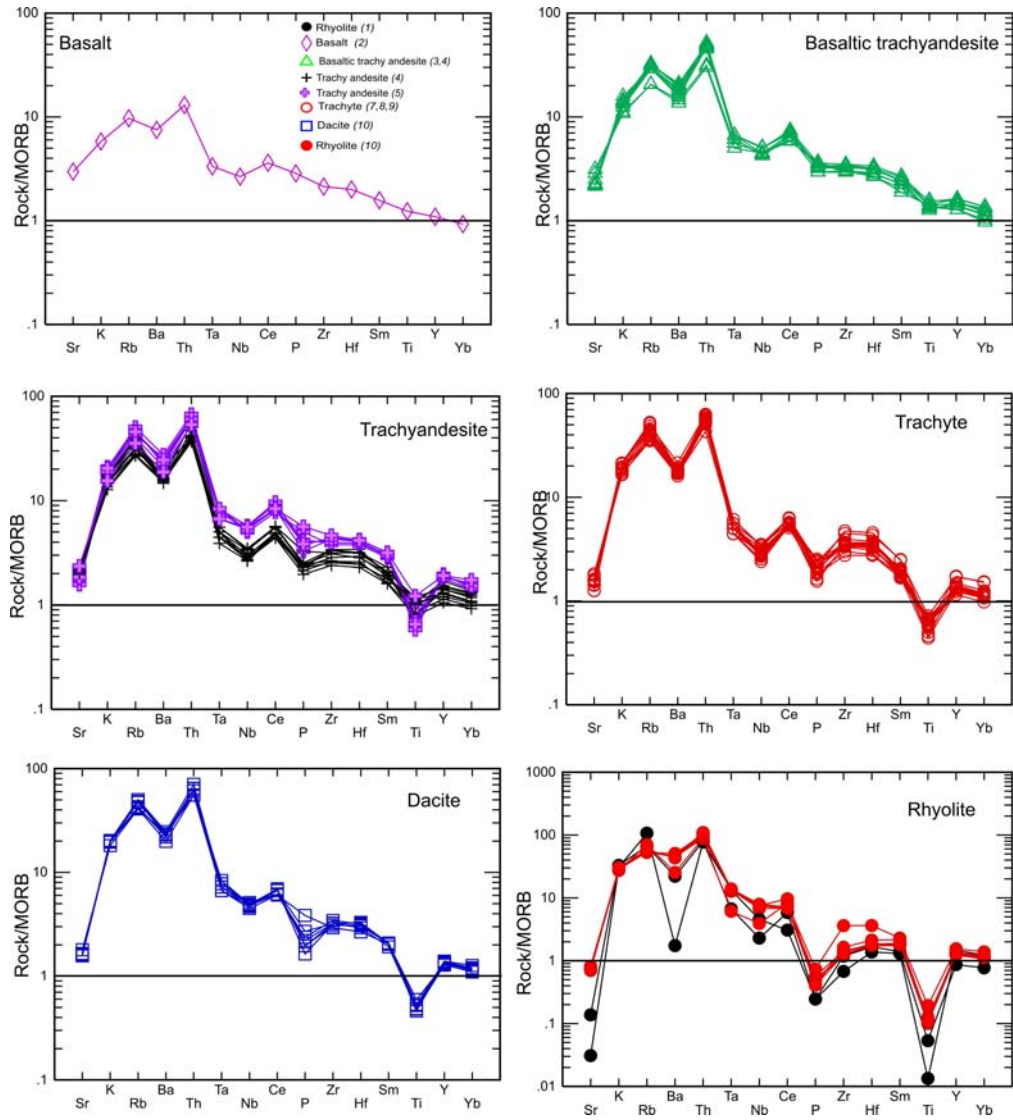


Figure 6.8 MORB normalized multi-element patterns of the Süphan volcanics (MORB normalizing values are from Pearce, 1983). Number in parenthesis in the legend correspond to the units in Figure 3.2.

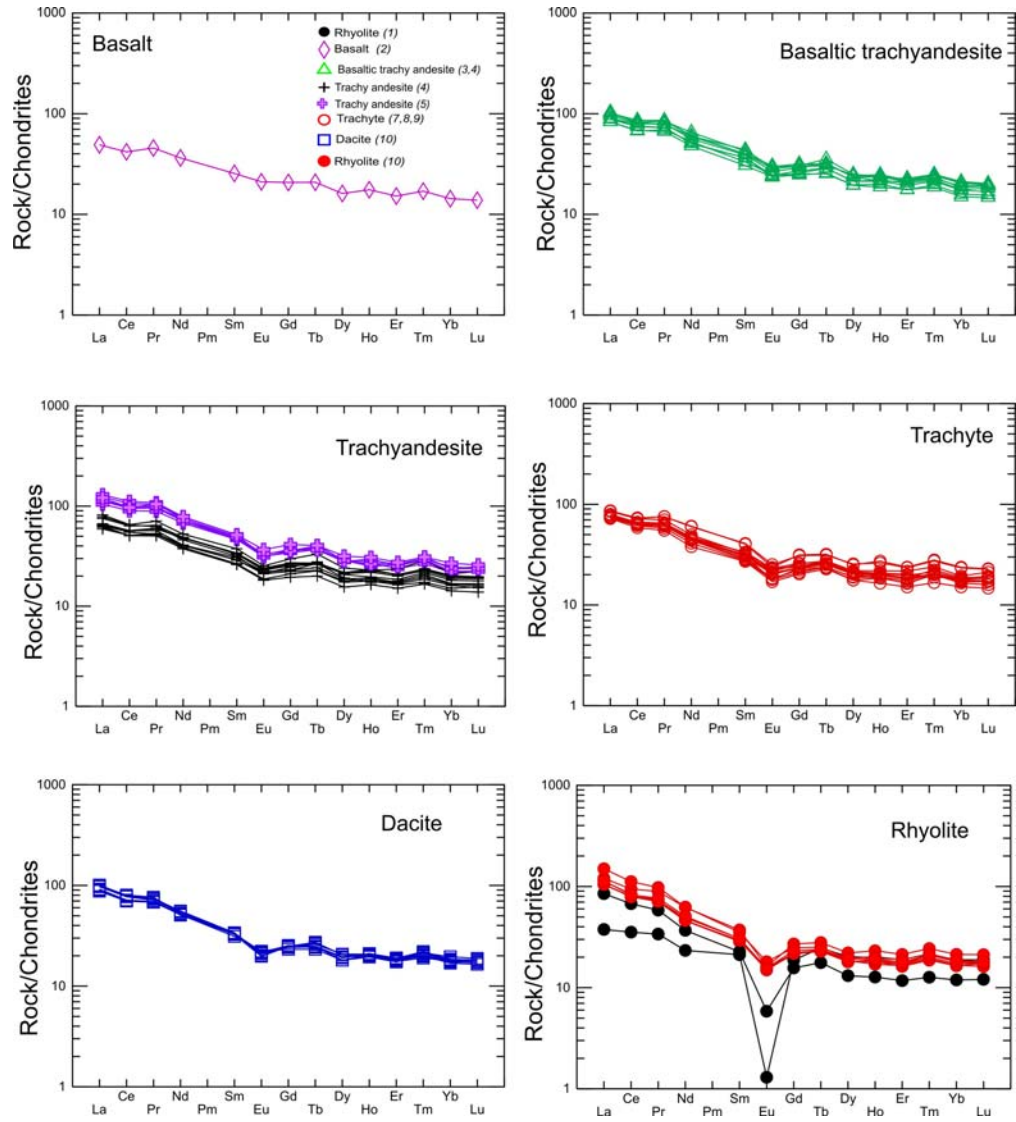


Figure 6.9 Chondrite normalized REE patterns of Süphan volcanics (Chondrite normalizing values are from Nakamura, 1974). Number in parenthesis in the legend correspond to the units in Figure 3.2.

6.3 Major, Trace and RE Element Geochemistry of Enclaves

Enclaves from the Süphan Stratovolcano are collected from dacitic - rhyolitic domes and trachytic lava flows. They are coarse (Sample No: 2007 6) and fine grained gabros (Sample No: 2005 41) , dolerites (Sample No: 2005 77 and 2005 4A) and microdiorites (Sample No: 2005 4B, 2005 29, 2005 34) Their contact with their host rocks are commonly sharp. In TAS diagram (Figure 6.10) enclaves show mainly basalt (Sample No: 2005 41, 2005 77, 2005 4A) basaltic trachyandesite (2007-6) and trachy-andesite (Sample No: 2005 4B, 2005 29, 2005 34) compositions, while host rocks cover trachyte-rhyolite range. SiO_2 and MgO content of the enclaves range between 50.7-61.8 and 1.8-7.3 respectively.

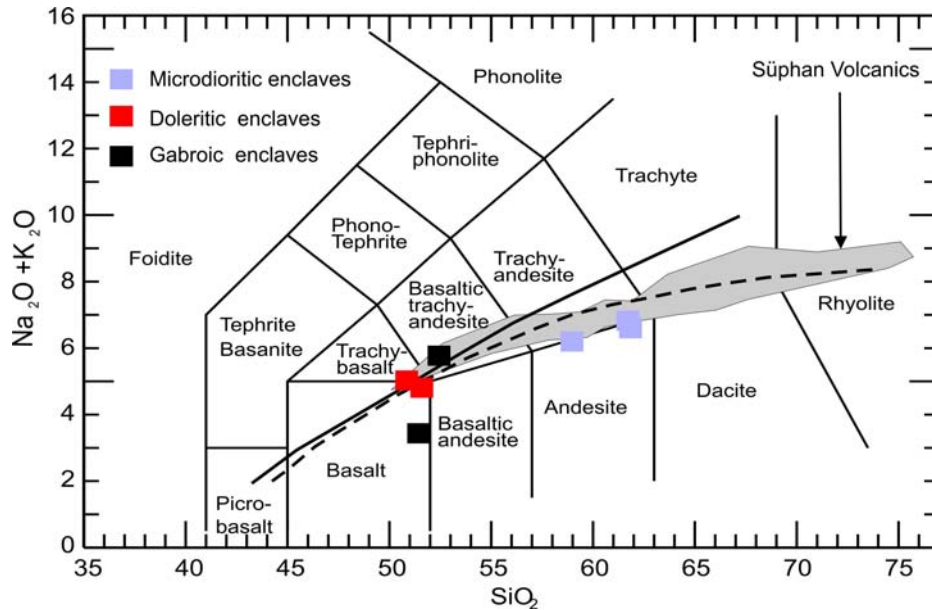


Figure 6.10 TAS diagram (Le Bas et al., 1986) of the Süphan enclaves. Subalkaline-alkaline divisions are from Miyashiro (1978) (dashed line) and Irvin&Baragar (1971) (solid line). (Shaded field represents the Süphan volcanics).

On AFM (Figure 6.11), K_2O-SiO_2 (Figure 6.12) and K_2O-Na_2O (Figure 6.13) diagrams enclaves have similar properties with the Süphan intermediate and mafic products rather than their host rocks (trachytes, dacites and rhyolites). They have mainly sodic nature and show calcalkaline affinity except fine grained gabbroic enclave (Sample 2005-41) which plots in the tholeiitic field.

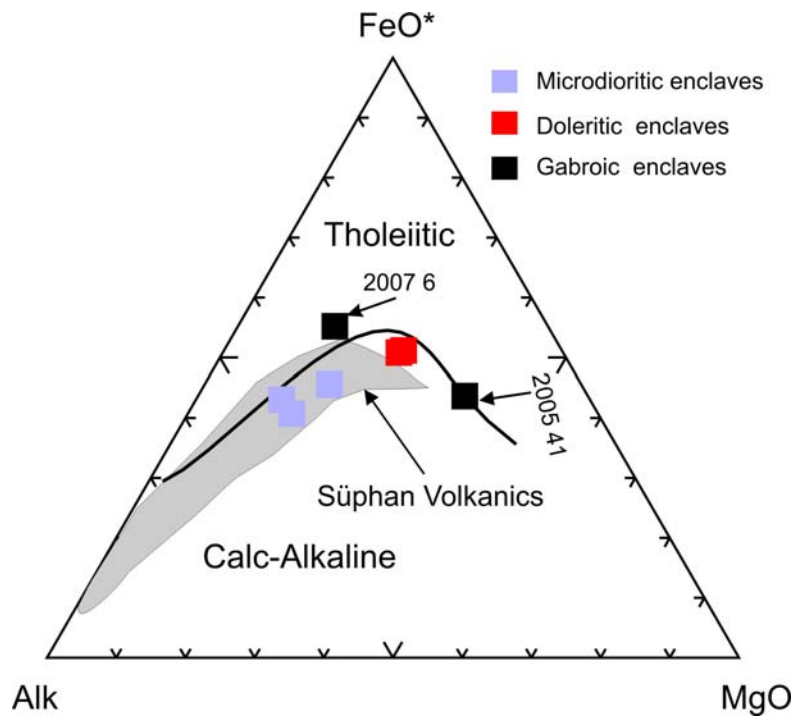


Figure 6.11 AFM diagram (Irvine&Baragar, 1971) of Süphan enclaves. FeO^* ; FeO , Alk ; $Na_2O + K_2O$. (Shaded field represents the Süphan volcanics).

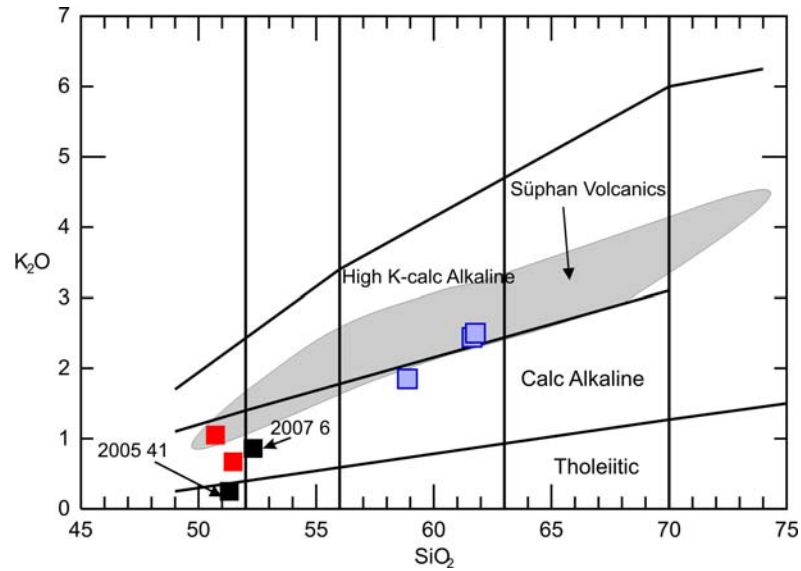


Figure 6.12 K₂O-SiO₂ diagram of Süphan enclaves (Peccerillo ve Taylor, 1976). (Shaded field represents the Süphan volcanics, symbols are same as Figure 5.11).

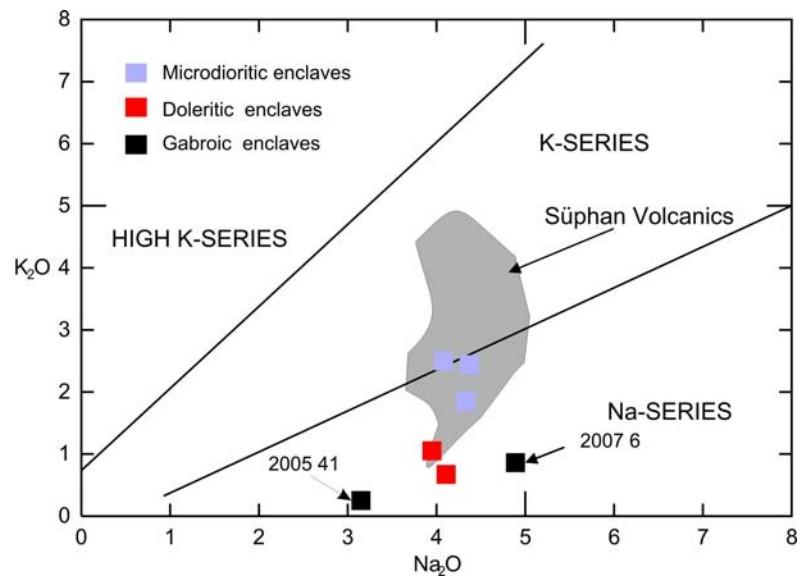


Figure 6.13 K₂O-Na₂O diagram (Middlemost 1975) of Süphan enclaves. (Shaded field represents the Süphan volcanics).

On Harker variation diagrams (Figure 6.14, Figure 6.15), Al_2O_3 , CaO, MgO, Fe_2O_3 , MnO, TiO_2 , Sr, Co, Sc, show negative and K_2O , Rb, U, Th show positive correlations with SiO_2 . Doleritic-microdioritic enclaves plot, in most of the variation diagrams, within the field defined by the host volcanics suggesting a co-magmatic origin with the Süphan lavas and relation to each other through fractional crystallization and/or magma mixing processes. On the other hand, fine and coarse grained gabbroic enclaves (sample 2005-41 and 2007-6, respectively) do not have compatible trends with Süphan lavas and other enclaves.

MORB normalized spider diagrams of enclaves are shown in Figure 6.16. Micro dioritic/doleritic enclaves (Figure 6.16a) in the Süphan volcanics have similar patterns with their host rocks (dacites and trachytes). LIL elements are enriched over HFS elements relative to the MORB and they have negative Ta and Nb anomalies. Fine grained gabbroic (sample 2005-41) and coarse grained gabbroic (2007-6) enclaves show two different trends in MORB normalized diagrams. Coarse grained gabbroic enclave from rhyolitic dome (Figure 6.16b) have hump pattern similar to the within plate trend. LIL and HFS elements are enriched relative to the MORB with small negative Ti anomaly.

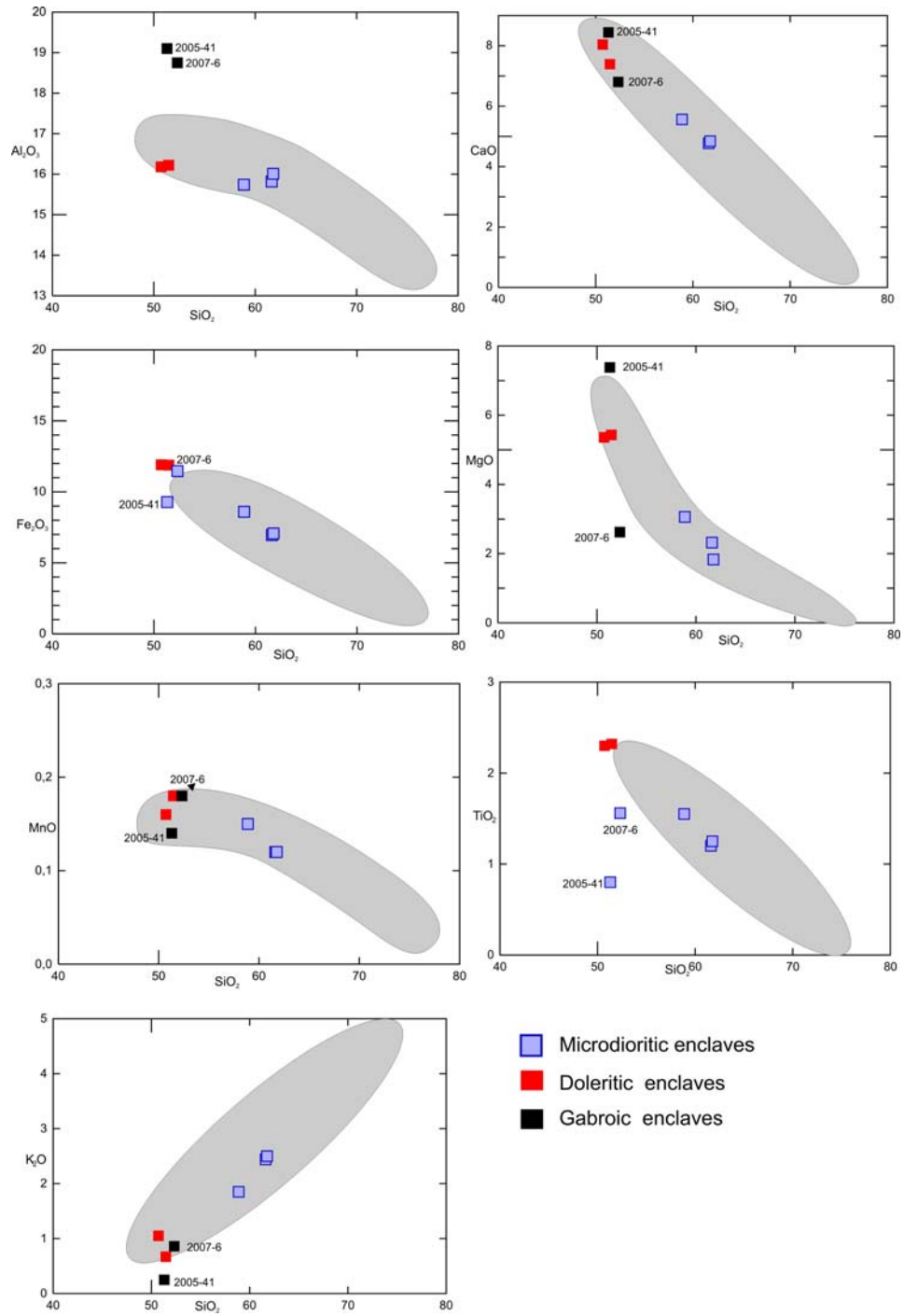


Figure 6.14 Major oxide variation diagrams of the Süphan enclaves (Shaded field represents the Süphan volcanics).

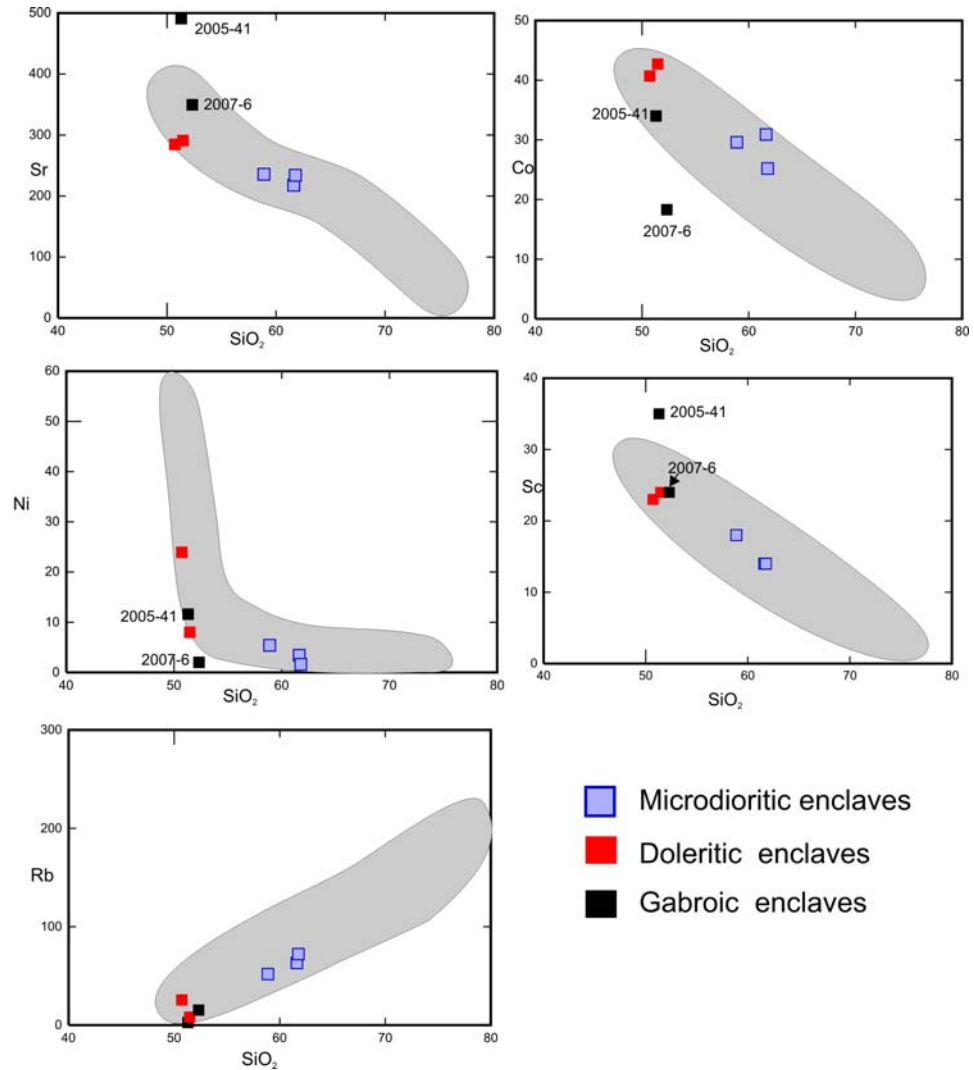


Figure 6.15 Trace element variation diagrams of Süphan enclaves (Shaded field represents the Süphan volcanics).

Fine grained gabbroic enclave, collected from the trachytic lava flows, has a different pattern from the other enclaves and the Süphan volcanics. It is depleted in HFS elements relative to the MORB and has distinct negative Nb and Ta troughs ($Rock/MORB < 1$) similar to the arc volcanism (Figure 6.16c). It is also depleted in K and Rb relative to the other enclaves and the Süphan volcanics.

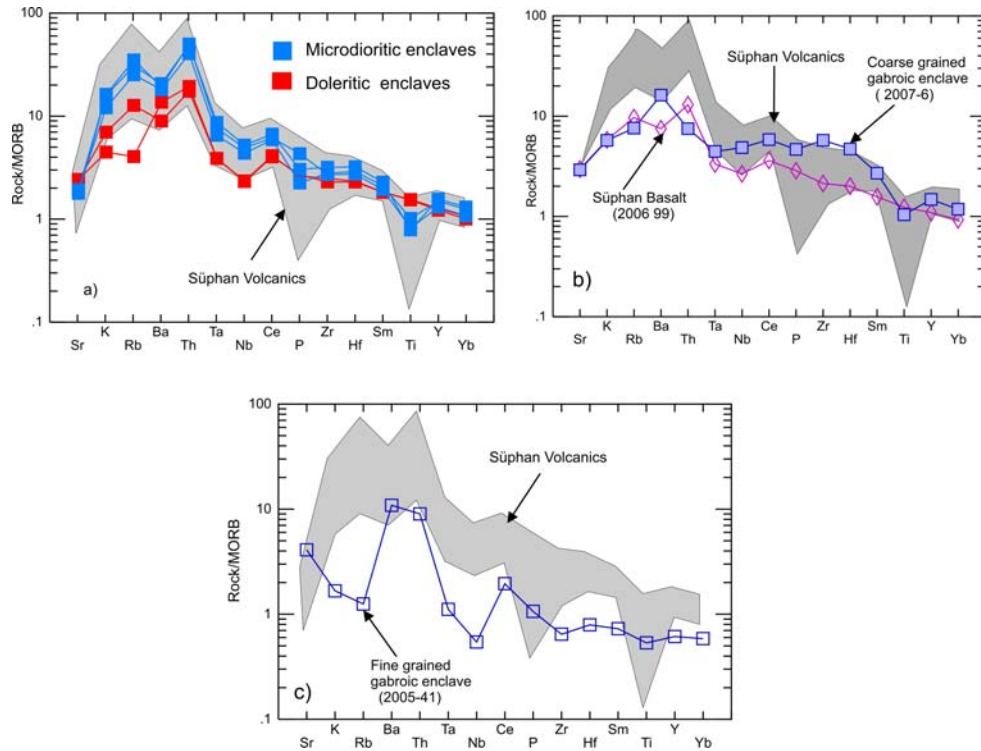


Figure 6.16 MORB normalized multi-element patterns of the Süphan enclaves (MORB normalizing values are from Pearce, 1983). (Shaded field represents the Süphan volcanics).

Chondrite normalized REE pattern of enclaves, except fine grained gabbroic sample, display patterns similar to those of Süphan volcanics (Figure 6.17). Fine grained gabbroic enclave (Sample No: 200 5 41) is depleted in REE contents relative to the other enclaves and the Süphan volcanics.

The observation that the doleritic and microdioritic enclaves have similar major, trace and RE element patterns with Süphan volcanics suggests that these enclaves are likely to represent the earlier products of the Süphan magmatism. The existence of the intersertial glass in microdioritic enclaves points to the presence of a crystal mush (not

completely solidified) at the sides and the roof of the magma chamber(s) from which and/or through which the host lavas were erupted.

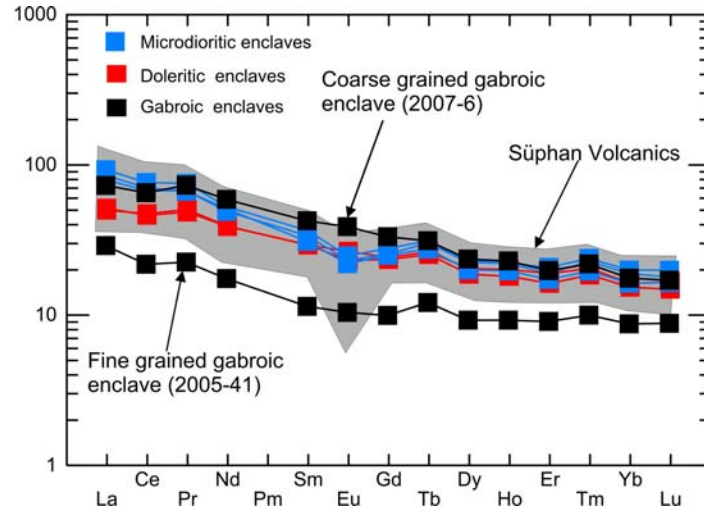


Figure 6.17 Chondrite normalized REE patterns of Süphan enclaves (Chondrite normalizing values are from Nakamura, 1974). (Shaded field represents the Süphan volcanics).

6.4 Isotope Geochemistry

Sr, Nd and Pb isotopic compositions of selected Süphan volcanics and enclaves are given in table 6.2. As can be seen from the table $^{87}\text{Sr}/^{86}\text{Sr}$, $^{143}\text{Nd}/^{144}\text{Nd}$, $^{208}\text{Pb}/^{204}\text{Pb}$, $^{207}\text{Pb}/^{204}\text{Pb}$ and $^{206}\text{Pb}/^{204}\text{Pb}$ ratios of Süphan volcanics are ranging between 0.703925 – 0.709579, 0.512520-0.512819 , 39.0585-39.4353, 15.6633-15.6943, and,19.0222-19.5497 respectively. $^{87}\text{Sr}/^{86}\text{Sr}$, $^{143}\text{Nd}/^{144}\text{Nd}$, $^{208}\text{Pb}/^{204}\text{Pb}$, $^{207}\text{Pb}/^{204}\text{Pb}$ and $^{206}\text{Pb}/^{204}\text{Pb}$ ratios of enclaves are in the range of 0.704596 - 0.706647, 0.512613 -0.512805, 39.2055-39.2690, 15.6757-15.6848 and 19.1849-19.1943, respectively.

The samples show relatively large variations in Sr-isotope composition (ϵ_{Sr} : -15.25 to +64.95) and moderate variations in ϵ_{Nd} values (-2.3 to + 3.5). The more radiogenic sample belongs to the older obsidian lava (sample 2005 69). On $^{87}\text{Sr}/^{86}\text{Sr}$ versus $^{143}\text{Nd}/^{144}\text{Nd}$ plot (Figure 6.18) mildly alkaline rocks (basalt, older basaltic trachy andesites (3) and older trachyandesitic (4) samples, a microdioritic enclave and a trachytic sample plot in the depleted quadrant of the diagram, however young transitional basaltic trachyandesites (4), trachyandesites, dacites, rhyolites and coarse grained gabbroic enclave plot in the enriched part of the diagram. Süphan volcanics display similar Nd-Sr isotopic compositions with Samoa, Society Islands and Kerguelen OIB mantle sources (Figure 6.18) which have Enriched Mantle (EM) components in their source regions. Similar to Figure 6.18, on Pb-Nd (Figure 6.19a) and Pb-Sr (Figure 6.19b) isotope plots Süphan volcanics fall between the mantle sources of MORB and EM II. On Pb-Pb, isotope plot, volcanic samples display radiogenic $^{208}\text{Pb}/^{204}\text{Pb}$, $^{207}\text{Pb}/^{204}\text{Pb}$ and $^{206}\text{Pb}/^{204}\text{Pb}$ values (Table 6.2, Figure 6.19c) and all samples are clustering in the EM II source region. (Figure 6.19c)

Table 6.2 Isotope compositions of the selected Süphan Volcanics.

Sample No	Rock Type	$^{143}\text{Nd}/^{144}\text{Nd} \pm 2\sigma$	$^{87}\text{Sr}/^{86}\text{Sr} \pm 2\sigma$	$^{208}\text{Pb}/^{204}\text{Pb} \pm 2\sigma$	$^{207}\text{Pb}/^{204}\text{Pb} \pm 2\sigma$	$^{206}\text{Pb}/^{204}\text{Pb} \pm 2\sigma$	ϵNd	ϵSr
2006-99	<i>Basalt</i>	0.512819 ± 7	0.703925 ± 7	39.0568 ± 20	15.6628 ± 7	19.0359 ± 9	3.53	-15.25
2005-61	<i>Bas. trachyand.</i>	0.512588 ± 6	0.706199 ± 7	-	-	-	-0.98	17.01
2005-62	<i>Bas. trachyand.</i>	0.512730 ± 7	0.704833 ± 8	39.1542 ± 20	15.6709 ± 7	19.1148 ± 10	1.79	-2.37
2005-68	<i>Bas. trachyand.</i>	0.512785 ± 6	0.706667 ± 8	39.2279 ± 21	15.6943 ± 8	19.0249 ± 9	2.87	23.65
2006-1	<i>Bas. trachyand.</i>	0.512615 ± 6	0.705939 ± 8	39.2198 ± 22	15.6888 ± 9	19.0245 ± 9	-0.45	13.32
2006-112	<i>Bas. trachyand.</i>	0.512739 ± 8	0.704680 ± 7	39.1258 ± 20	15.6779 ± 9	19.0549 ± 10	1.97	-4.54
2006-114	<i>Bas. trachyand.</i>	0.512577 ± 7	0.706764 ± 9	39.2213 ± 24	15.6932 ± 8	19.0222 ± 10	-1.19	25.02
2005-59	<i>Trachyand.</i>	0.512628 ± 6	0.706446 ± 7	39.2231 ± 23	15.6904 ± 8	19.0626 ± 9	-0.20	20.51
2006-6	<i>Trachyand.</i>	0.512774 ± 6	0.704683 ± 8	39.1234 ± 22	15.6760 ± 8	19.0537 ± 10	2.65	-4.5
2006-8	<i>Trachyand.</i>	-	0.707037 ± 8	39.2594 ± 31	15.6923 ± 9	19.0709 ± 12	-	28.89
2006-72	<i>Trachyand.</i>	0.512773 ± 7	0.704909 ± 8	39.1592 ± 47	15.6693 ± 14	19.1408 ± 19	2.63	-1.29
2006-74	<i>Trachyand.</i>	0.512520 ± 6	0.707180 ± 8	39.2649 ± 21	15.6991 ± 7	19.0296 ± 13	-2.30	30.92
2006-105	<i>Trachyand.</i>	0.512616 ± 10	0.706701 ± 7	39.2400 ± 37	15.6922 ± 14	19.0656 ± 15	-0.43	24.13
2005-10	<i>Trachyte</i>	0.512785 ± 6	0.705012 ± 8	39.1508 ± 18	15.6774 ± 7	19.1164 ± 7	2.87	0.17
2005-57	<i>Trachyte</i>	-	-	39.1489 ± 18	15.6745 ± 7	19.1281 ± 8	-	-
2006-59	<i>Trachyte</i>	0.512766 ± 7	0.704948 ± 8	39.1740 ± 20	15.6732 ± 8	19.1202 ± 9	2.50	-0.74
2007-2	<i>Trachyte</i>	0.512839 ± 6	0.704706 ± 8	39.0929 ± 19	15.6734 ± 8	19.0604 ± 9	3.92	-4.17
2005-28	<i>Dacite</i>	0.512660 ± 6	0.706387 ± 7	-	-	-	0.43	19.67
2006-110	<i>Dacite</i>	0.512765 ± 6	0.705566 ± 8	39.2433 ± 20	15.6738 ± 7	19.2392 ± 8	2.48	8.03
2007-4	<i>Dacite</i>	0.512670 ± 8	0.706270 ± 8	39.2622 ± 22	15.6853 ± 7	19.1918 ± 8	0.62	18.01
2005-69	<i>Rhyolite</i>	0.512691 ± 7	0.709579 ± 8	39.2329 ± 21	15.6766 ± 8	19.1162 ± 8	1.03	64.95
2007-5	<i>Rhyolite</i>	0.512801 ± 7	0.705238 ± 8	39.4335 ± 24	15.6783 ± 9	19.5498 ± 8	3.18	3.38
2005-52	<i>Rhyolite</i>	0.512805 ± 6	0.705252 ± 8	-	-	-	3.26	3.57
2005-4A	<i>Enclave</i>	0.512805 ± 7	0.704596 ± 8	39.2055 ± 41	15.6757 ± 15	19.1849 ± 20	3.26	-5.73
2007-6	<i>Enclave</i>	0.512613 ± 6	0.706647 ± 8	39.2690 ± 21	15.6848 ± 9	19.1943 ± 11	-0.49	23.36

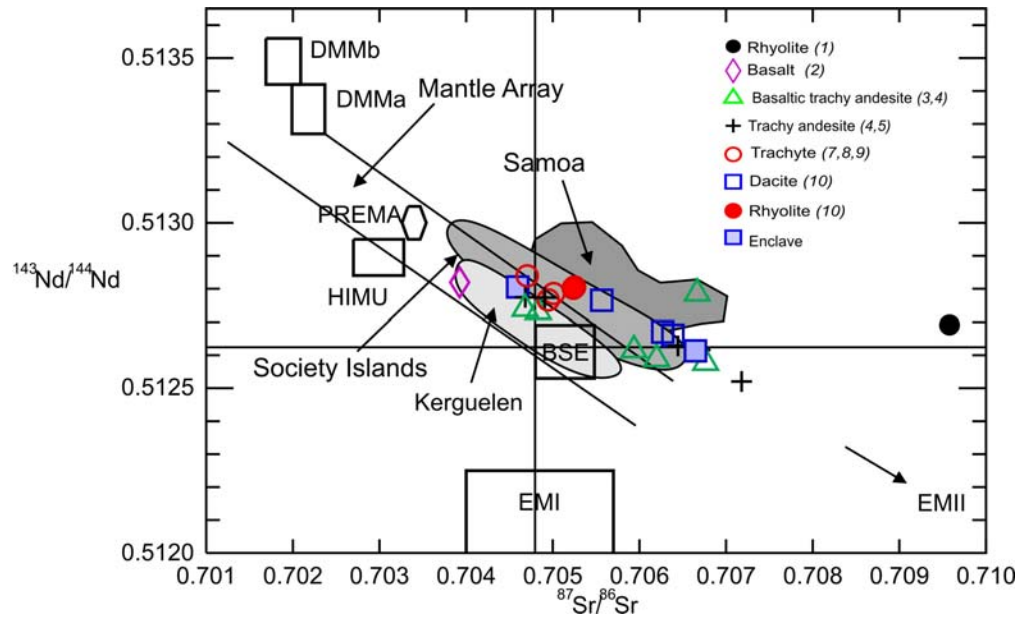


Figure 6.18 $^{143}\text{Nd}/^{144}\text{Nd}$ versus $^{87}\text{Sr}/^{86}\text{Sr}$ diagram of the Süphan volcanics (Data sources are from Zindler et al., 1982, Hart 1984b, Zindler and Hart 1986) Number in parenthesis in the legend correspond to the units in Figure 3.2.

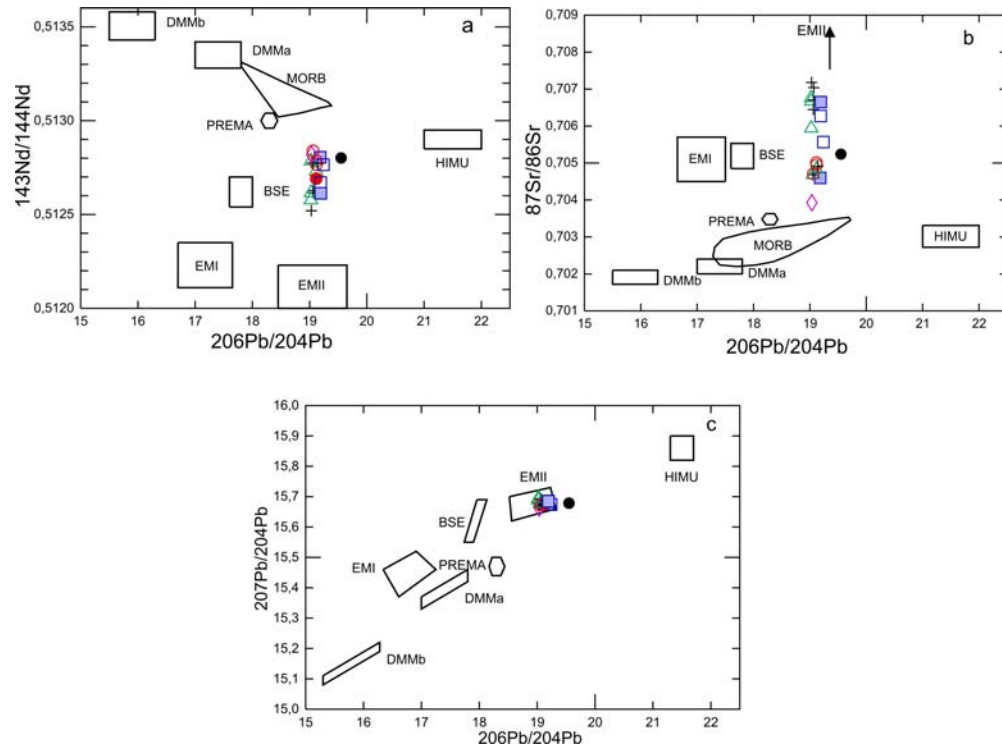


Figure 6.19 a) $^{143}\text{Nd}/^{144}\text{Nd} - ^{206}\text{Pb}/^{204}\text{Pb}$ b) $^{87}\text{Sr}/^{86}\text{Sr} - ^{206}\text{Pb}/^{204}\text{Pb}$ c) $^{207}\text{Pb}/^{204}\text{Pb} - ^{206}\text{Pb}/^{204}\text{Pb}$ isotop correlation diagrams of the Süphan volcanics (symbols are same as Figure 6.18, mantle reservoirs are taken from Zindler and Hart 1986).

CHAPTER 7

MINERAL CHEMISTRY

Minerals and glasses were analysed by electron microprobe (EMPA) at the University of Bristol using a CAMECA SX-100 five-spectrometer (WDS) instrument. Minerals were analyzed using a 20 kV accelerating voltage, 10 nA beam current and a 5 μ m beam diameter. Groundmass glasses and melt inclusions were analysed using a 15 kV accelerating voltage, 2-4 nA beam current and a 15 μ m beam diameter to minimize alkali migration (Humphreys et al. 2006). Calibration was carried out on a variety of natural and synthetic minerals and glasses. Data reduction used the PAP routine.

Electron microprobe analysis were carried on 15 different rock samples ranging compositions from basalts to rhyolites. Core and rim compositions of phenocrysts and core compositions of microlites obtained from these analysis.

In order to illustrate the evolution of mineral chemistry with changing host rock SiO₂ contents, a series of stacked histograms ranked downwards in order of increasing SiO₂ were presented. Selected mineral data are presented in Tables 7.1-7.5; the full dataset can be found in Appendix B.

Olivine

Olivine (Figure 7.1, Table 7.1) occurs in basalt, basaltic trachyandesites and trachyandesites as euhedral to subhedral phenocrysts. All crystals are normally zoned with Fo-rich cores. Olivine compositions (core, rim and microlite) display a wide range: Fo₅₃₋₈₀ for basalts; Fo₅₂₋₇₁ for basaltic trachyandesites; and Fo₃₇₋₇₅ for trachyandesites. Olivine microlite compositions have the lowest Fo values in basalts whereas microlites in basaltic trachyandesites overlap with phenocrysts compositions. Fo compositions of olivines decrease, in general, from basalt to trachyandesite, however one trachyandesitic sample (2006-6) contains olivine with core compositions (Fo₇₅) similar to those in basalt (Özdemir et al., 2011).

Clinopyroxene

Clinopyroxene (Figure 7.2 Table 7.2) is present in basalts to dacites with decreasing abundance. Clinopyroxene occurs in basaltic rocks as needle-like microcrysts, but forms phenocrysts in intermediate and acidic rocks. Most phenocrysts are augite, although diopside sometimes occurs in the rims of the phenocrysts in dacites. Augites are Ca-rich and have compositions in the range En₂₄₋₄₅, Fe₁₅₋₃₃, Wo₃₅₋₄₄.

Most clinopyroxenes are weakly normally-zoned. The mg-number of clinopyroxenes in basalts and dacites have limited ranges of 76-80 and 64-71, respectively. However mg-numbers of clinopyroxenes in basaltic trachyandesites, trachyanadesites, and trachytes display wide ranges between these two extremes (Özdemir et al., 2011).

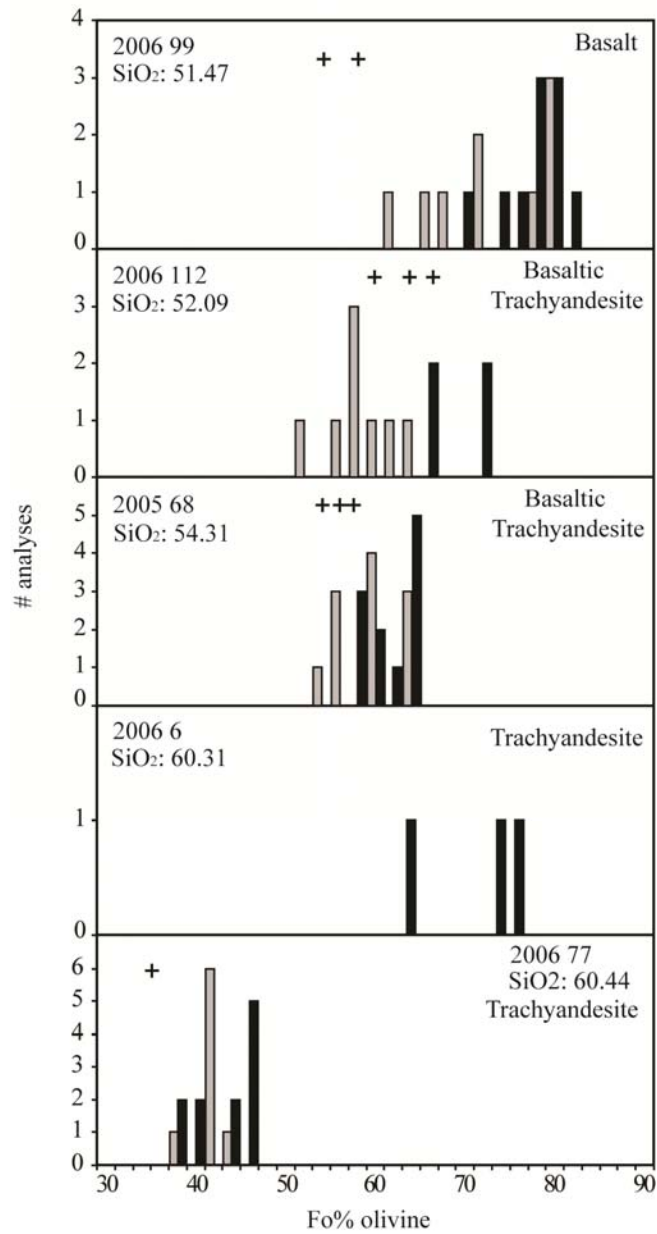


Figure 7.1 Frequency distribution diagrams for core, rim and microlite compositions of olivine. Black colored bars indicate core compositions, gray colored bars indicate rim compositions, crosses indicate microlites.

Table 7.1 Representative olivine compositions. FC, phenocryst sized free crystal; M, microlite

Sample	2006 99	2006 99	2006 99	2006 112	2006 112	2006 112	2005 68	2005 68	2005 68	2006 77	2006 77	2006 77	2006 6	2006 6
Grain	ol2c	ol2r	ol13c	ol1c	ol1r	olm2	ol3c	ol3r	olmic5	ol5c	ol5r	olmic1	ol1c	ol2c
Crystal type	FC	FC	M	FC	FC	FC	FC	FC	M	FC	FC	M	FC	FC
Position	core	rim	core	core	rim	core	core	rim	core	core	rim	core	core	core
SiO ₂	38.95	37.29	35.49	37.93	36.41	36.65	35.51	35.17	35.66	34.01	33.84	33.28	38.87	38.54
TiO ₂	0.01	0.03	0.06	0.02	0.03	0.04	0.05	0.16	0.04	0.04	0.01	0.08	0.01	0.01
Al ₂ O ₃	0.07	0.00	0.01	0.02	0.01	0.03	0.03	0.01	0.01	0.00	0.00	0.03	0.02	0.02
Cr ₂ O ₃	0.02	0.02	0.00	0.01	0.02	0.00	0.00	0.00	0.00	0.00	0.00	0.00	0.00	0.00
FeO	21.26	28.22	38.58	25.46	34.14	32.70	36.38	39.33	37.76	44.36	45.88	48.41	22.77	23.89
MnO	0.32	0.50	0.68	0.33	0.57	0.53	0.63	0.69	0.67	0.78	0.95	1.15	0.37	0.35
MgO	39.60	33.50	25.01	35.70	28.54	30.38	28.38	25.59	26.78	20.89	19.84	16.58	38.02	38.28
NiO	0.12	0.07	0.06	0.12	0.07	0.06	0.04	0.00	0.04	0.04	0.00	0.03	0.11	0.04
CaO	0.25	0.29	0.34	0.28	0.27	0.26	0.26	0.32	0.29	0.25	0.27	0.55	0.19	0.187
Total	100.60	99.92	100.24	99.92	100.12	100.70	101.28	101.28	101.24	100.37	100.81	100.10	100.36	101.3
Fo %	76.6	67.5	53.2	71.2	59.4	62.0	57.8	53.3	55.4	45.2	43.0	37.4	74.6	73.8

Table 7.2 Representative pyroxene compositions. FC, phenocryst sized free crystal; M,microlite

Sample	2006 99	2006 112	2005 68	2006 8	2006 8	2005 10	2005 10	2006 110	2006 112	2006 8	2006 8	2008 4	2007 4	2005 69	2005 69
Grain	cpx9c	cpx6c	cpx6	cp5c	cp5r	cp5cT	cp5rT	cpx2c	opx2c	op1r	op7c	op7c	op4c	opx1c	opx1r
Crystal type	M	FC	M	FC	FC	FC	FC	FC	FC	FC	FC	FC	FC	FC	FC
Position	core	core	core	core	rim	core	rim	core	core	rim	core	core	core	core	rim
SiO ₂	50.31	50.52	49.98	49.86	50.24	51.72	51.94	51.93	53.55	49.37	51.09	51.40	50.86	46.79	46.59
TiO ₂	1.69	1.90	1.41	0.31	0.48	0.43	0.40	0.24	0.49	0.16	0.21	0.14	0.11	0.13	0.10
Al ₂ O ₃	2.47	3.55	4.52	1.31	1.48	1.56	1.43	1.01	1.63	0.32	0.79	0.43	0.27	0.53	0.52
FeO	9.65	10.02	14.35	18.04	17.83	12.50	12.60	12.81	16.57	36.43	26.98	29.55	32.53	44.20	43.48
MnO	0.27	0.25	0.45	0.65	0.68	0.49	0.45	0.74	0.40	1.32	0.85	0.97	2.04	1.52	1.39
MgO	13.89	13.22	13.42	10.87	10.64	13.12	13.20	13.10	24.81	10.64	19.53	16.62	14.05	6.04	6.31
CaO	20.59	20.21	16.83	17.99	18.46	20.62	20.16	20.12	2.24	1.72	1.50	1.44	1.02	0.71	0.57
K ₂ O	0.01	0.04	0.07	0.09	0.01	0.01	0.02	0.01	0.01	0.00	0.02	0.03	0.00	0.01	0.00
Na ₂ O	0.52	0.55	1.17	0.37	0.36	0.33	0.34	0.25	0.07	0.07	0.12	0.02	0.02	0.01	0.00
Total	99.41	100.3	102.19	99.50	100.17	100.78	100.55	100.20	99.76	100.04	101.08	100.60	100.89	99.93	98.97
En	40.5	39.44	39.7	31.7	31.0	37.2	37.7	37.2	69.0	32.2	53.9	47.8	41.1	18.7	19.8
Fs	16.3	17.2	24.6	30.6	30.3	20.7	20.9	21.6	26.5	64.1	43.1	49.2	56.8	79.7	78.9
Wo	43.2	43.36	35.8	37.7	38.7	42.1	41.4	41.1	4.5	3.7	3.0	3.0	2.1	1.6	1.3
mg no	76.0	70.79	71.7	56.7	55.0	69.3	68.1	67.5	72.7	34.3	60.1	50.6	43.6	20.1	21.0

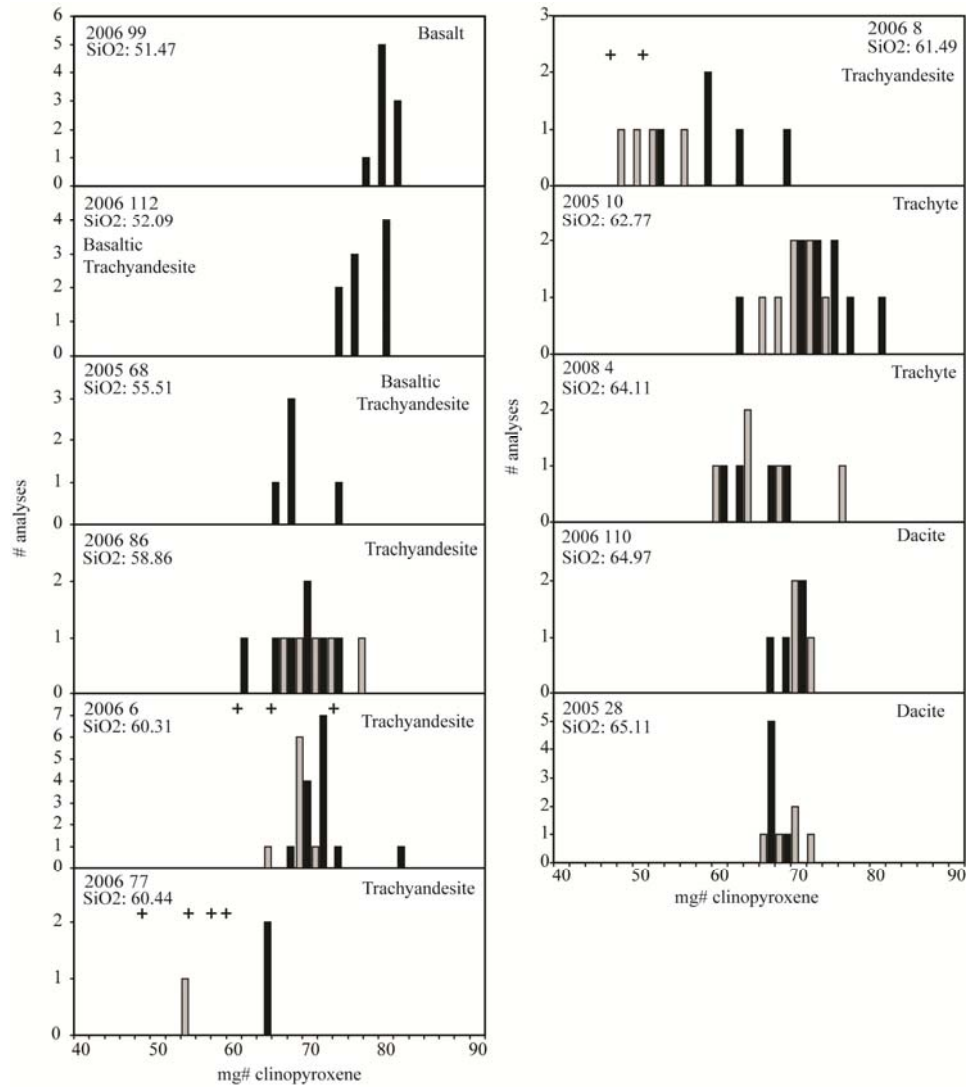


Figure 7.2 Frequency distribution diagrams for core, rim and microlite compositions of clinopyroxene. Black colored bars indicate core compositions, gray colored bars indicate rim compositions, crosses indicate microlites.

Orthopyroxene

Orthopyroxene (Figure 7.3, Table 7.2) is present in basaltic trachyandesites to rhyolites with increasing abundance. Orthopyroxenes ranges from enstatite to ferrosilite, with 1-4 mol% wollastonite component. Although there is quite considerable compositional overlap between samples, an older rhyolitic lava (2005-69) with distinctly lower mg# has higher FeO and lower CaO content than those from the other lavas. As for clinopyroxenes, the basalts and rhyolites show relatively limited ranges in mg-number (74-76 and 19-27, respectively), whereas intermediate rocks show a marked range between these two extremes. Ferrosilite compositions increase towards the felsic members. Trachyandesite sample 2006-8 is particularly remarkable in this regard with a range in mg-number from 34 to 60. Normally-zoned orthopyroxene phenocrysts with Mg-rich cores coexist with reversely-zoned orthopyroxene phenocrysts with Mg-rich rims in a single rock (Samples; 2005-10, 2006-6, 2006-86, 2006-110, 2008-4).

Feldspars

Plagioclase (Figure 7.4, Table 7.3) is the most abundant phenocryst and groundmass phase in all Süphan lavas. Plagioclase phenocrysts (An_{52-67}) in basalt typically display reverse zoning with cores slightly more An-rich than rims. Some display weakly oscillatory zoning. Microlite compositions are An_{48-59} in basalts. Some plagioclase phenocrysts contain inclusions of olivine, clinopyroxene and Fe-Ti oxides. Plagioclase in basaltic trachyandesites ranges between An_{40-54} (phenocrysts) and An_{36-50} (microlites). They also show normal, reverse and weakly oscillatory zoning. Most of them include pyroxene, olivine and Fe-Ti oxides. Only in one basaltic trachyandesitic rock (2006-77) is plagioclase found as inclusions in olivine and pyroxene minerals

suggesting plagioclase as the first crystallising phase (before olivine and pyroxenes) during fractionation.

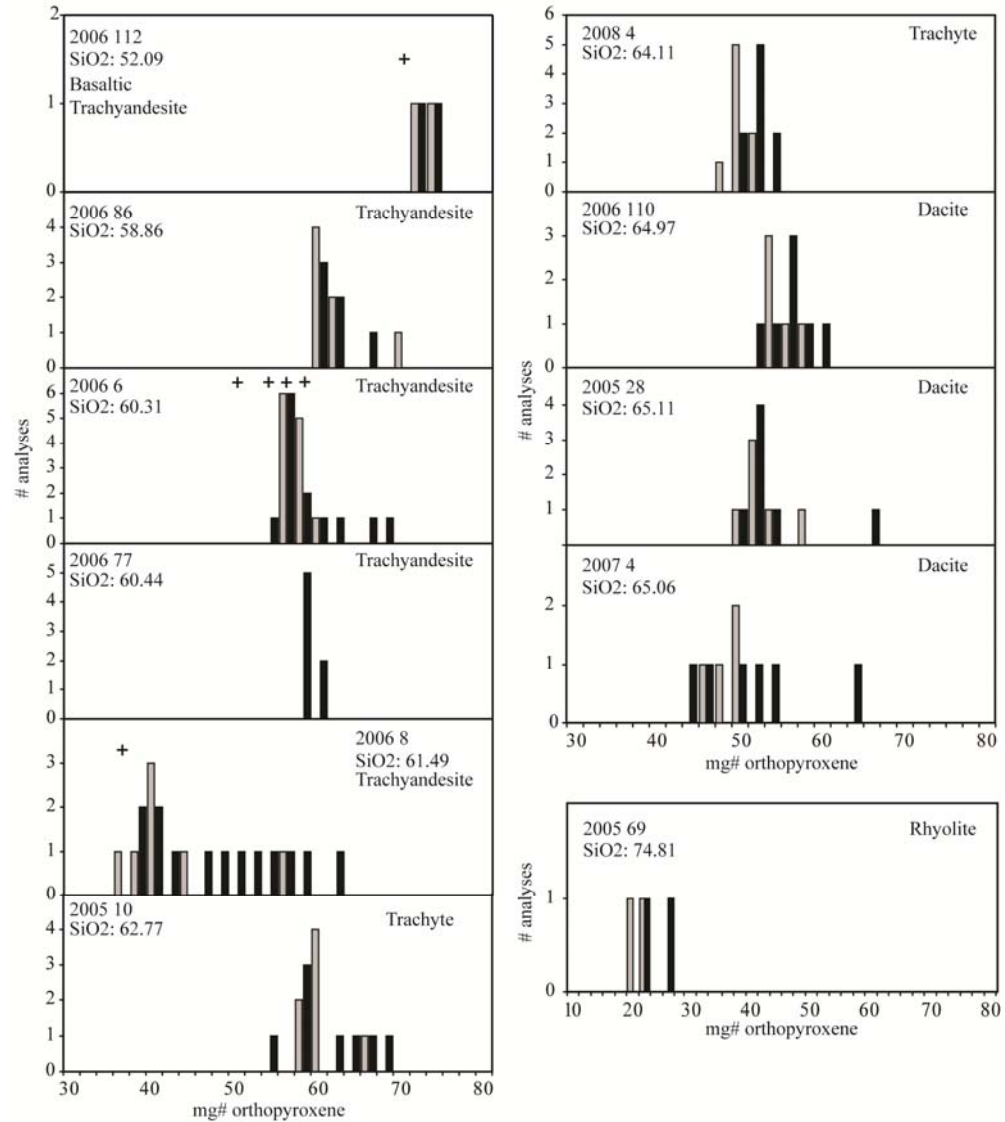


Figure 7.3 Frequency distribution diagrams for core, rim and microlite compositions of orthopyroxene. Black colored bars indicate core compositions, gray colored bars indicate rim compositions, crosses indicate microlites.

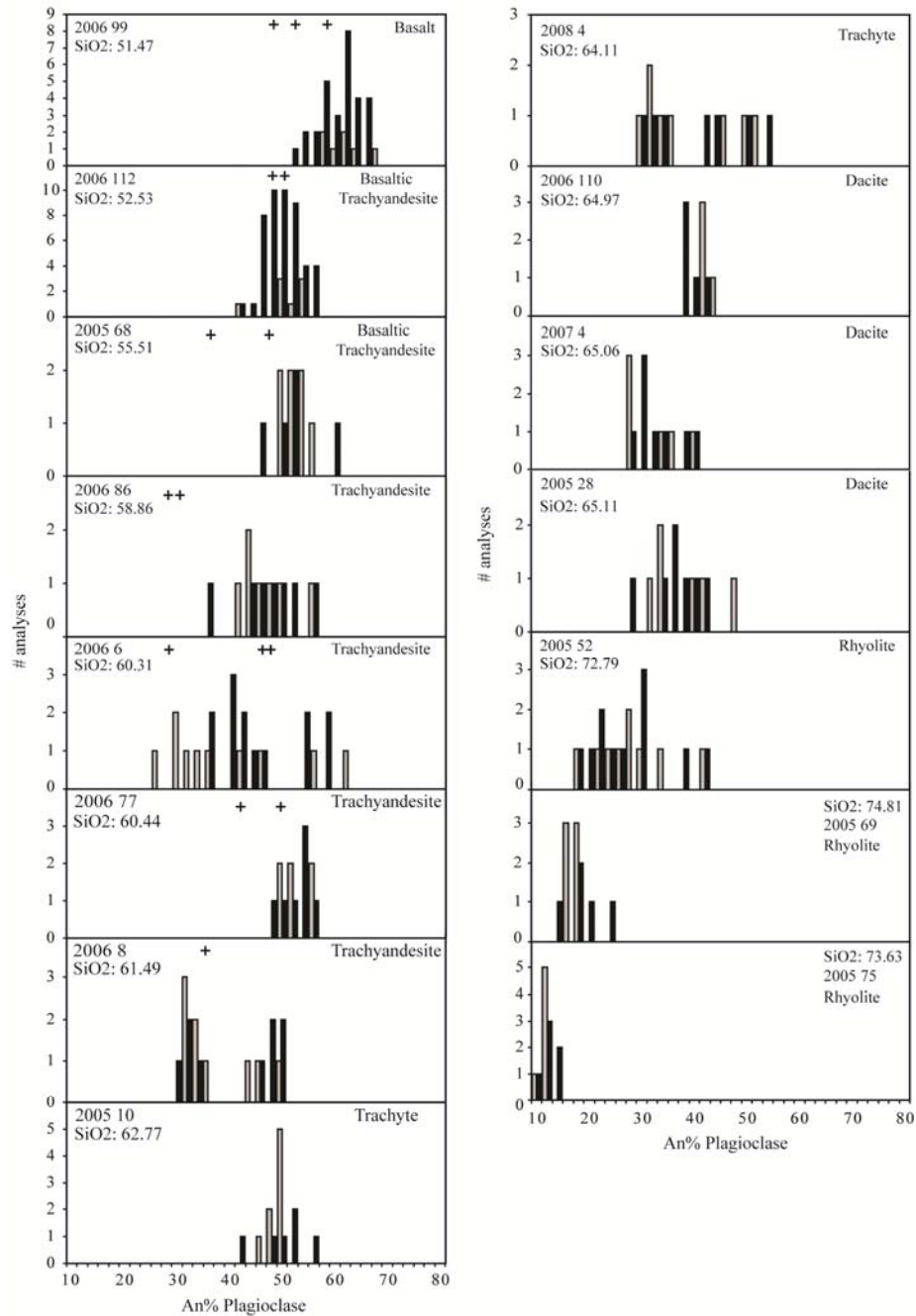


Figure 7.4 Frequency distribution diagrams for core, rim and microlite compositions of plagioclase. Black colored bars indicate core compositions, gray colored bars indicate rim compositions, crosses indicate microlites.

Plagioclases in trachytes and trachyandesites have similar textures to those in basaltic trachyandesites and most have melt, pyroxene and Fe-Ti inclusions indicating relatively late crystallisation. An content of phenocrysts displays a wide range (An_{25-61} in trachyandesites; An_{29-56} in trachytes); this is more apparent in samples 2006-6 and 2006-8. The majority of phenocrysts display reverse and weakly oscillatory zoning. Microlite compositions are An_{27-51} . Compositions of plagioclases in crystal clots in these lavas overlap with those of phenocrysts in the same sample. The amount of the plagioclase is markedly less in dacites and rhyolites. Plagioclase compositions in dacites are in the range An_{26-47} , displaying oscillatory and reverse zoning. An content of rhyolites are in the range An_{9-41} . The older rhyolitic samples (2005 69, 2005 75) have the lowest An content (An_{10-23}). Plagioclases in dacites and rhyolites are also found as inclusions in amphiboles and biotites.

In summary, plagioclase compositions tell a similar tale to olivine and pyroxenes, with relatively limited compositional range in the highest and lowest SiO_2 rocks and quite a wide range in intermediate rocks. K-feldspars are only found in rhyolitic samples and are sanidine in composition (ranging between $An_{1-2} Or_{61-82}$).

Table 7.3 Representative feldspar compositions. FC, phenocryst sized free crystal; M, microlite

Sample	2006 99	2006 99	2006 112	2006 112	2006 86	2005 10	2005 10	2005 28	2005 28	2005 75	2005 75	2005 52	2005 52	2005 75	2005 75
Grain	p1c	p1r	pl12c	pl12r	pl1mic	pl5c	pl5r	pl5c	pl5r	pl3c	pl3r	kf3c	kf3r	kf6c	kf6r
Crystal type	FC	FC	FC	FC	M	FC	FC	FC	FC	FC	FC	FC	FC	FC	FC
Position	core	rim	core	rim	core	core	rim	core	rim	core	rim	core	rim	core	rim
SiO ₂	53.22	51.38	55.54	54.69	61.21	58.45	56.74	58.12	56.25	64.70	64.96	65.02	63.32	65.28	64.88
TiO ₂	0.096	0.087	0.12	0.10	0.18	0.02	0.04	0.03	0.02	0.01	0.01	0.01	0.02	0.00	0.00
Al ₂ O ₃	28.79	30.29	27.30	27.77	23.19	27.88	26.45	25.78	27.02	21.84	21.42	18.82	18.90	18.80	18.67
FeO	0.51	0.51	0.53	0.51	0.77	0.38	0.37	0.29	0.30	0.06	0.05	0.07	0.08	0.03	0.04
MnO	0.01	0.00	0.02	0.00	0.00	0.00	0.04	0.00	0.01	0.00	0.00	0.00	0.00	0.01	0.00
MgO	0.12	0.09	0.10	0.10	0.04	0.04	0.05	0.01	0.00	0.00	0.00	0.00	0.00	0.00	0.00
CaO	12.36	13.41	10.07	10.85	5.68	10.14	9.78	8.54	10.07	2.77	2.37	0.16	0.17	0.10	0.12
Na ₂ O	4.76	4.16	5.91	5.23	7.10	5.88	6.12	6.57	5.89	9.74	9.54	3.10	2.99	3.54	3.54
K ₂ O	0.25	0.20	0.55	0.42	1.33	0.39	0.31	0.55	0.42	0.96	1.05	11.36	10.92	11.21	11.02
Total	100.13	100.12	100.14	99.66	99.51	103.18	99.91	99.89	99.98	100.07	99.39	98.54	96.41	98.98	98.28
An	58.1	63.4	47.0	52.1	28.2	47.7	46.1	40.5	47.4	12.9	11.3	0.8	0.9	0.5	0.6
Ab	40.5	35.5	49.9	45.5	63.9	50.1	52.2	56.4	50.2	81.8	82.7	29.1	29.1	32.2	32.6
Or	1.4	1.1	3.1	2.4	7.9	2.2	1.7	3.1	2.4	5.3	6.0	70.1	70.0	67.3	66.8

Amphibole

Euhedral and subhedral calcic amphibole phenocrysts are found in trachytes, dacites and rhyolites (Table 7.4). Following the nomenclature of Leake (1978), compositions are magnesiohastingsite-edenite in trachytes, and magnesiohornblende, tschermakite, edenite and ferrohornblende in dacites and rhyolites. Some amphibole phenocrysts show normal and reverse zoning with decreasing or increasing mg# from core to rim. Most amphiboles have opaque rims due to partial reaction and breakdown.

Biotite

Biotite is the most abundant ferromagnesian mineral in rhyolites and it also occurs occasionally in dacites (Table 7.4). Both normally and reverse-zoned crystals were found. Mg# of biotites range between 51-55 for dacites and 7-43 for rhyolites.

Fe-Ti Oxides

Fe-Ti oxides are titanomagnetite and ilmenite, typically occurring as coexisting groundmass crystals and as inclusions in the other phenocrysts. Rarely they occur as phenocrysts. Ulvospinel contents decrease from ≤ 83 mol % in basalt to 14-15 mol% in rhyolites; there is a correspondingly lesser change in the ilmenite content from 97 mol% to 85 mol% (Table 7.5).

Table 7.4 Representative amphibole and biotite compositions. FC, phenocryst sized free crystal; M, microlite

Sample	2008 4	2008 4	2005 28	2005 28	2006 110	2006 110	2005 52	2005 52	2005 69	2005 69	2005 52	2005 52
Grain	a1c	a1r	a2c	a2r	a5c	a5r	amp1c	amp3r	bio1c	bio1r	bio2c	bio2r
Crystal type	FC	FC	FC	FC	FC	FC	FC	FC	FC	FC	FC	FC
Position	core	rim	core	rim	core	rim	core	rim	core	rim	core	rim
SiO ₂	42.99	43.01	46.26	44.92	49.15	50.77	45.96	43.51	33.41	33.31	35.48	34.57
TiO ₂	2.47	2.65	1.94	2.18	0.92	0.63	1.28	1.75	4.80	5.19	3.20	3.61
Al ₂ O ₃	9.92	8.63	6.95	7.97	4.34	2.72	6.51	8.33	14.03	13.71	13.76	14.01
FeO	18.49	18.88	17.76	18.21	12.98	11.15	20.15	20.09	30.02	30.99	23.42	25.43
MnO	0.32	0.08	0.38	0.39	0.48	0.49	0.98	0.75	0.19	0.25	0.58	0.60
MgO	10.61	10.57	12.02	11.51	13.11	13.67	9.65	9.20	4.26	4.36	9.30	7.80
CaO	10.98	10.65	11.24	11.19	17.62	19.61	10.81	11.03	0.02	0.03	0.01	0.02
Na ₂ O	3.06	2.67	1.75	1.97	0.68	0.46	1.48	1.65	0.56	0.42	0.52	0.50
K ₂ O	0.64	0.69	0.642	0.861	0	0.007	0.614	0.936	8.59	8.09	8.21	8.27
Total	99.47	97.84	98.93	99.19	99.28	99.50	97.43	97.24	95.89	96.35	94.48	94.81
mg no	57.7	58.2	64.5	62.7	78.5	86	54.8	52.7	20.2	20.1	41.5	35.4

Table 7.5 Representative Fe-Ti oxide compositions. FC, phenocryst sized free crystal; M,microlite

Sample	2006 99	2006 99	2006 112	2006 112	2005 68	2005 68	2006 6	2006 6	2005 10	2005 10	2005 52	2005 52
Grain	mag3T	il	mag2	il1	mag6T	il1T	mag1	il2	mag5T	il3T	mag3	il1T
Crystal type	M	M	M	M	M	M	M	M	M	M	M	M
Position	core	core	core	core	core	core	core	core	core	core	core	core
SiO ₂	0.09	0.03	0.24	0.20	0.09	0.04	0.06	0.01	0.12	0.06	0.05	0.07
TiO ₂	14.15	48.60	1.87	46.28	21.79	47.36	12.77	50.38	20.68	49.98	5.11	47.14
Al ₂ O ₃	0.88	0.07	1.46	0.29	1.94	0.18	1.27	0.06	1.32	0.10	1.45	0.08
FeO(T)	76.18	44.27	86.74	43.04	69.06	46.39	78.55	40.62	74.07	47.61	84.92	49.11
MnO	0.27	0.58	0.18	0.19	0.63	0.59	0.18	0.60	0.66	0.80	1.13	2.21
MgO	0.87	3.10	0.72	0.33	1.76	2.39	0.39	0.70	1.32	2.06	0.20	0.59
Cr ₂ O ₃	0.37	0.04	0.23	0.26	0.15	0.03	0.06	0.02	0.05	0.00	0.03	0.01
Total	92.80	96.70	91.44	90.59	95.43	96.98	93.28	92.39	98.22	100.62	92.90	99.21
X Usp	0.40		0.6		0.7		0.4		0.6		0.1	
X Ilm		0.90		1.0		0.9		1.0		0.9		0.9

7.1 Chemistry of Melt Inclusions and Glasses

Melt inclusions and groundmass glasses offer the advantage over whole-rocks of revealing true liquid compositions (e.g. Reubi & Blundy 2009), which may be obscured by liquid-crystal mixing processes in rocks, especially when they are porphyritic. Glassy melt inclusions were identified in plagioclase and olivine from basaltic trachyandesites, in orthopyroxene, plagioclase and olivine from trachyandesites, in orthopyroxene and plagioclase from trachytes, in amphibole, orthopyroxene and clinopyroxene from dacites, and in biotites from rhyolites.

Melt inclusions in olivine, plagioclase, pyroxene, amphibole and biotite are randomly distributed from core to rim (Figure 7.5a). Some of them contain daughter crystals including Fe-Ti oxides, indicative of post-entrapment modification (Figure 7.5b). The size of the melt inclusions is up to 150 μm . In total 171 inclusions were analyzed (66 in olivine, 39 in plagioclase, 30 in orthopyroxene, 3 in clinopyroxene, 9 in amphibole, 24 in biotite) together with 183 matrix glasses (Table 7.6, Appendix C). By selecting melt inclusions from a wide variety of host phenocrysts we are able to minimize any effects of post-entrapment modification, which should have a different chemical influence for different hosts. Glass chemistry is plotted in figure 7.6, alongside whole rocks for comparison. All compositions are discussed on an anhydrous basis, although the shortfall from 100% in the analytical totals suggests dissolved volatile contents of ≤ 7.7 wt%.

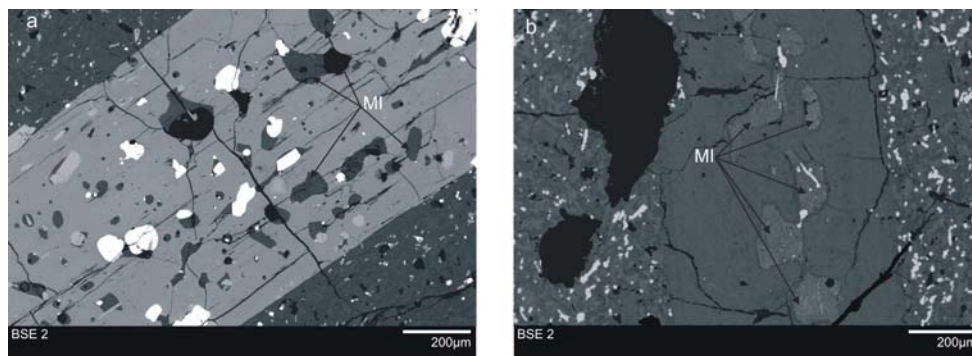


Figure 7.5 Melt inclusions (MIs) in Süphan volcanics a) BSE (Back-scattered Electron) image of MIs in orthopyroxene, MIs are randomly distributed from core to rim. b) BSE image of MIs in plagioclase, some of them contain some daughter crystals including Fe-Ti oxides.

Table 7.6 Representative compositions of melt inclusions and matrix glasses.

Sample	Melt Inclusions				Matrix Glasses		
	2005 68 pl3	2006 76 76_5	2006 1 6_11	2006 1 6_12	2006 86 G3	2005 10 G64	2005 28 G28
Host	pl	ol	ol	ol			
SiO ₂	71.10	61.48	63.00	63.07	70.48	73.09	76.63
TiO ₂	1.06	0.83	1.21	1.37	1.20	0.88	0.21
Al ₂ O ₃	12.90	17.06	15.33	15.25	13.32	12.52	10.49
FeO	1.98	1.40	2.12	1.21	3.63	2.15	0.81
MnO	0.05	0.00	0.06	0.00	0.05	0.06	0.00
MgO	0.30	0.30	0.74	0.05	0.33	0.12	0.00
CaO	0.56	0.42	2.68	0.82	0.82	0.32	0.26
Na ₂ O	5.10	4.42	2.96	4.99	4.06	3.77	2.26
K ₂ O	2.75	6.12	5.36	5.98	5.06	5.31	4.92
P ₂ O ₅	0.36	0.42	0.23	0.36	0.24	0.04	0.05
SO ₂	0.12	0.00	0.02	0.05	0.00	0.02	0.00
Cl	0.05	0.06	0.04	0.06	0.05	0.03	0.02
H ₂ O	3.68	7.46	6.25	6.74	0.75	1.69	4.29
Total	100.00	99.98	100.00	99.93	99.99	100.00	99.93

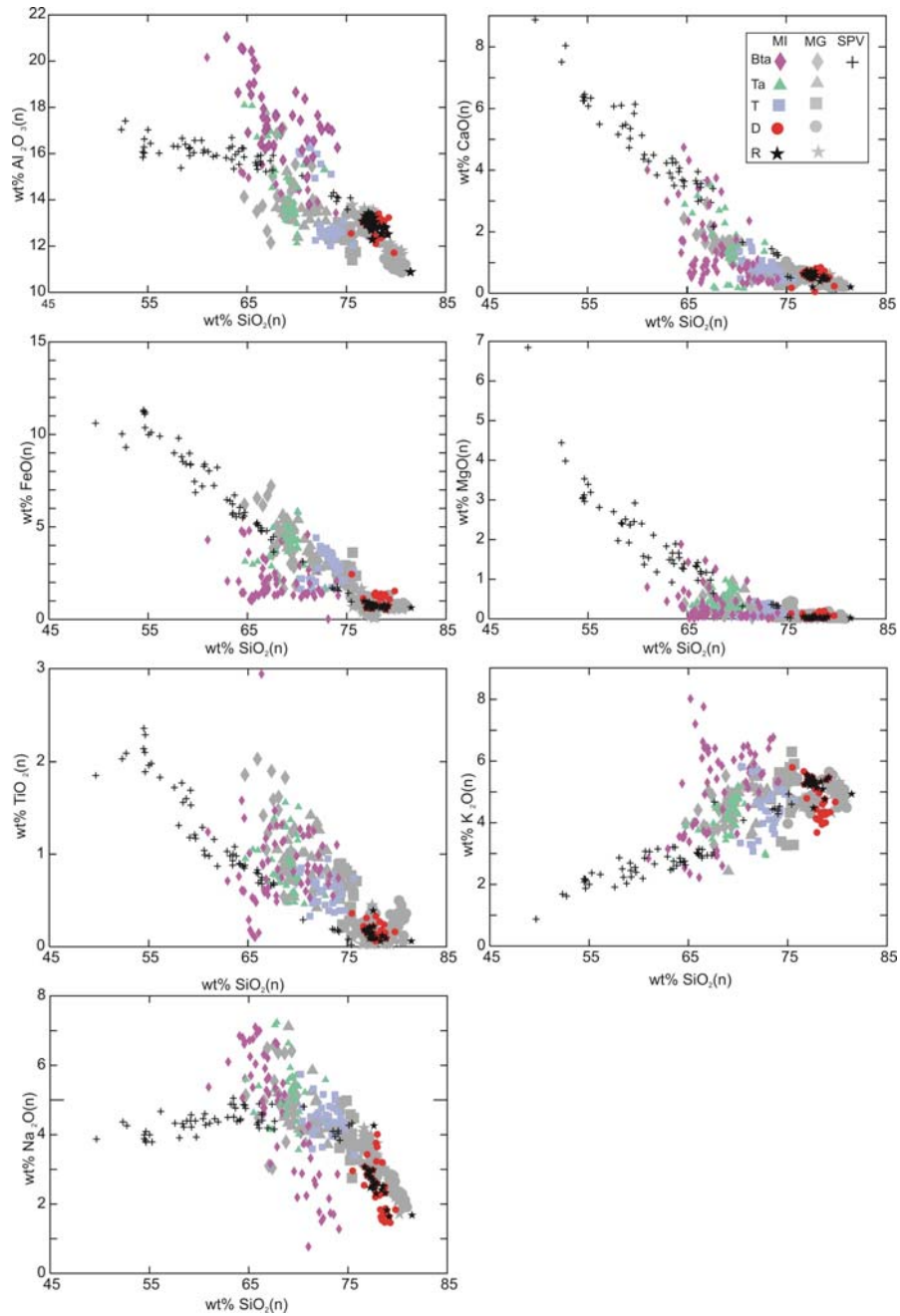


Figure 7.6 Major element variation diagrams for melt inclusions, matrix glasses and whole rocks of Süphan volcanics. (n) indicates anhydrous basis. Key to abbreviations: MI: melt inclusions, MG: matrix glasses, SPV: süphan volcanics, Bta: basaltic trachyandesite, Ta: trachyandesite, T: trachyte, D: dacite, R: rhyolite.

Melt inclusions (MI) from basaltic trachyandesites range in composition from trachyandesite to rhyolite with 61-74 wt% SiO₂ (on an anhydrous basis). The most striking features of melt inclusions in basaltic trachyandesites is the wide range of Al₂O₃, K₂O and Na₂O contents in the same sample. Relative to the whole rocks from Süphan, these melt inclusions are notably higher in Al₂O₃, Na₂O and K₂O, but lower in FeO, MgO and CaO. Matrix glasses in these rocks are trachyte and rhyolite with 65-72 percent SiO₂ (on an anhydrous basis). Most of them overlap with some part of the array defined by MI, however some of them are displaced to higher FeO and TiO₂ and lower Al₂O₃ content relative to the MIs. Again, there is rather poor correspondence between groundmass glasses and even the most evolved Süphan whole rocks.

Melt inclusions and matrix glasses from trachyandesites overlap in composition, from trachyte to rhyolite with 65-73 and 68-73 percent SiO₂, respectively. MIs in olivines and orthopyroxenes have higher Al₂O₃ and CaO content than those in plagioclases. There is some tendency to slightly higher Al₂O₃ and TiO₂ and lower CaO and MgO to MI in trachyandesites, but for the most part there is better correspondence between MI and the more evolved end of the whole-rock trend.

MI and matrix glasses from trachytes are rhyolite with 70-75, 73-76 percent SiO₂ respectively. MI in orthopyroxenes in these rocks have higher Al₂O₃ and CaO and lower FeO contents than MI in plagioclases, which may in part reflect differing degrees of post-entrapment crystallization of the host mineral. MI in orthopyroxenes can be grouped as low K and high K inclusions. There is also some bimodality in Al₂O₃, with a subordinate population of opx-hosted MI resembling those from basaltic trachyandesites with high Al₂O₃. The dominant (plagioclase-

hosted) population lies close to the evolved end of the whole rock trend, but displaced to slightly lower Al_2O_3 and higher TiO_2 .

MI and groundmass glasses from dacites and rhyolites have very similar rhyolitic compositions with 75-81 wt% SiO_2 . The lower SiO_2 end of these MI is a very good match for the most evolved whole rocks, although it is striking that the population as a whole define a trend that is oblique to that defined by whole rocks, e.g. it has a flatter slope for FeO and CaO versus SiO_2 , but a steeper slope for Al_2O_3 .

In summary, MI and groundmass glasses, as expected, are consistently more evolved than the rocks in which they occur. However, only the least evolved MI and groundmass glasses from rhyolites and dacites consistently reproduce the composition of any Süphan whole rock. In other rocks there are some MI that match whole rocks, but for the most part the MI compositions scatter quite widely, appearing to define trends that are quite oblique to the linear trends of the whole rocks. This is most marked in the rhyolite and dacite MI, but also apparent in trachyandesites and basaltic trachyandesites. The latter show the greatest compositional range in MI. Although some modification in chemistry due to post-entrapment crystallization is inevitable, the considerable range in, say, Al_2O_3 or TiO_2 , cannot be attributed to such a process as there is absolutely no textural evidence that the requisite amount of crystallization has occurred, either as daughter minerals or along MI walls. A final feature of the MI is the fact that some compositional bimodality is observed for some host minerals in some rocks. MI in trachytes show both high and low K_2O groups; MI in olivines in mildly alkaline basaltic trachyandesites have both high and low Na_2O and K_2O content in the same rock (Özdemir et al., 2011).

7.2 Intensive Parameters: Temperature and Pressure

Magma temperatures for Süphan volcanics were estimated by using coexisting Fe-Ti oxides and two pyroxenes, plagioclase–hornblende thermometry and plagioclase-liquid, olivine - liquid, and clinopyroxene-liquid equilibria. In order to eliminate mineral pairs that were not in equilibrium with each other at the time of eruption, only compositions of rims of touching grains have used. Fe-Ti oxide temperatures are exclusively from groundmass microlite pairs rather than phenocrysts. The Mg/Mn partitioning test for equilibrium (Bacon and Hirschmann, 1988) applied to the coexisting oxide pairs revealed that all of those used for temperature calculations plot between error limits of Bacon and Hirschmann (1988). In mineral - liquid temperature estimations, several measurements on groundmass glasses were performed for each rock sample , and the averages of these measurements were used for liquid composition.

The results from these diverse methods are given in Figure 7.7 and Table 7.7. In Figure 7.7 temperatures are plotted against the SiO₂ content of the host rock. Generally temperatures of Süphan lavas decrease progressively from ~1100°C in basalt to ~750°C in rhyolites, but there is significant scatter in intermediate rocks, which in some cases covers a range of almost 200 °C.

In basalt sample 2006-99 temperature estimate of 788°C derives from a single touching magnetite-ilmenite pair. As this is well below the liquidus of any basalt, regardless of H₂O content, and given that coexisting ilmenite and magnetite are rare in basalts, we suggest that this temperature comes from a xenocrystic pair of probable rhyolitic paragenesis.

Temperatures of basaltic trachyandesites are obtained from touching magnetite-ilmenite and clinopyroxene-orthopyroxene pairs, and plagioclase-liquid and clinopyroxene-liquid equilibria. Fe-Ti oxide temperatures range between 1057 and 1122 °C. Similar temperatures are obtained from touching clinopyroxene-orthopyroxene pairs, 1085⁰C. Plagioclase-liquid and clinopyroxene-liquid thermometers overlap each other (950-962 and 971°C, respectively), but are lower than those of the mineral-mineral pairs.

In trachyandesites temperatures were obtained from four different lavas (samples 2006-6, 2006-8, 2006-77, 2006-86). Fe-Ti oxide temperatures from 2006-8 and 2006-86 range from 792 to 966 °C, with the lower temperatures from 2006-8. Temperatures decrease from sample 2006-86 to sample 2006-8 with increasing host-rock SiO₂ (Figure 7.7). Two-pyroxene temperatures range between 912 and 1071°C (samples 2006-86, 2006-6, 2006-8). Plagioclase-liquid, olivine-liquid, clinopyroxene-liquid temperatures from sample 2007-77 are 933, 942 and 936°C, respectively. Generally two-pyroxene temperatures are slightly higher than the Fe-Ti oxide temperatures.

In trachytes temperatures are obtained from two different samples, 2005-10 and 2008-4, with the latter generally showing lower values. Fe-Ti oxide temperatures range between 827 and 958°C; two-pyroxene temperatures 860 and 989°C. A single plagioclase-hornblende temperature from sample 2008-4 gives 829°C.

In dacites temperatures are obtained from three different domes (2005-28, 2006-110, 2007-4). Fe-Ti oxide temperatures lie between 802 and 841°C; two-pyroxene temperatures range between 829 and 930°C; and hornblende-plagioclase temperatures are 791 and 898°C. Hornblende – plagioclase temperature of sample 2005-28 is lower than the other

temperatures of the same sample, whereas hornblende-plagioclase temperature of sample 2006 110 is higher. Three plagioclase-liquid temperatures obtained from sample 2007-4 display an average of 882 °C .

In rhyolites Fe-Ti oxide temperatures are obtained only from sample 2005-52 and range between 747 -774°C. These values match those of the supposed xenocrystic oxide pair in the basalt sample, suggesting a possible common origin. K-feldspar-plagioclase temperatures (sample no. 2005-52, 200-75) range from 765 to 819°C, in good agreement with oxides. Plagioclase-liquid temperatures are in the range of 806-895 °C; higher temperatures belong to the older rhyolitic lava flow (sample 2005 69).

Magma storage pressures can be estimated from the volatile contents of melt inclusions (Wallace et al., 1999; Schmit, 2001; Liu et al. 2006) provided there is evidence that the melt was volatile-saturated at the time the melt inclusions became sealed. Storage pressures can be calculated directly from saturation pressures for those melt inclusions where both H₂O and CO₂ data are available.

The software VolatileCalc of Newman and Lowenstern (2002) is used to estimate storage pressures of different rock groups of Süphan. H₂O and CO₂ contents of melt inclusions and estimated magma temperatures are needed for those calculations. Only H₂O contents are known from volatile-by-difference estimates in Süphan melt inclusions. The separate amounts of H₂O and CO₂ are not available.

The estimated maximum pressures are 320 Mpa for basaltictrachyandesites, 70 Mpa for trachyandesites, 120 Mpa for trachytes and rhyolites and 190 Mpa for dacites. The corresponding

maximum depths for these pressures assuming the density of surrounding rocks as $2,6 \text{ kg/m}^3$ are 12 km for basaltic trachyandesites, 3 km for trachyandesites, 4.5 km for trachytes and rhyolites and 7km for dacites (Özdemir et al., 2011).

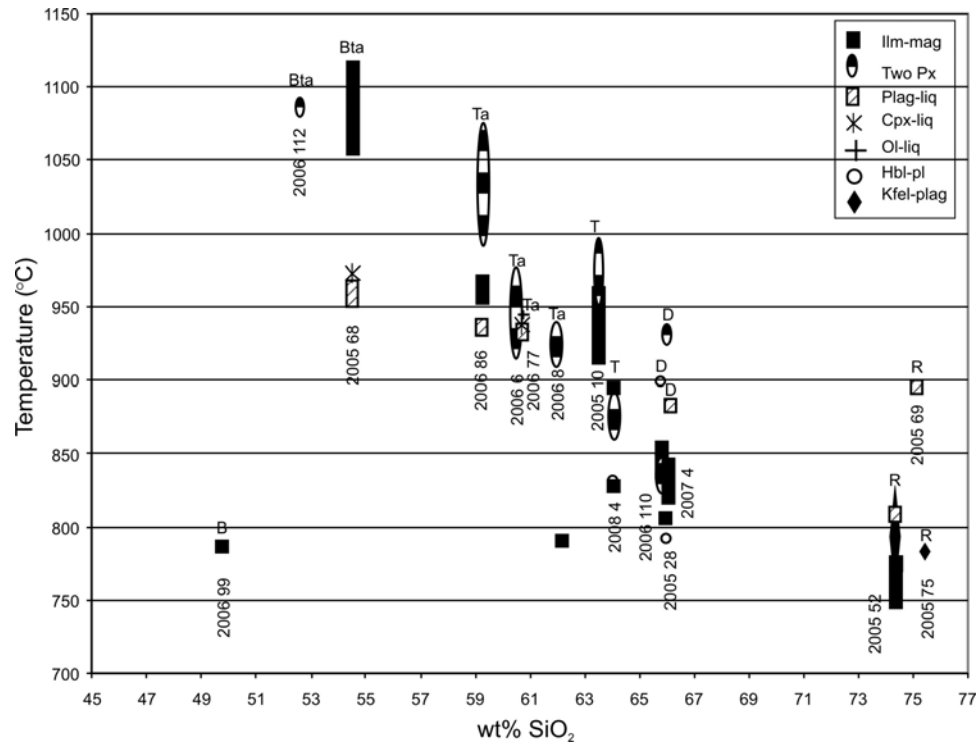


Figure 7.7 Calculated temperature versus SiO₂ plot for selected Süphan volcanics. Key to abbreviations: hbl: hornblend, ilm: ilmenite, kfel: K- feldspar, liq: liquid, mag:magnetite, plag: plagioclase, px: pyroxene, B: basalt, Bta: basaltic trachyandesite, Ta: trachyandesite, T: trachyte, D: dacite, R: rhyolite

Table 7.7 Temperatures estimated for Süphan magma using different methods.

Method	Andersen and Lindsley (1985); Stormer (1983) ilm-mag	Putirka (2008) Eq 23 plag-liq	Putirka (2008) Eq 33 cpx-liq	Lindsley Frost (1992) two px	Putirka (2008) Eq 22 ol-liq	Holand and Blundy (1994) hbl-plag	Putirka (2008) Eq 27a kfel-plag
Sample T	emperature (°C)						
2006 99	788	-	-	-	-	-	-
2006 112	-	-	-	1085	-	-	-
2005 68	1112 - 1057	950 - 963	971	-	-	-	-
2006 86	954 - 966	934 - 936	-	994 - 1071	-	-	-
2006 6	-	-	-	919 - 972	-	-	-
2006 77	-	933	936	-	942	-	-
2006 8	792	-	-	912 - 935	-	-	-
2005 10	914 - 958	-	-	946 - 989	-	-	-
2008 4	827 - 894	-	-	860 - 891	-	829	-
2006 110	836 - 853	-	-	829 - 843	-	898	-
2005 28	802	-	-	930	-	791	-
2007 4	819 -841	882	-	-	-	-	-
2005 52	747 - 774	806 - 809	-	-	-	-	764 - 819
2005 69	-	895	-	-	-	-	-
2005 75	-	-	-	-	-	-	781

7.3 Oxygen Fugacity

Oxygen fugacity is estimated from Fe–Ti oxide equilibria using the method of Andersen and Lindsley (1985); with the recalculation scheme of Stormer (1983) (Figure 7.8). Values obtained for basalt (xenocrystic pair), basaltic trachyandesites, trachyandesites and trachytes correspond to the FMQ (fayalite-magnetite-quartz) buffer. There is an apparent increase in fO_2 , relative to FMQ, in the more evolved rocks. Dacites correspond to $NNO \pm 0.3$ (nickel–nickel oxide); rhyolites to $NNO+1-1.4$.

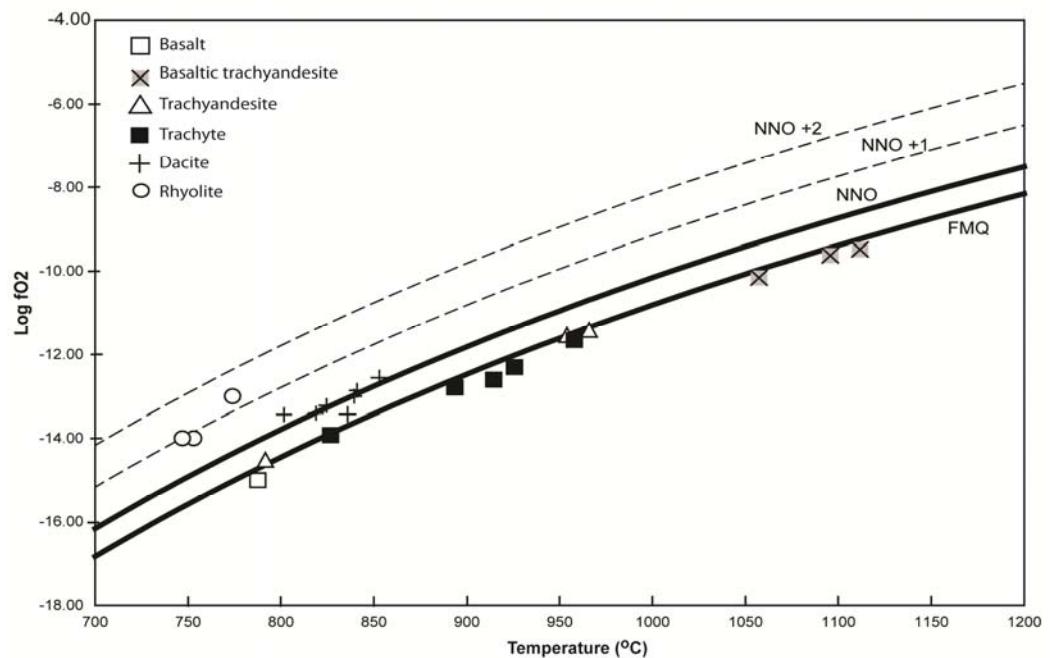


Figure 7.8 Temperature vs. oxygen fugacity, estimated from Fe-Ti equilibria in Süphan volcanics using the ILMAT program (Lepage 2003). Oxides were recalculated using Stormer (1983).

CHAPTER 8

DISCUSSION

8.1 Comparison to the Experimental Data

As has been outlined in Chapter 6, the mismatch between melt inclusions (MI) and whole rock compositions raises questions about liquid evolution at Süphan. If glasses record the composition of true (quenched) liquids, then what is the significance of the whole rock chemical variation, notably the marked linear trends apparent in harker diagrams (Figure 6.5)? This section attempts to address this question by using experimental studies (on volcanics from Trans-Mexican Volcanic Belt TMVB; Luhr 1990 and Kerguelen large igneous province, Freise et al, 2009) to help constrain liquid lines of descent, for comparison to glass and whole rock compositions at Süphan. A key question is the composition of the parent (basaltic) magma to chemical differentiation at Süphan. No melt inclusions were found in basaltic rocks which probably lie close to original liquid compositions. As there are no experimental determinations on Süphan rocks themselves, experimental studies on basalts which have similar major element composition to those at Süphan are used. The starting compositions of the experimental studies are shown in Figure 8.1 and Table 8.1. The experimental studies used for this comparison are given in Appendix D and Appendix E, along with ranges in pressure, temperature, H₂O content and fO₂.

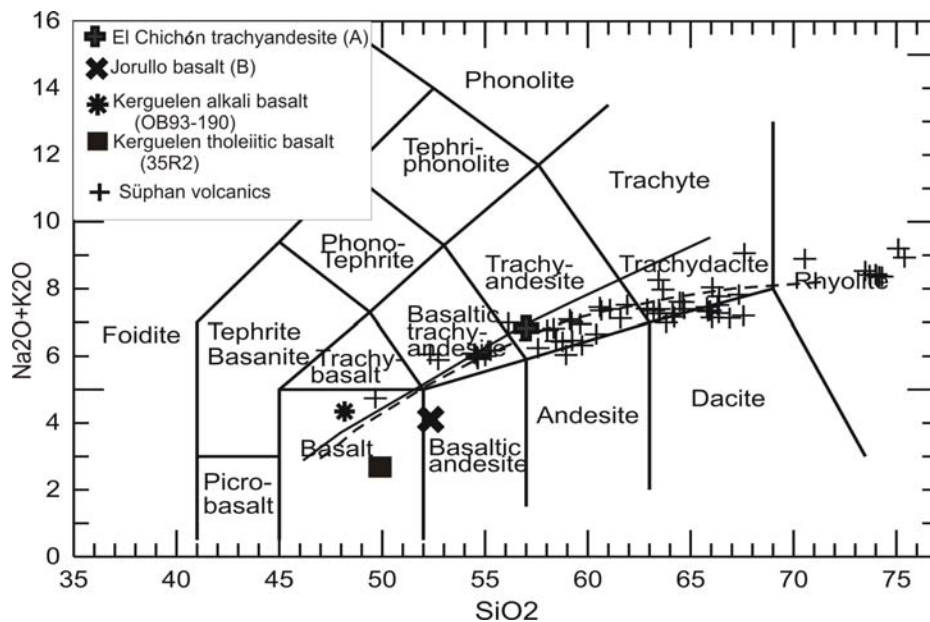


Figure 8.1 TAS diagram (Le Bas et al., 1986) of the Süphan volcanics and starting compositions of different experimental studies. Subalkaline-alkaline divisions are from Miyashiro (1978) (dashed line) and Irvin&Baragar (1971) (solid line). The data of El Chichón trachyandesite and Jorullo basalt are from Luhr 1990, Kerguelen alkali basalt (OB93 -190) and Kerguelen tholeiitic basalt (35R2) Freise et al, 2009.

Table 8.1 Major element compositions of starting materials (Data sources: A and B are from Luhr (1990), OB93-190 and 35RM are from Freise et al. (2009)).

	A	B	OB93-190	35RM
SiO ₂	57.75	53.04	48.84	50.40
TiO ₂	0.67	0.79	2.75	1.49
Al ₂ O ₃	18.52	16.53	16.14	14.84
FeO	-	-	11.85	11.00
Fe ₂ O ₃	6.4	8.25	-	-
MnO	0.19	0.14	-	-
MgO	2.31	9.44	5.86	6.82
CaO	7.22	8.41	9.76	12.57
Na ₂ O	4.33	3.24	3.12	2.62
K ₂ O	2.91	0.74	1.12	0.09

In Figure 8.2 Süphan data are compared to experimental melts of two volcanic rocks from the subduction-related Trans-Mexican Volcanic Belt (TMVB; Luhr1990). Magmas from the TMVB show a number of compositional similarities to those from eastern Anatolia. One rock is the trachyandesite erupted from El Chichón Volcano in 1982; the other is a primitive basalt erupted from Jorullo Volcano in 1759 (Table 8.1, Figure 8.2, Appendix D). Experimental crystallization of hydrous basaltic and andesitic melts over a range of crustal pressures (2-4 Kb) shows the possible liquid lines of descent during crustal differentiation (Figure 8.2). Experimentally-produced liquids describe curved fractionation trends that culminate in the compositions of silicic magmas and melt inclusions from Süphan. These curved trends are most marked for Al_2O_3 , MgO and FeO. For Al_2O_3 there is a fractionation peak at around 63 wt% SiO_2 ; for MgO and FeO there is an inflexion in the trend at ~59 wt% SiO_2 . The melt inclusions from Süphan basaltic trachyandesites, trachyandesites and trachytes are well matched by the experimental glass compositions. The whole rock compositions are not, however; they cut right across the liquid lines of descent produced experimentally. At the SiO_2 -rich end of the experimental array, however, there is a very good match between MI, from dacites and rhyolites, and some rhyolite whole-rocks themselves. It would appear from these experiments that differentiation from basalt to rhyolite is plausible, but not along the linear trends shown by Süphan whole-rocks. Instead, the MI provide a much better match to the liquid line of descent.

The second experimental dataset is from Kerguelen large igneous province (Table 8.1, Appendix E, Freise et al, 2009), an oceanic plateau produced by the early stages of activity of the Kerguelen hot spot and its interaction with Indian Ocean MORB-type component. Experimental melts were generated under fluid-saturated conditions at 500 MPa on two different basaltic compositions: a tholeiitic basalt from the Northern

Kerguelen Plateau and mildly alkalic basalt evolved from the Kerguelen Archipelago. In Figure 8.3 the experimental melts are compared to the whole rocks, MI and groundmass glasses from Süphan. A very similar story emerges as for the TMVB experimental studies shown in Figure 8.2 Experimental melts define curved liquid lines of descent for all oxides except CaO and K₂O, with a marked inflexion at 63 wt% SiO₂ for Al₂O₃. Although these experiments did not generate liquids with more than 66 wt% SiO₂, it is clear that the lower SiO₂ MI from Süphan provide a much better match to true liquids than do the whole rocks. This is most apparent for Al₂O₃ (Özdemir et al., 2011).

Figures 8.2 and 8.3 whole rock data match the experimental liquid line of descent in basaltic rocks and show curved fractionation trends until the rocks of 55% SiO₂. The intermediate rocks between 55 to 68% display linear chemical trends rather than the curved trends generated experimentally. This brings into question whether the rocks between 55-68 % SiO₂ are the products of mixing, rather than fractional crystallization, and the following sections are focused on a discussion of these alternatives.

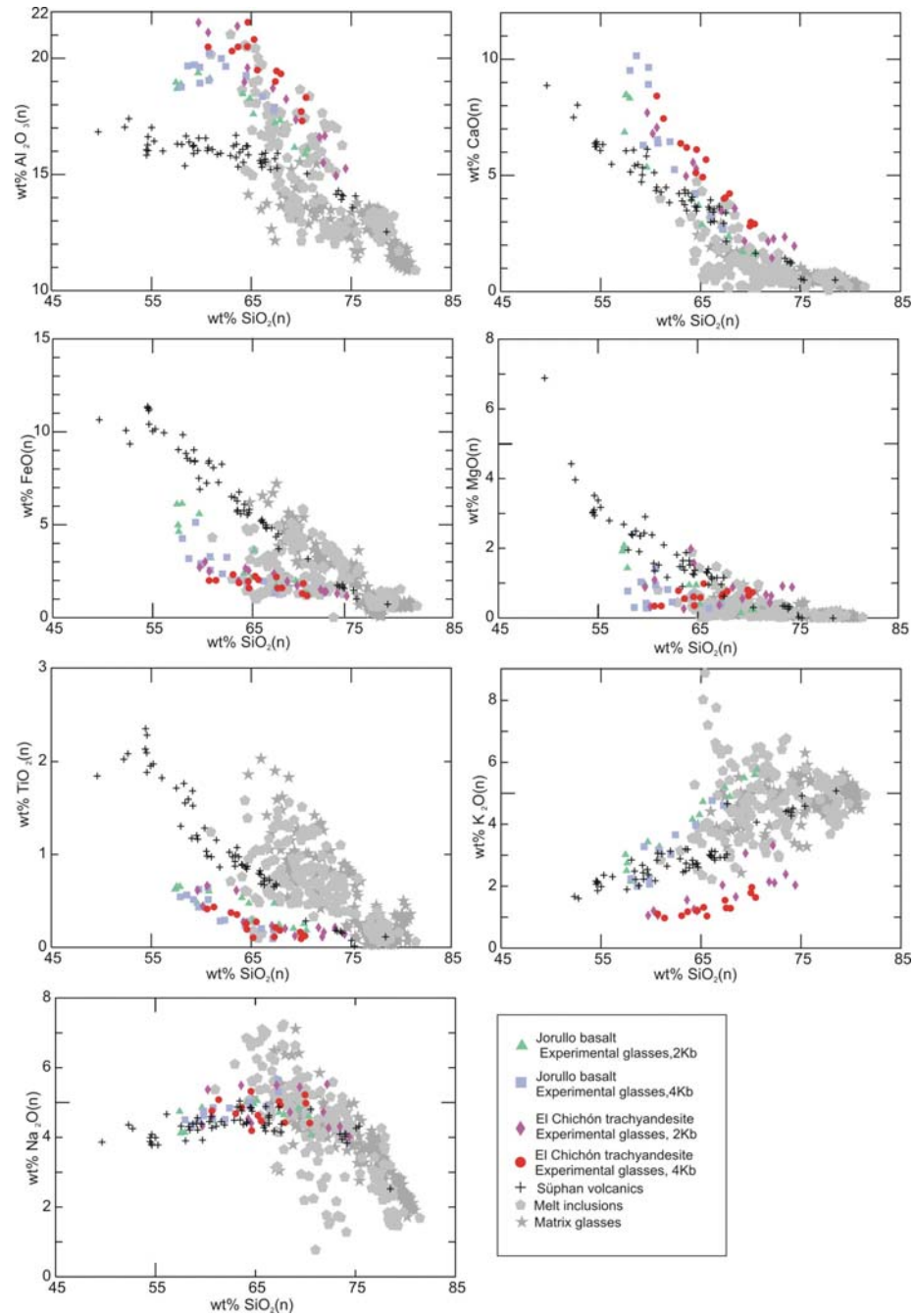


Figure 8.2 Comparison of chemical variation in melt inclusions, matrix glasses and whole rocks of Süphan volcanics with experimentally originated melts of two volcanic rocks from Trans-Mexican Volcanic Belt. (n) indicates anhydrous basis.

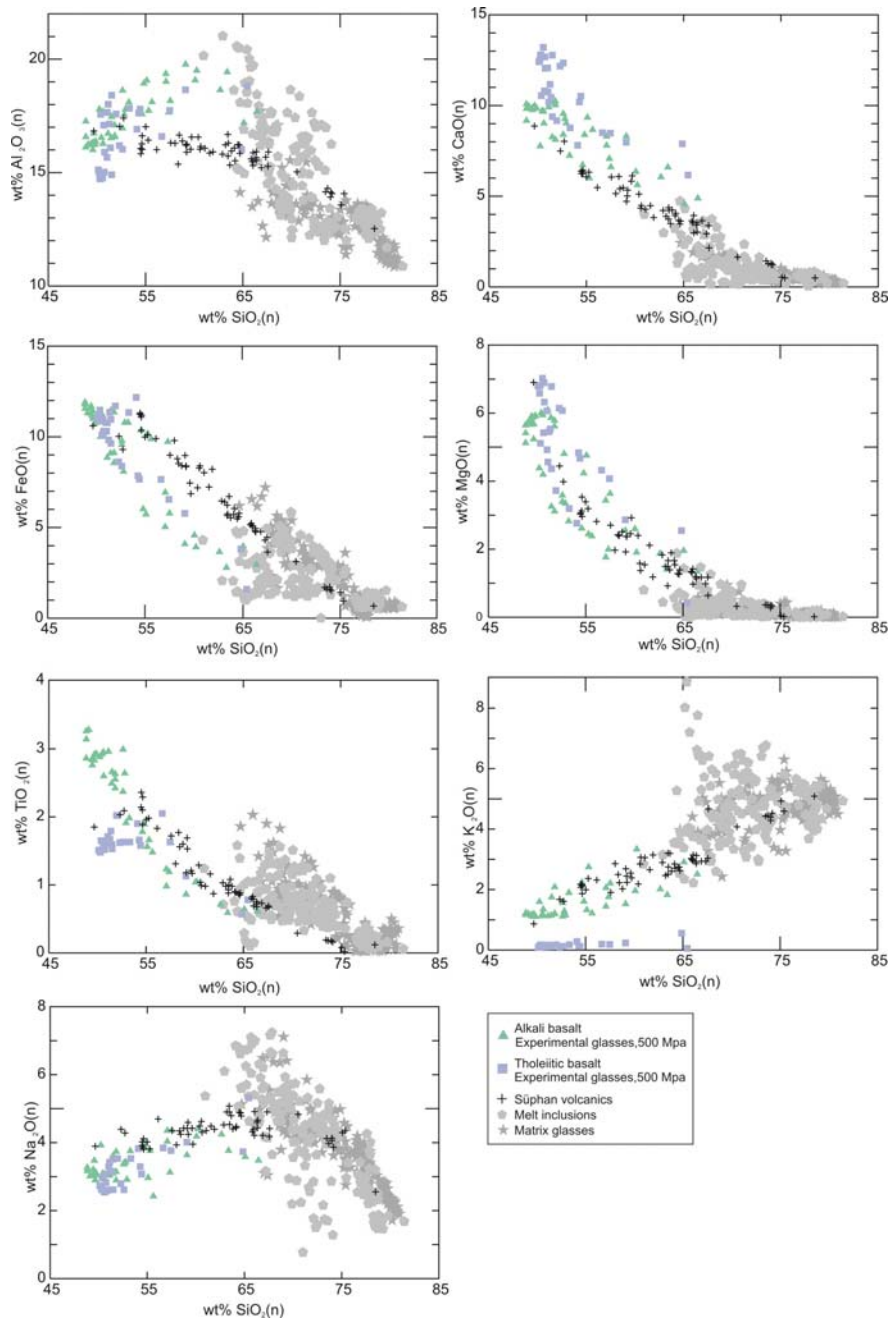


Figure 8.3 Comparison of chemical variation in melt inclusions, matrix glasses and whole rocks of Süphan volcanics with experimentally originated melts of two volcanic rocks from Kerguelen Large Igneous Province. (n) indicates anhydrous basis.

8.2 Magma mixing

The textural complexity of the phenocrysts, the wide temperature ranges obtained for trachytes, trachyandesites and dacites, and the linear geochemical trends are strongly suggestive of magma mixing in the evolution of Süphan volcanics. The two end-members involved in mixing appear to be rhyolite, with 75 wt% SiO₂ (anhydrous basis) and at ~750 °C, and basaltic trachyandesite with ~55 wt% SiO₂ (anhydrous basis) and at ~1100 °C. At lower SiO₂ contents the geochemical trends are no longer linear (Figure 8.2). It is therefore likely that the evolution from basalt to basaltic trachyandesite involved crystal fractionation rather than mixing. Mixing may have involved primarily the two different magma compositions given above. However, the presence of crystal clots suggests that some mixing also involved plutonic materials that became disrupted in the sub-volcanic plumbing system. Crystal clots contain almost exclusively gabbroic phases such that mixing would have involved rhyolitic liquids and solidified basalts. Disruption of the plutonic gabbros would have led first to the formation of glomerocrysts and then to dispersed xenocrysts, with varying degrees of rim overgrowth. Such crystals are widespread in the intermediate rocks at Süphan. Reubi & Blundy (2008) describe a very similar mixing process between plutonic materials and rhyolitic melts at Volcan Colima, Mexico. Their proposal, which is equally valid at Süphan, is that the sub-volcanic region contains numerous pockets of partially and fully crystallized basalts, which are encountered and disrupted by rhyolitic melts ascending through the system. Upon mixing and re-equilibration hybrid rocks are produced. If the mixing involved only rhyolite melt and plutonic fragments, then the melt composition in the hybrid magma will be broadly rhyolitic, notwithstanding any partial resorption of xenocrysts. If mixing involves rhyolitic and basalt liquids, then hybrid melts will be produced. As mixing is likely to have occurred at shallow

levels, the melt phase in the hybrid rocks will be expected to follow a low-pressure crystallization trend. This is recorded by the groundmass glasses and explains why the trends described by these glasses are different from the melt inclusion trends, discussed more fully below. The hypothesis that Süphan intermediate lavas are result of magma mixing of basaltic trachyandesitic and rhyolitic melts was tested by least - squares mixing calculations (Table 8.2 , method of Bryan et al., 1969 employed in IGPET software). The two end members for mixing calculations are chosen from basaltic trachyandesites (samples 2005 68 and 2006 112) at ~1100 °C and rhyolites at ~750 °C (samples 2005 69 and 2005 75). The SiO₂ contents of the basaltic trachyandesites and rhyolites are ranging between 52.87- 55.14 % and 75.20-75.47 % (on anhydrous basis), respectively. The blended mixing results are trachyandesites. The least square mixing solutions resulted in acceptable values for sum of squared residuals ($SR^2 < 1$) and give permissive evidence that intermediate lavas within the Süphan volcanics are related to the mixing of mafic (basaltic trachyandesites) and acidic (rhyolites) end members (Özdemir et al., 2011).

The fact that phenocryst zoning and anomalous temperature ranges are preserved in intermediate rocks indicates that mixing occurred on a timescale that was too short to permit full equilibration. In the case of Fe-Ti oxides, equilibration is known to occur on a timescale of days (Venezky & Rutherford 1999), suggesting that these minerals are most likely to preserve eruption temperatures. Indeed, all of our Fe-Ti oxide temperatures come from microlites rather than phenocrysts. Mixing may have occurred shortly before eruption, however, it is not possible to say at this stage whether mixing served as a trigger for eruption, as has been proposed at many other stratovolcanoes (e.g. Murphy et al 1998; Mortavazi & Sparks 2004).

Table 8.2 Table Least-Square mixing results for selected Süphan volcanics (H2O free).

	Test 1 Basaltic Trachyandesitic end-member 2006 112	Rhyolitic end-member 2007 75	Observed Trachyandesite 2006 95	Calculated Trachyandesite	Test 2 Basaltic Trachyandesitic end-member 2005 68	Rhyolitic end- member 2007 75	Observed Trachyandesite 2006 86	Calculated Trachyandesite
SiO ₂	52.87	75.47	60.08	59.99	55.14	75.47	59.72	59.87
TiO ₂	2.05	0.02	1.22	1.42	2.39	0.02	1.7	1.83
Al ₂ O ₃	17.2	14.08	16.15	16.24	16.01	14.08	16.04	15.55
Fe ₂ O ₃	9.11	0.86	6.75	6.53	10.3	0.86	7.58	8.09
MnO	0.14	0.07	0.13	0.12	0.18	0.07	0.13	0.16
MgO	4.49	0.02	2.47	3.09	3.1	0.02	2.39	2.38
CaO	7.58	0.5	5.87	5.37	6.32	0.5	5.06	4.95
Na ₂ O	4.42	4.34	4.44	4.39	4.05	4.34	4.61	4.12
K ₂ O	1.7	4.6	2.57	2.61	2.1	4.6	2.48	2.69
P ₂ O ₅	0.45	0.03	0.31	0.32	0.42	0.03	0.28	0.33
% Basaltic trachyandesite	68.7				76.6			
% Rhyolite	31.3				23.4			
SR ²	0.75				0.83			

Table 8.2. Continued

	Test 3 Basaltic Trachyandesitic end-member 2006 112	Rhyolitic end-member 2005 69	Observed Trachyandesite 2005 60	Calculated Trachyandesite
SiO ₂	52.87	75.2	62.04	61.94
TiO ₂	2.05	0.08	1.16	1.26
Al ₂ O ₃	17.2	13.59	15.98	15.76
Fe ₂ O ₃	9.11	1.28	6.56	5.95
MnO	0.14	0.03	0.13	0.1
MgO	4.49	0.04	2.13	2.7
CaO	7.58	0.54	4.51	4.75
Na ₂ O	4.42	4.27	4.49	4.36
K ₂ O	1.7	4.94	2.68	3.01
P ₂ O ₅	0.45	0.03	0.31	0.28
<hr/>				
% Basaltic				
trachyandesite	59.7			
% Rhyolite				
	40.3			
SR ²	0.93			

8.3 Fractional crystallization

A striking feature of the Süphan rocks is the discrepancy between chemical trends of melt inclusions and those of whole rocks (Figure 8.2, 8.3). Melt inclusions cover a wide compositional range, but lie at the evolved end of the spectrum defined by whole rocks. There are no melt inclusions with less than 61 wt% SiO₂, with the vast majority having ≥65 wt%. This echoes Reubi & Blundy's (2009) study of arc volcanoes worldwide, in which they found a dearth of truly andesitic melt inclusions with 60-70 wt% SiO₂, despite a wide continuum in whole rock chemistry. The melt inclusions at Süphan derive from a wide range of host phenocryst types, which rules out post-entrapment crystallization as a primary source of chemical variation, although we cannot rule out some post-entrapment processes in generating scatter.

The trends described by Süphan melt inclusions are consistent with crystallization trends obtained experimentally on hydrous magmas (Luhr 1990 and Freise et al., 2009, Figures 8.2, 8.3) similar in composition to the more mafic end of the Süphan whole rock spectrum. The evidence for high Al₂O₃ in some melt inclusions is consistent with the presence of H₂O in the parent magmas responsible for these trends, which will lead to the suppression of plagioclase crystallization. The magnitude of the Al₂O₃ peak and the SiO₂ content at which it occurs are indicative of the H₂O content of the parent magma and the pressure at which crystallization occurred. The experimental data presented in Figures 8.2 and 8.3, albeit from slightly different bulk compositions to those at Süphan, give a good match to the melt inclusions, suggesting that H₂O pressures of 200-500 Mpa prevailed during crystallization. If the magmas were H₂O-saturated, this would place crystallization at depths of 6-15 km beneath the volcano; greater depths are inferred for the H₂O-undersaturated case. Analysis of H₂O and CO₂ in melt inclusions is

required to better constrain these depths, as would experimental studies of the Süphan rocks themselves. The melt inclusions also show high TiO_2 , which is not matched by any of the experiments. This may reflect delayed onset of ilmenite or titanomagnetite crystallization at Süphan, a consequence of the lower $f\text{O}_2$ compared to experiments.

The melt inclusion trends do not intersect the whole rock trends until ~ 70 wt% SiO_2 , suggesting that these are the only whole rocks more differentiated than basaltic trachyandesite that could plausibly represent true liquids. This accords with our proposal above that the mixing processes that occurred beneath Süphan involved rhyolitic melts (*sensu lato*) and both basaltic trachyandesite liquids and gabbroic plutonic rocks.

The logical interpretation of the discrepant whole rock and melt inclusion trends is that the crystals preserving melt inclusions grew from melts that described true fractionation trends occurring at depth. These crystals were entrained from the source region by ascending magmas, become redistributed and rimmed at shallow level by magma mixing and mingling processes. These processes served to generate linear chemical trends that almost entirely obscure the chemical variations generated by crystal fractionation. Some groundmass glasses have compositions similar to melt inclusions, e.g. in terms of high Al_2O_3 and TiO_2 (Figure 8.1, 8.2) and these may represent aliquots of liquid added to the shallow system. Piecemeal construction of a shallow magma body by repeated incursions of magma from a deeper storage region have been documented at Nevado de Toluca Volcano in Mexico by Smith et al (2009). The majority of the groundmass glasses, however, are displaced to higher SiO_2 and, as proposed above, appear to reflect closed system crystallization at shallow levels following mixing (Özdemir et al., 2011).

8.4 Crustal Contamination

The above discussion on mixing and fractional crystallization points to the presence of a felsic (rhyolitic) melt in the evolution of Süphan volcanism in addition to the mantle-derived mafic magma. This felsic magma might have been produced either as a result of magmatic differentiation of, or represent the product of crustal melting induced by, the mantle-derived mafic magma. Regarding the latter, relatively large ranges of isotopic compositions (Sr, Nd) suggests additional contributions from lower and/or upper crustal sources. On $^{87}\text{Sr}/^{86}\text{Sr}$ and $^{143}\text{Nd}/^{144}\text{Nd}$ vs SiO_2 plots (Figure 8.4a,b), most of the Süphan volcanics display positive correlation on $^{87}\text{Sr}/^{86}\text{Sr}$ and a roughly negative trend on $^{143}\text{Nd}/^{144}\text{Nd}$ vs. SiO_2 plots. These observations suggest that some of the Süphan volcanics have been contaminated by a component with high $^{87}\text{Sr}/^{86}\text{Sr}$ and low $^{143}\text{Nd}/^{144}\text{Nd}$ compositions. A plausible contaminant would be the upper crust which have interacted with Süphan volcanics during their ascent or in subvolcanic magma chambers.

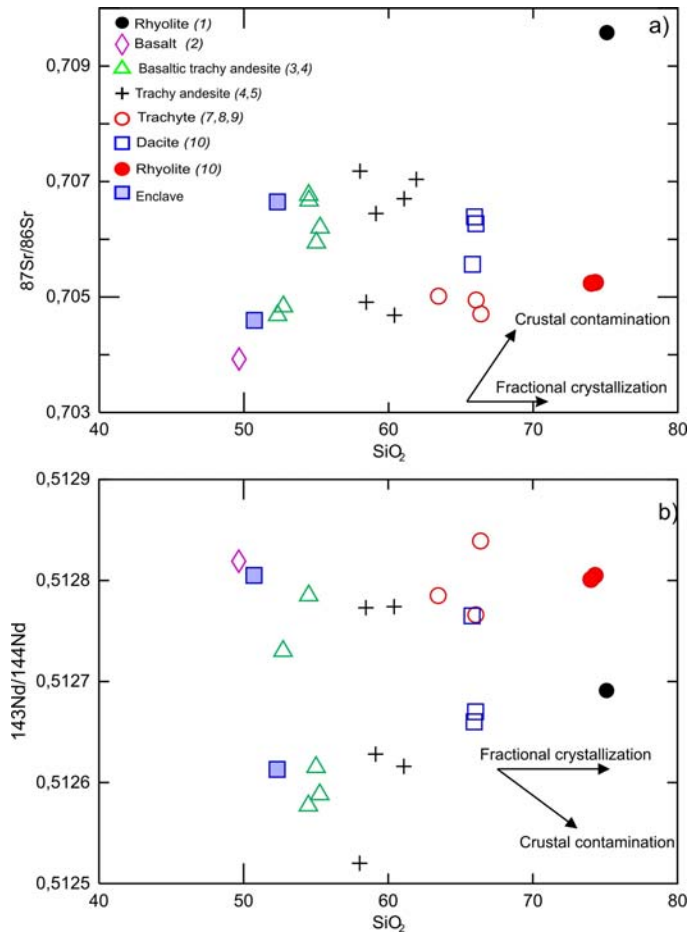


Figure 8.4 a) ⁸⁷Sr/⁸⁶Sr vs SiO₂ and **b)** ¹⁴³Nd/¹⁴⁴Nd vs SiO₂ diagrams of the Süphan volcanics. Number in parenthesis in the legend correspond to the units in Figure 3.2.

In an attempt to examine this possibility, mixing calculations (using the equations given by Langmuir et al., 1978) were performed for two cases: i) the mafic and felsic end-members are assigned compositions representative of trachyandesitic lava (sample 2006 112) and a rhyolitic sample (2005 69), respectively (the end-members used for major element modeling) and ii) the mafic end-member is assigned the composition of trachyandesitic lava (sample 2006 112) and the felsic member is assigned an upper crustal composition. The mixing curves

produced are shown in Fig. 8.5. As can be seen from Figure 8.5, the mixing trajectory constructed for the first case can accommodate only a few data points belonging to intermediate and felsic samples. Most of the Süphan basaltic, intermediate and felsic samples are placed over the mixing curve and indicate a more radiogenic $^{87}\text{Sr}/^{86}\text{Sr}$ source. In the second case (felsic end member with upper crustal composition), only one sample is encompassed by the mixing trajectory.

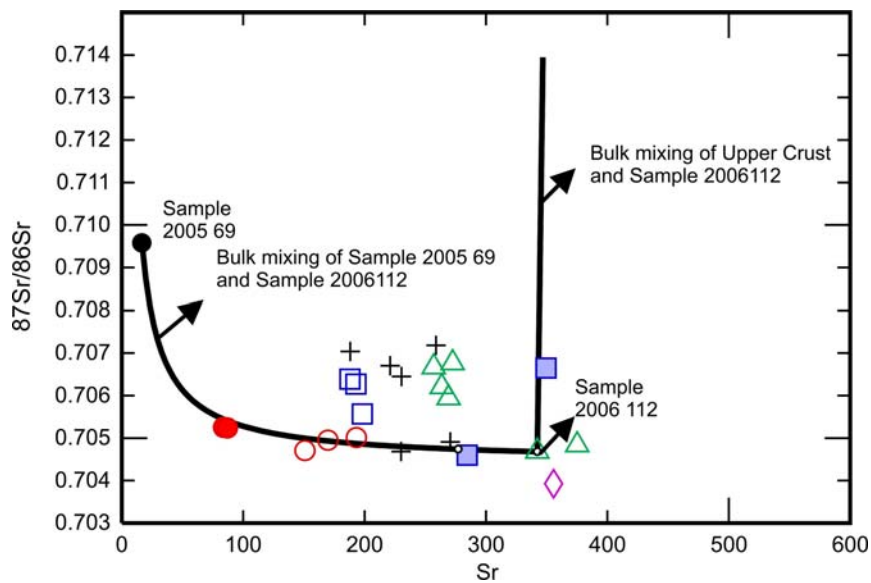


Figure 8.5 Mixing trajectories between sample 2006 122 & sample 2005 69, and between sample 2006 112 & Upper crust. Data source for upper crust is from Taylor and Mc Lennan (1985). Symbols are same as Figure 8.4.

As a further assesment, quantitative calculation of the amounts of fractional crystallization and assimilation of continental crust for Sr-Nd isotopes and Sr element concentrations was performed by using the energy constrained-assimilation fractional crystallization (EC-AFC) model of Spera and Bohrson (2001) and Bohrson and Spera (2001). The energy - constrained assimilation and fractional crystallization (EC-

AFC) provides accurate approach to the expressing of AFC processes. EC-AFC is a self-consistent formulation of energy, mass and species conservation for a magma body undergoing concurrent assimilation-fractional crystallization with or without recharge (Spera and Bohrson, 2001, Bohrson and Spera ,2001). The model tracks the system as magma cools and crystallizes and wallrock heats up and partially melts. There are two types of initial parameters in the EC-AFC model: thermal and compositional parameters (Bohrson and Spera ,2001). The thermal and compositional parameters of EC-AFC calculation for Süphan volcanics are given in Table 8.3. The thermal parameters are those used by Bohrson and Spera (2001) for standart upper and lower crust . Compositional parameters of assimilants are taken from Bohrson and Spera, (2001). Sample 2006 99 was taken as the starting value for the Süphan volcanics due to its most primitive nature (mg# 60,) within the Süphan volcanics. The bulk partition coefficients (KD) values of the assimilants (lower and upper crust) are taken from Bohrson and Spera (2001). Bulk distribution coefficient for Sample 2006 99 is calculated using the modal mineralogical composition of the sample and the Sr, Nd elemental partition coefficients taken from <http://www.earthref.org/> (Table 8.4). The results of the EC-AFC modeling are demonstrated in Figure 8.6a and 8.6b. On $^{87}\text{Sr}/^{86}\text{Sr}$ versus Sr plot, both upper and lower crustal EC-AFC curves are shown (Figure 8.6a). The Süphan lavas seems to be conformable with the curve of the upper crustal contaminant rather than the lower crust. Most of the intermediate and more differentiated samples of the Süphan display about 8% upper crustal assimilant in their composition. A similar result is obtained in figure 8.6b where the samples which contain radiogenic $^{87}\text{Sr}/^{86}\text{Sr}$ and low $^{143}\text{Nd}/^{144}\text{Nd}$ plot on the 8 % contaminant part of the EC_AFC curve.

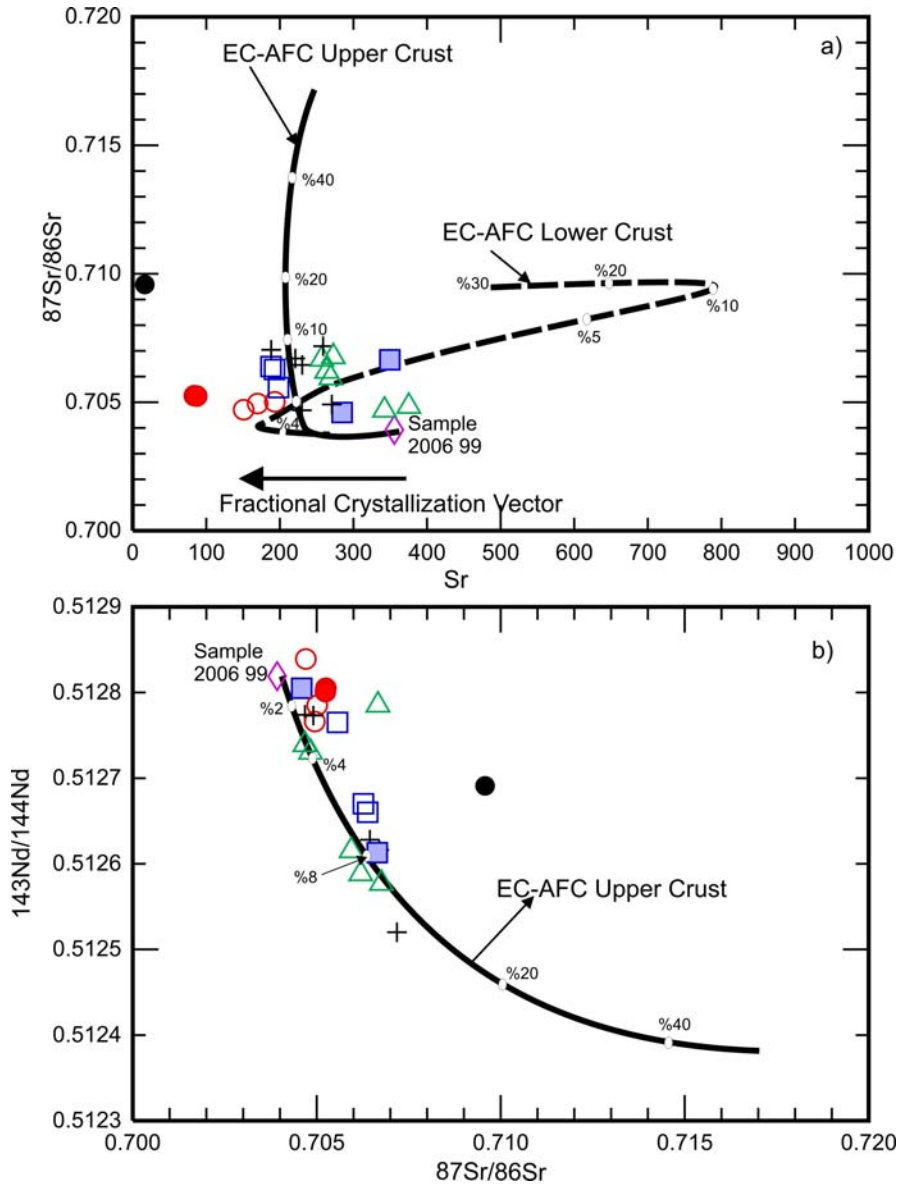


Figure 8.6 $^{87}\text{Sr}/^{86}\text{Sr}$ vs Sr (ppm) (a) and $^{143}\text{Nd}/^{144}\text{Nd}$ vs $^{87}\text{Sr}/^{86}\text{Sr}$ (b) with model EC-AFC curves calculated using the model of Spera and Bohrsen (2001). Small circles on the curves indicate percentage of assimilated contaminant. Bulk distribution coefficients are calculated using the modal mineralogical composition of the sample 2006 99 (Plagioclase_{0.5}+Clinopyroxene_{0.3}+Olivine_{0.18}+Ilmenite_{0.02}). Symbols are same as figure 8.4

Table 8.3 EC-AFC (Spera and Bohrsen, 2001) parameters for Süphan volcanics and potential contaminants (lower and upper crust).

<i>Thermal Parameters</i>					
	T (°C) Upper crust	T (°C) Lower crust		Upper crust	Lower crust
Magma liquidus temperature	1280	1320	Crystallization enthalpy (J/kg)	39600	39600
Magma initial temperature	1280	1320	Isobaric specific heat of magma (J/kg per K)	1484	1484
Assimilant liquidus temperature	1000	1100	Fusion enthalpy (J/kg)	270000	350000
Assimilant initial temperature	300	600	Isobaric specific heat of assimilant (J/kg per K)	1370	1388
Solidus temperature	900	950			
Equilibration temperature	980	980			
<i>Compositional parameters</i>					
	Sr	Nd			
Sample 2006 99					
Magma initial concentration (ppm)	356	23			
Magma isotope ratio	0.70392	0.512819			
Magma trace element distribution coefficient	1.5	0.09			
<i>Assimilant (upper crust)</i>					
Assimilant initial concentration (ppm)	350	26			
Assimilant isotope ratio	0.722	0.5118			
Assimilant trace element distribution coefficient	1.5	0.25			
<i>Assimilant (lower crust)</i>					
Assimilant initial concentration (ppm)	230	12.7			
Assimilant isotope ratio	0.71	0.513			
Assimilant trace element distribution coefficient	0.05	0.25			

Table 8.4 Partition coefficients of elements used for EC-AFC modelling

Mineral	Sr	Nd
Plagioclase	2.94 (a)	0.069 (b)
Clinopyroxene	0.16 (c)	0.18 (d)
Olivine	0.02 (c)	0.0023 (e)
Ilmenite	2.3	0.00048 (d)

Data source: Geochemical Earth Reference Model home page; <http://www.earthref.org>, (a); Matsui et al., (1977), (b); Schnetzler and Philpotts, (1970), (c); Villemant et al., (1981), (d); Zack and Brumm, (1988), (e); Fujimaki et al., (1984).

8.5 Mantle Source

8.5.1 Partial Melting

To establish the nature of the mantle sources, partial melting models using the rare earth element (REE) ratios have been constructed to determine the conditions of partial melting along with the facies mineralogy and chemistry using the methodology of Shaw (1970). REE ratios are useful for restriction of the extent and depth of the partial melting.

Partial melting of either a garnet or spinel peridotite will enrich the LREE contents (e.g. La) in the melt and produce La/Yb variations with variable degrees of melting. Garnet-facies melts will produce higher La/Yb ratios relative to the spinel - facies melts (Shaw et al., 2003 Peters et al., 2008). Enrichment of MREE (e.g. Dy) relative to the HREE (e.g. Yb) depend on whether garnet exists as a residual phase during melting, as HREE are preferentially retained by garnet during melting (high $D_{Yb} \sim$

4.0-15) relative to MREE (Dy) (Shaw et al., 2003 Peters et al., 2008). Thus, Dy/Yb ratios increase with decreasing degree of partial melting in the garnet facies. However, melting of a spinel peridotite will result in a minimal variation in Dy/Yb ratios. Figure 8.7 represents $(Dy/Yb)_N$ vs $(La/Yb)_N$, and Yb vs La/Yb data for the Süphan volcanics, along with the trajectories for non-modal batch melts of garnet and spinel peridotite sources. Because of the absence of mantle xenoliths from eastern Anatolian volcanics, primitive mantle composition is taken for the modeling calculations. Source concentrations of primitive mantle values, partition coefficients and mineral assemblages of spinel and garnet peridotites are from McKenzie and O'Nions (1991). Mineral proportions that incorporated to the non-modal batch melts are from Thirlwall et al., 1994, Shaw et al., 2003, Peters et al., 2008). In figure 8.7a and b, mafic samples ($\%SiO_2 < 55$, basaltic, basaltic trachyandesitic and doleritic enclaves which are co-magmatic with the Süphan volcanics) are shown. Results obtained from figures (Figure 8.7a,b) depict that melting of garnet or spinel facies could not alone reproduce Süphan mafic rocks. To test the contribution of both spinel and garnet facies in the origin of the Süphan volcanics, two component mixing lines/curves (Langmiur et al., 1978) are drawn. Alkaline basaltic lava and two doleritic co-magmatic enclaves plot between mixing lines of 2-5% melting of garnet and spinel facies.. The contribution of the garnet and spinel facies in the genesis of the volcanics seems to correspond to a garnet/spinel ratio of about 40/60 in figure 8.7 a and 50/50 in figure 8.7 b. The differentiated basaltic trachyandesitic samples (relative to the basaltic sample) plot between mixing lines of 1-2 % melting of garnet and spinel facies, with a ratio of ~50Gt-50 Sp (Fig. 8.7 a,b). Enrichment of La/Yb ratio of basaltic trachyandesites (relative to basalts) could be related to the crustal contamination (EC-AFC processes) that these samples were subjected as has been discussed in section 8.4.

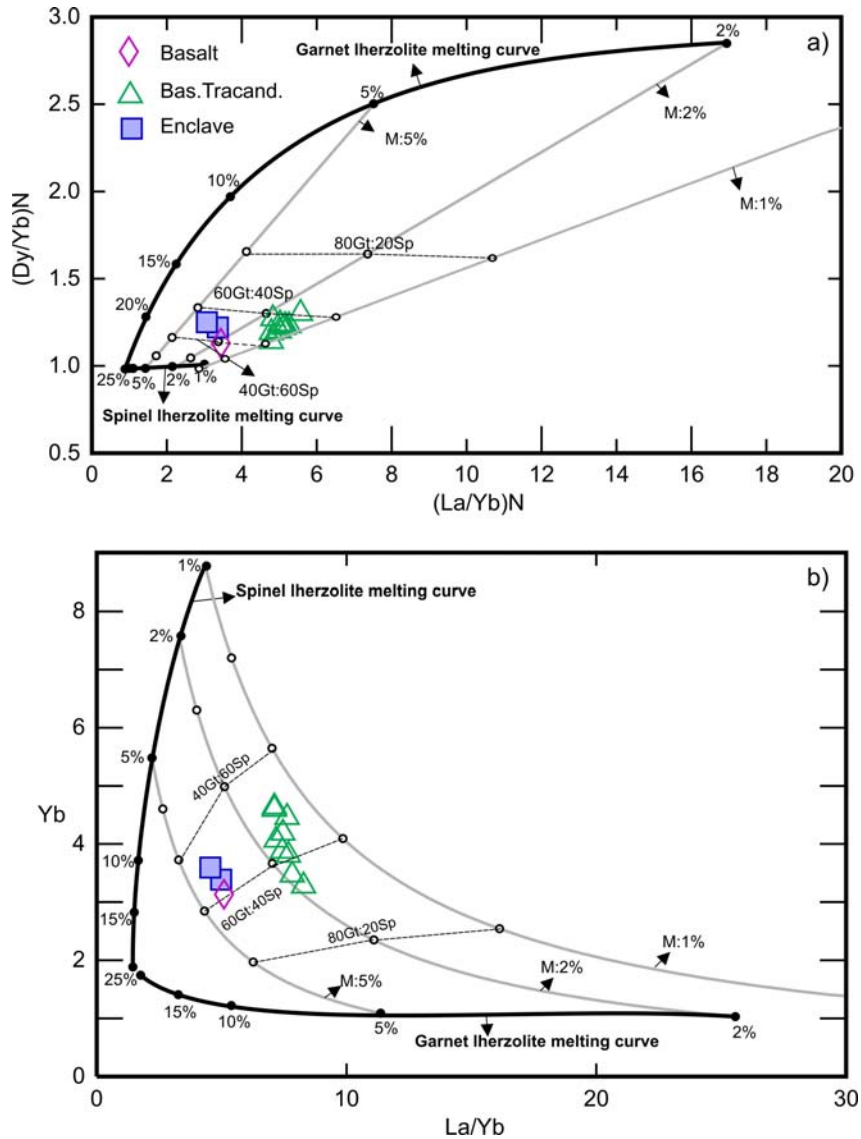


Figure 8.7 (a-b). Calculated partial melting curves assuming non-modal batch melting of garnet (Gt) and spinel (Sp) lherzolite sources for Süphan Volcanics (garnet lherzolite: 0.598ol, 0.211 opx, 0.076cpx, 0.115 grt, melting proportions: 0.05 ol, 0.2 opx, 0.3 cpx, 0.45 grt; spinel lherzolite 0.578 ol, 0.27 opx, 0.119 cpx, 0.033 sp, melting proportions: 0.1 ol, 0.27 opx, 0.5 cpx, 0.13 sp; Thirlwall et al., 1994, Shaw et al., 2003, Peters et al., 2008). The composition of the primitive mantle and distribution coefficients are from McKenzie and O'nions (1991). M:1%, M:2% and M:5% represents mixing lines between 1%, 2% and 5% melts from garnet and spinel peridotites.

8.5.2 Subduction Components

A key feature of the Süphan volcanics is the LILE enrichment and the presence of negative HFSE (Nb and Ta in particular) anomalies (Figure 5.7) which is opposite to the signature of the oceanic basalts and suggesting similarities with magmas generated in subduction related tectonic settings.

Previous studies have shown that subduction related metasomatic components can be broadly classified into two groups : (1) fluids, derived from dehydration of either altered oceanic crust (Tatsumi et al., 1986; Hawkesworth et al., 1993, 1997; Turner et al., 1996; Turner, 2002) or subducted sediments (Ryan et al., 1995; Class et al., 2000; Elburg et al., 2002); (2) partial melts of subducted sediment or the oceanic crust itself (Hawkesworth et al., 1993, 1997; Varoon et al., 1993; Elliot et al., 1997; Elburg et al., 2002). Important geochemical distinctions can be recognized between arc volcanic rocks in which the magma sources are modified by a subduction-derived fluid and those that are enriched by subducted sediments or partial melt (Hawkesworth et al., 1997; Elburg et al., 2002). It has been shown that some LILE (e.g. Rb, Ba, Sr, U) are mobile in aqueous fluids because these elements are water soluble; however, the REE and HFSE (e.g. Ce, Th, Nb, Zr and Ta) are less mobile or immobile in a fluid phase because they are relatively water insoluble trace elements (Sheppard and Taylor, 1992; Turner et al., 1997; Elburg et al., 2002; Turner 2002). This characteristics leads to high concentrations of some water-soluble LILE and other fluid mobile elements (e.g. Rb, Ba), and very low contents of HFSE in the subduction - derived fluid. Thus, those volcanic rocks whose source was strongly metasomatized by a fluid component are likely to have higher, Ba/Th (>170; Hawkesworth et al., 1997), Pb/Ce (> 0.1; Elburg et al., 2002) and Ba/La ratios than rocks whose source was enriched by

partial melts of oceanic crust and subducted sediments (Sheppard and Taylor, 1992; Elburg et al., 2002). In contrast, arc volcanics with a strong imprint of a subduction related partial melt or subducted sediment in their source region have higher Th/Ce (> 0.15 ; Hawkesworth et al., 1997), $^{87}\text{Sr} / ^{86}\text{Sr}$, $^{206}\text{Pb} / ^{204}\text{Pb}$ (Hawkesworth et al., 1997; Guo et al., 2006) and lower Ba/La (Sheppard and Taylor, 1992) than those related to fluid metasomatism of their mantle source. Both fluid and melt (or bulk subducted sediment) related metasomatism could be responsible for the negative Nb-Ta anomalies of the Süphan volcanics.

All of the Süphan primitive volcanic rocks have lower Ba/Th (< 170) ratios and display values akin to the global subducting sediment composition (GLOSS; Plank and Langmuir 1998, Figure 8.8a). Pb/Ce (< 0.1), Ba/La (Figure 8.8b), Th/Ce (most of them > 0.5) ratios support that mantle source of the Süphan volcanics modified by bulk sediment or a partial melt of subducted sediment rather than fluids from subducted oceanic crust or subducted sediments.

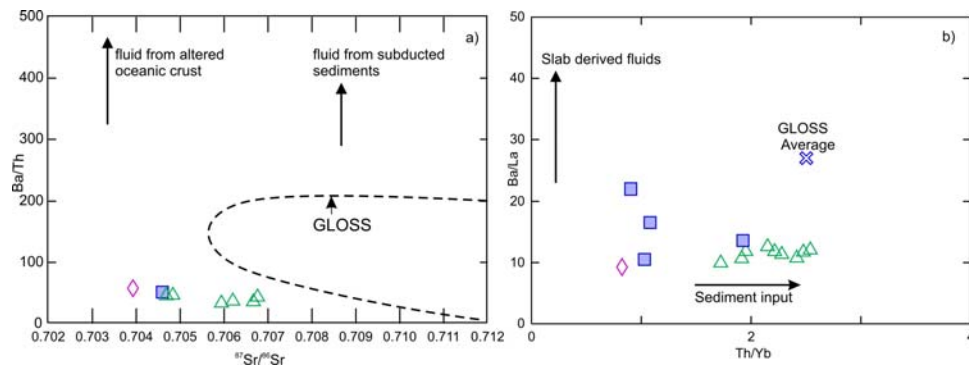


Figure 8.8 a) Ba/Th vs $^{87}\text{Sr}/^{86}\text{Sr}$, b) Ba/La vs Th/Yb, diagrams of Süphan volcanics. Symbols are same as in Figure 8.7. GLOSS and GLOSS average are from Plank and Langmuir (1998).

$^{206}\text{Pb}/^{204}\text{Pb}$, $^{207}\text{Pb}/^{204}\text{Pb}$, $^{208}\text{Pb}/^{204}\text{Pb}$ isotopic ratios also support sediment contribution to the mantle source of the Süphan volcanics. Higher Pb isotopic ratios of Süphan overlap with the GLOSS and EM II component (Figure 8.9). GLOSS is dominated by terrigenous material and therefore similar to the upper continental crust in composition (Plank and Langmuir, 1998). Source for the EM II component are generally accepted to have formed by subducted terrigenous sediments (Weaver, 1991), recycling of delaminated subcontinental lithosphere into the mantle (e.g. Hawkesworth et al., 1986, 1988, 1990) and a pyroxenitic source component which occurred from previous subduction related volcanic rocks within the lithosphere (Timm et al., 2009).

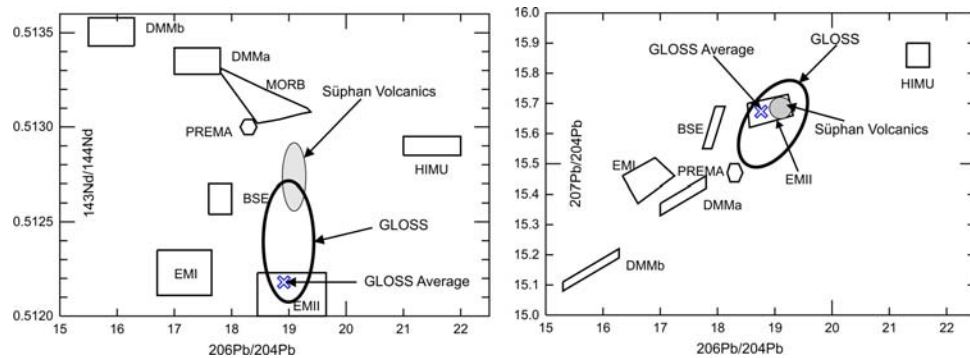


Figure 8.9 $^{143}\text{Nd}/^{144}\text{Nd}$ vs $^{206}\text{Pb}/^{204}\text{Pb}$ and $^{207}\text{Pb}/^{204}\text{Pb}$ vs $^{206}\text{Pb}/^{204}\text{Pb}$ diagrams of the Süphan volcanics.

8.6 Magmatic Plumbing Beneath Süphan

Mineral and melt inclusions chemistry allow to place some constraints on the sub-volcanic magma plumbing beneath Süphan (Figure 8.10). Two-stage petrogenetic model, similar to that envisaged by Annen et al (2006), can be proposed for Süphan. Mantle-derived hydrous basalt

stalls in the lower to mid-crust, whereupon it crystallizes to produce evolved melts. The thermal structure of this deep crustal hot zone is complex and evolves with time, such that it may contain a wide variety of melts of differing SiO₂ content distributed across a wide depth range. The characteristic feature of these melts is the delayed crystallization of plagioclase due to elevated H₂O, leading to high Al₂O₃ in intermediate liquids. Lack of sufficient experimental information or data on dissolved H₂O and CO₂ in melt inclusions prevents to constrain the exact depth range over which the hot zone is developed. Nevertheless, the crust in this region is reported to have an average thickness of 45 km (Angus et al., 2006; Özacar, 2008) and Angus et al. (2006) describe a crustal low velocity zone at ~25 km depth below Quaternary volcanic centers (e.g. Süphan, Nemrut) which most likely represents a pocket of partial melt in the middle crust. The match between experimental melts and melt inclusions (Figures 8.2, 8.3) suggests that pressures are at least 200-500 MPa. Assimilation of older crustal rocks may accompany differentiation in the deep crust. However, assimilation has had little influence based on the major element chemistry, given the close correspondence to experimentally generated liquid lines of descent and isotopic compositions of the volcanics. (see also section 5.5.4).

Once generated in the deep crust, melts are buoyant due to elevated SiO₂ and H₂O and can ascend to shallower levels in the crust, plausibly entraining solid residues as they leave the hot zone. The presence of Al-rich melt inclusions of intermediate composition strongly supports crystal entrainment. These melt inclusions represent snapshots of melt evolution occurring within the hot zone. Ascending melts, with or without their cargo of entrained crystals, are arrested at shallow level where they construct a sub-volcanic magma reservoir. The level of arrest may reflect the onset of H₂O saturation which leads to copious crystallization and a marked increase in viscosity (Annen et al 2006). Without melt

inclusion volatile contents the depth of the sub-volcanic reservoir cannot be constrained, although maximum volatile-by-difference estimates of melt inclusions for different rock groups range between 3.0 and 7.7 wt%, which would suggest H₂O saturation pressures of around 70-320 MPa, or 3-12 km depth. In any event the sub-volcanic reservoir is somewhat shallower than the source region. Various melts and their entrained residues meet and interact in the shallow storage region, leading to a wide variety of mixing and mingling phenomena that define the final chemical distribution of erupted magma types. Mixing may involve contrasted magmas (e.g. rhyolite and basaltic trachyandesite) or evolved melt (rhyolite) and solidified gabbro. It is likely that both processes operated in tandem, resulting in linear whole-rock chemical trends, hybrid magmas, glomerocrysts and dispersed, rimmed xenocrysts. It is unclear to what extent mixing and mingling served as a trigger for eruptions.

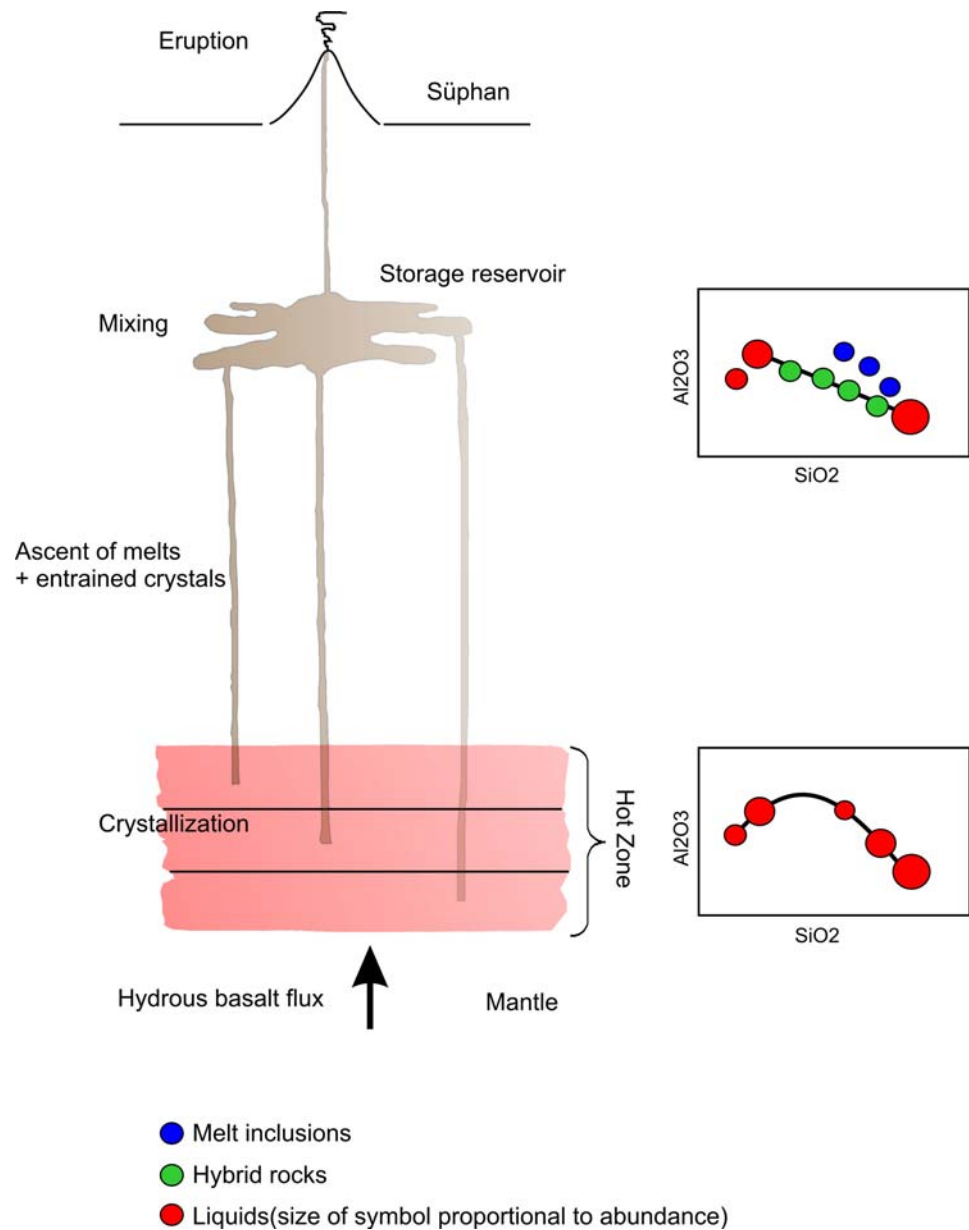


Figure 8.10 Schematic representation of intracrustal magma plumbing system beneath Süphan Stratovolcano (not to scale) showing that fractional crystallization predominates in the deep source region, whereas mixing processes predominate in the shallow storage region. Right hand panels show chemical variation schematically in terms of Al₂O₃ vs SiO₂.

8.7 Magmato-Tectonic History and Role of Lithospheric Mantle

Nature of the tectonism in eastern Anatolia is characterized by a transition from N-S directed compressional-contractual regime (post-collisional convergence) in Middle Miocene-Early Pliocene to compressional-extensional regime (tectonic escape) in Early Pliocene – Recent time interval (Koçyiğit et al., 2001; Bozkurt, 2001). The major structures formed during the former tectonic regime are the E-W trending thrust to reverse faults and E-W trending folds, whereas the latter regime has been dominated by strike-slip faulting. Strike slip faults are the main constituents of the neotectonic structures of the region. Koçyiğit et al. (2001) classified the neotectonic structures of the eastern Anatolia as *i)* dextral to sinistral strike slip faults, *ii)* strike slip basins, and *iii)* N-S trending fissures and lines of Plio-Quaternary volcanoes. These faults cut, displace and deform Plio-Quaternary basins and volcanic rocks of the region. Most of the volcanic edifices of the eastern Anatolia are located on these structural features.

The nature and the source of the magmatism in eastern Anatolia is still a matter of debate. There are several hypotheses about the origin of the magmatism, and lithospheric structure beneath eastern Anatolia. Two main models proposed are partial lithospheric delamination (Pearce et al., 1990) and slab break off (Şengör et al., 2003; Keskin 2003).

Keskin (2003) claimed that volcanic activity in Eastern Anatolia began earlier in the north (11–13 Ma) than in the south, migrating towards south with time. This migration was accompanied by changes in lava chemistry in the north - south direction. Volcanic products erupted in the north around the Erzurum-Kars plateau are calc-alkaline in character with a distinct subduction signature. However, volcanics in the south around the Mus,-Nemrut-Tendürek volcanoes are alkaline with an

intraplate signature (Pearce et al., 1990). The volcanic rocks of the Bingöl and Süphan volcanoes display transitional chemical characteristics.

However, the data accumulated so far on Eastern Anatolian volcanics support neither a monotonic age progression nor any systematic change in geochemical nature with time from north to south (e.g 15 Ma aged Aladağ andezites (Lebedev et al., 2010) and 11.9 -12.6 Ma aged Sarıçimen quartz monzodiorites (Çolakoğlu and Arehart , 2010) are situated in the southern parts of eastern Anatolia). The nonuniform distribution of ages and geochemical characters of volcanics, along with the recent findings from geophysical studies (i.e. Sandvol et al. 2003a, b; Zor et al. 2003; Angus et al. 2006; Gok et al. 2007; Özacar et al. 2008) in eastern Anatolia cast doubt on validity of only lithospheric mantle source (e.g. Pearce 1990, Yılmaz et al., 1998; Kheirkhah et al. 2009) or only asthenospheric mantle source with/without subduction component (Keskin 2003, 2007; Şengör et al., 2008) in the generation of the widespread volcanism in the region.

To evaluate the relative roles of the lithospheric and asthenospheric sources, as well as the melting degrees and melting depths, Süphan volcanics are compared here with the other volcanics of the region as taken from the previous studies (see Table 8.5). For this purpose, to avoid the effects of fractional crystallization, only rocks with < % 53 SiO₂ and > % 4.5 MgO are chosen (Table 8.5). Data which are used for interpretations are grouped as Miocene-Pliocene (Erzurum-Kars, Muş, Meydan) and Quaternary lavas (Ağrı, Nemrut, Süphan, Tendürek). Karacadağ volcanics which display within-plate character are also used for comparison.

Table 8.5 Representative major and trace element data from eastern Anatolian volcanics.

	Area	Source	Sample	SiO ₂	Al ₂ O ₃	Fe ₂ O ₃	FeO	FeO ^t	Fe ₂ O ₃ ^t	CaO	MgO	Na ₂ O	K ₂ O	TiO ₂	MnO	P ₂ O ₅	LOI	Tot
MIOCENE-PLIOCENE	Meydan	1	MA 23mp	48.00	18.02	3.24	5.23			10.82	7.29	3.68	0.78	1.19	0.16	0.37	0.51	99.29
	Meydan	1	MA 27mp	50.28	14.91	3.41	4.64			10.49	10.41	4.05	1.08	0.99	0.10	0.31	0.18	100.85
	Meydan	1	MA 230mp	47.81	17.26	4.14	7.09			9.16	5.86	5.39	1.16	1.59	0.18	0.53	0.04	100.21
	Muş	2	4	45.65	17.46				14.11	9.06	4.58	4.58	1.16	2.72	0.19	0.72		100.23
	Muş	2	26	45.17	15.54				15.78	8.29	4.86	4.22	1.21	3.68	0.25	1.22		100.22
	Muş	3	2112mp	50.10	15.56				12.60	8.00	4.60	3.92	1.32	2.86	0.20	0.49		99.65
	Muş	3	2113	47.50	16.50				12.42	8.56	5.92	2.86	1.00	2.84	0.18	44.00		141.78
	EKP	4	HO-1mp	50.92	17.21	2.97	5.41			8.42	5.93	3.51	1.03	1.35	0.17	0.30		97.22
	EKP	5	MK144mp	48.80	15.18				9.10	11.40	8.40	3.29	1.08	1.34	0.33	0.54	2.47	101.93
EKP	5	MK139mp	49.70	17.03				9.77	9.78	7.06	4.06	0.73	1.47	0.15	0.31	0.30	100.36	
QUATERNARY	Tendürek	6	T-38	47.80	17.01			11.14		10.50	6.42	3.96	0.55	2.07	0.19	0.34		99.98
	Tendürek	6	T-64	46.79	17.62			11.44		9.43	5.06	5.47	1.28	2.18	0.20	0.58		100.05
	Süphan	7	S6_99	51.47	17.44				10.98	9.19	7.15	4.01	0.90	1.92	0.17	0.36	0.00	103.59
	Nemrut	8	cu-34	46.14	16.39					8.58	5.90	3.46	0.81	3.10	0.19	0.57	0.10	85.24
	Nemrut	8	NCu17	46.49	16.52				12.67	8.65	6.25	3.05	1.34	2.15	0.18	0.45	1.70	99.45
	Nemrut	8	NÖka23	47.00	16.05				13.62	9.17	6.08	3.47	0.78	2.75	0.19	0.40	0.10	99.61
	Ağrı	3	A3132	51.40	17.54				9.88	8.42	6.68	4.12	0.86	2.08	0.15	0.33		101.46
	Ağrı	9	AMu 18.25	48.95	16.37				8.86	10.61	5.16	4.49	0.55	1.60	0.14	0.26	3.14	100.13
	Ağrı	9	AMu 20.26	49.64	16.39				9.84	9.14	6.93	4.51	1.06	1.67	0.16	0.42	0.45	100.21
	Ağrı	6	A 30-1	51.84	18.30			8.89		7.99	5.06	4.60	0.37	1.78	0.14	0.28		99.25
	Ağrı	6	A 30-5	52.11	18.33			9.06		7.97	5.20	4.95	0.58	1.79	0.14	0.28		100.41
	Ağrı	6	A30-10	51.20	17.79			9.07		8.32	6.22	4.32	0.75	1.74	0.15	0.35		99.91
	Ağrı	6	A30-12	51.35	17.59			9.08		8.47	6.54	4.30	0.82	1.73	0.15	0.38		100.41
	Ağrı	6	A-13	52.72	18.65			8.81		7.84	4.87	4.40	0.57	1.78	0.15	0.29		100.08
	Ağrı	6	A36-A	52.32	18.59			8.70		7.84	4.85	4.65	0.55	1.77	0.15	0.30		99.72
	Karacadağ	10	3MO 142	48.50	13.60						9.52	8.13	3.06	0.86	2.40	0.20	0.35	0.85
Karacadağ	10	3MO 134																0.00
Karacadağ	10	3MO 59	48.40	16.50					11.10	9.96	5.79	3.49	1.26	2.99	0.22	0.28	1.23	101.22
Karacadağ	10	3MO 84	43.30	14.30					15.80	10.50	6.94	2.90	0.80	4.76	0.26	0.40	0.46	100.42
Karacadağ	10	3MO 114	46.60	12.60					12.40	10.20	11.40	2.66	0.95	2.71	0.18	0.35	0.81	100.86
Karacadağ	10	3MO 103	46.90	12.50					12.80	9.62	11.80	2.67	0.91	2.26	0.25	0.36	1.76	101.83
Karacadağ	10	3MO 118																0.00
Karacadağ	10	3MO 110	44.30	11.80					13.60	9.38	9.62	4.63	1.97	3.54	0.21	0.98	0.22	100.25

Table 8.5. continued

	Area	Source	Sample	Th	Ta	Rb	Sr	Y	Ba	U	Ga	Hf	Nb	Pb	Zr	La	Ce
MIOCENE-PLIOCENE	Meydan	1	MA 23mp	5.00		14.0	630.0	31.0	326.0		17.00			0.00	129.0	22.30	47.31
	Meydan	1	MA 27mp	11.00		28.0	429.0	25.0	306.0		17.00			6.00	131.0	21.51	44.31
	Meydan	1	MA 230mp	8.00		37.0	673.0	32.0	417.0		18.00			8.00	199.0	27.03	60.15
	Muş	2	4	2.20		18.6	1081.7	30.4	155.2	14.00	23.20	5.40	21.7		339.2	25.00	50.00
	Muş	2	26	3.20		25.1	578.2	50.1	169.1	11.00	32.30	6.60	22.9		368.0	27.00	73.00
	Muş	3	2112mp	3.00	1.51	28.0	393.0	39.0	180.0	0.73		8.37	21.0	6.00	313.0	28.60	77.74
	Muş	3	2113	3.00	1.14	22.0	397.0	31.0	153.0	1.10		6.77	13.0	8.00	211.0	23.48	62.18
	EKP	4	HO-1mp	7.35	0.97	54.1	342.0		429.0	2.40		4.00				22.30	42.90
	EKP	5	MK144mp	3.34	0.71	18.0	867.0	26.0	533.0	1.03	16.00	2.80	15.0	5.60	119.0	30.60	68.90
EKP	5	MK139mp	1.65	0.53	9.0	507.0	25.0	461.0	0.70	22.00	2.60	11.0	2.60	147.0	13.50	29.60	
QUATERNARY	Tendürek	6	T-38			6.4	420.0		147.0						15.30	38.70	
	Tendürek	6	T-64			22.9	589.0		314.0						32.50	71.00	
	Süphan	7	S6_99	2.60	0.60	19.4	355.7	32.8	150.0	0.80	18.20	4.80	9.3		191.7	16.20	36.10
	Nemrut	8	Cu-34	1.80	0.80	13.8	512.7	36.6	180.0	0.60	25.00	5.10	13.8	1.60	215.0	20.20	53.70
	Nemrut	8	NCu17	4.20	0.80	37.9	493.6	34.4	266.0	1.00	23.80	5.60	14.2	3.10	223.3	23.20	54.30
	Nemrut	8	NÖka23	2.50	0.80	16.1	408.7	37.2	70.0	0.90	23.50	4.90	12.7	1.70	211.4	17.50	40.80
	Ağrı	3	A3132	3.00	0.43	11.0	531.0	26.0	221.0	0.30		4.23	10.1	3.00	187.0	18.90	52.72
	Ağrı	9	AMu 18.25	1.48	0.33	7.0	523.0	27.0	213.0	0.81	17.10	3.64	5.0	3.23	172.0	11.05	26.05
	Ağrı	9	AMu 20.26	2.10	0.66	15.0	571.0	29.0	309.0	0.62	16.70	3.71	12.0	4.36	172.0	20.79	43.98
	Ağrı	6	A 30-1			9.0	424.0	29.0	93.0			4.09	6.0		184.0	11.90	31.00
	Ağrı	6	A 30-5			10.0	459.0	29.0	105.0				7.0		193.0		
	Ağrı	6	A30-10			11.0	536.0	30.0	147.0			4.00	10.0		190.0		
	Ağrı	6	A30-12			13.0	566.0	28.0	160.0			4.16	11.0		188.0	17.60	41.00
	Ağrı	6	A-13			8.0	434.0	30.0	154.0				7.0		182.0	11.30	29.00
	Ağrı	6	A36-A			10.0	431.0	29.0	161.0				6.0		181.0	13.10	32.00
Karacadağ	10	3MO 142	2.60	1.00	22.0	368.0	22.0	178.0	0.70	23.00	3.50	19.0		122.0	15.00	34.30	
Karacadağ	10	3MO 134	2.50	0.90	15.0	398.0	25.0	192.0	0.60	24.00	3.50	17.0		123.0	14.80	31.50	
Karacadağ	10	3MO 59	2.60	1.60	16.0	599.0	24.0	162.0	0.90	26.00	5.00	29.0		193.0	22.60	50.10	
Karacadağ	10	3MO 84	1.50	1.70	9.0	739.0	21.0	256.0	0.40	25.00	4.00	32.0		147.0	20.70	46.30	
Karacadağ	10	3MO 114	1.70	1.50	11.0	530.0	19.0	219.0	0.50	22.00	3.80	28.0		139.0	17.90	40.60	
Karacadağ	10	3MO 103	2.20	1.40	12.0	459.0	20.0	258.0	0.70	21.00	3.50	26.0		133.0	18.80	41.60	
Karacadağ	10	3MO 118	2.70	2.50	10.0	854.0	20.0	179.0	1.10	27.00	5.60	48.0		219.0	33.20	71.20	
Karacadağ	10	3MO 110	5.30	4.80	23.0	1000.0	26.0	332.0	1.70	28.00	7.00	90.0		277.0	50.90	103.00	

Table 8.5 continued

	Area	Source	Sample	Pr	Nd	Sm	Eu	Gd	Tb	Dy	Ho	Er	Tm	Yb	Lu
MIOCENE-PLIOCENE	Meydan	1	MA 23mp	5.63	21.75	4.15	1.43	4.04	0.58	3.59	0.66	1.90	0.27	1.76	0.25
	Meydan	1	MA 27mp	5.19	19.77	3.81	1.27	3.82	0.57	3.33	0.63	1.84	0.25	1.69	0.24
	Meydan	1	MA 230mp	6.91	22.87	5.09	1.75	1.88	0.61	1.67	0.60	1.38	0.25	1.68	0.26
	Muş	2	4		31.60	6.60	1.90		0.78					2.80	0.5
	Muş	2	26		43.20	9.70	3.60		1.70					4.10	0.7
	Muş	3	2112mp		44.10	8.45	2.40		1.13					4.00	0.61
	Muş	3	2113		32.38	7.07	1.90		0.87					3.07	0.45
	EKP	4	HO-1mp		19.50	4.33	1.24		0.72					2.62	4
	EKP	5	MK144mp	8.30	33.70	6.14	1.74	5.70	0.71	4.05	0.83	2.20	0.32	2.18	0.34
EKP	5	MK139mp	3.80	15.80	3.64	1.33	4.10	0.65	4.14	0.80	2.46	0.35	2.37	0.35	
QUATERNARY	Tendürek	6	T-38		21.80	5.56	2.03		1.05					3.41	0.5
	Tendürek	6	T-64		34.00	7.35	2.46		1.26					3.97	0.53
	Süphan	7	S6_99	5.11	22.90	5.18	1.62	5.73	0.98	5.53	1.23	3.42	0.51	3.15	0.47
	Nemrut	8	Cu-34	6.48	28.30	6.60	2.18	6.55	1.12	6.51	1.20	3.54	0.49	3.41	0.42
	Nemrut	8	NCu17	6.63	31.50	6.30	2.07	6.62	1.09	6.07	1.14	3.43	0.47	3.00	0.45
	Nemrut	8	NÖka23	5.49	25.60	6.30	1.79	6.49	1.11	6.74	1.28	3.46	0.49	3.64	0.47
	Ağrı	3	A3132		26.64	5.17	1.63		0.69					2.46	0.41
	Ağrı	9	AMu 18.25	3.74	17.33	4.19	1.46	4.84	0.78	4.57	0.93	2.49	0.39	2.40	0.4
	Ağrı	9	AMu 20.26	5.81	24.34	5.19	1.66	5.47	0.85	4.94	1.00	2.70	0.43	2.61	0.43
	Ağrı	6	A 30-1		18.50	4.66	1.75		0.86					2.70	0.4
	Ağrı	6	A 30-5												
	Ağrı	6	A30-10												
	Ağrı	6	A30-12		21.50	4.87	1.77		0.90					2.50	0.36
	Ağrı	6	A-13		17.50	4.34	1.70		0.84					2.60	0.41
Ağrı	6	A36-A		18.30	4.36	1.76		0.86					2.90	0.45	
Karacadağ	10	3MO 142	4.20	16.90	4.30	1.53	4.60	0.70	4.00	0.70	2.10	0.28	1.60	0.25	
Karacadağ	10	3MO 134	3.83	16.10	4.30	1.57	4.90	0.80	4.40	0.90	2.30	0.31	1.90	0.27	
Karacadağ	10	3MO 59	5.44	22.90	5.80	2.01	5.60	0.90	4.80	0.90	2.30	0.30	1.80	0.25	
Karacadağ	10	3MO 84	5.71	23.10	5.70	2.07	5.60	0.80	4.10	0.70	1.90	0.24	1.40	0.18	
Karacadağ	10	3MO 114	4.94	19.20	4.80	1.74	4.80	0.70	3.70	0.70	1.70	0.22	1.30	0.19	
Karacadağ	10	3MO 103	4.95	19.70	4.70	1.68	4.70	0.70	3.70	0.70	1.80	0.24	1.40	0.2	
Karacadağ	10	3MO 118	8.48	32.90	7.30	2.53	6.70	0.90	4.30	0.70	1.70	0.20	1.10	0.15	
Karacadağ	10	3MO 110	11.90	43.50	9.70	3.22	8.70	1.20	5.60	0.90	2.20	0.26	1.40	0.18	

Table 8.5 continued

	Area	Source	Sample	La/Yb	Dy/Yb	Dy/YbN	La/Sm	Sm/Yb
MIOCENE-PLIOCENE	Meydan	1	MA 23mp	12.67	2.04	1.31	5.37	2.36
	Meydan	1	MA 27mp	12.73	1.97	1.26	5.65	2.25
	Meydan	1	MA 230mp	16.09	0.99	0.64	5.31	3.03
	Muş	2	4	8.93	0.00	0.00	3.79	2.36
	Muş	2	26	6.59	0.00	0.00	2.78	2.37
	Muş	3	2112mp	7.15	0.00	0.00	3.38	2.11
	Muş	3	2113	7.65	0.00	0.00	3.32	2.30
	EKP	4	HO-1mp	8.51	0.00	0.00	5.15	1.65
	EKP	5	MK144mp	14.04	1.86	1.19	4.98	2.82
	EKP	5	MK139mp	5.70	1.75	1.12	3.71	1.54
QUATERNARY	Tendürek	6	T-38	4.49	0.00	0.00	2.75	1.63
	Tendürek	6	T-64	8.19	0.00	0.00	4.42	1.85
	Süphan	7	S6_99	5.14	1.76	1.13	3.13	1.64
	Nemrut	8	cu-34	5.92	1.91	1.22	3.06	1.94
	Nemrut	8	NCu17	7.73	2.02	1.30	3.68	2.10
	Nemrut	8	NÖka23	4.81	1.85	1.19	2.78	1.73
	Ağrı	3	A3132	7.68	0.00	0.00	3.66	2.10
	Ağrı	9	AMu 18.25	4.60	1.90	1.22	2.64	1.75
	Ağrı	9	AMu 20.26	7.97	1.89	1.21	4.01	1.99
	Ağrı	6	A 30-1	4.41		0.00	2.55	1.73
	Ağrı	6	A 30-5					
	Ağrı	6	A30-10					
	Ağrı	6	A30-12	7.04			3.61	1.95
	Ağrı	6	A-13	4.35			2.60	1.67
	Ağrı	6	A36-A	4.52			3.00	1.50
	Karacadağ	10	3MO 142	9.38	2.50	1.60	3.49	2.69
	Karacadağ	10	3MO 134	7.79	2.32	1.49	3.44	2.26
	Karacadağ	10	3MO 59	12.56	2.67	1.71	3.90	3.22
	Karacadağ	10	3MO 84	14.79	2.93	1.88	3.63	4.07
	Karacadağ	10	3MO 114	13.77	2.85	1.83	3.73	3.69
	Karacadağ	10	3MO 103	13.43	2.64	1.70	4.00	3.36
	Karacadağ	10	3MO 118	30.18	3.91	2.51	4.55	6.64
	Karacadağ	10	3MO 110	36.36	4.00	2.57	5.25	6.93

Source for data; 1; Arslan (1994), 2; Buket & Temel (1998), 3; Pearce et al. (1990), 4; Ercan et al. (1990), 5; Keskin et al. (1998), 6; Gülen (1984), 7; this study, 8; Özdemir et al. (2006), 9; Kheirkhah et al. (2009), 10; Lustrino et al. (2010).

Concentrations of REE can be used to search for the presence of garnet in the source of the volcanic rocks. Garnet strongly retain HREE, and therefore magmas derived from garnet-bearing source have high LREE/ HREE (Blundy et al., 1998). La/Yb ratios range between 12.67-16.09 for Meydan, 5.70-14.04 for Erzurum-Kars, 6.59-8.93 for Muş 4.49-8.19 for Tendürek, 4.35-7.97 for Ağrı, and 4.81-7.73 for Nemrut; the ratio is 5.14 for Süphan. It is apparent that the enrichment of the LREE/HREE is decreasing from Miocene-Pliocene aged (Meydan, Erzurum-Kars, Muş) volcanic rocks to Quaternary (Tendürek , Ağrı, Nemrut, Süphan,) volcanic fields. The MREE/HREE ratio of Dy/Yb may also support the presence of garnet in the source region. $(Dy/Yb)_N$ ratios of < 1.06 characterize melts derived from a spinel lherzolite source (Blundy et al., 1998). All of the Eastern Anatolian volcanics have a ratio of $(Dy/Yb)_N > 1.06$ further supporting the presence of garnet in the source.

Another attempt can be done by using Sm/Yb vs La/Sm plot (Figure 8.11).. Miocene - Pliocene lavas plot between mixing lines of 0.1-3 % melting of garnet and spinel facies. The contribution of the garnet and spinel facies in the genesis of the volcanics seems to correspond to a garnet/spinel ratio between 75/25 - 60/40. However, garnet/spinel ratio of the two volcanic samples from Erzurum-Kars is 40/60. Quaternary lavas of the eastern Anatolia (Ağrı, Nemrut, Süphan, Tendürek) display different positions in the diagram. It is apparent from the figure that garnet contribution is decreasing in the genesis of the these Quaternary lavas and also melting degree is increasing (1-5 %, majority plotting in the 5 % area.) Karacadağ samples display various degree of melting between 0. 1% - 7 % and have a garnet contribution more than 80% in their genesis.

Recent geophysical studies reveal a range of 60-80 km for the thickness of the lithosphere in eastern Anatolia, with an average thickness of 75 km (Angus et al., 2006; Özacar et al, 2008). This thickness is less than the normal thickness of a lithosphere, but still implying presence of mantle lithosphere beneath the crust of the eastern Anatolia. Thin lithospheric mantle beneath the region, can be reformed by cooling of the asthenosphere (Keskin, 2007) or remnant of some lithospheric mantle prior to the asthenospheric upwelling. With the spinel to garnet transition at a depth of ~ 80 km (Takahashi and Kushiro, 1983), it is likely to say that spinel peridotite facies (<80 km) comprises most of the lower lithosphere beneath eastern Anatolia. Garnet peridotite facies (>80 km) is primarily part of the asthenosphere beneath the region.

Melting trajectories using the available data depict that eastern Anatolian volcanics are result of various mixing between asthenospheric and lithospheric sources. In a broad approximation, melting degree and contribution of the spinel facies (lithospheric contribution) is increasing from Miocene-Pliocene to Quaternary volcanics. Both slab break off or partial loss of lower lithosphere can be responsible for the asthenospheric upwelling and widespread volcanism in the region.

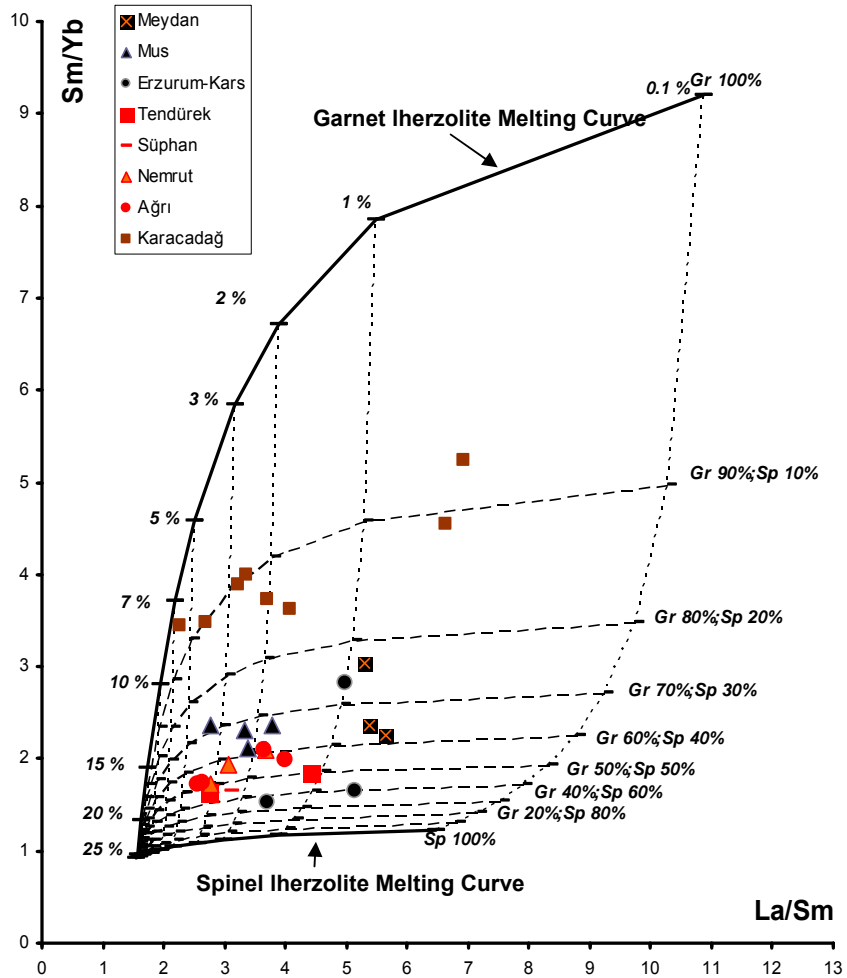


Figure 8.11 Calculated partial melting curves assuming non-modal batch melting of garnet (Gt) and spinel (Sp) lherzolite sources for eastern Anatolian volcanics (dotted lines: mixing between garnet and spinel lherzolite melts; dashed lines: garnet/spinel ratio on the mixing lines, F: degree of melting. Garnet lherzolite : 0.598ol, 0.211 opx, 0.076cpx, 0.115 grt, melting proportions: 0.05 ol, 0.2 opx, 0.3 cpx, 0.45 grt; spinel lherzolite 0.578 ol, 0.27 opx, 0.119 cpx, 0.033 sp, melting proportions: 0.1 ol, 0.27 opx, 0.5 cpx, 0.13 sp; Thirlwall et al., 1994, Shaw et al., 2003, Peters et al., 2008). The composition of the primitive mantle and distribution coefficients are from McKenzie and O’Nions (1991).

CHAPTER 9

CONCLUSIONS

The main conclusions drawn from the thesis study can be summarized as follows;

- Volcanic products of the Süphan stratovolcano were emplaced over the Miocene and Pliocene-Pleistocene sedimentary units in eastern Anatolia. Products of the Süphan volcanism extend over an area of about 2000 km² between Malazgirt, Patnos and Adilcevaz towns. Initial products of Süphan volcanism are debris avalanche and phase I pyroclastic rocks. The first lava flows observed around the volcano are rhyolitic obsidian flows. These acidic units are overlain by basaltic, basaltic trachyandesitic, trachandesitic lava flows. Several plinian eruptions and a block and ash flow overlay these basic and intermediate units. Trachytic lava flows and rhyolitic/dacitic domes occurred as the last eruption phase of the main cone. The most recent product of volcanism is phreatomagmatic and includes a maar occurrence at the southern parts of the volcano.
- Ar-Ar data obtained from the different levels of the volcanostratigraphic succession suggest that the evolution of volcanism took place between 0.76 Ma-0.06 Ma BP.

- On the basis of the mineral paragenesis, the lava flows/domes are classified as 6 major groups corresponding to different compositions. The basalt, basaltic trachyandesites, trachyandesites contain *plagioclase + c linopyroxene ± o livine ± orthopyroxene* minerals. Trachytes and dacites include *plagioclase + cli nopyroxene + orth opyroxene ± a mphibole ± biotite* phenocrysts. Rhyolites are characterized by *plagioclase ± orthopyroxene ± amphibole + biotite + quartz + K-feldspar*.
- Major element contents reveal that volcanic products of Süphan cover a broad compositional spectrum from basalt to rhyolite. They display transition between subalkaline and alkaline character. The lavas which have the mildly alkaline character are the older lavas of the volcano and overall the character of the volcanism seems to have turned into transitional and subalkaline with time.
- On the basis of trace and RE elements data, volcanics of the Suphan Stratovolcano exhibit enrichment in light rare earth elements (LREE) over heavy rare earth elements (HREE), and large ion lithophile elements (LILE) over high field strength elements (HFSE) with negative Nb and Ta anomalies. Distinctive depletion of Nb and Ta points to the presence of a subduction component in the mantle source of the Süphan volcanics.
- Enclaves from the Suphan Stratovolcano are collected from dacitic - rhyolitic domes and trachytic lava flows. They were classified as coarse and fine grained gabros, dolerites and microdiorites. Doleritic and microdioritic enclaves have major, trace and REE patterns similiar to those of Süphan volcanics, suggesting that these enclaves are likely to represent the earlier

products of the Süphan magmatism. Coarse grained gabbroic enclave displays similarities to the within plate volcanism, while fine grained gabbroic enclave has arc volcanism affinity with its distinct negative Nb and Ta anomalies.

- Mineral chemistry and textures indicate that magma mixing played an important role in the petrogenesis of Süphan volcanism. Intermediate magmas show a wide range of mineral compositions, for pyroxene, olivine and plagioclase, that are intermediate between those of basalts and rhyolites.
- Glassy melt inclusions were identified in plagioclase, olivine, orthopyroxene, clinopyroxene, amphibole and biotites from rocks of the Süphan ranging from basaltic trachyandesites to rhyolites. Most part of the melt inclusion compositions define trends that are quite oblique to the linear trends of the whole rocks. .
- Mineral thermometry of Süphan volcanics yields a wide range of temperatures between rhyolite (~750 °C) and basalt (~1100 °C). The estimated maximum pressures are 320 Mpa for basaltic trachyandesites, 70 Mpa for trachyandesites, 120 Mpa for trachytes and rhyolites and 190 Mpa for dacites. The corresponding maximum depths for these pressures are 12 km for basaltic trachyandesites, 3 km for trachyandesites, 4.5 km for trachytes and rhyolites, and 7km for dacites.
- The textural complexity of the phenocrysts, the wide temperature ranges obtained for trachytes, trachyandesites and dacites, and the linear geochemical trends are strongly suggestive of magma mixing in the evolution of Süphan volcanics. Comparison of whole rock data and melt inclusion contents in Süphan to

experimental data from basaltic and trachyandesitic magmas of similar composition indicate that the melt inclusions describe true liquid lines of descent from a common hydrous parent at H₂O pressures of ≤ 500 MPa

- Crustal contamination and melting models using the isotopic compositions and REE data reveal that Süphan volcanics were derived from mixing of both lithospheric and asthenospheric mantle sources and were affected by upper crustal contamination on the way to surface.
- LILE enrichment and the presence of negative HFSE (Nb and Ta in particular) anomalies in the Süphan volcanics are attributed to the mantle source of the Süphan volcanics modified by bulk sediment or partial melt of subducted sediment, rather than fluids from subducted oceanic crust or subducted sediments.
- A two-stage petrogenetic model can be proposed for Süphan volcanism based on the mineral and melt inclusions chemistry. Mantle-derived hydrous basalt stalls in the lower to mid-crust, whereupon it crystallizes to produce evolved melts. A variety of evolved melts then ascended to shallow level where they interacted. The presence of glomerocrysts in many lavas suggests that cogenetic plutonic rocks were also involved in the interaction process.
- Melting trajectories using the available data from eastern Anatolia suggest that eastern Anatolian volcanics have been resulted from various degrees of mixing between asthenospheric and lithospheric sources.

- Any attempt for the construction of time-space relationship of the volcanic products, any possible trend in temporal evolution and spatial distribution of volcanism requires more data covering the whole region.

▪

REFERENCES

- Agard, P., Omrani, J., Jolivet, L., and Mouthereau, F., 2005. Convergence history across Zagros (Iran): Constraints from collisional and earlier deformation. *International Journal of Earth Sciences*, 94, 401–419, doi: 10.1007/s00531-005-0481-4.
- Alavi, M., 1994. Tectonics of the Zagros orogenic belt of Iran—New data and interpretations: *Tectonophysics*, 229, 211–238, doi: 10.1016/0040-1951 (94)90030-2.
- Al-Lazki, A., Seber, D., Sandvol, E., Turkelli, N., Mohamad, R., Barazangi, M., 2003. Tomographic Pn velocity and anisotropy structure beneath the Anatolian plateau (eastern Turkey) and the surrounding regions. *Geophysical Research Letters* 30 (24), 8043, doi:10.1029/2003GL017391.
- Allen, M., and Armstrong, H.A., 2008. Arabia–Eurasia collision and the forcing of mid-Cenozoic global cooling. *Palaeogeography, Palaeoclimatology, Palaeoecology*, 265, 52–58, doi: 10.1016/j.palaeo.2008.04.021.
- Anderson, D.J. and Lindsley, D.H., 1985. New (and final!) models for the Ti-magnetite/Ilmenite geothermometer and oxygen barometer. *EOS Trans* 66, 416.

- Angus D.A., Wilson D.C., Sandvol E., Ni J.F., 2006. Lithospheric structure of the Arabian and Eurasian collision zone in Eastern Turkey from S-wave receiver functions. *Geophysical Journal International* 166 (3):1335-1346.
- Arslan, M., 1994. Mineralogy, geochemistry, petrology and petrogenesis of the Meydan-Zilan (Erciş-Van, Turkey) area volcanic rocks. PhD Thesis, University of Glasgow; UK.
- Aydar, E., Gourgaud, A., Ulusoy, I., Digonnet, F., Labazuy, P., Sen, E., Bayhan, H., Kurttaş, T., Tolluoğlu, A.Ü., 2003. Morphological analysis of active Mount Nemrut stratovolcano, eastern Turkey: evidences and possible impact areas of future eruption. *Journal of Volcanology and Geothermal Research* 123:301-312.
- Bacon, C.R, Hirschmann, M.M., 1988. Mg/Mn partitioning as a test for equilibrium between coexisting Fe-Ti oxides. *American Mineralogist*,73,57-61.
- Berberian, M., and King, G., 1981, Toward a paleogeography and tectonic evolution of Iran. *Canadian Journal of Earth Sciences*, 18, 210–265, doi: 10.1139/e81-163.
- Blundy, J.D., Robinson, J.A.C., Wood, B.J., 1998. Heavy REE are compatible in clinopyroxene on the spinel lherzolite solidus. *Earth and Planetary Science Letters* ,160, 493–504.
- Bohrson, W. A. & Spera, F. J., 2001. Energy-constrained open-system magmatic processes II: application of energy-constrained assimilation– fractional crystallisation (EC-AFC) model to magmatic systems. *Journal of Petrology*, 42, 1019–1041.

- Bozkurt, E., 2001. Neotectonics of Turkey- a synthesis. *Geodinamica Acta*, 14, 3-30.
- Bryan, W.B., Finger, I. & Chayes, F. 1969. Estimating proportions in petrographic mixing equations by least-square approximation. *Science*, 163, 926–927.
- Buket, E., and Temel, A., 1998. Major-element, trace-element, and Sr-Nd isotopic geochemistry and genesis of Varto Mus, volcanic rocks, Eastern Turkey: *Journal of Volcanology and Geothermal Research*, 85, 405– 422, doi: 10.1016/S0377-0273(98)00064-X.
- Cas, R.A.F, and Wright, J.V., 1987. *Volcanic successions*. Chapman & Hall, London, 528 pp.
- Class, C., Miller, D. M., Goldstein, S. L., Langmuir, C. H., 2000. Distinguishing melt and fluid subduction components in Umnak volcanics: Aleutian arc. *Geochemistry, Geophysics, Geosystems* 1, 1999GC000010.
- Çakır, Ö., Erduran, M., Çınar, H., and Yılmaztürk, A., 2000. Forward modeling receiver functions for crustal structure beneath station TBZ (Trabzon, Turkey): *Geophysical Journal International*, 140, 341–356, doi: 10.1046/j.1365-246x.2000.00023.x.
- Çolakoğlu, A.L., Arehart, G.B., 2010. The petrogenesis of Sariçimen (Çaldıran-Van) quartz monzodiorite: Implication for initiation of magmatism (Late Medial Miocene) in the east Anatolian collision zone, Turkey. *Lithos*, 119, 607-620.

- Demirtaşı, E., Pisoni, C., 1965. Ahlat–Adilcevaz bölgesinin jeolojisi (Van Gölü kuzeyi). Maden Tetkik ve Arama Enstitüsü Dergisi, 64, 22–36.
- Dewey J.F, Hempton M.R, Kidd W.S.F, Şaroğlu F, Şengör A.M.C., 1986. Shortening of continental lithosphere: the neotectonics of Eastern Anatolia - a young collision zone. In: Coward MP, Riea AC (eds) Collision Tectonics. Geological Society of London, Spec Publ., 19, 3-36.
- Dhont D., Chorowicz J., 2006. Review of the neotectonics of the Eastern Turkish–Armenian Plateau by geomorphic analysis of digital elevation model imagery: International Journal of Earth Sciences, 95, 34–49, doi:10.1007/s00531–005–0020–3.
- Dolmaz, M.N., Elitok, Ö., Kalyoncuoğlu, U.Y., 2008. Interpretation of low seismicity in the Eastern Anatolian Collisional Zone using geophysical (Seismicity and Aeromagnetic) and geological data. Pure and Applied Geophysics, 165, 311–330.
- Elburg, M. A., Bergen, M. V., Hoogewerff, J., Foden, J., Vroon, P., Zulkarnain, I., Nasution, A., 2002. Geochemical trends across an arc–continent collision zone: magma sources and slab–wedge transfer processes below the Pantar Strait volcanoes, Indonesia. Geochimica et Cosmochimica Acta, 66, 2771–2789.
- Elliott, T., Planck, T., Zindler, A., White, W., Bourdon, B., 1997. Element transport from slab to volcanic front at the Mariana arc. Journal of Geophysical Research ,102, 14991–15019.

- Ercan, T., Fujitani, T., Matsuda, J., Notsu, K., Tokel, S., Tadahide, U.İ., 1990. Doğu ve Güneydoğu Anadolu Neojen-Kuvaterner volkanitlerine ilişkin yeni jeokimyasal, radyometrik ve izotopik verilerin yorumu. MTA dergisi 110, 143-164.
- Freise, M., Holtz, F., Nowak, M., Scoates, J.S., Strauss, H., 2009. Differentiation and crystallization conditions of basalts from the Kerguelen large igneous province: an experimental study. Contributions to Mineralogy and Petrology, 158, 505-527, doi:10.1007/s00410-009-0394-5.
- Fujimaki, H., Tatsumoto, M. and Aoki, K.-i., 1984. Partition coefficients of Hf, Zr, and REE between phenocrysts and groundmasses. Journal of Geophysical Research, 89, 662-672.
- Glicken, H., 1982. Criteria for identification of large volcanic debris avalanches (abstr). Eos, Trans Am Geophys Union, 63, 1141.
- Glicken, H., 1996. Rockslide-Debris Avalanche of May 18, 1980, Mount St. Helens Volcano, USGS Open-File Report 96-677. USGS, Washington, 1–90.
- Gok, R., Pasyanos, M.E., Zor, E., 2007. Lithospheric structure of the continent–continent collision zone: eastern Turkey. Geophysical Journal International, 169, 1079–1088.
- Göncüoğlu, M.C., and Turhan, N., 1984. Geology of the Bitlis metamorphic belt, in Tekeli, O., and Göncüoğlu, M.C., eds., Proceedings of the International Symposium on the Geology of the Taurus Belt: Ankara, Turkey. Mineral Research and Exploration Institute, 237–244.

- Guo, Z., Wilson, M., Liu, J., Mao, Q., 2006. Post-collisional, Potassic and Ultrapotassic Magmatism of the Northern Tibetan Plateau: Constraints on Characteristics of the Mantle Source, Geodynamic Setting and Uplift Mechanisms. *Journal of Petrology*, 47, 1177-1220.
- Gülen, L., 1984. Sr, Nd, Pd isotope and trace elements geochemistry of calc-alkaline and alkaline volcanics, eastern Turkey. PhD Thesis, Massachusetts Inst Tech., USA.
- Hall, R., 1976. Ophiolite emplacement and the evolution of the Taurus suture zone, southeastern Turkey: *Geological Society of America Bulletin*, 87, 1078–1088.
- Hafkenscheid, E., Wortel, M.J.R., and Spakman, W., 2006, Subduction history of the Tethyan region derived from seismic tomography and tectonic reconstructions, *Journal of Geophysical Research, Solid Earth*, 111, B8, article no. B08401.
- Hart, S. R., 1984b. A large-scale isotope anomaly in the Southern Hemisphere mantle. *Nature*, 309, 753-57.
- Hawkesworth, C.J., Taylor, P.N., Palacz, Z., 1986. Evidence from the Parana of SouthBrazil for a continental contribution to Dupal basalts. *Nature* 322, 356-359.
- Hawkesworth, C.J., Mantovani, M.S.M. and Peate, D.W., 1988. Lithosphere remobilisation during Parana CFB magmatism. In: Cox, K.G. & Menzies, M.A. (eds) *Oceanic and continental lithosphere: Similarities and differences*. *Journal of Petrology, Special Volume*, 205-223.

- Hawkesworth, C.J., Kempton, P.D., Rogers, N.W., Ellam, R.M. and Von Calsteren, P.W., 1990. Continental mantle lithosphere and shallow level enrichment processes in the Earth's mantle. *Earth & Planetary Science Letters*, 96, 256-268.
- Hawkesworth, C. J., Gallagher, K., Hergt, J. M., McDermott, F., 1993. Mantle and slab contributions in arc magmas. *Annual Review of Earth and Planetary Sciences*, 21, 175–204.
- Hawkesworth, C. J., Turner, S. P., McDermott, F., Peate, D. W., van Calsteren, P., 1997. U–Th isotopes in arc magmas: implications for element transfer from the subducted crust. *Science*, 276, 551–555.
- Holland, T., Blundy, J.D., 1994. Non-ideal interactions in calcic amphiboles and their bearing on amphibole–plagioclase thermometry. *Contributions to Mineralogy and Petrology*, 116, 433–447.
- Humphreys, M.C.S., Kearns, S.L., Blundy, J.D., 2006 SIMS investigation of electron-beam damage to hydrous, rhyolitic glasses: Implications for melt inclusion analysis. *American Mineralogist*, 91, 667-679.
- Innocenti, F., Mazzuoli, R., Pasquare, G., Redicci di Brozolo, F., Villari, L., 1976. Evolution of the volcanism in the area of interaction between the Arabian, Anatolian and Iranian plates (Lake Van, Eastern Turkey). *Journal Volcanology and Geothermal Research* 1, 103-112.

Innocenti, F., Manetti, P., Mazzuoli, R., Pasquaré, G., and Villari, L., 1982a, Anatolia and north-western Iran, in *Andesites*, Ed. R.S. Thorpe, John Wiley & Sons.

Innocenti, F., Mazzuoli, R., Pasquaré, G., Radicati di Brozolo, F., and Villari, L., 1982b. Tertiary and Quaternary volcanism of the Erzurum-Kars area (Eastern Turkey): Geochronological data and geodynamic evolution: *Journal of Volcanology and Geothermal Research*, 13,223–240, doi: 10.1016/0377-0273(82)90052-X.

Irvine T.N, Baragar W.R.A., 1971. A guide to the chemical classification of the common volcanic rocks. *Canadian Journal of Earth Sciences*, 8, 523-548.

Jolivet, L., and Faccenna, C., 2000. Mediterranean extension and the Africa-Eurasia collision. *Tectonics*, 19, 1095–1106, doi: 10.1029/2000TC900018.

Karaoğlu, Ö., Özdemir, Y., Tolluoğlu, A.Ü., Karabıyıköğlu, M., Köse, O., Froger, J.L., 2005 Stratigraphy of the volcanic products around Nemrut Caldera: implications for reconstruction of the Caldera Formation. *Turkish Journal of Earth Sciences*, 14, 123–143

Karapetian, S.G., Jrbashian, R.T., and Mnatsakanian, A.K., 2001, Late collision rhyolitic volcanism in the north-eastern part of the Armenian Highland: *Journal of Volcanology and Geothermal Research*, 112 (1–4), 189–220. doi: 10.1016/S0377-273(01)00241-4.

Keskin, M., 2003. Magma generation by slab steepening and breakoff beneath a subduction-accretion complex: An alternative model for

collision-related volcanism in Eastern Anatolia, Turkey. *Geophysical Research Letters*, 30(24),1-4. doi.10.1029/2003GI018019.

Keskin, M., 2007. Eastern Anatolia: a hot spot in a collision zone without a mantle plume. In: Foulhrt GR and Jurdy D (eds) *Plates, Plumes, and Planetary Processes*. Geological Society of America, Special Paper., 430, 693–722.

Keskin, M., Pearce, J.A., Mitchell, J.G., 1998. Volcano-stratigraphy and geochemistry of collision-related volcanism on the Erzurum-Kars Plateau, North Eastern Turkey. *Journal of Volcanology and Geothermal Research.*, 85,355– 404.

Kheirkhah M., Allen M.B., Emami M., 2009. Quaternary syn-collision magmatism from the Iran/Turkey borderlands. *Journal of Volcanology and Geothermal Research*, 182, 1–12.

Koçyiğit, A., Yılmaz, A., Adamina, S., Kuloshvili, S., 2001. Neotectonics of East Anatolian Plateau (Turkey) and Lesser Caucasus: implication for transition from thrusting to strike-slip faulting. *Geodinamica Acta*,14, 177-195.

Langmuir, C., Vocke, R., Hanson, G. and Hart, S., 1978. A general mixing equation with applications to Icelandic basalts. *Earth and Planetary Science Letters*, 37, 380-392.

Leake ,B.E .,1978. Nomenclature of amphiboles. *American Mineralogist* 63: 1023–1052.

- Le Bas, M. J., Le Maitre, R. W., Streckeisen, A., Zannettin, B., 1986. A classification of volcanic rocks based on the total alkali-silica diagram. *Journal of Petrology*, 27, 745-750.
- Lebedev, V.A., Sharkov, E.V., Keskin, M., Oyan, V., 2010. Erratum: Geochronology of Late Cenozoic Volcanism in the Area of Lake Van, Turkey: An Example of Developmental Dynamics for Magmatic Processes. *Doklady Earth Sciences*, 433(2), 1031-1037.
- Lei, J., Zhao, D., 2007. Teleseismic evidence for a break-off subducting slab under Eastern Turkey. *Earth and Planetary Science Letters*, 257, 14–28.
- Lepage, L.D., 2003. ILMAT: an Excel worksheet for ilmenite-magnetite geothermometry and geobarometry. *Computes and Geosciences*, 29, 673–678.
- Lindsley, D.H and Frost, B.R., 1992. Equilibria among Fe–Ti oxides, pyroxenes, olivine, and quartz: Part I. Theory. *American Mineralogist*, 77, 987–1003.
- Liu, Y., Anderson, A.T., Wilson, C.J.N., Davis, A.M. and Steele, I.M., 2006. Mixing and differentiation in the Oruanui rhyolitic magma, Taupo, New Zealand: evidence from volatiles and trace elements in melt inclusions, *Contributions to Mineralogy and Petrology*, 151, 71–87.
- Luhr, J.F., 1990. Experimental phase relations of water- and sulfur-saturated arc magmas and the 1982 eruptions of El Chichón Volcano. *Journal of Petrology*, 31, 1071-1114.

- Lustrino, M., Keskin, M., Mattioli, M., Lebedev, V., Chugaev, A., Sharkov, E., Kavak, O., 2010. Early activity of the largest Cenozoic shield volcano in the circum-Mediterranean area: Mt. Karacadağ, SE Turkey. *European Journal of Mineralogy*, 22, 343-362.
- Matsui, Y., Onuma, N., Nagasawa, H., Higuchi, H. and Banno, S., 1977. Crystal structure control in trace element partition between crystal and magma. *Tectonics*, 100, 315-324.
- Mc Kenzie, D. P., O'Nions, R. K., 1991. Partial melt distributions from inversion of rare earth element concentrations. *Journal of Petrology*, 32, 1021-1091.
- Middlemost, E. A. K., 1975. The basalt clan. *Earth Science Reviews*, 11, 337-364.
- Miyashiro, A. 1978 Nature of alkalic volcanic rocks series. *Contributions to Mineralogy and Petrology*, 66, 91-104.
- Mortazavi, M and Sparks, R.S.J., 2004. Origin of rhyolite and rhyodacite lavas and associated mafic inclusions of Cape Akrotiri, Santorini: the role of wet basalt in generating calcalkaline silicic magmas. *Contributions to Mineralogy Petrology*, 146, 397–413.
- Murphy, M.D, Sparks, R.S.J., Barclay, J., et al., 1998. The role of magma mixing in triggering the current eruption at the Soufrie`re Hills volcano, Montserrat, West Indies. *Geophysical Research Letters*, 25, 433–3436.

- Nakamura, N., 1974. Determination of REE, Ba, Mg, Na and K in carbonaceous and ordinary chondrites. *Geochimica et Cosmochimica Acta*, 38, 757-775.
- Newman, S. and Lowenstern, J.B., 2002. VolatileCalc: a silicate melt-H₂O-CO₂ solution model written in Visual Basic for Excel. *Computer and Geosciences*, 28, 597-604.
- Notsu, K., Fujitoni, T., Ui, T., Matsuda, J., Ercan, T., 1995. Geochemical features of collision related volcanic rocks in central and Eastern Anatolia, Turkey. *Journal of Volcanology and Geothermal Research*, 64,171-192.
- Oberhänsli, R., Candan, O., Bousquet, R., Rimmelé, G., Okay, A., and Goff, J.B., 2010. Alpine HP evolution of the eastern Bitlis complex, SE Turkey: *Geological Society of London Special Publication*, 340, 461-483.
- Ogata A., Nakamura K., Nagao K. and Akimoto S.,1989. K-Ar age of young volcanic rocks of Turkey. 1989 annual meeting of the Geochemical Society of Japan, ICO 3.
- Okay, A.I., Zattin, M., Cavazza, W., 2010. Apatite fission-track data for the Miocene Arabia-Eurasia collision. *Geology*, 38, 35-38.
- Oyan, V., 2004. Bölükyazı-Hizan (Bitlis Masifi) Çevresindeki Na-Feldispat Oluşumlarının Jeolojik Özellikleri ve Ekonomik Önemi (Yüksek Lisans Tezi), Yüzüncü Yıl Üniversitesi, Fen Bilimleri Enstitüsü, Van.

- Özacar, A.A., Gilbert, H., Zandt, G., 2008. Upper mantle discontinuity structure beneath East Anatolian Plateau (Turkey) from receiver functions. *Earth and Planetary Science Letters*, 269, 426-434.
- Özdemir, Y., Karoğlu, Ö., Tolluoğlu, A.Ü., Güleç, N., 2006. Volcanostratigraphy and petrogenesis of the Nemrut stratovolcano (East Anatolian High Plateau): The most recent post-collisional volcanism in Turkey. *Chemical Geology*, 226,189–211.
- Özdemir, Y., Blundy, J.D., Güleç, N., 2011. The importance of fractional crystallization and magma mixing in controlling chemical differentiation at Süphan Stratovolcano, Eastern Anatolia, Turkey. *Contributions to Mineralogy and Petrology*, in press.
- Peccerillo, A. & Taylor, S. R.,1976. Geochemistry of Eocene calc-alkaline volcanic rocks from the Kastamonu area, Northern Turkey. *Contributions to Mineralogy and Petrology*, 58, 63–81.
- Pearce, J.A., 1983. The role of sub-continental lithosphere in magma genesis at destructive plate margins. In: Hawkesworth CJ and Norry MJ (eds) *Continental Basalt and Mantle Xenoliths*. Shiva Publishing Limited, Cheshire, 230-249.
- Pearce J.A., Bender J.F., De Long S.E., Kidd, W.S.F., Low, P.J., Güner, Y., Şaroğlu, F., Yılmaz, Y., Moorbath, S., Mitchell, J.G., 1990. Genesis of collision volcanism in Eastern Anatolia, Turkey. *Journal of Volcanology Geothermal Research*, 44,189–229.

- Peters, T.J., Menzies, M., Thirlwall, M., Kyle, P., 2008. Zuni-Bandera volcanism, Rio Grande, USA – melt formation in garnet- and spinel-facies mantle straddling the asthenosphere-lithosphere boundary. *Lithos*, 102(1-2), 295-315.
- Piromallo, A., and Morelli, P., 2003. P wave tomography of the mantle under the Alpine-Mediterranean area: *Journal of Geophysical Research*, 108, doi: 10.1029/2002JB001757.
- Plank, T. & Langmuir, C. H., 1998. The chemical composition of subducting sediment and its consequences for the crust and mantle. *Chemical Geology* 145, 325–394.
- Putirka, K.D., 2008. Thermometers and barometers for volcanic systems. In: Putirka KD and Tepley F (eds) *Reviews in Mineralogy and Geochemistry.*, 69, 61-120.
- Reubi, O., Blundy, J.D., 2008. Assimilation of plutonic roots, formation of high-K “exotic” melt inclusions and genesis of andesitic magmas at Volcán de Colima, Mexico. *Journal of Petrology*, 49, 2221-2243.
- Reubi, O., Blundy, J.D., 2009. A dearth of intermediate melts at subduction zone volcanoes and the petrogenesis of arc andesites. *Nature*, 461,1269-1273.
- Robertson, A.H.F., Parlak, O., Rızaoğlu, T., Ünlügenç, Ü., İnan, N., Taslı, K., and Ustaömer, T., 2007, Tectonic evolution of the South Tethyan ocean: Evidence from the Eastern Taurus Mountains (Elazığ region, SE Turkey), *in* Ries, A.C., Butler, R.W.H., and Graham, R.H., eds., *Deformation of Continental Crust*. Geological Society of London Special Publication,272, 231–270.

- Ryan, J. G., Morris, J., Tera, F., Leeman, W. P., Tsvetkov, A., 1995. Cross-arc geochemical variations in the Kurile arc as a function of slab depth. *Science* 270, 625–627.
- Sandvol, E., Türkelli, N., Barazangi, M., 2003a. The eastern Turkey seismic experiment: the study of a young continent-continent collision. *Geophysical Research Letters* 30(24), 8038, doi: 10.1029/2003GL018912.
- Schmitt, A.K., 2001. Gas-saturated crystallization and degassing in large-volume, crystal-rich dacitic magmas from the Altiplano-Puna, northern Chile, *Journal of Geophysical Research*, 106 , 30561–30578.
- Schnetzler, C.C. and Philpotts, J.A., 1970. Partition coefficients of rare-earth elements between igneous matrix material and rock-forming mineral phenocrysts; II. *Geochimica et Cosmochimica Acta*, 34 (3), 331-340. doi: 10.1016/0016-7037(70)90110-9.
- Shaw, J.E., Baker, J.A., Menzies, M.A., Thirlwall, M.F., Ibrahim, K.M., 2003. Petrogenesis of the largest intraplate volcanic field on the Arabian Plate (Jordan): a mixed lithosphere–asthenosphere source activated by lithospheric extension. *Journal of Petrology*, 44, 1657–1679.
- Sheppard, S. & Taylor, W. R., 1992. Barium- and LREE-rich, olivine–mica- lamprophyres with affinities to lamproites, Mt. Bunday, Northern Territory, Australia. *Lithos*, 28, 303–325.

- Siebert, L., 1984. Large volcanic debris avalanches: characteristics of source areas, deposits, and associated eruptions. *Journal of Volcanology and Geothermal Research*, 22:163-197.
- Siebert, L., Glicken, H., Ui, T., 1987. Volcanic hazards from Bezymianny- and Bandai-type eruptions. *Bulletin of Volcanology*, 49, 435-459.
- Sigurdsson, H., Houghton, B.F., McNutt, S.R., Rymer, H., Stix, J., 2000. *Encyclopedia of Volcanoes*. Academic press, San Diego.
- Smith, V.C., Blundy, J.D., Arce, J.L., 2009. A temporal record of magma accumulation and evolution beneath Nevado de Toluca, Mexico, preserved in plagioclase phenocrysts. *Journal of Petrology*, 50, 405-426, doi:10.1093/petrology/egp005.
- Spera, F. J. & Bohron, W. A., 2001. Energy-constrained open-system magmatic processes I: general model and energy-constrained assimilation-fractional crystallisation (EC-AFC) formulation. *Journal of Petrology*, 42, 999-1018.
- Stormer, Jr J.C., 1983. The effects of recalculation on estimates of temperature and oxygen fugacity from analyses of multicomponent iron-titanium oxides. *American Mineralogist*, 68 (5-6), 586–594.
- Şen, P.A., Teme, I A., Gourgaud, A., 2004. Petrogenetic modeling of Quaternary post- collisional volcanism: a case study of central and eastern Anatolia. *Geological Magazine*, 141, 81-98.

- Şengör, A.M.C., 1990. A new model for the late Palaeozoic–Mesozoic tectonic evolution of Iran and implications for Oman, *in* Robertson, A.H.F., et al., eds., *The geology and tectonics of the Oman region: Geological Society of London Special Publication*, 49,. 797 – 831.
- Şengör, A.M.C., Görür, N., and Şaroğlu, F., 1985. Strikeslip faulting and related basin formation in zones of tectonic escape: Turkey as a case study, *in* Biddle, K.D., and Christie-Blick, N., eds., *Strike-Slip Deformation, Basin Formation and Sedimentation. Society of Economic Paleontologists and Mineralogists Special Publication*, 17, 227–264.
- Şengör, A.M.C., Özeren, S., Genç, T., Zor, E., 2003. East Anatolian high plateau as a mantle supported, north-south shortened domal structure. *Geophysical Research Letters*, 30. doi: 10.1029/2003GL017858.
- Şengör, A.M.C., Özeren, S., Keskin, M., Sakınç, M., Özbakir, A.D., Kayan, I., 2008. Eastern Turkish high plateau as a small Turkic-type orogen: Implications for post-collisional crust-forming processes in Turkic-type orogens. *Earth Science Reviews*, 90,1-48.
- Şengün, M., 1984. Bitlis Masifi Tatvan güneyinin jeolojik/petrografik incelenmesi (Doktora tezi, basılmamış). H.Ü. Fen Bilimleri Enstitüsü, Ankara.
- Takahashi, E., Kushiro, I., 1983. Melting of a dry peridotite at high pressures and basalt magma genesis. *American Mineralogist*, 68, 859–879.

- Taylor, S.R., Mc Lennan, S.M., 1985. The continental crust: its composition and evolution. Blackwell, Oxford Press, 312.
- Tatsumi, Y., D. J. Hamilton, Nesbitt, R. W., 1986. Chemical characterization of fluid phase released from a subducted lithosphere and origin of arc magmas: Evidence from high-pressure experiments and natural rocks, *Journal of Volcanology and Geothermal. Research*, 29, 293–309.
- Tchalenko, J.S., 1977. Reconnaissance of seismicity and tectonics at northern border of Arabian plate (Lake Van region). *Rev Geog Phy Geol Dyn.*, 19, 89–207.
- Thirlwall, M.F., Upton, B.G.J., Jenkins, C., 1994. Interaction between continental lithosphere and the Iceland plume-Sr–Nd–Pb isotope geochemistry of Tertiary basalts, NE Greenland. *Journal of Petrology*, 35, 839–879.
- Timm, C., Hoernle, K., van den Bogaard, P., Bindeman, I., Weaver, S., 2009. Geochemical evolution of intraplate volcanism at Banks Peninsula, New Zealand: Interaction between asthenospheric and Lithospheric melts. *Journal of Petrology*, 50 (6), 1-35.
- Tolluođlu, A. Ü., Erkan, Y., 1982. Mutki (Bitlis) yöresindeki bölgesel metamorfik kayaçların petrografik incelenmesi. *Yerbilimleri Dergisi*, 9 (1), 73-91.
- Topuz, G., R. Altherr, A. Kalt, M. Satör, O. Werner, Schwarz, W.H., 2004. Aluminous granulites from the Pulur complex, NE Turkey: a case of partial melting, efficient melt extraction and crystallization, *Lithos*, 72, 183-207.

- Turner, S. P., 2002. On the time-scales of magmatism at island-arc volcanoes. *Philosophical Transactions of the Royal Society of London, Mathematical, Physical and Engineering Sciences*, 360, 2853–2871.
- Turner, S., Hawkesworth, C., van Calsteren, P., Heath, E., Macdonald, R., Black, S., 1996. U-series isotopes and destructive plate margin magma genesis in the Lesser Antilles. *Earth and Planetary Science Letters*, 142, 191–207.
- Venezky, D.Y., Rutherford, M.J., 1999. Petrology and Fe–Ti oxide reequilibration of the 1991 Mount Unzen mixed magma. *Journal of Volcanology and Geothermal Research*, 89, 213–230.
- Villemant, B., Jaffrezic, H., Joron, J.L. and Treuil, M., 1981. Distribution Coefficients of Major and Trace-Elements - Fractional Crystallization in the Alkali Basalt Series of Chaîne-Des-Puys (Massif Central, France). *Geochimica et Cosmochimica Acta* 45 (11), 1997-2016. doi: 10.1016/0016-7037(81)90055-7.
- Vroon, P. Z., Van Bergen, M. J., White, W. M., Varekamp, J. C., 1993. Sr–Nd–Pb isotope systematics of the Banda Arc, Indonesia: combined subduction and assimilation of continental material. *Journal of Geophysical Research*, 98, 22349–22366.
- Wallace, P.J, Anderson, A. T. & Davis, A. M., 1999. Gradients in H₂O, CO₂, and exsolved gas in a large-volume silicic magma system: interpreting the record preserved in melt inclusions from the Bishop Tuff. *Journal of Geophysical Research*, 104, 20097–20122.

- Weaver, B.L., 1991. The origin of ocean island basalt end-member compositions: trace element and isotopic constraints. *Earth and Planetary Science Letters* 104, 381–397.
- Yeşilova, Ç., Yakupoğlu, T., 2007. Adilcevaz Kireçtaşının (Van Gölü Kuzeyi) Mikrofasiyes Özellikleri, *Türkiye Jeoloji Bülteni*, Cilt 50, Sayı 1, 27-39.
- Yılmaz, Y., 1993. New evidence and model on the evolution of the southeast Anatolian orogen: *Geological Society of America Bulletin*, 105, 252–271.
- Yılmaz, Y., Şaroğlu, F., Güner, Y., 1987. Initiation of the neomagmatism in East Anatolia. *Tectonophysics*, 137, 177-199.
- Yılmaz, Y., Güner, Y., Şaroğlu, F., 1998. Geology of the Quaternary volcanic centres of the East Anatolia. *Journal of Volcanology and Geothermal Research*, 85, 173-210.
- Zack, T. and Brumm, R., 1998. Ilmenite/liquid partition coefficients of 26 trace elements determined through ilmenite/clinopyroxene partitioning in garnet pyroxene. In: 7th International Kimberlite Conference. Gurney, J.J., Gurney, J.L., Pascoe, M.D. and Richardson, S.H. (Editors), Red Roof Design, Cape Town. 986-988.
- Zindler, A.E., Jagoutz, E., and Goldstein, S., 1982. Nd, Sr and Pb isotopic systematics in a three-component mantle: A new perspective. *Nature*, 298, 519-523.
- Zindler, A. and Hart, S.R., 1986. Chemical geodynamics. *Ann. Rev. Earth Planet. Sci.* ,14, 1986, 493–57.

Zor, E. 2008. Tomographic evidence of slab detachment beneath eastern Turkey and Caucasus. *Geophysical Journal International*, 175, 1273–1282, doi: 10.1111/j.1365-246X.2008.03946.x.

Zor, E., Sandvol., E., Gurbuz, C., Turkelli, N., Seber, D., Barazangi, M., 2003. The crustal structure of East Anatolian plateau from receiver functions. *Geophysical Research Letters* 30(24), 8044, doi: 10.1029/2003GLO18192.

Table A.1 UTM Coordinates of samples

Sample	Rock Type	Coordinates (UTM)	Sample	Rock Type	Coordinates (UTM)
2005 69	Rhyolite (1)	E: 3005125 N: 4306000	2005 68 (2007 24)	Basaltic Trachyand.(4)	E: 305400 N: 4298325
2005 75	Rhyolite (1)	E: 309150 N: 4304610	2006 79	Trachyand.(4)	E: 303375 N: 4316075
2006 99	Basalt (2)	E: 308527 N: 4326028	2006 86	Trachyand.(4)	E: 306250 N: 4314150
2006 112	Basaltic Trachyand.(3)	E: 306850 N: 4324175	2006 89	Trachyand.(4)	E: 307325 N: 4317250
2005 62	Basaltic Trachyand.(3)	E: 322750 N: 4299531	2006 95	Trachyand.(4)	E: 307500 N: 4320000
2005 61	Basaltic Trachyand.(3)	E: 323125 N: 4301150	2006 118	Trachyand.(4)	E: 314325 N: 4321800
2006 114	Basaltic	E: 308850	2006 72	Trachyand.(4)	E: 301750
2006 116	Trachyand.(4)	N: 4324375	2006 74	Trachyand.(4)	N: 4313625
2006 76	Basaltic Trachyand.(4)	E: 296250 N: 4315650	2006 77	Trachyand.(4)	E: 300750 N: 4314250
2006 1	Basaltic Trachyand.(4)	E: 321680 N: 4317013	2006 81	Trachyand.(4)	E: 303750 N: 4315750
2006 130	Basaltic Trachyand.(4)	E: 310000 N: 4330250	2006 6	Trachyand.(4)	E: 305875 N: 431755
2007 23	Basaltic Trachyand.(4)	E: 303550 N: 4305625			E: 320856 N: 4317534

UTM Coordinates of samples

APPENDIX A

Table A.1 Continued.

Sample	Rock Type	Coordinates (UTM)	Sample	Rock Type	Coordinates (UTM)	Sample	Rock Type	Coordinates (UTM)
2005 60	Trachyand.(4)	E: 323800 N: 4299828	2005 25	Trachyte (8)	E: 321533 N: 4308290	2006 101	Dacite (10)	E: 311250 N: 4319373
2006 131	Trachyand.(4)	E: 304750 N: 4325600	2005 38	Trachyte (8)	E: 311800 N: 4312000	2006 108	Dacite (10)	E: 311250 N: 4314175
2006 102	Trachyand.(5)	E: 307875 N: 4321125	2006 14	Trachyte (8)	E: 323000 N: 4314550	2006 110	Dacite (10)	E: 311875 N: 4316250
2007 19A	Trachyand.(5)	E: 307300 N: 4306625	2006 27	Trachyte (8)	E: 317325 N: 4309500	2006 111	Dacite (10)	E: 310500 N: 4313575
2005 59	Trachyand.(5)	E: 326250 N: 4306200	2006 59	Trachyte (9)	E: 304700 N: 4310000	2007 4	Dacite (10)	E: 3113890 N: 4308266
2006 105	Trachyand.(5)	E: 310300 N: 4318500	2005 1	Dacite (10)	E: 320100 N: 4314900	2005 52	Rhyolite (10)	E: 308940 N: 4305650
2006 8	Trachyand.(5)	E: 31875 N: 4316625	2005 3	Dacite (10)	E: 319313 N: 4314934	2005 63	Rhyolite (10)	E: 313525 N: 4299000
2005 55	Trachyte (7)	E: 315200 N: 4306800	2005 28	Dacite (10)	E: 319370 N: 4311480	2006 135	Rhyolite (10)	E: 313000 N: 4310250
2005 51	Trachyte (7)	E: 318091 N: 4306865	2006 43	Dacite (10)	E: 310274 N: 4306625	2006 137	Rhyolite (10)	E: 319145 N: 4308405
2008 4	Trachyte (7)	E: 314855 N: 4301609	2006 47	Dacite (10)	E: 309623 N: 4306515	2007 5	Rhyolite (10)	E: 312000 N: 4311000
2005 10	Trachyte (8)	E: 325798 N: 4311602						

Table B.1 Compositions of minerals from Süphan Volcano.**Olivine**

Sample 2006 99	Crystal type	Analysis location	SiO ₂	TiO ₂	Al ₂ O ₃	Cr ₂ O ₃	FeO	MnO	MgO	NiO	CaO	Total	Fo %	
200699	ol1c	free crystal	core	39,03	0,01	0,04	0,02	20,29	0,31	40,27	0,09	0,25	100,31	77,7
200699	ol2c	free crystal	core	38,95	0,01	0,07	0,02	21,26	0,32	39,60	0,12	0,25	100,60	76,6
200699	ol2r	free crystal	rim	37,29	0,03	0,00	0,02	28,22	0,50	33,50	0,07	0,29	99,92	67,5
200699	ol3c	free crystal	core	37,50	0,02	0,03	0,01	26,81	0,39	34,87	0,08	0,25	99,95	69,6
200699	ol3r	free crystal	rim	36,18	0,03	0,00	0,00	32,69	0,63	28,93	0,05	0,32	98,84	60,7
200699	ol4c	free crystal	core	38,68	0,02	0,03	0,02	21,89	0,35	38,78	0,07	0,27	100,12	75,7
200699	ol4r	free crystal	rim	36,92	0,03	0,04	0,00	30,08	0,51	32,51	0,08	0,28	100,45	65,5
200699	ol5c	free crystal	core	38,40	0,02	0,03	0,01	23,53	0,37	37,73	0,09	0,24	100,42	73,8
200699	ol5r	free crystal	rim	37,80	0,04	0,02	0,02	26,13	0,46	35,39	0,11	0,26	100,23	70,3
200699	ol6c	free crystal	core	39,28	0,03	0,04	0,00	18,20	0,24	42,31	0,10	0,23	100,43	80,4
200699	ol6r	free crystal	rim	38,96	0,01	0,07	0,03	18,58	0,30	41,28	0,11	0,23	99,57	79,6
200699	ol7c	free crystal	core	38,95	0,01	0,04	0,02	20,31	0,31	40,45	0,10	0,23	100,41	77,8
200699	ol7r	free crystal	rim	38,77	0,01	0,04	0,01	20,53	0,34	40,09	0,18	0,22	100,19	77,4
200699	ol8m	microlite	core	36,00	0,05	0,02	0,00	36,38	0,64	26,61	0,04	0,36	100,09	56,2
200699	ol9c	free crystal	core	39,34	0,02	0,05	0,01	18,77	0,24	41,53	0,09	0,21	100,28	79,6
200699	ol9r	free crystal	rim	39,41	0,02	0,05	0,03	18,60	0,26	41,67	0,11	0,23	100,37	79,8
200699	ol10c	free crystal	core	39,20	0,01	0,01	0,01	18,56	0,27	41,35	0,12	0,22	99,75	79,7
200699	ol10r	free crystal	rim	39,19	0,02	0,03	0,01	19,39	0,29	41,12	0,12	0,23	100,39	78,8
200699	ol11c	free crystal	core	39,09	0,05	0,04	0,06	19,46	0,25	40,98	0,12	0,26	100,33	78,7
200699	ol11r	free crystal	rim	38,03	0,01	0,09	0,01	24,87	0,38	36,41	0,08	0,25	100,13	72,0
200699	ol12c	microlite	core	35,28	0,05	0,02	0,00	38,55	0,73	25,27	0,04	0,36	100,30	53,4
200699	ol13c	microlite	core	35,49	0,06	0,01	0,00	38,58	0,68	25,01	0,06	0,34	100,24	53,2

Table B.1 Continued.

Olivine

Sample	2006	112	Crystal type	Analysis location	SiO2	TiO2	Al2O3	Cr2O3	FeO	MnO	MgO	NiO	CaO	Total	Fo %
2006112	ol1c	free crystal	core	37,93	0,02	0,02	0,01	25,46	0,33	35,70	0,12	0,28	99,88	71,2	
2006112	ol1r	free crystal	rim	36,41	0,03	0,01	0,02	34,14	0,57	28,54	0,07	0,27	100,04	59,4	
2006112	ol2r	free crystal	rim	36,90	0,03	0,01	0,01	31,09	0,54	30,43	0,07	0,29	99,36	63,2	
2006112	ol3r	free crystal	rim	35,20	0,03	0,03	0,00	39,52	0,64	24,38	0,01	0,28	100,10	52,0	
2006112	ol4c	free crystal	core	36,97	0,02	0,02	0,00	29,81	0,49	32,43	0,08	0,29	100,11	65,6	
2006112	ol4r	free crystal	rim	35,85	0,03	0,01	0,00	35,80	0,60	27,07	0,02	0,28	99,67	57,0	
2006112	ol5r	free crystal	rim	35,50	0,04	0,01	0,00	36,92	0,64	26,18	0,04	0,28	99,62	55,4	
2006112	ol6r	free crystal	rim	36,10	0,03	0,00	0,01	35,86	0,60	26,79	0,01	0,29	99,70	56,7	
2006112	olmic1	microlite	core	36,91	0,02	0,01	0,00	29,92	0,41	32,20	0,09	0,32	99,88	65,4	
2006112	ol7r	free crystal	rim	35,97	0,04	0,02	0,01	35,11	0,59	27,44	0,05	0,29	99,53	57,8	
2006112	ol8c	free crystal	core	37,77	0,03	0,05	0,01	25,61	0,41	35,60	0,08	0,26	99,83	70,9	
2006112	ol8r	free crystal	rim	36,22	0,03	0,04	0,00	32,63	0,55	29,62	0,05	0,30	99,44	61,4	
2006112	ol9rim	free crystal	rim	36,98	0,02	0,04	0,01	30,45	0,52	31,72	0,06	0,29	100,09	64,6	
2006112	olmic2	microlite	core	36,65	0,04	0,03	0,00	32,70	0,53	30,38	0,06	0,26	100,65	62,0	
2006112	olmic3	microlite	core	37,28	0,03	0,01	0,02	28,35	0,43	33,55	0,09	0,28	100,04	67,5	
Sample 2005 68															
200568	clol1c	crystal clot	core	36,47	0,02	0,03	0,00	32,01	0,49	31,94	0,02	0,20	101,18	63,7	
200568	clol1r	crystal clot	rim	36,79	0,03	0,05	0,01	32,82	0,55	31,11	0,01	0,19	101,55	62,4	
200568	clol2c	crystal clot	core	36,88	0,03	0,03	0,00	32,25	0,52	31,34	0,06	0,19	101,29	63,0	
200568	clol2r	crystal clot	rim	36,67	0,03	0,05	0,01	32,01	0,49	30,47	0,02	0,24	99,99	62,6	
200568	ol1c	free crystal	core	35,95	0,02	0,02	0,01	34,58	0,60	28,81	0,02	0,21	100,22	59,3	
200568	ol1r	free crystal	rim	35,41	0,05	0,01	0,00	37,67	0,65	26,90	0,02	0,24	100,94	55,6	
200568	ol2c	free crystal	core	37,03	0,28	0,05	0,00	35,40	0,63	28,09	0,00	0,29	101,76	58,2	
200568	ol2r	free crystal	rim	35,54	0,03	0,04	0,00	37,74	0,64	26,96	0,00	0,30	101,26	55,6	
200568	ol3c	free crystal	core	35,51	0,05	0,03	0,00	36,38	0,63	28,38	0,04	0,26	101,28	57,8	
200568	ol3r	free crystal	rim	35,17	0,16	0,01	0,00	39,33	0,69	25,59	0,00	0,32	101,28	53,3	

Table B.1Continued

Olivine														
Sample	2005 68	Crystal type	Analysis location	SiO2	TiO2	Al2O3	Cr2O3	FeO	MnO	MgO	NiO	CaO	Total	Fo %
200568	ol5c	free crystal	core	35,86	0,03	0,02	0,00	36,25	0,60	28,01	0,02	0,26	101,06	57,5
200568	ol5r	free crystal	rim	35,65	0,04	0,01	0,00	38,44	0,68	25,90	0,02	0,28	101,03	54,1
200568	ol6c	free crystal	core	35,98	0,02	0,04	0,00	31,85	0,52	31,09	0,03	0,26	99,79	63,1
200568	ol6r	free crystal	rim	36,53	0,02	0,01	0,01	32,60	0,56	30,87	0,07	0,17	100,85	62,4
200568	ol7c	free crystal	core	36,12	0,03	0,05	0,00	36,34	0,63	27,61	0,02	0,22	101,02	57,1
200568	ol7r	free crystal	rim	36,18	0,02	0,03	0,00	34,71	0,54	29,28	0,00	0,22	100,99	59,7
200568	ol8c	free crystal	core	36,50	0,02	0,04	0,00	32,91	0,52	30,70	0,04	0,21	100,93	62,1
200568	ol8r	free crystal	rim	35,93	0,04	0,01	0,00	35,79	0,61	28,35	0,02	0,23	100,98	58,1
200568	ol9c	free crystal	core	36,66	0,01	0,04	0,00	32,03	0,51	31,31	0,02	0,19	100,77	63,2
200568	ol9r	free crystal	rim	35,99	0,03	0,01	0,00	35,29	0,59	28,54	0,00	0,21	100,67	58,6
200568	olmic1	microlite	core	35,47	0,06	0,05	0,01	38,05	0,67	26,50	0,00	0,27	101,06	55,0
200568	olmic2	microlite	core	36,02	0,06	0,01	0,01	36,47	0,63	27,49	0,01	0,26	100,96	56,9
200568	olmic3	microlite	core	35,42	0,04	0,04	0,00	37,44	0,63	26,80	0,03	0,37	100,77	55,6
200568	olmic4	microlite	core	35,83	0,02	0,03	0,00	35,78	0,59	28,40	0,05	0,28	100,99	58,2
200568	olmic5	microlite	core	35,66	0,04	0,01	0,00	37,76	0,67	26,78	0,04	0,29	101,24	55,4
Sample	2006 77													
200677	ol1c77	free crystal	core	34,09	0,03	0,02	0,00	45,49	0,79	20,50	0,00	0,24	101,15	44,1
200677	ol1r677	free crystal	rim	33,52	0,03	0,00	0,00	47,24	1,06	18,28	0,00	0,33	100,46	40,3
200677	ol2c	free crystal	core	34,05	0,04	0,03	0,00	44,97	0,77	21,13	0,00	0,26	101,25	45,2
200677	ol2mic	microlite	core	33,20	0,10	0,00	0,00	48,60	1,14	16,63	0,03	0,40	100,09	37,3
200677	ol2r	free crystal	rim	33,65	0,04	0,00	0,00	46,37	1,03	19,21	0,01	0,24	100,55	41,9
200677	ol3c	free crystal	core	33,92	0,03	0,02	0,01	45,64	0,89	19,22	0,04	0,24	100,01	42,4
200677	ol3r	free crystal	rim	33,51	0,04	0,02	0,01	47,26	0,99	18,19	0,01	0,33	100,35	40,2
200677	ol4c	free crystal	core	33,80	0,03	0,03	0,00	45,53	0,89	20,02	0,03	0,27	100,59	43,5
200677	ol4r	free crystal	rim	33,72	0,02	0,01	0,00	46,08	1,02	19,08	0,02	0,32	100,27	41,9
200677	ol5c	free crystal	core	34,01	0,04	0,00	0,00	44,36	0,78	20,89	0,04	0,25	100,37	45,2
200677	ol5r	free crystal	rim	33,84	0,01	0,00	0,00	45,88	0,95	19,84	0,00	0,27	100,81	43,0

Table B.1Continued**Olivine**

Sample 2006 77	Crystal type	Analysis location	SiO₂	TiO₂	Al₂O₃	Cr₂O₃	FeO	MnO	MgO	NiO	CaO	Total	Fo %	
200677	ol7c	free crystal	core	34,44	0,02	0,02	0,01	45,06	0,74	20,77	0,13	0,21	101,39	44,7
200677	ol7r	free crystal	rim	34,14	0,02	0,02	0,00	46,63	0,93	19,18	0,01	0,23	101,17	41,8
200677	ol8c	free crystal	core	33,33	0,03	0,04	0,00	48,05	1,08	17,87	0,00	0,36	100,76	39,3
200677	ol8r	free crystal	rim	33,28	0,05	0,01	0,00	48,71	1,21	16,72	0,02	0,36	100,37	37,4
200677	ol9c	free crystal	core	33,46	0,04	0,00	0,01	48,11	1,14	17,41	0,01	0,38	100,56	38,6
200677	olmic1	microlite	core	33,28	0,08	0,03	0,00	48,41	1,15	16,58	0,03	0,55	100,10	37,4
Sample 2006 6														
20066	ol1c	free crystal	core	38,87	0,01	0,02	0,00	22,77	0,37	38,02	0,11	0,19	100,36	74,6
20066	ol2c	free crystal	core	38,54	0,01	0,02	0,00	23,89	0,35	38,28	0,04	0,19	101,33	73,8
20066	ol2r	free crystal	rim	35,18	0,02	0,24	0,00	30,60	0,42	29,21	0,02	0,38	96,08	62,7

Table B.1Continued

Clinopyroxene

Sample		Crystal type	A. Loc	SiO ₂	TiO ₂	Al ₂ O ₃	FeO	MnO	MgO	CaO	K ₂ O	Na ₂ O	Total	En	Fs	Wo	mg#
200699	cpx1c	microlite	core	49,72	1,80	2,86	8,81	0,20	14,09	20,75	0,03	0,59	98,86	41,4	14,8	43,8	79,9
200699	cpx2c	microlite	core	51,67	1,23	1,79	8,86	0,24	14,88	21,23	0,02	0,47	100,39	42,2	14,5	43,3	79,9
200699	cpx3c	microlite	core	49,76	1,81	2,96	9,13	0,28	13,99	20,69	0,00	0,48	99,11	41,0	15,5	43,5	77,7
200699	cpx4c	microlite	core	49,48	1,92	3,22	8,97	0,24	13,96	20,68	0,01	0,46	98,94	41,1	15,2	43,7	77,8
200699	cpx5c	microlite	core	50,55	1,67	2,42	9,00	0,21	14,13	20,89	0,01	0,51	99,39	41,2	15,1	43,8	77,3
200699	cpx6c	microlite	core	49,14	2,04	3,55	9,19	0,22	13,84	20,25	0,01	0,54	98,76	41,1	15,7	43,2	77,4
200699	cpx7c	microlite	core	47,88	2,40	3,69	10,52	0,28	12,70	20,19	0,13	0,65	98,44	38,2	18,2	43,6	75,9
200699	cpx8c	microlite	core	49,79	1,79	2,81	9,02	0,21	14,10	20,71	0,02	0,56	99,00	41,3	15,2	43,6	79,2
200699	cpx9c	microlite	core	50,31	1,69	2,47	9,65	0,27	13,89	20,59	0,01	0,52	99,41	40,5	16,3	43,2	76,0
Sample 2006 112																	
2006112	cpx1c	microlite	core	51,72	1,09	1,56	10,81	0,29	15,56	18,06	0,01	0,33	99,43	44,8	17,9	37,3	73,3
2006112	cpx2c	microlite	core	49,92	1,41	1,99	11,33	0,30	13,62	19,86	0,01	0,47	98,91	39,6	19,0	41,5	73,6
2006112	cpx3c	microlite	core	51,57	1,14	1,33	11,10	0,29	14,36	19,36	0,02	0,42	99,59	41,4	18,4	40,1	72,0
2006112	cpx4c	microlite	core	50,53	1,52	2,74	9,14	0,32	14,32	20,44	0,02	0,43	99,45	41,7	15,5	42,8	76,8
2006112	cpx5c	microlite	core	50,06	1,74	2,81	10,29	0,31	14,14	19,96	0,02	0,51	99,84	41,1	17,3	41,7	76,1
2006112	cpx6c	free crystal	core	50,52	1,90	3,55	10,02	0,25	13,22	20,21	0,04	0,55	100,26	39,4	17,2	43,4	70,8
2006112	cpx6r	free crystal	rim	50,45	1,61	2,33	10,53	0,25	13,68	20,41	0,01	0,51	99,77	39,8	17,6	42,6	74,0
2006112	cpx7T	microlite	core	50,24	1,42	2,48	9,06	0,25	14,41	20,42	0,00	0,41	98,71	42,0	15,2	42,8	77,8
2006112	cpx9	microlite	core	49,74	1,80	3,05	9,78	0,26	13,90	20,25	0,01	0,54	99,34	40,8	16,5	42,7	76,7
Sample 2005 68																	
200568	cpx1c	microlite	core	48,57	3,95	1,77	16,05	0,46	13,59	17,10	0,01	0,30	101,79	38,7	26,4	35,0	64,0
200568	cpx2	microlite	core	50,13	1,16	1,95	15,08	0,46	13,63	16,95	0,00	0,31	99,67	39,5	25,3	35,3	65,0
200568	cpx3	microlite	core	48,69	1,86	2,68	14,38	0,45	12,48	18,67	0,00	0,00	99,22	36,5	24,3	39,2	62,6
200568	cpx6	microlite	core	49,98	1,41	4,52	14,35	0,45	13,42	16,83	0,07	1,17	102,19	39,7	24,6	35,8	71,7
200568	cpx7	microlite	core	49,74	1,43	2,41	14,67	0,44	12,50	18,72	0,02	0,36	100,28	36,3	24,6	39,1	64,3

Table B.1Continued

Clinopyroxene

Sample 2005 77		Crystal type	Analysis location	SiO₂	TiO₂	Al₂O₃	FeO	MnO	MgO	CaO	K₂O	Na₂O	Total	En	Fs	Wo	mg#
2005 77	cpx1c	free crystal	core	50,40	0,62	2,06	14,69	0,40	12,69	18,20	0,00	0,21	99,27	37,1	24,7	38,2	62,6
2005 77	cpx1r	free crystal	rim	48,81	0,61	2,01	14,25	0,41	9,17	19,06	0,01	0,26	94,60	29,5	26,4	44,1	53,4
2005 77	cpx2c	free crystal	core	50,30	0,59	1,87	15,36	0,48	12,76	17,68	0,02	0,33	99,38	37,2	25,9	37,0	63,2
2005 77	cpmic1	microlite	core	49,01	0,93	2,60	19,58	0,68	9,50	16,41	0,10	0,44	99,25	29,1	34,8	36,1	47,9
2005 77	cpmic2	microlite	core	50,18	0,73	1,45	16,88	0,60	11,33	18,54	0,03	0,26	100,00	32,9	28,5	38,7	57,7
2005 77	cpmic3	microlite	core	49,24	0,84	1,59	16,92	0,53	10,35	18,95	0,03	0,40	98,85	30,7	29,0	40,3	56,1
2005 77	cpmic4	microlite	core	50,48	0,81	1,73	16,98	0,60	10,70	18,42	0,07	0,39	100,17	31,6	29,2	39,2	54,7
Sample 2006 6																	
20066	cpx1c	free crystal	core	51,82	0,23	0,84	13,61	0,62	12,28	20,30	0,01	0,46	100,15	35,2	22,9	41,9	65,6
20066	cpx1r	free crystal	rim	51,59	0,25	0,92	14,09	0,60	11,78	20,26	0,01	0,41	99,90	34,1	23,8	42,1	62,8
20066	cp2cT	free crystal	core	51,62	0,32	1,08	12,78	0,50	13,10	20,31	0,01	0,34	100,08	37,3	21,2	41,5	69,0
20066	cp2rT	free crystal	rim	51,92	0,36	1,22	12,99	0,49	12,93	20,39	0,03	0,33	100,68	36,8	21,5	41,7	67,5
20066	cp3cT	free crystal	core	51,91	0,37	1,30	12,43	0,44	13,15	20,71	0,01	0,41	100,73	37,3	20,5	42,2	69,9
20066	cp3rT	free crystal	rim	51,95	0,24	0,85	12,78	0,46	13,16	20,53	0,01	0,37	100,35	37,2	21,0	41,7	69,3
20066	cp4cT	free crystal	core	51,51	0,30	1,05	12,83	0,46	13,04	20,31	0,00	0,45	99,94	37,2	21,2	41,6	69,8
20066	cp4rT	free crystal	rim	51,99	0,25	1,07	12,89	0,50	12,79	20,39	0,02	0,34	100,25	36,6	21,5	41,9	66,8
20066	cp5c	free crystal	core	51,92	0,25	0,91	13,11	0,56	12,71	20,25	0,00	0,50	100,20	36,4	22,0	41,7	67,7
20066	cp5r	free crystal	rim	51,63	0,40	1,21	12,66	0,50	12,81	20,44	0,00	0,36	100,01	36,7	21,2	42,1	67,7
20066	cp6cT	free crystal	core	51,40	0,36	1,39	13,40	0,52	12,62	20,34	0,01	0,48	100,52	36,0	22,3	41,7	68,3
20066	cp6rT	free crystal	rim	51,79	0,30	1,03	12,73	0,52	12,74	20,38	0,01	0,40	99,90	36,6	21,4	42,0	67,5
20066	cp7c	free crystal	core	50,91	0,64	2,75	9,58	0,26	14,08	21,22	0,00	0,40	99,84	40,4	15,8	43,8	78,1
20066	cp7r	free crystal	rim	51,57	0,29	1,01	13,45	0,50	12,47	20,37	0,00	0,38	100,04	35,7	22,4	41,9	66,2
20066	cp8c	free crystal	core	51,87	0,26	0,92	12,76	0,50	13,00	20,56	0,01	0,30	100,16	36,9	21,1	42,0	68,1
20066	cp8r	free crystal	rim	51,53	0,26	0,90	13,49	0,51	12,66	20,39	0,01	0,43	100,17	36,0	22,3	41,7	68,0
20066	cp9cT	free crystal	core	51,71	0,23	0,88	12,76	0,47	12,90	20,62	0,00	0,42	99,99	36,7	21,1	42,2	69,3
20066	cp9rT	free crystal	rim	51,41	0,34	1,34	13,45	0,53	12,54	20,10	0,01	0,46	100,17	36,0	22,5	41,5	67,0
20066	cp10cT	free crystal	core	51,57	0,39	1,20	12,49	0,46	13,39	20,34	0,00	0,47	100,30	38,0	20,6	41,4	71,6

Table B.1Continued
Clinopyroxene

Sample 2006 6		Crystal type	Analysis location	SiO₂	TiO₂	Al₂O₃	FeO	MnO	MgO	CaO	K₂O	Na₂O	Total	En	Fs	Wo	mg#
20066	cpcl1c	free crystal	core	51,92	0,26	1,00	13,16	0,54	12,75	20,47	0,00	0,35	100,44	36,3	21,9	41,9	67,0
20066	cpcl2c	free crystal	core	51,77	0,30	1,00	12,93	0,48	12,77	20,48	0,01	0,40	100,13	36,5	21,5	42,0	67,8
20066	cpcl3c	free crystal	core	51,57	0,44	1,47	12,49	0,47	12,78	20,67	0,00	0,46	100,34	36,6	20,8	42,6	69,1
20066	cpx1micT	microlite	core	53,40	0,47	1,61	15,62	0,52	12,71	16,33	0,23	0,58	101,46	37,9	27,0	35,0	59,2
20066	cp2micT	microlite	core	50,54	0,99	2,25	13,07	0,43	15,54	16,83	0,03	0,27	99,95	44,1	21,5	34,4	72,9
20066	cp3micT	microlite	core	52,02	0,34	0,97	13,21	0,47	12,54	20,38	0,01	0,38	100,32	36,0	22,0	42,0	65,5
Sample 2006 8																	
20068	cp1c	free crystal	core	49,31	0,30	0,99	19,55	0,77	9,74	17,64	0,00	0,25	98,56	28,8	33,7	37,5	50,1
20068	cp1r	free crystal	rim	50,54	0,24	0,83	19,35	0,71	9,25	18,90	0,01	0,30	100,12	27,1	33,0	39,9	48,0
20068	cp2micT	microlite	core	50,08	0,28	1,11	19,22	0,77	9,67	18,53	0,02	0,23	99,91	28,3	32,8	38,9	50,0
20068	cp3micT	microlite	core	50,48	0,21	0,78	20,77	0,83	8,77	18,40	0,00	0,41	100,64	25,7	35,5	38,8	45,7
20068	cp5c	free crystal	core	49,86	0,31	1,31	18,04	0,65	10,87	17,99	0,09	0,37	99,50	31,7	30,6	37,7	56,7
20068	cp5r	free crystal	rim	50,24	0,48	1,48	17,83	0,68	10,64	18,46	0,01	0,36	100,17	31,0	30,3	38,7	55,0
20068	cp6c	free crystal	core	50,15	0,64	2,08	15,26	0,67	11,34	19,64	0,00	0,37	100,15	33,0	26,0	41,0	61,3
20068	cp6r	free crystal	rim	49,59	0,52	1,57	19,11	0,71	9,35	18,82	0,00	0,35	100,01	27,5	32,7	39,8	50,0
20068	cp7c	free crystal	core	51,97	0,21	2,13	14,65	0,66	11,54	19,86	0,36	0,94	102,31	33,5	25,0	41,5	66,9
20068	cp7r	free crystal	rim	50,29	0,25	0,71	19,78	0,78	9,13	18,82	0,01	0,32	100,09	26,7	33,7	39,6	47,9
20068	cpcl1cT	free crystal	core	50,58	0,48	1,37	16,39	0,60	10,72	19,54	0,01	0,33	100,04	31,3	27,8	40,9	56,7
Sample 2006 86																	
2006_86	cpx1cT	free crystal	core	51,31	0,54	1,36	12,48	0,51	13,57	18,81	0,00	0,30	98,90	39,5	21,2	39,3	67,6
2006_86	cpx1rT	free crystal	rim	51,86	0,47	1,17	12,10	0,51	13,58	19,75	0,00	0,37	99,82	39,0	20,3	40,7	69,4
2006_86	cpx2cT	free crystal	core	50,94	0,51	1,19	14,55	0,56	12,49	18,39	0,00	0,40	99,03	36,5	24,8	38,7	62,9
2006_86	cpx2rT	free crystal	rim	50,85	0,49	1,14	14,45	0,53	12,91	18,40	0,00	0,29	99,06	37,4	24,3	38,3	64,3
2006_86	cpx3cT	free crystal	core	50,02	1,05	2,31	12,08	0,43	13,15	19,57	0,00	0,44	99,05	38,4	20,5	41,1	70,6
2006_86	cpx3rT	free crystal	rim	51,30	0,53	1,21	13,03	0,49	13,49	18,68	0,00	0,35	99,09	39,1	22,0	38,9	67,3
2006_86	cpkx1	inclusion	core	51,66	0,50	1,30	12,72	0,54	13,62	19,04	0,02	0,36	99,77	39,2	21,4	39,4	68,3

Table B.1Continued
Clinopyroxene

Sample 2006 86		Crystal type	Analysis location	SiO₂	TiO₂	Al₂O₃	FeO	MnO	MgO	CaO	K₂O	Na₂O	Total	En	Fs	Wo	mg#
2006_86	cp2k	inclusion	core	51,38	0,55	1,31	13,09	0,48	13,42	18,91	0,01	0,30	99,46	38,7	22,0	39,3	66,8
2006_86	cpcl1cT	crystal clot	core	51,17	0,60	1,70	16,27	0,54	11,52	18,16	0,01	0,56	100,52	33,9	27,7	38,4	58,2
2006_86	cpcl1rT	crystal clot	rim	50,99	1,12	2,85	11,33	0,38	14,69	18,28	0,00	0,33	99,98	42,7	19,1	38,2	71,5
2006_86	cpcl2c	crystal clot	core	51,62	0,57	1,52	13,27	0,54	13,34	18,75	0,00	0,35	99,96	38,6	22,4	39,0	66,0
2006_86	cpcl2r	crystal clot	rim	51,85	0,86	1,73	10,71	0,34	15,95	18,23	0,01	0,28	99,96	45,3	17,6	37,2	75,3
Sample 2005 10																	
2005 10	cp1cT	free crystal	core	51,29	0,43	1,37	12,74	0,47	13,00	20,83	0,04	0,37	100,53	36,7	20,9	42,3	70,8
2005 10	cp1rT	free crystal	rim	51,87	0,46	1,50	12,51	0,43	13,58	20,53	0,01	0,43	101,32	38,2	20,4	41,4	71,9
2005 10	cp2cT	free crystal	core	49,41	0,65	2,54	11,33	0,33	13,72	20,10	0,03	0,52	98,61	39,5	18,9	41,6	78,6
2005 10	cp2rT	free crystal	rim	51,66	0,62	1,94	11,33	0,37	14,17	20,20	0,01	0,33	100,63	40,2	18,6	41,2	73,2
2005 10	cp3ct	free crystal	core	51,90	0,41	1,36	12,01	0,46	13,62	21,00	0,01	0,36	101,13	38,1	19,6	42,3	72,8
2005 10	cp3rt	free crystal	rim	52,10	0,44	1,31	12,01	0,45	13,42	20,71	0,03	0,35	100,81	38,0	19,8	42,2	70,4
2005 10	cp4c	free crystal	core	51,10	0,66	2,20	12,19	0,46	13,60	20,69	0,03	0,43	101,35	38,2	20,0	41,8	74,3
2005 10	cp5cT	free crystal	core	51,72	0,43	1,56	12,50	0,49	13,12	20,62	0,01	0,33	100,78	37,2	20,7	42,1	69,3
2005 10	cp5rT	free crystal	rim	51,94	0,40	1,43	12,60	0,45	13,20	20,16	0,02	0,34	100,55	37,7	20,9	41,4	68,1
2005 10	cp6cT	free crystal	core	52,24	0,19	0,77	14,30	0,59	11,62	20,85	0,00	0,31	100,89	33,2	23,9	42,9	61,1
2005 10	cp6rT	free crystal	rim	51,72	0,42	1,47	12,84	0,47	12,94	20,34	0,00	0,37	100,56	36,9	21,3	41,7	67,9
2005 10	cpcl1c	crystal clot	core	51,69	0,48	1,58	12,02	0,38	13,41	21,04	0,00	0,35	100,95	37,8	19,6	42,6	71,9
2005 10	cpcl2c	crystal clot	core	52,10	0,37	1,26	12,63	0,51	13,59	20,26	0,01	0,32	101,07	38,2	20,8	41,0	70,0
2005 10	cpcl2r	crystal clot	rim	51,60	0,54	1,83	12,16	0,44	13,22	20,75	0,01	0,31	100,85	37,5	20,1	42,4	69,9
2005 10	cpcl3cT	crystal clot	core	51,72	0,40	1,47	12,43	0,48	13,13	20,96	0,03	0,60	101,20	37,0	20,4	42,5	73,1
2005 10	cpcl3rT	crystal clot	rim	51,98	0,53	1,72	14,78	0,52	13,85	17,06	0,01	0,37	100,81	39,9	24,8	35,3	64,1
Sample 2008 4																	
2008 4	cp1c	free crystal	core	51,80	0,29	0,95	13,81	0,55	11,96	20,66	0,00	0,42	100,44	34,3	23,1	42,6	64,2
2008 4	cp1r	free crystal	rim	51,89	0,20	0,81	14,72	0,00	11,37	20,63	0,00	0,36	99,98	33,0	24,0	43,0	59,4
2008 4	cp2cT	free crystal	core	52,21	0,17	0,83	14,40	0,59	11,61	20,73	0,00	0,38	100,92	33,2	24,1	42,7	61,5

Table B.1Continued
Clinopyroxene

Sample 2008 4		Crystal type	Analysis location	SiO₂	TiO₂	Al₂O₃	FeO	MnO	MgO	CaO	K₂O	Na₂O	Total	En	Fs	Wo	mg#
2008 4	cp2rT	free crystal	rim	52,44	0,24	0,87	14,36	0,51	11,99	20,37	0,01	0,40	101,19	34,3	23,9	41,8	62,1
2008 4	cpx3r	free crystal	rim	50,44	0,34	1,19	13,83	0,52	13,20	20,88	0,01	0,43	100,84	36,4	22,2	41,4	75,1
2008 4	cp4c	free crystal	core	53,36	0,19	0,86	14,36	0,54	11,42	21,25	0,03	0,41	102,42	32,6	23,9	43,6	59,5
2008 4	cp4r	free crystal	rim	51,99	0,20	0,89	14,47	0,55	11,68	21,25	0,00	0,33	101,36	33,0	23,8	43,2	63,0
2008 4	cp5cT	free crystal	core	52,03	0,27	1,02	13,42	0,59	12,33	21,21	0,01	0,35	101,23	34,8	22,2	43,0	66,6
2008 4	cp5rT	free crystal	rim	51,81	0,27	0,91	13,61	0,57	12,17	21,06	0,01	0,38	100,79	34,5	22,6	42,9	66,0
Sample 2005 28																	
200528	cp1c	free crystal	core	51,50	0,19	1,09	14,21	0,56	11,92	21,00	0,01	0,48	100,94	33,8	23,5	42,8	66,3
200528	cp1r	free crystal	rim	52,03	0,16	0,68	12,93	0,55	12,31	22,13	0,01	0,37	101,17	34,4	21,2	44,5	69,2
200528	cp2c	free crystal	core	51,56	0,26	1,17	14,79	0,55	11,78	20,70	0,01	0,48	101,31	33,4	24,4	42,2	64,5
200528	cp2r	free crystal	rim	51,67	0,14	0,85	14,82	0,61	11,48	21,21	0,01	0,47	101,25	32,4	24,5	43,1	64,0
200528	cp3c	free crystal	core	51,78	0,15	0,82	13,91	0,57	11,95	21,51	0,00	0,36	101,04	33,6	22,9	43,5	66,0
200528	cp3r	free crystal	rim	51,68	0,16	0,87	13,67	0,53	11,91	21,60	0,02	0,52	100,97	33,6	22,5	43,8	68,0
200528	cp4c	free crystal	core	51,89	0,18	0,69	14,17	0,66	11,86	21,31	0,01	0,42	101,18	33,4	23,4	43,1	65,5
200528	cp4r	free crystal	rim	51,51	0,46	1,59	12,37	0,52	12,48	21,45	0,00	0,43	100,81	35,5	20,6	43,9	69,5
200528	cp5cT	free crystal	core	52,22	0,16	0,76	13,82	0,62	11,88	21,55	0,00	0,45	101,46	33,5	22,8	43,7	65,7
200528	cp6c	free crystal	core	51,61	0,13	0,70	14,17	0,61	11,58	21,39	0,02	0,44	100,66	32,9	23,5	43,6	65,1
200528	cp6r	free crystal	rim	51,99	0,16	0,74	12,63	0,57	12,42	21,92	0,01	0,43	100,88	34,9	20,8	44,3	70,0
Sample 6 110																	
2006110	cp1cT	free crystal	core	51,38	0,25	1,09	13,28	0,82	12,54	19,63	0,01	0,37	99,36	36,3	22,9	40,8	65,8
2006110	cp1rT	free crystal	rim	51,35	0,26	0,99	12,44	0,68	12,60	20,85	0,00	0,30	99,48	36,0	21,1	42,9	68,4
2006110	cpx2c	free crystal	core	51,93	0,24	1,01	12,81	0,74	13,10	20,12	0,01	0,25	100,20	37,2	21,6	41,1	67,5
2006110	cpx2r	free crystal	rim	51,83	0,30	1,24	12,43	0,62	12,90	20,95	0,04	0,35	100,66	36,6	20,8	42,7	69,6
2006110	cpx3c	free crystal	core	51,68	0,22	0,81	12,31	0,68	13,25	20,02	0,00	0,35	99,33	37,9	20,9	41,2	69,5
2006110	cpx3r	free crystal	rim	51,61	0,23	0,86	11,63	0,62	13,24	20,83	0,02	0,29	99,33	37,7	19,6	42,7	71,1
2006110	cpx4cT	free crystal	core	51,00	0,30	1,01	12,84	0,74	13,07	19,85	0,00	0,32	99,12	37,4	21,8	40,8	69,4

Table B.1Continued

Orthopyroxene

Sample 2006 112		Crystal type	A. Loc.	SiO ₂	TiO ₂	Al ₂ O ₃	FeO	MnO	MgO	CaO	K ₂ O	Na ₂ O	Total	En	Fs	Wo	mg#
2006112	op2c	free crystal	core	53,55	0,49	1,63	16,57	0,40	24,81	2,24	0,01	0,07	99,76	69,0	26,5	4,5	72,7
2006112	op2r	free crystal	rim	52,82	0,54	1,62	17,71	0,33	23,89	2,21	0,00	0,10	99,21	67,1	28,4	4,5	70,9
2006112	op3micT	microlitr	core	52,24	0,55	1,70	18,01	0,39	23,34	2,30	0,06	0,11	98,71	66,1	29,2	4,7	70,6
2006112	op3c	free crystal	core	53,47	0,43	1,34	17,48	0,41	24,21	2,18	0,01	0,15	99,68	67,6	28,0	4,4	71,5
2006112	op3r	free crystal	rim	53,49	0,55	1,79	16,58	0,36	24,15	2,28	0,00	0,06	99,26	68,4	26,9	4,6	72,2
Sample 2006 6																	
20066	op1c	free crystal	core	52,26	0,19	0,59	25,38	0,93	18,77	1,62	0,03	0,03	99,79	54,1	42,5	3,4	56,9
20066	op1r	free crystal	rim	51,71	0,26	0,62	26,04	0,84	18,69	1,64	0,01	0,13	99,93	53,5	43,2	3,4	56,9
20066	op2cT	free crystal	core	50,04	0,28	0,72	28,67	1,04	16,47	2,05	0,03	0,15	99,45	47,6	48,2	4,3	52,8
20066	op2rT	free crystal	rim	51,44	0,20	0,41	26,67	0,89	17,84	1,94	0,04	0,15	99,58	51,4	44,6	4,0	55,3
20066	op3c	free crystal	core	51,95	0,30	0,42	26,96	0,94	17,88	1,47	0,01	0,06	99,98	51,7	45,3	3,0	54,2
20066	op3r	free crystal	rim	51,72	0,16	0,46	26,94	0,95	18,25	1,38	0,01	0,08	99,95	52,3	44,9	2,8	55,3
20066	op4cT	free crystal	core	51,19	0,22	0,54	25,05	0,80	19,46	2,11	0,02	0,06	99,46	54,8	40,9	4,3	60,3
20066	op4rT	free crystal	rim	52,01	0,19	0,57	25,20	0,84	19,08	1,59	0,03	0,11	99,62	54,8	41,9	3,3	57,8
20066	op5cT	free crystal	core	51,62	0,26	0,66	26,49	0,85	18,20	1,57	0,01	0,06	99,71	52,5	44,2	3,3	55,2
20066	op5rT	free crystal	rim	51,28	0,21	0,53	26,35	0,88	18,36	1,62	0,02	0,11	99,36	52,8	43,9	3,3	56,5
20066	op6cT	free crystal	core	51,92	0,30	1,32	24,38	0,71	20,06	1,39	0,01	0,02	100,10	57,1	40,1	2,8	59,9
20066	op6rT	free crystal	rim	51,90	0,29	0,93	26,72	0,89	18,22	1,49	0,02	0,04	100,51	52,4	44,5	3,1	54,9
20066	op7cT	free crystal	core	52,78	0,33	1,56	20,78	0,47	22,53	1,52	0,00	0,08	100,05	63,4	33,5	3,1	66,2
20066	op7rT	free crystal	rim	51,82	0,20	0,73	25,97	0,82	18,70	1,46	0,01	0,05	99,76	53,8	43,2	3,0	56,3
20066	op8cT	free crystal	core	51,05	0,23	0,57	26,72	0,89	18,47	1,49	0,01	0,05	99,48	52,7	44,2	3,1	56,6
20066	op8rT	free crystal	rim	51,36	0,19	0,75	27,01	0,94	18,69	1,56	0,00	0,05	100,55	52,7	44,2	3,1	57,1
20066	op9cT	free crystal	core	51,74	0,20	0,63	26,91	0,82	18,16	1,50	0,00	0,04	100,00	52,2	44,7	3,1	54,8
20066	op9rT	free crystal	rim	51,40	0,19	0,51	27,02	0,89	18,16	1,60	0,01	0,02	99,80	51,9	44,8	3,3	55,3
20066	op10cT	free crystal	core	53,14	0,25	1,10	20,98	0,54	22,56	1,70	0,00	0,00	100,26	62,9	33,7	3,4	65,9
20066	op10rT	free crystal	rim	51,86	0,27	1,18	24,36	0,69	20,01	1,34	0,00	0,05	99,76	57,1	40,1	2,8	59,8
20066	op1micT	microlite	core	49,26	0,21	1,01	27,86	0,92	15,68	1,64	0,11	0,11	96,77	47,5	48,9	3,6	50,6

Table B.1Continued

Orthopyroxene

Sample 2006 6		Crystal type	A. Loc.	SiO₂	TiO₂	Al₂O₃	FeO	MnO	MgO	CaO	K₂O	Na₂O	Total	En	Fs	Wo	mg#
20066	op2mic	microlite	core	51,59	0,22	0,75	26,15	0,85	18,52	1,55	0,01	0,02	99,65	53,2	43,6	3,2	56,0
20066	op3mic	microlite	core	52,01	0,35	0,99	24,96	0,81	19,36	1,60	0,01	0,03	100,12	55,4	41,4	3,3	58,1
20066	op4mic	microlite	core	51,46	0,19	0,49	27,46	0,88	17,72	1,50	0,00	0,04	99,74	51,1	45,8	3,1	53,8
20066	opcl1c	crystal clot	core	51,68	0,24	0,59	26,65	0,94	18,35	1,53	0,00	0,02	100,01	52,5	44,3	3,1	55,4
20066	opcl1r	crystal clot	core	51,41	0,25	0,68	27,03	0,94	18,23	1,54	0,00	0,04	100,12	52,0	44,8	3,2	55,5
20066	opcl2cT	crystal clot	core	51,80	0,19	0,56	26,74	0,89	18,13	1,45	0,02	0,02	99,80	52,3	44,7	3,0	54,7
20066	opcl2rT	crystal clot	rim	51,80	0,24	0,57	26,13	0,87	18,24	1,48	0,02	0,03	99,38	52,9	44,0	3,1	55,4
20066	opcl3cT	crystal clot	core	51,61	0,25	0,58	26,72	0,87	18,03	1,60	0,00	0,03	99,69	52,0	44,7	3,3	54,6
Sample 2006 8																	
20068	op1c8	free crystal	core	50,65	0,19	0,74	28,11	0,95	13,87	4,89	0,02	0,08	99,50	41,2	48,4	10,4	46,8
20068	op1r8	free crystal	rim	49,37	0,16	0,32	36,43	1,32	10,64	1,72	0,00	0,07	100,04	32,2	64,1	3,7	34,3
20068	op2c	free crystal	core	49,53	0,18	0,37	34,83	1,14	11,68	1,71	0,00	0,04	99,48	35,3	61,0	3,7	37,4
20068	op2r	free crystal	rim	49,47	0,19	0,36	35,20	1,27	11,66	1,67	0,01	0,05	99,87	35,0	61,4	3,6	37,3
20068	op3c	free crystal	core	51,12	0,27	0,63	28,34	0,94	16,84	1,78	0,00	0,05	99,95	48,7	47,6	3,7	51,8
20068	op3r	free crystal	rim	49,97	0,24	0,47	34,58	1,20	12,57	1,64	0,00	0,00	100,65	37,2	59,4	3,5	39,5
20068	op3cT	free crystal	core	51,67	0,24	0,53	28,29	0,93	17,22	1,63	0,01	0,04	100,55	49,5	47,1	3,4	52,2
20068	op3rT	free crystal	rim	50,06	0,17	0,38	33,89	1,28	12,51	1,69	0,00	0,05	100,03	37,4	59,0	3,6	39,7
20068	op4c	free crystal	core	49,53	0,23	0,36	34,70	1,21	12,16	1,65	0,01	0,08	99,94	36,3	60,2	3,5	38,9
20068	op5c	free crystal	core	50,96	0,25	0,54	30,01	0,96	15,74	1,66	0,00	0,06	100,19	45,9	50,7	3,5	48,5
20068	op5r	free crystal	rim	49,66	0,29	0,58	34,21	1,07	12,44	1,69	0,01	0,04	100,00	37,2	59,2	3,6	39,5
20068	op6cT	free crystal	core	50,00	0,30	0,55	33,59	1,10	12,94	1,71	0,00	0,09	100,29	38,5	57,9	3,7	40,9
20068	op7c	free crystal	core	51,09	0,21	0,79	26,98	0,85	19,53	1,50	0,02	0,12	101,08	53,9	43,1	3,0	60,1
20068	op7r	free crystal	rim	49,26	0,30	1,23	28,22	0,92	17,37	1,74	0,01	0,07	99,12	49,7	46,8	3,6	55,6
20068	op8c	free crystal	core	50,30	0,26	0,48	31,87	0,98	14,22	1,67	0,00	0,07	99,85	42,0	54,5	3,5	44,5
20068	opcl1cT	crystal clot	core	51,99	0,26	0,73	25,65	0,91	19,12	1,58	0,01	0,07	100,32	54,4	42,4	3,2	57,7
20068	opcl1rT	crystal clot	rim	49,27	0,33	0,59	33,69	0,99	13,59	1,81	0,01	0,08	100,35	39,6	56,7	3,8	43,6
20068	opcl2c	crystal clot	core	51,03	0,32	1,27	26,78	0,82	17,71	1,83	0,00	0,01	99,77	51,3	44,9	3,8	54,3

Table B.1Continued
Orthopyroxene

Sample 2006 8		Crystal type	A. Loc.	SiO₂	TiO₂	Al₂O₃	FeO	MnO	MgO	CaO	K₂O	Na₂O	Total	En	Fs	Wo	mg#
20068	opcl3c	crystal clot	core	49,60	0,21	0,44	34,82	1,15	12,00	1,71	0,01	0,05	100,00	35,9	60,4	3,7	38,3
20068	opcl4cT	crystal clot	core	49,09	0,33	0,69	35,24	1,13	11,62	1,64	0,00	0,05	99,79	35,0	61,5	3,5	37,3
20068	opmic	microlite	core	49,09	0,17	0,39	36,00	1,17	10,93	1,77	0,00	0,07	99,60	33,1	63,1	3,9	35,4
Sample 2006 77																	
2006_77	opx2c	free crystal	core	51,46	0,35	1,33	25,88	0,60	18,79	1,90	0,01	0,03	100,34	53,7	42,4	3,9	57,1
2006_77	opx2r	free crystal	core	51,71	0,35	1,30	24,99	0,58	19,43	1,85	0,02	0,02	100,24	55,3	40,9	3,8	58,7
2006_77	opx3	free crystal	core	51,33	0,33	1,13	26,36	0,69	18,45	1,87	0,00	0,06	100,23	52,8	43,4	3,8	56,4
2006_77	opx3c	free crystal	core	51,97	0,19	0,38	26,00	0,89	18,99	1,66	0,02	0,06	100,15	53,8	42,8	3,4	57,4
2006_77	opx4c	free crystal	core	52,10	0,30	0,57	25,80	0,82	18,98	1,85	0,00	0,06	100,48	53,9	42,4	3,8	57,3
2006_77	opx5c	free crystal	core	52,01	0,27	0,49	25,47	0,81	19,34	1,76	0,00	0,06	100,21	54,7	41,7	3,6	58,4
2006_77	opx6c	free crystal	core	52,14	0,33	0,59	25,56	0,83	19,10	1,80	0,01	0,00	100,38	54,2	42,1	3,7	57,3
Sample 2006 86																	
200686	opcl1c	crystal clot	core	53,03	0,34	0,99	21,37	0,63	21,85	1,82	0,01	0,05	100,09	61,6	34,8	3,7	64,6
200686	opcl1r	crystal clot	rim	52,38	0,50	2,18	19,55	0,44	23,10	1,79	0,00	0,08	100,02	64,9	31,5	3,6	68,6
200686	opcl2rT	crystal clot	rim	52,16	0,33	0,81	23,52	0,74	20,36	1,97	0,00	0,04	99,93	57,5	38,5	4,0	61,3
200686	opx1cT	free crystal	core	52,13	0,29	0,60	24,19	0,78	19,99	1,79	0,01	0,05	99,82	56,6	39,7	3,6	60,1
200686	opx1rT	free crystal	rim	51,49	0,34	0,68	24,21	0,82	19,48	1,78	0,00	0,07	98,89	56,0	40,4	3,7	59,4
200686	opx2c	free crystal	core	51,84	0,22	0,74	24,21	0,85	19,72	1,81	0,00	0,09	99,47	56,2	40,1	3,7	60,0
200686	opx2r	free crystal	rim	52,66	0,26	0,69	24,08	0,82	20,13	1,64	0,02	0,00	100,30	57,1	39,6	3,3	59,8
200686	opx3cT	free crystal	core	50,91	0,29	0,80	25,15	0,81	19,12	1,78	0,00	0,03	98,88	54,7	41,7	3,7	58,9
200686	opx3rT	free crystal	rim	51,81	0,30	0,58	24,52	0,81	19,46	1,82	0,00	0,00	99,30	55,6	40,6	3,7	58,7
200686	opx4c	free crystal	core	52,23	0,35	0,97	23,92	0,75	20,12	1,71	0,00	0,01	100,05	57,2	39,3	3,5	60,0
200686	opx4r	free crystal	rim	51,38	0,43	1,45	22,93	0,69	20,46	1,71	0,00	0,01	99,07	58,5	37,9	3,5	62,0
200686	opx5cT	free crystal	core	51,34	0,31	0,69	23,88	0,75	19,89	1,79	0,01	0,05	98,70	56,8	39,5	3,7	60,8
200686	opx5rT	free crystal	rim	51,64	0,29	0,56	24,09	0,77	19,80	1,70	0,00	0,04	98,89	56,6	39,9	3,5	60,0

Table B.1Continued
Orthopyroxene

Sample 2008 4		Crystal type	A. Loc.	SiO₂	TiO₂	Al₂O₃	FeO	MnO	MgO	CaO	K₂O	Na₂O	Total	En	Fs	Wo	mg#
20084	op1c	free crystal	core	52,01	0,16	0,40	28,84	0,92	17,23	1,43	0,02	0,05	101,05	49,3	47,8	2,9	51,8
20084	op1r	free crystal	rim	50,71	0,24	1,03	29,02	0,99	16,27	1,92	0,03	0,03	100,22	47,2	48,8	4,0	50,7
20084	op2c	free crystal	core	49,12	0,10	0,28	30,20	1,12	16,24	1,30	0,06	0,20	98,62	46,7	50,6	2,7	52,7
20084	op2r	free crystal	rim	50,73	0,15	0,41	30,11	1,09	15,36	1,30	0,01	0,07	99,23	45,4	51,8	2,8	47,6
20084	op3c	free crystal	core	50,92	0,20	0,63	29,75	1,03	16,54	1,45	0,01	0,04	100,58	47,5	49,5	3,0	50,9
20084	op3r	free crystal	rim	51,40	0,13	0,40	30,34	1,13	15,90	1,30	0,00	0,06	100,67	46,1	51,2	2,7	48,5
20084	op4c	free crystal	core	51,92	0,16	0,40	29,86	0,99	16,32	1,35	0,04	0,11	101,15	47,2	50,0	2,8	49,4
20084	op4r	free crystal	rim	50,82	0,13	0,39	30,53	1,05	15,65	1,38	0,05	0,16	100,17	45,6	51,6	2,9	48,8
20084	op5c	free crystal	core	51,12	0,20	0,58	30,47	1,25	15,61	1,42	0,02	0,11	100,78	45,3	51,7	3,0	48,3
20084	op6c	free crystal	core	51,39	0,17	0,48	30,12	0,98	16,57	1,33	0,00	0,05	101,09	47,4	49,9	2,7	50,3
20084	op6r	free crystal	rim	51,55	0,15	0,42	30,03	1,05	16,14	1,39	0,04	0,29	101,07	46,7	50,4	2,9	50,1
20084	op7c	free crystal	core	51,40	0,14	0,43	29,55	0,97	16,62	1,44	0,03	0,02	100,60	47,8	49,2	3,0	50,6
20084	op7r	free crystal	rim	51,62	0,14	0,41	30,32	1,10	16,03	1,31	0,00	0,09	101,02	46,3	50,9	2,7	48,7
20084	op8cT	free crystal	core	51,09	0,28	0,71	29,98	0,98	16,82	1,26	0,00	0,06	101,18	47,9	49,5	2,6	51,3
20084	op8rT	free crystal	rim	51,12	0,30	0,38	30,08	1,10	16,22	1,44	0,01	0,07	100,71	46,7	50,4	3,0	49,8
20084	op9cT	free crystal	core	51,65	0,21	0,64	27,84	0,85	17,48	1,33	0,00	0,08	100,08	50,6	46,6	2,8	52,8
20084	op9rT	free crystal	rim	51,33	0,24	0,45	30,00	1,05	15,96	1,35	0,01	0,09	100,48	46,5	50,7	2,8	48,8
Sample 2005 10																	
200510	op1c	free crystal	core	52,78	0,28	0,86	25,04	0,79	19,35	1,54	0,00	0,07	100,71	55,4	41,5	3,2	57,9
200510	op1r	free crystal	rim	53,66	0,30	1,10	24,24	0,74	18,91	1,72	0,02	0,10	100,79	55,4	41,0	3,6	58,2
200510	op2c	free crystal	core	59,84	0,19	0,00	24,86	0,80	15,31	1,54	0,21	0,23	102,96	49,7	46,7	3,6	52,3
200510	op2r	free crystal	rim	53,08	0,33	1,09	22,37	0,63	22,06	1,81	0,02	0,16	101,54	60,8	35,6	3,6	65,5
200510	op4cT	free crystal	core	53,40	0,39	1,56	25,87	1,06	14,50	3,35	0,58	0,47	101,19	45,3	47,2	7,5	50,0
200510	op5c	free crystal	core	51,97	0,22	0,65	24,84	0,81	21,49	1,58	0,04	0,15	101,74	58,1	38,9	3,1	65,3
200510	op5r	free crystal	rim	51,93	0,22	0,64	25,54	0,83	19,57	1,67	0,03	0,09	100,52	55,0	41,6	3,4	59,3
200510	op6c	free crystal	core	53,51	0,36	1,40	25,83	1,07	15,81	3,76	0,33	0,47	102,55	47,0	44,9	8,0	52,2
200510	op7c	free crystal	core	53,20	0,37	1,32	19,94	0,58	23,19	1,71	0,02	0,04	100,38	64,5	32,0	3,4	67,8

Table B.1Continued

Orthopyroxene

Sample	2005 10	Crystal type	A. Loc.	SiO ₂	TiO ₂	Al ₂ O ₃	FeO	MnO	MgO	CaO	K ₂ O	Na ₂ O	Total	En	Fs	Wo	mg#
200510	op7r	free crystal	rim	52,22	0,25	0,82	24,77	0,81	19,73	1,61	0,01	0,08	100,30	56,0	40,7	3,3	59,2
200510	op8cT	free crystal	core	52,27	0,34	1,28	23,75	0,77	20,47	1,72	0,01	0,04	100,64	57,7	38,8	3,5	61,2
200510	op8rT	free crystal	rim	52,65	0,25	1,00	24,98	0,82	19,02	1,60	0,09	0,09	100,51	54,9	41,8	3,3	57,6
200510	op10cT	free crystal	core	52,36	0,21	0,59	26,13	0,86	19,12	1,52	0,00	0,05	100,83	54,1	42,8	3,1	57,1
200510	op10rT	free crystal	rim	52,21	0,24	0,73	26,09	0,78	19,08	1,55	0,00	0,06	100,74	54,1	42,7	3,2	57,1
200510	op11cT	free crystal	core	51,19	0,31	0,40	28,42	1,19	15,00	3,63	0,03	0,18	100,36	43,8	48,5	7,6	48,9
200510	op12c	free crystal	core	51,84	0,21	0,63	25,49	0,89	19,16	1,45	0,02	0,07	99,75	54,7	42,3	3,0	57,9
200510	opcl1c	crystal clot	core	52,17	0,38	1,31	22,90	0,69	20,83	2,12	0,01	0,06	100,48	58,5	37,2	4,3	62,9
200510	opcl1r	crystal clot	rim	52,26	0,29	0,70	25,41	0,73	19,36	1,59	0,00	0,12	100,45	55,0	41,7	3,3	58,1
2005 10	op9r	free crystal	rim	52,10	0,29	0,96	24,30	0,73	20,03	1,62	0,01	0,13	100,17	56,8	39,9	3,3	60,4
Sample 2007 4																	
20074	op1c	free crystal	core	51,53	0,10	0,31	28,09	1,38	17,72	1,20	0,01	0,02	100,35	50,4	47,1	2,5	53,8
20074	op1r	free crystal	rim	51,34	0,12	0,43	30,34	1,13	16,34	1,14	0,00	0,05	100,90	46,9	50,7	2,3	49,6
20074	op2c	free crystal	core	51,48	0,09	0,29	29,40	1,30	16,94	1,21	0,02	0,02	100,75	48,3	49,2	2,5	51,5
20074	op2r	free crystal	rim	50,70	0,13	0,46	30,28	1,32	16,04	1,11	0,01	0,06	100,11	46,4	51,3	2,3	49,6
20074	op3c	free crystal	core	50,38	0,08	0,40	31,96	1,81	14,64	1,14	0,02	0,02	100,45	42,5	55,1	2,4	45,9
20074	op3r	free crystal	rim	50,60	0,10	0,37	31,74	1,68	15,07	1,13	0,01	0,04	100,75	43,5	54,2	2,3	46,9
20074	op4	free crystal	core	51,16	0,13	0,50	30,41	1,16	16,36	1,23	0,03	0,00	100,98	46,8	50,7	2,5	49,9
20074	op4c	free crystal	core	50,86	0,11	0,27	32,53	2,04	14,05	1,02	0,00	0,02	100,89	41,1	56,8	2,1	43,6
20074	op4r	free crystal	rim	50,81	0,09	0,29	32,03	1,73	14,86	0,95	0,01	0,04	100,81	43,1	55,0	2,0	45,9
20074	op5	free crystal	core	51,64	0,42	1,85	23,76	0,68	20,81	1,43	0,01	0,06	100,66	58,5	38,6	2,9	62,6
Sample 2005 28																	
200528	op1c	free crystal	core	51,15	0,15	0,51	29,55	1,04	17,21	1,28	0,00	0,04	100,94	48,8	48,6	2,6	52,5
200528	op1r	free crystal	rim	51,32	0,13	0,47	29,61	1,08	16,73	1,25	0,01	0,00	100,59	48,0	49,4	2,6	50,8
200528	op2c	free crystal	core	51,07	0,17	0,65	30,11	1,11	16,66	1,19	0,01	0,09	101,06	47,5	50,0	2,4	51,1
200528	op2r	free crystal	rim	50,81	0,16	0,55	28,82	1,03	16,85	1,36	0,02	0,06	99,66	48,7	48,4	2,8	52,0

Table B.1Continued

Orthopyroxene

Sample	Crystal type	A.Loc.	SiO ₂	TiO ₂	Al ₂ O ₃	FeO	MnO	MgO	CaO	K ₂ O	Na ₂ O	Total	En	Fs	Wo	mg#	
200528	op3c	free crystal	core	51,38	0,09	0,31	30,04	1,13	16,63	1,26	0,02	0,01	100,87	47,5	49,9	2,6	50,5
200528	op3r	free crystal	rim	51,36	0,13	0,36	30,37	1,10	16,36	1,37	0,01	0,00	101,07	46,7	50,5	2,8	49,7
200528	op4c	free crystal	core	51,05	0,39	0,71	29,62	1,13	16,76	1,30	0,01	0,06	101,03	48,0	49,4	2,7	51,3
200528	op4r	free crystal	rim	50,41	0,30	1,44	29,23	1,07	16,36	1,81	0,01	0,11	100,73	47,2	49,1	3,8	51,5
200528	op5c	free crystal	core	51,35	0,17	0,69	29,75	1,18	16,91	1,21	0,01	0,00	101,28	48,1	49,4	2,5	51,3
200528	op6c	free crystal	core	50,84	0,16	0,53	30,41	1,10	16,05	1,38	0,01	0,02	100,49	46,2	50,9	2,9	49,4
200528	op6r	free crystal	rim	51,36	0,11	0,43	29,03	1,09	17,29	1,25	0,00	0,07	100,62	49,3	48,2	2,6	52,7
200528	op7c	free crystal	core	52,74	0,40	2,19	22,15	0,55	21,87	1,68	0,02	0,03	101,63	61,1	35,6	3,4	64,4
200528	op7r	free crystal	rim	51,29	0,28	1,72	26,03	0,82	19,12	1,40	0,00	0,02	100,67	54,3	42,8	2,8	57,9
Sample 2006 110																	
2006110	opx1c	free crystal	core	50,64	0,15	0,62	28,43	1,61	16,80	1,15	0,00	0,06	99,45	48,7	48,9	2,4	52,3
2006110	opx1r	free crystal	core	51,26	0,12	0,36	27,94	1,45	17,31	0,96	0,04	0,05	99,49	50,2	47,8	2,0	52,9
2006110	opx2c	free crystal	core	51,39	0,20	0,86	24,72	1,05	19,13	1,41	0,00	0,01	98,78	55,3	41,8	2,9	58,1
2006110	opx2r	free crystal	rim	49,74	0,10	0,67	28,93	1,32	17,53	0,78	0,02	0,04	99,12	50,0	48,4	1,6	54,8
2006110	opx3c	free crystal	core	50,87	0,09	0,51	29,01	1,39	16,53	0,84	0,01	0,03	99,27	48,3	49,9	1,8	50,6
2006110	opx3r	free crystal	rim	51,49	0,21	0,87	24,99	1,01	19,10	1,47	0,02	0,00	99,16	55,0	42,0	3,0	57,9
2006110	opx4k	inclusion	core	51,09	0,13	0,38	26,25	1,23	18,50	1,19	0,01	0,02	98,81	53,2	44,3	2,5	56,6
2006110	op5cT	free crystal	core	50,71	0,19	0,81	26,00	1,13	17,95	1,42	0,00	0,00	98,20	52,5	44,5	3,0	55,3
2006110	op5rT	free crystal	rim	50,95	0,11	0,33	27,64	1,35	17,27	1,01	0,02	0,05	98,72	50,4	47,5	2,1	53,0
2006110	op6k	free crystal	core	50,76	0,20	0,80	26,05	1,30	18,08	1,38	0,00	0,02	98,59	52,5	44,6	2,9	55,8
2006110	opx7cT	free crystal	core	52,04	0,08	0,36	26,56	1,29	18,61	1,09	0,01	0,01	100,04	53,1	44,6	2,2	55,8
2006110	opx7rT	free crystal	rim	50,85	0,16	0,43	28,11	1,41	17,11	1,05	0,00	0,04	99,15	49,7	48,1	2,2	52,6
Sample 2005 69																	
200569	opx1c	free crystal	core	46,79	0,13	0,53	44,20	1,52	6,04	0,71	0,01	0,01	99,93	18,7	79,7	1,6	20,1
200569	opx1r	free crystal	rim	46,59	0,10	0,52	43,48	1,39	6,31	0,57	0,00	0,00	98,97	19,8	78,9	1,3	21,0
200569	opx2c	free crystal	core	47,46	0,12	0,70	41,30	1,27	7,53	0,67	0,02	0,10	99,17	23,6	74,9	1,5	24,8
200569	opx2r	free crystal	rim	46,55	0,11	0,44	43,28	1,43	5,91	0,62	0,02	0,10	98,45	18,8	79,8	1,4	19,9

Table B.1Continued

Feldspars																
Sample 2006 99		Crystal type	A. Loc.	SiO₂	TiO₂	Al₂O₃	FeO	MnO	MgO	CaO	Na₂O	K₂O	Total	An	Ab	Or
200699	p1c	free crystal	core	53,22	0,096	28,79	0,51	0,01	0,12	12,36	4,76	0,25	100,13	58,1	40,5	1,4
200699	p1r	free crystal	rim	51,38	0,087	30,29	0,51	0,00	0,09	13,41	4,16	0,20	100,12	63,4	35,5	1,1
200699	p2c	free crystal	core	54,01	0,097	28,11	0,47	0,00	0,12	11,47	5,10	0,25	99,62	54,6	44,0	1,4
200699	p2r	free crystal	rim	51,67	0,076	29,51	0,39	0,02	0,12	13,37	4,42	0,21	99,78	61,9	37,0	1,1
200699	pm1	microlite	core	52,71	0,114	29,08	0,68	0,00	0,03	12,35	4,55	0,32	99,81	59,0	39,3	1,8
200699	p3c	free crystal	core	52,04	0,084	28,23	0,50	0,00	0,16	11,89	5,85	0,27	99,01	52,2	46,4	1,4
200699	p4c	free crystal	core	53,44	0,107	28,49	0,48	0,01	0,13	11,96	4,73	0,21	99,55	57,6	41,2	1,2
200699	p4r	free crystal	rim	52,25	0,096	29,58	0,37	0,00	0,07	12,94	4,38	0,22	99,91	61,3	37,5	1,2
200699	p5c	free crystal	core	53,5	0,086	28,48	0,42	0,00	0,13	11,83	4,93	0,23	99,62	56,2	42,4	1,3
200699	p6c	free crystal	core	53	0,084	28,84	0,41	0,00	0,13	12,25	4,70	0,23	99,64	58,3	40,5	1,3
200699	p7c	free crystal	core	53,58	0,116	28,45	0,44	0,00	0,14	11,93	5,03	0,25	99,93	55,9	42,7	1,4
200699	p7r	free crystal	rim	53,13	0,106	28,92	0,61	0,01	0,07	11,87	4,82	0,31	99,85	56,6	41,6	1,8
200699	p8c	free crystal	core	52,55	0,063	29,45	0,51	0,01	0,03	12,48	4,60	0,27	99,95	59,1	39,4	1,5
200699	pl9c	free crystal	core	53,14	0,077	28,70	0,41	0,02	0,12	12,11	4,88	0,24	99,70	57,0	41,6	1,3
200699	pl9r	free crystal	rim	52,58	0,079	29,20	0,39	0,00	0,11	12,57	4,64	0,18	99,74	59,4	39,6	1,0
200699	pl10r	free crystal	rim	50,97	0,07	30,37	0,52	0,00	0,10	13,92	3,73	0,17	99,85	66,7	32,4	0,9
200699	pl10c	free crystal	core	51,34	0,053	30,05	0,37	0,02	0,15	13,56	4,12	0,12	99,77	64,1	35,2	0,7
200699	pl11c	free crystal	core	54,63	0,097	27,71	0,48	0,03	0,09	10,88	5,35	0,36	99,64	51,8	46,1	2,1
200699	pl11r	free crystal	rim	53,06	0,115	28,97	0,53	0,00	0,07	12,10	4,75	0,27	99,87	57,6	40,9	1,5
200699	plm2	microlite	core	54,13	0,135	28,07	0,93	0,01	0,02	11,14	5,34	0,32	100,11	52,6	45,6	1,8
200699	plm3	microlite	core	55,06	0,182	26,99	1,27	0,00	0,08	10,52	5,91	0,45	100,45	48,4	49,2	2,5
Sample 2006 112																
2006112	pl1m_112	free crystal	core	55,72	0,13	27,01	0,44	0,00	0,08	9,99	5,96	0,59	99,92	46,5	50,2	3,3
2006112	pl1r_112	free crystal	rim	54,01	0,11	28,15	0,48	0,00	0,10	11,34	5,14	0,38	99,71	53,8	44,1	2,1
2006112	pl2z	free crystal	core	55,43	0,10	27,15	0,47	0,02	0,08	10,34	5,61	0,53	99,74	48,9	48,1	3,0

Table B.1Continued

Feldspars

Sample	2006	112	Crystal type	A. Loc.	SiO ₂	TiO ₂	Al ₂ O ₃	FeO	MnO	MgO	CaO	Na ₂ O	K ₂ O	Total	An	Ab	Or
2006112	pl2c		free crystal	core	55,44	0,11	27,20	0,50	0,00	0,10	10,11	5,77	0,49	99,73	47,8	49,4	2,8
2006112	plmic2c		microlite	core	55,26	0,16	27,32	0,75	0,02	0,02	10,13	5,90	0,38	99,95	47,6	50,2	2,1
2006112	pl3c		free crystal	core	53,42	0,10	28,44	0,37	0,03	0,10	11,65	4,99	0,36	99,48	55,2	42,8	2,1
2006112	pl3r		free crystal	rim	55,00	0,11	27,40	0,46	0,03	0,09	10,66	5,75	0,46	99,95	49,3	48,2	2,5
2006112	plmic3		microlite	core	55,56	0,11	26,99	0,60	0,00	0,07	10,22	5,85	0,49	99,90	47,7	49,5	2,7
2006112	pl4z		free crystal	core	55,27	0,12	27,25	0,51	0,03	0,09	10,38	5,68	0,50	99,82	48,8	48,4	2,8
2006112	pl4z		free crystal	rim	55,06	0,10	28,04	0,48	0,00	0,10	10,75	5,42	0,49	100,43	50,8	46,4	2,7
2006112	pl5c		free crystal	core	55,02	0,10	27,46	0,55	0,01	0,08	10,87	5,34	0,43	99,86	51,7	45,9	2,4
2006112	pl5r		free crystal	rim	54,30	0,11	27,89	0,51	0,02	0,09	11,15	5,35	0,44	99,87	52,2	45,3	2,4
2006112	pl6z		free crystal	core	56,31	0,10	26,41	0,43	0,03	0,08	9,32	6,04	0,66	99,38	44,3	52,0	3,7
2006112	pl6z		free crystal	rim	54,63	0,11	27,69	0,50	0,01	0,10	11,31	5,38	0,41	100,16	52,5	45,2	2,3
2006112	plmic4		microlite	core	54,58	0,12	27,52	0,59	0,00	0,05	10,53	5,56	0,44	99,38	49,9	47,6	2,5
2006112	pl7c		free crystal	core	55,51	0,11	27,35	0,47	0,01	0,07	10,52	5,60	0,56	100,18	49,3	47,6	3,1
2006112	pl7r		free crystal	rim	57,63	0,11	25,95	0,43	0,00	0,08	8,53	6,54	0,79	100,07	40,0	55,5	4,4
2006112	pl8r		free crystal	rim	54,31	0,09	27,64	0,52	0,00	0,10	10,40	5,65	0,43	99,14	49,2	48,4	2,4
2006112	pl9z		free crystal	core	54,86	0,10	27,46	0,53	0,00	0,08	10,81	5,41	0,50	99,75	51,0	46,2	2,8
2006112	pl9z		free crystal	rim	54,50	0,11	27,45	0,58	0,01	0,10	10,69	5,63	0,46	99,53	49,9	47,6	2,6
2006112	pl10c		free crystal	core	57,35	0,11	25,95	0,47	0,01	0,11	8,74	6,57	0,69	100,00	40,7	55,4	3,8
2006112	pl10r		free crystal	rim	54,24	0,12	27,65	0,52	0,04	0,10	10,87	5,48	0,44	99,45	51,0	46,5	2,4
2006112	pl11c		free crystal	core	56,14	0,09	26,68	0,41	0,01	0,07	9,59	6,27	0,59	99,86	44,3	52,4	3,3
2006112	pl11r		free crystal	rim	55,56	0,12	27,04	0,54	0,02	0,10	10,15	5,73	0,51	99,77	48,0	49,1	2,9
2006112	pl12c		free crystal	core	55,54	0,12	27,30	0,53	0,02	0,10	10,07	5,91	0,55	100,14	47,0	49,9	3,1
2006112	pl12r		free crystal	rim	54,69	0,10	27,77	0,51	0,00	0,10	10,85	5,23	0,42	99,66	52,1	45,5	2,4

Table B.1Continued

Feldspars

Sample 2005 68		Crystal type	A. Loc.	SiO ₂	TiO ₂	Al ₂ O ₃	FeO	MnO	MgO	CaO	Na ₂ O	K ₂ O	Total	An	Ab	Or
200568	pl1r	free crystal	rim	55,33	0,10	26,84	0,50	0,02	0,08	10,19	5,69	0,50	99,24	48,3	48,9	2,8
200568	pl3c	free crystal	core	52,64	0,07	28,92	0,51	0,02	0,07	12,49	4,69	0,30	99,71	58,5	39,8	1,7
200568	pl3r	free crystal	rim	54,79	0,10	27,74	0,58	0,01	0,09	10,83	5,52	0,41	100,07	50,8	46,9	2,3
200568	pl4c	free crystal	core	55,31	0,13	27,06	0,59	0,00	0,10	10,34	5,32	0,46	99,31	50,4	46,9	2,6
200568	pl4r	free crystal	rim	54,10	0,12	27,20	0,60	0,01	0,09	10,88	5,29	0,46	98,76	51,8	45,6	2,6
200568	pl5r	free crystal	rim	54,58	0,11	27,68	0,54	0,04	0,08	11,13	5,34	0,41	99,90	52,3	45,4	2,3
200568	pl6c	free crystal	core	54,86	0,10	27,38	0,47	0,00	0,06	10,69	5,24	0,56	99,36	51,3	45,5	3,2
200568	pl6r	free crystal	rim	53,67	0,07	28,43	0,49	0,02	0,08	11,74	4,95	0,33	99,78	55,7	42,5	1,9
200568	pl7c	free crystal	core	55,65	0,12	27,11	0,55	0,01	0,09	10,33	5,67	0,43	99,96	49,0	48,6	2,4
200568	pl7r	free crystal	rim	54,81	0,09	27,65	0,52	0,00	0,08	10,99	5,17	0,43	99,74	52,7	44,9	2,4
200568	pl8c	free crystal	core	56,20	0,12	26,57	0,50	0,01	0,06	9,57	6,06	0,70	99,77	44,8	51,3	3,9
200568	pl9r	free crystal	rim	55,69	0,10	27,31	0,56	0,01	0,08	10,46	5,58	0,50	100,30	49,5	47,7	2,8
200568	plmic1	microlite	core	59,10	0,15	24,87	0,75	0,00	0,08	7,66	6,99	0,89	100,49	35,9	59,2	5,0
200568	plmic2	microlite	core	55,80	0,11	27,02	0,66	0,01	0,07	10,28	5,75	0,47	100,17	48,4	49,0	2,6
Sample 2006 77																
2006 77	pl1c	free crystal	core	56,02	0,03	26,70	0,39	0,00	0,03	9,86	5,95	0,41	99,37	46,7	51,0	2,3
2006 77	pl1r	free crystal	rim	54,02	0,04	28,28	0,36	0,02	0,04	11,46	5,04	0,33	99,60	54,6	43,5	1,9
2006 77	pl2c	free crystal	core	54,50	0,03	28,01	0,37	0,00	0,04	11,02	5,43	0,35	99,76	51,8	46,2	2,0
2006 77	pl2r	free crystal	rim	54,27	0,04	28,27	0,40	0,00	0,04	11,15	5,44	0,38	99,98	52,0	45,9	2,1
2006 77	pl3c	free crystal	core	54,42	0,05	27,96	0,41	0,00	0,04	11,03	5,22	0,32	99,46	52,9	45,3	1,8
2006 77	pl3mic	microlite	core	56,80	0,07	25,95	0,62	0,03	0,04	8,86	6,13	0,72	99,22	42,6	53,3	4,1
2006 77	pl4c	free crystal	core	54,17	0,03	28,37	0,33	0,02	0,05	11,25	5,27	0,30	99,79	53,2	45,1	1,7
2006 77	pl4mic	microlite	core	54,57	0,05	27,60	0,39	0,00	0,04	10,86	5,53	0,40	99,44	50,9	46,9	2,2
2006 77	pl4r	free crystal	rim	54,77	0,03	28,02	0,41	0,01	0,04	10,83	5,35	0,38	99,83	51,7	46,2	2,1
2006 77	pl5c	free crystal	core	53,88	0,03	28,34	0,35	0,01	0,05	11,55	5,18	0,29	99,68	54,3	44,1	1,6

Table B.1Continued

Feldspars

Sample 2006 77		Crystal type	A. Loc.	SiO ₂	TiO ₂	Al ₂ O ₃	FeO	MnO	MgO	CaO	Na ₂ O	K ₂ O	Total	An	Ab	Or
2006 77	pl5r	free crystal	rim	53,95	0,03	28,46	0,37	0,03	0,04	11,53	5,15	0,32	99,88	54,3	43,9	1,8
2006 77	pl6c	free crystal	core	54,66	0,03	27,78	0,49	0,00	0,05	10,93	5,15	0,35	99,44	52,9	45,1	2,0
2006 77	pl6r	free crystal	rim	55,39	0,04	27,08	0,47	0,02	0,04	10,23	5,62	0,43	99,32	48,9	48,6	2,5
2006 77	pl7c	free crystal	core	54,95	0,04	27,39	0,31	0,01	0,04	10,40	5,53	0,38	99,04	49,9	48,0	2,2
2006 77	pl7r	free crystal	rim	55,00	0,03	27,48	0,40	0,00	0,05	10,50	5,60	0,39	99,45	49,8	48,0	2,2
Sample 2006 6																
20066	pl1c	free crystal	core	58,14	0,03	25,63	0,38	0,03	0,03	8,35	6,82	0,64	100,05	38,9	57,5	3,6
20066	pl1r	free crystal	rim	59,74	0,02	24,67	0,40	0,00	0,02	6,96	7,39	0,82	100,03	32,6	62,8	4,6
20066	pl2c	free crystal	core	54,10	0,04	28,27	0,51	0,00	0,04	11,34	5,19	0,33	99,81	53,7	44,5	1,9
20066	pl2r	free crystal	rim	52,12	0,07	29,36	0,74	0,02	0,05	12,95	4,49	0,24	100,03	60,6	38,0	1,3
20066	pl1mic	microlite	core	61,17	0,02	23,93	0,31	0,01	0,01	5,94	8,01	1,03	100,44	27,4	66,9	5,7
20066	pl2mic	microlite	core	55,64	0,06	27,57	0,64	0,00	0,02	10,44	5,78	0,43	100,56	48,8	48,8	2,4
20066	pl2mic	microlite	core	56,43	0,06	26,89	0,62	0,02	0,03	9,83	6,01	0,47	100,36	46,2	51,2	2,6
20066	pl3c	free crystal	core	54,79	0,04	28,62	0,29	0,02	0,03	11,42	5,44	0,35	100,98	52,7	45,4	1,9
20066	pl3r	free crystal	rim	60,82	0,02	24,36	0,38	0,00	0,02	6,25	7,69	0,99	100,52	29,3	65,2	5,5
20066	pl4c	free crystal	core	53,20	0,04	29,16	0,29	0,00	0,02	12,36	4,77	0,29	100,13	57,9	40,5	1,6
20066	pl4r	free crystal	rim	58,73	0,02	25,23	0,35	0,03	0,01	7,78	7,22	0,66	100,02	36,0	60,4	3,6
20066	pl5z	free crystal	core	57,09	0,03	26,57	0,33	0,00	0,02	9,21	6,38	0,53	100,15	43,1	54,0	2,9
20066	pl6c	free crystal	core	56,33	0,04	27,28	0,28	0,01	0,01	9,92	6,25	0,46	100,58	45,6	51,9	2,5
20066	pl6r	free crystal	rim	59,99	0,02	24,57	0,31	0,02	0,02	6,76	7,45	0,87	100,00	31,8	63,4	4,9
20066	pl7c	free crystal	core	53,62	0,04	28,87	0,34	0,02	0,01	12,00	4,81	0,30	100,02	57,0	41,3	1,7
20066	pl7r	free crystal	rim	61,81	0,04	23,09	0,43	0,02	0,02	5,32	8,31	0,94	99,98	24,8	70,0	5,2
20066	pl8c	free crystal	core	59,35	0,02	24,95	0,39	0,01	0,02	7,49	7,06	0,75	100,05	35,4	60,4	4,2
20066	pl8r	free crystal	rim	57,79	0,03	25,98	0,41	0,00	0,03	8,59	6,68	0,58	100,09	40,2	56,6	3,3
20066	pl9c	free crystal	core	59,26	0,01	25,27	0,27	0,00	0,01	7,66	7,13	0,67	100,28	35,8	60,4	3,8

Table B.1Continued

Feldspars

Sample 2006 6		Crystal type	A. Loc.	SiO₂	TiO₂	Al₂O₃	FeO	MnO	MgO	CaO	Na₂O	K₂O	Total	An	Ab	Or
20066	pl9r	free crystal	rim	53,67	0,07	28,23	0,72	0,03	0,05	11,96	5,17	0,32	100,22	55,1	43,1	1,8
20066	plcl1c	crystal clot	core	57,59	0,04	26,00	0,28	0,01	0,02	8,58	6,74	0,55	99,83	40,0	56,9	3,1
20066	plcl1r	crystal clot	rim	60,53	0,01	24,17	0,36	0,03	0,02	6,32	7,78	0,95	100,17	29,3	65,4	5,3
20066	plcl2c	crystal clot	core	58,10	0,06	25,96	0,45	0,00	0,02	8,38	6,78	0,59	100,34	39,2	57,5	3,3
20066	plcl2r	crystal clot	rim	56,53	0,07	26,87	0,48	0,00	0,03	9,64	6,02	0,47	100,10	45,7	51,6	2,6
Sample 2006 8																
20068	pl1c	free crystal	core	55,32	0,02	27,94	0,24	0,00	0,01	10,56	5,73	0,41	100,22	49,3	48,4	2,3
20068	pl1r	free crystal	rim	59,98	0,03	24,53	0,29	0,01	0,01	6,60	7,46	0,94	99,84	31,1	63,6	5,3
20068	pl3c	free crystal	core	56,17	0,03	27,22	0,23	0,00	0,00	9,81	5,95	0,43	99,84	46,5	51,0	2,4
20068	pl3r	free crystal	rim	60,14	0,01	24,52	0,27	0,00	0,01	6,80	7,39	0,90	100,04	32,0	62,9	5,0
20068	pl4c	free crystal	core	59,89	0,02	24,46	0,25	0,00	0,02	6,80	7,47	0,89	99,80	31,8	63,2	5,0
20068	pl4r	free crystal	rim	57,41	0,03	26,49	0,29	0,01	0,01	9,14	6,34	0,60	100,31	42,9	53,8	3,3
20068	pl5c	free crystal	core	60,42	0,02	24,43	0,28	0,00	0,01	6,51	7,60	0,88	100,15	30,5	64,5	4,9
20068	pl5r	free crystal	rim	60,31	0,02	24,41	0,25	0,00	0,02	6,58	7,78	0,97	100,33	30,2	64,5	5,3
20068	pl6c	free crystal	core	60,93	0,04	23,87	0,26	0,00	0,01	5,99	7,70	1,09	99,89	28,2	65,7	6,1
20068	pl6r	free crystal	rim	59,10	0,02	25,24	0,22	0,00	0,00	7,50	7,34	0,74	100,18	34,6	61,3	4,1
20068	pl7c	free crystal	core	59,99	0,03	24,75	0,31	0,01	0,01	6,84	7,40	0,86	100,19	32,2	63,0	4,8
20068	pl7r	free crystal	rim	60,45	0,04	24,29	0,24	0,00	0,01	6,51	7,56	0,94	100,04	30,6	64,2	5,3
20068	pl8c	free crystal	core	56,03	0,03	27,36	0,28	0,00	0,00	10,14	6,20	0,44	100,48	46,4	51,3	2,4
20068	pl8r	free crystal	rim	59,84	0,02	24,79	0,24	0,03	0,02	7,11	7,33	0,80	100,19	33,4	62,2	4,5
20068	plcl1c	crystal clot	core	56,61	0,04	26,97	0,27	0,00	0,01	9,69	6,22	0,50	100,31	45,0	52,3	2,8
20068	plcl1r	crystal clot	rim	61,26	0,02	23,44	0,26	0,00	0,01	5,61	7,80	1,14	99,53	26,6	66,9	6,4
20068	plcl2c	crystal clot	core	55,59	0,05	27,64	0,25	0,02	0,02	10,33	5,79	0,42	100,10	48,5	49,2	2,4
20068	plcl2r	crystal clot	rim	59,56	0,03	24,74	0,27	0,00	0,01	7,11	7,34	0,87	99,92	33,2	62,0	4,8
20068	plmic3	microlite	core	59,10	0,01	25,34	0,28	0,00	0,01	7,59	6,95	0,77	100,04	36,0	59,7	4,3

Table B.1Continued
Feldspars

Sample 2006 86		Crystal type	A. Loc.	SiO₂	TiO₂	Al₂O₃	FeO	MnO	MgO	CaO	Na₂O	K₂O	Total	An	Ab	Or
2006_86	6_86pl1c	free crystal	core	55,78	0,09	27,29	0,52	0,02	0,05	9,83	5,86	0,37	99,80	47,1	50,8	2,1
2006_86	6_86pl1r	free crystal	rim	55,69	0,09	27,17	0,45	0,00	0,04	9,56	5,78	0,39	99,17	46,7	51,1	2,2
2006_86	clp11c	crystal clot	core	55,13	0,08	28,23	0,55	0,00	0,06	10,72	5,32	0,30	100,38	51,8	46,5	1,7
2006_86	clp11r	crystal clot	rim	54,34	0,07	28,41	0,65	0,00	0,09	11,32	5,10	0,26	100,22	54,3	44,2	1,5
2006_86	pl1mic	microlite	core	61,21	0,18	23,19	0,77	0,00	0,04	5,68	7,10	1,33	99,51	28,2	63,9	7,9
2006_86	pl2c	free crystal	core	53,97	0,10	29,08	0,49	0,00	0,03	11,42	5,18	0,26	100,52	54,1	44,4	1,5
2006_86	pl2r	free crystal	rim	57,22	0,04	26,59	0,37	0,00	0,04	8,81	6,36	0,43	99,84	42,3	55,3	2,4
2006_86	pl3c	free crystal	core	56,45	0,05	27,43	0,37	0,00	0,04	9,50	5,94	0,39	100,18	45,9	51,9	2,3
2006_86	pl3r	free crystal	rim	56,88	0,05	27,16	0,40	0,01	0,03	9,33	6,25	0,40	100,51	44,2	53,6	2,2
2006_86	pl4c	free crystal	core	57,41	0,05	26,57	0,36	0,01	0,04	8,78	6,12	0,38	99,73	43,2	54,5	2,3
2006_86	pl4r	free crystal	rim	57,14	0,05	27,00	0,35	0,00	0,04	9,25	6,25	0,43	100,50	43,9	53,7	2,4
2006_86	pl5c	free crystal	core	59,35	0,03	25,19	0,38	0,00	0,04	7,20	6,97	0,58	99,74	35,1	61,5	3,4
2006_86	pl5r	free crystal	rim	58,48	0,05	26,50	0,41	0,00	0,04	8,42	6,52	0,46	100,87	40,6	56,8	2,6
2006_86	plcl2c	crystal clot	core	55,88	0,08	27,67	0,51	0,01	0,05	10,03	5,49	0,36	100,09	49,2	48,7	2,1
2006_86	plcl2r	crystal clot	rim	56,11	0,07	27,51	0,53	0,03	0,06	9,96	5,70	0,34	100,30	48,2	49,9	1,9
2006_86	plmic2	microlite	core	62,13	0,12	23,47	0,77	0,02	0,08	5,53	7,29	1,27	100,67	27,3	65,2	7,5
Sample 2008 4																
20084	pl1c	free crystal	core	61,33	0,01	24,36	0,22	0,02	0,01	6,20	7,86	0,61	100,61	29,3	67,2	3,5
20084	pl1r	free crystal	rim	60,44	0,00	24,13	0,24	0,00	0,01	6,45	7,28	0,56	99,12	31,8	64,9	3,3
20084	pl2cT	free crystal	core	55,19	0,02	27,99	0,37	0,00	0,04	11,19	5,40	0,24	100,44	52,7	46,0	1,3
20084	pl2rT	free crystal	rim	55,79	0,06	27,51	0,49	0,01	0,01	10,63	5,61	0,26	100,39	50,4	48,1	1,5
20084	pl3c	free crystal	core	58,72	0,03	25,99	0,24	0,01	0,03	8,51	6,62	0,37	100,52	40,6	57,2	2,1
20084	pl3r	free crystal	rim	60,33	0,03	24,20	0,25	0,01	0,01	6,73	7,28	0,60	99,45	32,6	63,9	3,5
20084	pl4c	free crystal	core	57,77	0,04	26,43	0,26	0,00	0,01	8,83	6,44	0,29	100,07	42,4	55,9	1,7
20084	pl4r	free crystal	rim	57,38	0,05	26,63	0,29	0,00	0,00	9,49	6,14	0,28	100,25	45,3	53,1	1,6

Table B.1Continued
Feldspars

Sample 2008 4		Crystal type	A. Loc.	SiO₂	TiO₂	Al₂O₃	FeO	MnO	MgO	CaO	Na₂O	K₂O	Total	An	Ab	Or
20084	pl5cT	free crystal	core	60,00	0,02	24,95	0,22	0,00	0,01	6,93	7,26	0,64	100,03	33,3	63,1	3,7
20084	pl6r	free crystal	rim	59,39	0,04	24,81	0,30	0,01	0,03	7,37	7,06	0,56	99,57	35,4	61,4	3,2
20084	pl7cT	free crystal	core	55,92	0,03	27,53	0,37	0,00	0,06	10,58	5,83	0,27	100,59	49,3	49,2	1,5
20084	pl7rT	free crystal	rim	55,30	0,03	27,02	0,40	0,01	0,04	10,53	5,80	0,30	99,43	49,3	49,1	1,6
20084	pl8c	free crystal	core	61,24	0,00	24,32	0,24	0,01	0,00	6,45	7,63	0,58	100,48	30,8	65,9	3,3
20084	pl8r	free crystal	rim	61,47	0,02	24,15	0,24	0,00	0,00	6,32	7,78	0,59	100,57	29,9	66,7	3,3
20084	pl9r	free crystal	rim	60,95	0,02	23,74	0,21	0,00	0,01	6,26	7,51	0,61	99,32	30,4	66,0	3,5
Sample 2005 10																
200510	pl1c	free crystal	core	58,61	0,02	25,14	0,36	0,00	0,02	8,37	6,58	0,47	99,56	40,1	57,2	2,7
200510	pl1r	free crystal	rim	56,45	0,02	27,02	0,38	0,00	0,03	10,39	5,90	0,28	100,48	48,5	49,9	1,6
200510	pl3r	free crystal	rim	57,00	0,05	27,28	0,41	0,01	0,04	10,30	5,82	0,33	101,25	48,5	49,6	1,8
200510	pl4r	free crystal	rim	57,42	0,02	26,17	0,36	0,01	0,03	9,53	6,33	0,32	100,20	44,6	53,6	1,8
200510	pl5c	free crystal	core	58,45	0,02	27,88	0,38	0,00	0,04	10,14	5,88	0,39	103,18	47,7	50,1	2,2
200510	pl5r	free crystal	core	56,74	0,04	26,45	0,37	0,04	0,05	9,78	6,12	0,31	99,91	46,1	52,2	1,7
200510	pl6c	free crystal	core	56,10	0,08	27,54	0,29	0,01	0,02	10,34	5,68	0,26	100,32	49,4	49,1	1,5
200510	pl6r	free crystal	rim	56,22	0,03	27,14	0,35	0,00	0,03	10,18	5,59	0,28	99,83	49,3	49,0	1,6
200510	pl7c	free crystal	core	54,36	0,06	28,22	0,41	0,00	0,05	11,64	4,94	0,25	99,93	55,7	42,8	1,4
200510	pl7r	free crystal	rim	56,16	0,04	27,16	0,37	0,02	0,03	9,89	5,72	0,31	99,69	48,0	50,2	1,8
200510	plcl1c	crystal clot	core	55,97	0,07	27,28	0,43	0,01	0,04	10,54	5,56	0,27	100,16	50,4	48,1	1,5
200510	plcl1r	crystal clot	rim	56,73	0,04	26,99	0,37	0,00	0,04	10,07	5,99	0,31	100,54	47,3	51,0	1,7
200510	plcl2c	crystal clot	core	55,98	0,03	27,33	0,35	0,01	0,03	10,62	5,54	0,25	100,15	50,7	47,9	1,4
200510	plcl2r	crystal clot	rim	56,14	0,02	27,20	0,37	0,00	0,04	10,25	5,60	0,26	99,87	49,6	49,0	1,5

Table B.1Continued
Feldspars

Sample 2007 4		Crystal type	Analysis location	SiO ₂	TiO ₂	Al ₂ O ₃	FeO	MnO	MgO	CaO	Na ₂ O	K ₂ O	Total	An	Ab	Or
20074	pl1c			free crystal	core	60,78	0,02	23,95	0,19	0,00	0,01	6,33	7,80	0,72	99,81	29,7
20074	pl1r	free crystal	rim	61,85	0,02	23,51	0,21	0,01	0,02	5,88	7,97	0,79	100,25	27,7	67,9	4,4
20074	pl2c	free crystal	core	61,72	0,00	23,65	0,21	0,00	0,01	5,76	7,61	0,72	99,68	28,3	67,5	4,2
20074	pl3c	free crystal	core	58,56	0,03	25,24	0,25	0,00	0,03	8,03	6,87	0,47	99,47	38,2	59,1	2,6
20074	pl3r	free crystal	rim	60,10	0,00	24,36	0,23	0,02	0,01	7,03	7,37	0,56	99,68	33,4	63,4	3,1
20074	pl4c	free crystal	core	59,47	0,03	25,10	0,20	0,01	0,00	7,58	6,97	0,54	99,90	36,4	60,6	3,1
20074	pl4r	free crystal	rim	58,96	0,03	25,00	0,20	0,03	0,00	7,50	7,14	0,48	99,35	35,7	61,6	2,7
20074	pl5c	free crystal	core	62,26	0,02	23,20	0,21	0,02	0,00	5,57	8,04	0,79	100,11	26,4	69,1	4,4
20074	pl6cT	free crystal	core	60,10	0,02	24,50	0,24	0,01	0,00	6,89	7,47	0,67	99,91	32,5	63,7	3,8
20074	pl6rT	free crystal	rim	62,07	0,04	23,52	0,35	0,01	0,01	5,62	7,85	0,86	100,33	27,0	68,1	4,9
20074	pl7c	free crystal	core	60,93	0,01	23,70	0,30	0,02	0,02	6,28	7,72	0,76	99,74	29,7	66,0	4,3
20074	pl7r	free crystal	rim	61,38	0,00	23,62	0,20	0,02	0,01	5,83	7,86	0,77	99,69	27,8	67,8	4,4
20074	pl8cT	free crystal	core	60,89	0,01	24,17	0,24	0,00	0,00	6,46	7,72	0,68	100,16	30,4	65,8	3,8
20074	pl8rT	free crystal	rim	58,24	0,02	25,70	0,25	0,00	0,01	8,42	6,76	0,47	99,87	39,7	57,6	2,7
Sample 2005 28																
200528	28pl1z	free crystal	core	61,02	0,01	23,93	0,21	0,02	0,01	6,15	7,67	0,87	99,88	29,2	65,9	4,9
200528	pl2c	free crystal	core	60,20	0,00	24,22	0,21	0,00	0,00	6,87	7,46	0,72	99,69	32,4	63,6	4,0
200528	pl2r	free crystal	rim	60,44	0,01	24,51	0,24	0,00	0,00	6,80	7,29	0,78	100,07	32,5	63,1	4,4
200528	pl3c	free crystal	core	59,51	0,01	25,03	0,25	0,01	0,02	7,34	7,14	0,69	99,98	34,8	61,3	3,9
200528	pl3r	free crystal	rim	60,55	0,01	24,00	0,25	0,01	0,00	6,55	7,60	0,78	99,76	30,8	64,8	4,4
200528	pl4c	free crystal	core	51,11	0,02	25,75	0,30	0,00	0,03	8,84	11,59	3,19	100,83	26,3	62,4	11,3
200528	pl4r	free crystal	rim	57,93	0,03	25,92	0,34	0,01	0,02	8,63	6,58	0,50	99,95	40,8	56,3	2,8
200528	pl5c	free crystal	core	58,12	0,03	25,78	0,29	0,00	0,01	8,54	6,57	0,55	99,89	40,5	56,4	3,1
200528	pl5r	free crystal	rim	56,25	0,02	27,02	0,30	0,01	0,00	10,07	5,89	0,42	99,98	47,4	50,2	2,4
200528	pl6c	free crystal	core	58,56	0,02	25,58	0,23	0,00	0,01	8,36	6,69	0,58	100,04	39,5	57,2	3,3

Table B.1Continued

Feldspars																
Sample 2005 28		Crystal type	Analysis location	SiO₂	TiO₂	Al₂O₃	FeO	MnO	MgO	CaO	Na₂O	K₂O	Total	An	Ab	Or
200528	pl6r	free crystal	rim	58,53	0,04	25,43	0,23	0,00	0,02	8,00	6,60	0,61	99,46	38,7	57,8	3,5
200528	pl7c	free crystal	core	59,50	0,03	24,79	0,20	0,00	0,02	7,32	7,19	0,66	99,71	34,7	61,6	3,7
200528	pl7r	free crystal	rim	59,96	0,00	24,43	0,22	0,00	0,00	6,85	7,15	0,74	99,35	33,1	62,6	4,3
200528	pl8cT	free crystal	core	58,94	0,03	25,21	0,34	0,01	0,01	7,82	6,79	0,61	99,75	37,6	59,0	3,5
Sample 2006 110																
2006_110	pl1z	free crystal	core	58,36	0,02	25,89	0,26	0,00	0,02	7,84	6,97	0,45	99,80	37,3	60,1	2,5
2006_110	pl2c	free crystal	core	59,11	0,03	25,46	0,25	0,00	0,01	7,53	7,07	0,49	99,96	36,0	61,2	2,8
2006_110	pl2r	free crystal	rim	57,50	0,03	26,40	0,31	0,00	0,01	8,78	6,49	0,42	99,96	41,7	55,9	2,4
2006_110	pl3cT	free crystal	core	57,47	0,03	26,55	0,31	0,00	0,01	8,63	6,36	0,40	99,75	41,9	55,8	2,3
2006_110	pl3rT	free crystal	rim	57,27	0,02	26,43	0,29	0,02	0,02	8,64	6,40	0,40	99,48	41,7	56,0	2,3
2006_110	pl4c	free crystal	core	58,09	0,01	26,17	0,22	0,01	0,02	8,28	6,71	0,40	99,91	39,6	58,1	2,3
2006_110	pl4r	free crystal	rim	57,14	0,00	26,64	0,28	0,04	0,01	8,74	6,52	0,34	99,72	41,7	56,4	1,9
2006_110	pl5c	free crystal	core	58,44	0,05	25,92	0,46	0,01	0,03	8,04	7,07	0,39	100,42	37,8	60,0	2,2
2006_110	pl5r	free crystal	rim	56,83	0,03	26,60	0,38	0,02	0,03	8,95	6,35	0,32	99,52	43,0	55,2	1,9
Sample 2005 69																
2005_69	69pl1lc	free crystal	core	63,77	0,01	22,37	0,11	0,00	0,00	3,45	8,76	1,41	99,88	16,4	75,5	8,0
2005_69	69pl1r	free crystal	rim	64,33	0,01	22,10	0,09	0,00	0,00	3,32	8,77	1,42	100,04	15,9	76,0	8,1
2005_69	pl2c	free crystal	core	63,02	0,03	22,58	0,10	0,00	0,00	3,73	8,36	1,01	98,83	18,6	75,4	6,0
2005_69	pl2r	free crystal	rim	63,37	0,01	22,17	0,08	0,02	0,01	3,30	8,65	1,34	98,94	16,1	76,2	7,8
2005_69	pl3r	free crystal	rim	63,70	0,00	22,14	0,09	0,02	0,00	3,44	9,04	1,44	99,86	16,0	76,1	8,0
2005_69	pl4c	free crystal	core	61,90	0,01	23,65	0,15	0,02	0,00	5,01	8,33	0,95	100,01	23,6	71,1	5,3
2005_69	pl4r	free crystal	rim	63,56	0,02	22,37	0,11	0,02	0,00	3,40	8,71	1,37	99,57	16,3	75,8	7,8
2005_69	pl5c	free crystal	core	63,65	0,02	22,50	0,09	0,00	0,00	3,55	8,49	1,26	99,56	17,4	75,3	7,4
2005_69	pl5r	free crystal	rim	65,44	0,01	22,79	0,07	0,02	0,00	3,39	8,58	1,30	101,60	16,5	75,9	7,6
2005_69	pl6c	free crystal	core	64,77	0,00	21,67	0,05	0,00	0,00	2,72	8,60	1,67	99,48	13,4	76,8	9,8

Table B.1Continued

Feldspars

Sample 2005 69		Crystal type	Analysis location	SiO ₂	TiO ₂	Al ₂ O ₃	FeO	MnO	MgO	CaO	Na ₂ O	K ₂ O	Total	An	Ab	Or
2005_69	pl6r			free crystal	rim	64,41	0,00	21,93	0,08	0,01	0,00	3,03	8,85	1,44	99,75	14,6
Sample 2005 52																
2005 52	plag1c	free crystal	core	62,26	0,01	25,07	0,17	0,00	0,01	5,86	7,44	0,66	101,48	29,1	67,0	3,9
2005 52	plag1r	free crystal	rim	59,64	0,02	25,22	0,20	0,00	0,00	6,71	7,14	0,57	99,50	33,0	63,6	3,3
2005 52	plag2c	free crystal	core	62,37	0,00	22,93	0,17	0,02	0,01	4,31	8,35	0,90	99,06	21,0	73,7	5,2
2005 52	plag2r	free crystal	rim	60,73	0,00	23,93	0,17	0,00	0,01	5,31	7,88	0,71	98,74	26,0	69,8	4,2
2005 52	pl3cT	free crystal	core	63,10	0,00	22,52	0,12	0,00	0,00	3,90	8,40	1,21	99,26	19,0	74,0	7,0
2005 52	pl3rT	free crystal	rim	63,62	0,01	22,58	0,11	0,00	0,00	3,55	8,50	1,24	99,61	17,4	75,4	7,2
2005 52	pl4c	free crystal	core	57,69	0,01	26,83	0,20	0,00	0,01	8,31	6,56	0,36	99,96	40,3	57,6	2,1
2005 52	pl4r	free crystal	rim	63,03	0,00	23,32	0,17	0,00	0,00	4,37	8,37	0,82	100,09	21,3	73,9	4,7
2005 52	pl5c	free crystal	core	57,94	0,01	26,29	0,20	0,01	0,04	7,79	6,80	0,41	99,50	37,8	59,8	2,4
2005 52	pl5r	free crystal	rim	56,89	0,03	26,43	0,25	0,00	0,00	8,32	6,40	0,34	98,65	41,0	57,0	2,0
2005 52	pl6cT	free crystal	core	62,80	0,02	23,16	0,14	0,01	0,00	4,47	8,50	0,92	100,02	21,3	73,4	5,2
2005 52	pl7c	inclusion	core	60,28	0,02	24,33	0,15	0,00	0,01	6,02	7,59	0,59	99,01	29,4	67,1	3,5
2005 52	pl7k	free crystal	core	62,93	0,00	22,02	0,16	0,00	0,00	3,59	8,44	1,53	98,67	17,3	73,8	8,8
2005 52	pl7r	free crystal	rim	61,97	0,01	23,86	0,16	0,00	0,00	5,07	8,18	0,71	99,97	24,5	71,5	4,1
2005 52	pl8c	free crystal	core	61,70	0,01	23,69	0,17	0,00	0,00	5,20	8,12	0,75	99,64	25,0	70,7	4,3
2005 52	pl8r	free crystal	rim	61,13	0,01	24,15	0,16	0,00	0,00	5,65	7,95	0,66	99,71	27,1	69,1	3,8
2005 52	pl9cT	free crystal	core	61,88	0,01	23,27	0,16	0,00	0,00	4,73	8,08	0,89	99,03	23,2	71,6	5,2
2005 52	pl9rT	free crystal	rim	61,67	0,00	23,41	0,16	0,01	0,01	4,68	8,11	0,81	98,86	23,0	72,2	4,8
2005 52	pl10cT	free crystal	core	60,78	0,01	24,63	0,23	0,00	0,01	5,92	7,81	0,63	100,01	28,5	67,9	3,6
2005 52	pl10rT	free crystal	rim	60,55	0,00	24,93	0,25	0,01	0,00	6,10	7,66	0,55	100,05	29,6	67,2	3,1
2005 52	kf1c	free crystal	core	63,33	0,02	18,84	0,09	0,01	0,00	0,13	2,79	11,16	96,37	0,7	27,3	72,0
2005 52	kf1r	free crystal	rim	63,08	0,01	18,84	0,08	0,00	0,00	0,16	3,03	11,05	96,26	0,9	29,2	70,0
2005 52	kf2c	free crystal	core	63,63	0,02	18,90	0,09	0,01	0,00	0,16	2,90	11,34	97,04	0,8	27,7	71,5

Table B.1Continued
Feldspars

Sample 2005 52		Crystal type	Analysis location	SiO₂	TiO₂	Al₂O₃	FeO	MnO	MgO	CaO	Na₂O	K₂O	Total	An	Ab	Or
2005 52	kf2r	free crystal	rim	63,62	0,02	18,71	0,06	0,00	0,00	0,13	2,85	11,29	96,68	0,7	27,6	71,8
2005 52	kf3c	free crystal	core	65,02	0,01	18,82	0,07	0,00	0,00	0,16	3,10	11,36	98,54	0,8	29,1	70,1
2005 52	kf3r	free crystal	rim	63,32	0,02	18,90	0,08	0,00	0,00	0,17	2,99	10,92	96,41	0,9	29,1	70,0
2005 52	kf4r	free crystal	rim	64,05	0,01	18,71	0,08	0,01	0,01	0,09	2,71	11,75	97,41	0,5	25,9	73,7
2005 52	kf5cT	free crystal	core	63,21	0,01	18,66	0,08	0,00	0,00	0,11	2,58	11,31	95,97	0,6	25,6	73,8
2005 52	kf6c	free crystal	core	62,63	0,04	18,69	0,07	0,00	0,00	0,17	2,70	11,32	95,62	0,9	26,4	72,7
2005 52	kf7rT	free crystal	rim	64,14	0,01	18,78	0,08	0,00	0,00	0,12	2,72	11,70	97,55	0,6	26,0	73,4
2005 52	kf8c	free crystal	core	62,71	0,04	18,79	0,08	0,01	0,00	0,19	2,93	10,88	95,63	1,0	28,8	70,2
2005 52	kf8r	free crystal	rim	64,59	0,02	18,81	0,09	0,00	0,00	0,16	2,94	11,58	98,18	0,8	27,6	71,5
2005 52	kf9c	free crystal	core	62,77	0,03	18,80	0,10	0,02	0,00	0,16	2,82	11,58	96,26	0,8	26,8	72,4
2005 52	kf9r	free crystal	rim	62,75	0,03	18,64	0,10	0,00	0,00	0,16	2,75	11,69	96,12	0,8	26,1	73,0
2005 52	kr10rT	free crystal	rim	63,81	0,02	18,87	0,08	0,03	0,00	0,15	2,99	11,91	97,87	0,8	27,4	71,8
Sample 2005 75																
2005 75	pl1c	free crystal	core	65,28	0,01	21,29	0,05	0,00	0,00	2,34	9,65	1,02	99,64	11,1	83,1	5,8
2005 75	pl1r	free crystal	rim	64,46	0,00	21,37	0,06	0,00	0,00	2,48	9,47	1,00	98,84	11,9	82,3	5,7
2005 75	pl2cT	free crystal	core	65,63	0,00	21,30	0,05	0,02	0,00	2,22	9,76	1,02	100,01	10,5	83,7	5,8
2005 75	pl2rT	free crystal	rim	64,96	0,00	20,75	0,05	0,00	0,00	1,94	9,51	1,18	98,40	9,5	83,7	6,8
2005 75	pl3c	free crystal	core	64,70	0,01	21,84	0,06	0,00	0,00	2,77	9,74	0,96	100,07	12,9	81,8	5,3
2005 75	pl3r	free crystal	rim	64,96	0,01	21,42	0,05	0,00	0,00	2,37	9,54	1,05	99,39	11,3	82,7	6,0
2005 75	pl4c	free crystal	core	64,08	0,00	21,27	0,07	0,00	0,00	2,50	9,84	1,01	98,77	11,6	82,8	5,6
2005 75	pl4r	free crystal	rim	64,27	0,00	21,15	0,07	0,00	0,01	2,42	9,38	1,11	98,40	11,7	81,9	6,4
2005 75	pl5c	free crystal	core	65,85	0,00	21,22	0,07	0,02	0,00	2,09	9,88	1,14	100,27	9,8	83,8	6,4
2005 75	pl5r	free crystal	rim	65,10	0,00	21,53	0,06	0,02	0,00	2,35	9,65	1,09	99,81	11,1	82,7	6,2
2005 75	pl6c	free crystal	core	64,31	0,00	21,62	0,06	0,00	0,00	2,60	9,66	1,02	99,26	12,2	82,1	5,7
2005 75	pl6r	free crystal	rim	64,60	0,00	21,38	0,05	0,02	0,00	2,49	9,66	1,10	99,30	11,7	82,2	6,1

Table B.1Continued

Feldspars

Sample 2005 75		Crystal type	Analysis location	SiO ₂	TiO ₂	Al ₂ O ₃	FeO	MnO	MgO	CaO	Na ₂ O	K ₂ O	Total	An	Ab	Or
2005 75	kf1rT	free crystal	rim	64,97	0,01	18,72	0,05	0,00	0,00	0,11	3,47	11,24	98,57	0,6	31,8	67,7
2005 75	kf2cT	free crystal	core	65,51	0,00	18,80	0,03	0,00	0,00	0,16	3,71	10,91	99,12	0,8	33,8	65,4
2005 75	kf2rT	free crystal	rim	65,40	0,00	18,76	0,04	0,00	0,00	0,10	3,45	11,11	98,85	0,5	31,9	67,6
2005 75	kf3mic	microlite	core	65,22	0,00	18,76	0,03	0,00	0,00	0,12	3,49	11,01	98,65	0,6	32,3	67,1
2005 75	kf4c	free crystal	core	65,30	0,00	18,84	0,04	0,00	0,00	0,13	3,79	11,17	99,27	0,7	33,8	65,5
2005 75	kf4r	free crystal	rim	64,81	0,02	18,79	0,03	0,00	0,00	0,12	3,64	11,16	98,56	0,6	32,9	66,5
2005 75	kf5c	free crystal	core	65,26	0,00	18,74	0,04	0,03	0,00	0,08	3,49	11,05	98,70	0,4	32,3	67,3
2005 75	kf5r	free crystal	rim	64,65	0,00	18,50	0,04	0,00	0,01	0,10	3,37	11,14	97,80	0,5	31,3	68,2
2005 75	kf6c	free crystal	core	65,30	0,01	18,66	0,02	0,01	0,00	0,12	3,40	11,17	98,68	0,6	31,5	67,9
2005 75	kf6c	free crystal	core	65,17	0,00	18,71	0,05	0,00	0,01	0,10	3,50	11,07	98,61	0,5	32,3	67,2
2005 75	kf6c	free crystal	core	65,28	0,00	18,80	0,03	0,01	0,00	0,10	3,54	11,21	98,98	0,5	32,2	67,3
2005 75	kf6r	free crystal	rim	64,88	0,00	18,67	0,04	0,00	0,00	0,12	3,54	11,02	98,28	0,6	32,6	66,8

Table B.1Continued
Amphibole

Sample 2008 4		Crystal type	Analysis location	SiO₂	TiO₂	Al₂O₃	FeO	MnO	MgO	CaO	Na₂O	K₂O	Total	mg #
2008 4	a1c	free crystal	core	42,99	2,47	9,92	18,49	0,32	10,61	10,98	3,06	0,64	99,47	57,7
2008 4	a1r	free crystal	rim	43,01	2,65	8,63	18,88	0,08	10,57	10,65	2,67	0,69	97,84	58,2
2008 4	a2c	free crystal	core	43,56	2,65	9,19	23,26	0,39	10,16	9,41	1,73	0,30	100,66	47,2
2008 4	a3c	free crystal	core	43,82	2,81	8,79	18,88	0,34	10,67	11,07	2,36	0,64	99,38	58,5
2008 4	a3r	free crystal	rim	43,67	2,77	8,65	18,27	0,36	10,95	11,31	2,89	0,66	99,52	56,7
2008 4	a3cT	free crystal	core	42,21	3,38	10,89	16,63	0,27	11,20	10,72	2,70	0,51	98,50	64,8
2008 4	a3r	free crystal	rim	44,16	2,75	8,74	18,55	0,33	10,85	11,03	2,35	0,63	99,38	59,3
2008 4	a3rT	free crystal	core	44,09	2,97	9,32	15,04	0,28	11,98	12,44	2,28	0,42	98,84	58,9
2008 4	a5cT	free crystal	rim	43,48	2,76	8,74	19,19	0,05	10,50	11,09	2,27	0,72	98,78	57
2008 4	a6c	free crystal	core	44,25	2,77	8,92	17,90	0,34	10,81	11,13	2,59	0,72	99,42	56,8
2008 4	a6r	free crystal	rim	43,63	2,74	8,63	18,27	0,33	10,50	10,72	2,58	0,66	98,05	57,2
2008 4	a7c	free crystal	core	41,80	2,98	13,20	18,34	0,30	7,91	9,28	3,60	0,68	98,08	47,8
2008 4	a7r	free crystal	rim	42,75	3,48	10,10	18,08	0,34	10,36	11,12	2,49	0,54	99,25	57,2
2008 4	a8c	free crystal	core	41,89	3,06	9,63	18,41	0,34	10,17	10,82	2,55	0,56	97,42	57,8
2008 4	a8r	free crystal	rim	42,67	2,82	8,38	20,94	0,35	9,60	11,10	2,35	0,75	98,96	52,8
2008 4	a9c	free crystal	core	42,34	2,64	8,34	17,92	0,36	10,85	11,24	2,40	0,68	96,78	58,8
2008 4	a10cT	free crystal	core	42,44	3,57	10,80	15,82	0,27	11,59	10,92	3,21	0,50	99,11	63
2008 4	a10rT	free crystal	rim	42,47	3,75	10,48	16,27	0,30	11,63	11,26	2,79	0,55	99,51	63,2
2008 4	a11c	free crystal	core	42,53	2,57	8,80	16,43	0,31	10,41	10,19	2,26	0,66	94,15	60
Sample 2007 4														
2007 4	a1c	free crystal	core	44,97	2,19	7,65	18,39	0,39	11,21	11,27	2,093	0,8	98,93	59,50
2007 4	a1r	free crystal	rim	45,27	2,049	7,415	18,65	0,423	11,28	11,34	1,945	0,7	99,07	60,30
2007 4	a2cT	free crystal	core	46,23	1,735	6,678	16,05	0,419	12,96	11,42	1,853	0,576	97,92	68,2
2007 4	a3c	free crystal	core	45,28	1,941	7,124	18,45	0,43	11,52	11,23	1,699	0,773	98,44	62,9
2007 4	a3r	free crystal	rim	44,28	2,06	8,148	18,41	0,398	11,37	11,34	2,018	0,669	98,70	62,5

Table B.1Continued
Amphibole

Sample 2007 4		Crystal type	Analysis location	SiO₂	TiO₂	Al₂O₃	FeO	MnO	MgO	CaO	Na₂O	K₂O	Total	mg #
2007 4	a4c	free crystal	core	43,15	2,688	9,027	20,15	0,414	9,962	10,96	2,109	0,808	99,27	56,9
2007 4	a4r	free crystal	rim	45,63	1,966	7,261	18,3	0,443	11,59	11,13	1,66	0,776	98,76	63,9
2007 4	a5c	free crystal	core	45,47	1,857	6,879	18,46	0,555	11,26	11,26	1,801	0,659	98,21	60,7
2007 4	a6c	free crystal	core	44,87	1,925	7,626	19,67	0,424	10,86	10,78	1,719	0,865	98,73	62,4
2007 4	a6r	free crystal	rim	44,91	2,049	7,559	20,6	0,445	10,15	10,84	1,755	0,829	99,13	57,5
2007 4	a7c	free crystal	core	46,07	1,854	6,891	18,66	0,44	11,55	10,92	1,619	0,631	98,63	64,6
2007 4	a8c	free crystal	core	45,83	1,656	6,969	17,65	0,499	12,09	11,14	1,789	0,641	98,27	66,4
2007 4	a8r	free crystal	rim	43,68	2,074	8,621	18,56	0,488	10,92	10,86	1,917	0,832	97,96	63,4
2007 4	a9	free crystal	core	47,55	1,121	5,694	20,09	0,647	11,26	10,73	1,385	0,461	98,95	51
2007 4	a10c	free crystal	core	41,19	4,284	11,89	14,33	0,309	12,94	10,44	2,525	0,559	98,45	81,4
2007 4	a10r	free crystal	core	42,02	3,76	11,35	13,86	0,272	13,01	11,28	2,581	0,61	98,74	73,4
2007 4	a11cT	free crystal	core	45,36	1,86	7,12	19,82	0,57	10,45	11,31	1,639	0,681	98,82	57,10
2007 4	a11rT	free crystal	rim	45,26	1,76	7,05	20,01	0,57	10,79	11,05	1,739	0,662	98,88	60,70
2007 4	a12c	free crystal	core	45,46	1,86	7,47	17,90	0,50	11,85	11,38	1,825	0,658	98,91	64,40
2007 4	a12r	free crystal	rim	46,27	1,96	7,25	16,26	0,40	12,90	11,43	1,802	0,582	98,86	68,70
2007 4	a13cT	free crystal	core	44,74	2,03	7,36	19,89	0,40	10,53	11,01	1,661	0,826	98,44	59
Sample 2005 28														
2005 28	a1c	free crystal	core	44,43	2,07	8,05	18,82	0,40	10,87	11,43	1,86	0,828	98,76	58,8
2005 28	a1r	free crystal	rim	44,57	2,21	8,11	18,30	0,36	11,23	11,31	2,11	0,819	99,02	60,2
2005 28	a2c	free crystal	core	46,26	1,94	6,95	17,76	0,38	12,02	11,24	1,75	0,642	98,93	64,5
2005 28	a2r	free crystal	rim	44,92	2,18	7,97	18,21	0,39	11,51	11,19	1,97	0,861	99,19	62,7
2005 28	a3c	free crystal	core	44,98	2,26	7,87	18,20	0,37	11,23	11,40	2,04	0,751	99,11	59,4
2005 28	a3r	free crystal	rim	45,03	2,21	7,85	17,76	0,33	11,74	11,43	1,96	0,871	99,17	62,2
2005 28	a4c	free crystal	core	45,20	2,13	7,54	18,12	0,35	11,62	11,24	1,76	0,767	98,71	63,3
2005 28	a4r	free crystal	rim	45,02	2,11	7,91	17,38	0,34	11,98	11,19	2,02	0,82	98,77	64,8

Table B.1Continued

Amphibole

Sample 2005 28		Crystal type	Analysis location	SiO₂	TiO₂	Al₂O₃	FeO	MnO	MgO	CaO	Na₂O	K₂O	Total	mg #
2005 28	a5c	free crystal	core	46,78	1,77	6,61	16,83	0,32	12,68	11,30	1,69	0,652	98,64	67,1
2005 28	a5r	free crystal	rim	46,16	1,94	7,19	18,05	0,38	11,75	11,26	1,93	0,734	99,38	62,2
2005 28	a6c	free crystal	core	44,92	2,16	7,74	17,50	0,30	11,87	11,22	2,12	0,793	98,62	63,3
2005 28	a6r	free crystal	rim	45,45	2,03	7,44	17,41	0,29	11,99	11,17	1,89	0,781	98,45	64,4
2005 28	a7c	free crystal	core	42,61	1,54	8,46	17,95	0,35	14,07	9,20	2,54	0,71	97,43	64
2005 28	a7r	free crystal	rim	44,54	2,20	7,75	17,76	0,36	11,77	11,24	2,08	0,645	98,35	64
2005 28	a8cT	free crystal	core	45,00	2,20	7,81	17,68	0,34	12,05	11,41	1,77	0,807	99,07	65,6
2005 28	a8rT	free crystal	rim	44,46	2,52	8,06	17,61	0,31	11,60	11,41	2,10	0,708	98,78	61,6
Sample 2006 110														
2006 110	110a1c	free crystal	core	47,16	1,35	6,48	16,98	0,57	12,27	10,72	1,63	0,456	97,61	68,7
2006 110	110a1r	free crystal	rim	47,44	1,26	5,96	16,51	0,47	12,63	10,81	1,53	0,44	97,04	69,6
2006 110	a2cT	free crystal	core	45,54	1,50	6,98	17,14	0,44	12,19	10,63	1,59	0,668	96,68	70,6
2006 110	a2r	free crystal	rim	41,79	3,05	10,09	17,44	0,45	10,68	10,70	2,40	0,592	97,20	63
2006 110	a3c	free crystal	core	42,96	2,55	9,19	17,54	0,40	10,90	11,01	2,09	0,939	97,57	61,2
2006 110	a3r	free crystal	rim	43,33	2,62	9,14	16,43	0,37	11,45	11,20	2,06	0,804	97,40	63,1
2006 110	a4c	free crystal	core	42,34	3,03	10,20	15,48	0,39	11,70	11,13	2,39	0,61	97,27	65,7
2006 110	a4r	free crystal	rim	42,97	2,44	9,70	16,36	0,40	11,53	10,76	2,13	0,606	96,90	67,8
2006 110	a5c	free crystal	core	49,15	0,92	4,34	12,98	0,48	13,11	17,62	0,68	0	99,28	78,5
2006 110	a5r	free crystal	rim	50,77	0,63	2,72	11,15	0,49	13,67	19,61	0,46	0,007	99,50	86
2006 110	a6c	free crystal	core	46,62	1,73	6,95	17,05	0,44	12,39	10,75	1,59	0,691	98,19	69,7
2006 110	a6r	free crystal	rim	46,99	1,41	6,25	17,42	0,49	12,31	10,74	1,58	0,567	97,74	68,9

Table B.1Continued

Amphibole														
Sample 2005 52	Crystal type	Analysis location	SiO₂	TiO₂	Al₂O₃	FeO	MnO	MgO	CaO	Na₂O	K₂O	Total	mg #	
2005 52	a1c	free crystal	core	45,96	1,28	6,51	20,15	0,98	9,65	10,81	1,48	0,614	97,43	54,8
2005 52	amp1r	free crystal	rim	43,40	1,69	8,24	21,22	0,93	8,51	10,90	1,62	0,938	97,44	49,8
2005 52	amp2c	free crystal	core	43,61	1,53	8,28	21,22	0,98	8,40	10,99	1,63	0,951	97,58	48,6
2005 52	amp3c	free crystal	core	40,83	1,97	8,55	20,44	0,88	8,62	10,99	1,87	0,767	94,93	51,4
2005 52	amp3r	free crystal	rim	43,51	1,75	8,33	20,09	0,75	9,20	11,03	1,65	0,936	97,24	52,7
2005 52	amp4cT	free crystal	core	45,30	2,15	8,07	15,56	0,45	12,51	11,12	1,92	0,62	97,70	68,5
2005 52	amp4rT	free crystal	rim	44,25	1,49	8,11	19,15	0,67	10,14	10,97	1,70	0,87	97,34	58,0

Table B.1Continued

Biotite

Sample 2007 4		Crystal type	Analysis location	SiO₂	TiO₂	Al₂O₃	FeO	MnO	MgO	CaO	Na₂O	K₂O	Total	mg #
2007 4	bi1c	free crystal	core	36,61	5,08	13,16	20,20	0,17	11,95	0,02	0,67	8,61	96,46	51,3
2007 4	bi1r	free crystal	rim	36,99	4,89	13,21	19,36	0,15	12,37	0,03	0,77	8,67	96,44	53,2
2007 4	bi2c	free crystal	core	36,95	4,99	13,02	19,19	0,16	12,44	0,08	0,83	8,38	96,04	53,6
2007 4	bi2r	free crystal	rim	37,16	5,00	13,35	18,63	0,10	12,76	0,02	0,80	8,26	96,07	55,0
Sample 2005 69														
2005 69	bio1c	free crystal	core	33,41	4,80	14,03	30,02	0,19	4,26	0,02	0,56	8,59	95,89	20,2
2005 69	bio1r	free crystal	rim	33,31	5,19	13,71	30,99	0,25	4,36	0,03	0,42	8,09	96,35	20,1
2005 69	bio2c	free crystal	core	33,70	4,90	13,78	29,61	0,18	4,54	0,02	0,52	8,70	95,96	21,5
2005 69	bio2r	free crystal	rim	33,78	4,95	14,23	29,23	0,21	4,48	0,03	0,48	8,52	95,92	21,4
2005 69	bio3c	free crystal	core	33,49	4,81	14,48	30,08	0,24	3,36	0,04	0,47	8,42	95,40	16,6
2005 69	biok	inclusion	core	31,70	4,71	14,22	30,78	0,24	3,32	0,02	0,54	8,64	94,16	16,1
Sample 2005 52														
2005 52	52bio1c	free crystal	core	36,19	4,40	13,13	23,57	0,44	9,22	0,04	0,36	8,38	95,71	41,1
2005 52	52bio1r	free crystal	rim	35,42	4,45	13,24	23,94	0,48	9,01	0,02	0,32	8,51	95,38	40,2
2005 52	bio2c	free crystal	core	35,48	3,20	13,76	23,42	0,58	9,30	0,01	0,52	8,21	94,48	41,5
2005 52	bio2r	free crystal	rim	34,57	3,61	14,01	25,43	0,60	7,80	0,02	0,50	8,27	94,81	35,4
2005 52	bio3c	free crystal	core	35,73	4,47	12,80	23,77	0,52	9,11	0,00	0,36	8,38	95,15	40,6
2005 52	bio3r	free crystal	rim	35,71	4,62	13,43	23,63	0,48	8,79	0,03	0,44	8,46	95,60	39,9
2005 52	bio4mic	microlite	core	34,64	3,52	14,05	24,75	0,58	8,04	0,02	0,52	8,25	94,38	36,7
2005 52	bio6mic	microlite	core	35,15	3,00	13,56	22,76	0,50	9,65	0,01	0,39	8,56	93,58	43,0

Table B.1Continued**Biotite**

Sample	2005 75	Crystal type	Analysis location	SiO₂	TiO₂	Al₂O₃	FeO	MnO	MgO	CaO	Na₂O	K₂O	Total	mg #
2005 75	5_75bio1c	free crystal	core	33,10	3,08	14,50	34,46	0,58	1,92	0,02	0,50	8,14	96,31	9,1
2005 75	5_75bio1r	free crystal	rim	33,05	2,80	14,52	34,32	0,55	1,82	0,03	0,47	8,13	95,68	8,7
2005 75	bio2c	free crystal	core	32,79	2,30	14,92	35,20	0,64	1,57	0,01	0,42	8,24	96,09	7,4
2005 75	bio2r	free crystal	rim	32,47	2,08	15,26	35,13	0,73	1,65	0,00	0,52	8,22	96,06	7,7
2005 75	bio3c	free crystal	core	33,15	2,50	14,67	34,88	0,71	1,68	0,00	0,38	8,23	96,22	7,9
2005 75	bio3r	free crystal	rim	33,51	2,58	15,75	33,20	0,64	1,59	0,03	0,27	8,03	95,61	7,9
2005 75	bio4r	free crystal	rim	32,22	2,19	14,96	34,71	0,64	1,82	0,02	0,44	8,13	95,12	8,5
2005 75	bio5c	free crystal	core	32,55	2,33	14,96	34,80	0,65	1,75	0,01	0,42	8,24	95,71	8,2
2005 75	bio5r	free crystal	rim	32,20	2,41	14,75	34,45	0,64	1,77	0,03	0,38	8,22	94,86	8,4
2005 75	biomic	microlite	core	32,27	2,36	14,53	34,35	0,66	1,64	0,04	0,38	8,07	94,31	7,8

Table B.1Continued
Fe-Ti Oxides

Sample	2006 99	Crystal type	Analysis location	SiO₂	TiO₂	Al₂O₃	FeO (T)	MnO	MgO	Cr₂O₃	Total	X Usp	X Ilm
2006 99	mag3T	microlite	core	0,09	14,15	0,88	76,18	0,27	0,87	0,37	92,80	0,426	
2006 99	mag 1	microlite	core	0,07	17,93	0,30	71,53	0,65	1,06	0,08	91,61	0,529	
2006 99	il3T	microlite	core	0,01	48,61	0,03	43,73	0,84	2,95	0,07	96,23		0,930
2006 99	il 1	microlite	core	0,03	48,60	0,07	44,27	0,58	3,10	0,04	96,70		0,924
2006 99	il 2	microlite	core	0,04	48,28	0,04	44,03	0,54	3,11	0,05	96,09		0,923
2006 99	il 3	microlite	core	0,02	47,70	0,08	44,24	0,55	3,04	0,05	95,67		0,916
Sample 2006 112													
2006 112	mag 1	microlite	core	1,18	23,86	0,99	59,82	0,33	0,77	0,60	87,57	0,835	
2006 112	mag2	microlite	core	0,24	1,87	1,46	86,74	0,18	0,72	0,23	91,44	0,568	
2006 112	il1	microlite	core	0,20	46,28	0,29	43,04	0,19	0,33	0,26	90,59		0,977
2006 112	il2	microlite	core	0,07	47,88	0,14	43,54	0,53	1,70	0,02	93,87		0,950
2006 112	il3T	microlite	core	0,02	47,70	0,08	44,24	0,55	3,04	0,05	95,67		0,916
Sample 2005 68													
2005 68	mag3T	microlite	core	0,17	22,93	1,80	68,34	0,51	1,65	0,10	95,49	0,694	
2005 68	mag4T	microlite	core	0,13	22,03	1,94	68,41	0,60	1,38	0,09	94,58	0,677	
2005 68	mag6T	microlite	core	0,09	21,79	1,94	69,06	0,63	1,76	0,15	95,43	0,659	
2005 68	il1T	microlite	core	0,04	47,36	0,18	46,39	0,59	2,39	0,03	96,98		0,903
2005 68	il2T	microlite	core	0,12	46,18	0,19	46,27	0,60	1,98	0,03	95,37		0,899
2005 68	il4T	microlite	core	0,11	47,20	0,19	46,38	0,59	2,39	0,04	96,90		0,902
Sample 2006 77													
2006 77	mag1	microlite	core	0,47	20,57	1,99	70,10	0,62	1,69	0,10	95,54	0,627	95,54
2006 77	mag2	microlite	core	0,11	20,74	1,87	71,25	0,55	0,01	0,09	94,62	0,653	94,62
2006 77	mag3	microlite	core	0,04	20,99	1,89	71,78	0,63	0,00	0,04	95,37	0,693	95,37
2006 77	mag4	microlite	core	0,14	19,68	1,64	69,26	0,61	1,47	0,02	92,83	0,653	92,83

Table B.1Continued

Fe-Ti Oxides

Sample 2006 77	Crystal type	Analysis location	SiO₂	TiO₂	Al₂O₃	FeO (T)	MnO	MgO	Cr₂O₃	Total	X Usp	X Ilm	
2006 77	mag5	microlite	core	0,09	22,47	1,68	69,95	0,64	1,81	0,05	96,68	0,658	96,68
2006 77	mag6	microlite	core	0,10	22,30	1,69	69,42	0,66	1,86	0,03	96,05	0,661	96,05
2006 77	mag 7	microlite	core	0,09	22,51	1,69	69,26	0,66	1,78	0,05	96,05	0,668	96,05
Sample 2006 6													
2006 6	mag1	microlite	core	0,06	12,77	1,27	78,55	0,18	0,39	0,06	93,28	0,389	
2006 6	mag2	microlite	core	0,06	8,21	1,08	82,43	0,39	0,43	0,05	92,65	0,245	
2006 6	mag3	microlite	core	0,08	20,72	0,85	69,84	0,58	0,71	0,05	92,81	0,628	
2006 6	il1	microlite	core	0,03	46,75	0,04	46,30	0,83	1,23	0,01	95,18		0,917
2006 6	il3	microlite	core	0,05	46,13	0,05	47,85	0,69	0,95	0,01	95,73		0,903
2006 6	il4	microlite	core	0,03	46,30	0,05	48,03	0,65	0,91	0,02	96,00		0,891
2006 6	il5	microlite	core	0,02	46,19	0,05	48,45	0,58	1,38	0,02	96,70		0,888
2006 6	il6	microlite	core	0,00	46,29	0,08	48,03	0,51	1,60	0,03	96,53		0,891
Sample 2006 8													
2006 8	mag1	microlite	core	0,10	18,05	1,26	74,16	0,73	0,79	0,02	95,11	0,594	
2006 8	mag1	microlite	core	0,07	19,43	2,40	70,61	0,56	1,33	0,05	94,44	0,604	
2006 8	mag2	microlite	core	0,06	18,11	1,30	73,41	0,70	1,23	0,04	94,85	0,534	
2006 8	mag2	microlite	core	0,09	19,16	1,52	72,51	0,65	0,92	0,03	94,88	0,577	
2006 8	mag4T	microlite	core	0,11	12,10	1,62	80,00	0,40	0,44	0,01	94,68	0,365	
2006 8	magcl1	microlite	core	0,10	19,85	1,56	72,16	0,69	1,07	0,03	95,47	0,594	
2006 8	magcl2	microlite	core	0,11	19,37	1,46	72,69	0,69	1,02	0,03	95,38	0,578	
2006 8	il1	microlite	core	0,01	47,59	0,11	46,51	0,87	1,50	0,00	96,60		0,918
2006 8	il2	microlite	core	0,03	47,29	0,11	46,19	0,91	1,52	0,00	96,06		0,917
2006 8	il3T	microlite	core	0,00	47,48	0,06	46,12	0,95	1,59	0,00	96,20		0,917
2006 8	ilcl1	microlite	core	0,02	47,76	0,12	46,04	0,82	1,61	0,00	96,37		0,923
2006 8	ilcl2	microlite	core	0,01	47,72	0,15	45,92	0,93	1,73	0,00	96,45		0,920

Table B.1Continued
Fe-Ti Oxides

Sample 2006 86		Crystal type	Analysis location	SiO₂	TiO₂	Al₂O₃	FeO (T)	MnO	MgO	Cr₂O₃	Total	X Usp	X Ilm
2006 86	mag1	microlite	core	0,09	18,68	2,25	72,92	0,56	2,11	0,03	96,65	0,550	
2006 86	clmag1	microlite	core	0,09	17,44	2,86	71,79	0,53	2,34	0,04	95,09	0,530	
2006 86	mag2T	microlite	core	0,08	18,85	2,27	71,10	0,57	2,25	0,06	95,18	0,564	
2006 86	mag3T	microlite	core	0,08	19,81	2,13	71,62	0,56	2,18	0,06	96,43	0,584	
2006 86	cli1	microlite	core	0,04	46,45	0,31	46,97	0,56	2,99	0,03	97,36		0,875
2006 86	il1	microlite	core	0,01	48,37	0,25	45,62	0,59	3,55	0,00	98,40		0,898
2006 86	il2T	microlite	core	0,02	47,82	0,21	45,81	0,63	3,08	0,00	97,57		0,899
2006 86	il3T	microlite	core	0,02	48,01	0,20	45,83	0,57	3,05	0,01	97,69		0,902
Sample 2008 4													
2008 4	mag1	microlite	core	0,08	14,67	1,82	78,99	0,53	1,14	0,05	97,28	0,427	
2008 4	mag2	microlite	core	0,10	15,06	1,72	78,87	0,52	1,00	0,02	97,30	0,439	
2008 4	mag3	microlite	core	0,10	14,30	1,65	77,78	0,50	1,01	0,03	95,37	0,422	
2008 4	mag4	microlite	core	0,77	14,75	1,82	78,53	0,50	1,24	0,01	97,61	0,436	
2008 4	mag5	microlite	core	0,13	18,30	1,52	74,96	0,54	0,77	0,03	96,24	0,544	
2008 4	il1	microlite	core	0,00	47,42	0,15	48,34	0,70	2,27	0,00	98,89		0,884
2008 4	il2	microlite	core	0,00	49,84	0,12	48,36	0,75	1,91	0,00	100,98		0,917
2008 4	il3	microlite	core	0,03	49,73	0,14	48,11	0,74	2,17	0,03	100,96		0,912
2008 4	il4T	microlite	core	0,05	49,56	0,12	48,35	0,71	1,84	0,01	100,65		0,917
2008 4	il5T	microlite	core	0,05	49,78	0,12	47,60	0,66	2,29	0,01	100,51		0,917
Sample 2005 10													
2005 10	mag1	microlite	core	0,12	18,92	1,91	75,18	0,60	1,38	0,02	98,13	0,551	
2005 10	mag 2	microlite	core	0,10	18,96	2,43	74,51	0,58	1,62	0,04	98,24	0,560	
2005 10	mag 3	microlite	core	0,11	18,32	1,89	75,46	0,64	1,32	0,05	97,80	0,535	
2005 10	magcl2T	microlite	core	0,11	20,69	1,29	74,64	0,57	1,47	0,00	98,76	0,586	
2005 10	mag4T	microlite	core	0,13	20,78	1,28	73,86	0,77	1,29	0,01	98,12	0,595	

Table B.1Continued
Fe-Ti Oxides

Sample 2005 10		Crystal type	Analysis location	SiO₂	TiO₂	Al₂O₃	FeO (T)	MnO	MgO	Cr₂O₃	Total	X Usp	X Ilm
2005 10	mag5T	microlite	core	0,12	20,68	1,32	74,07	0,66	1,32	0,05	98,22	0,592	
2005 10	il2T	microlite	core	0,01	48,86	0,17	47,55	0,80	2,16	0,00	99,54		0,909
2005 10	il3T	microlite	core	0,06	49,98	0,10	47,61	0,80	2,06	0,00	100,62		0,923
2005 10	ilcl2T	microlite	core	0,01	49,86	0,14	47,72	0,69	2,27	0,00	100,69		0,917
2005 10	il1	microlite	core	0,00	50,09	0,19	47,31	0,71	2,25	0,02	100,57		0,917
Sample 200 7 4													
2007 4	mag1	microlite	core	0,10	11,78	1,61	81,76	0,52	0,95	0,04	96,75	0,341	
2007 4	mag2	microlite	core	0,06	11,17	1,52	82,72	0,53	0,80	0,07	96,88	0,320	
2007 4	mag3T	microlite	core	0,09	11,31	1,51	83,02	0,52	0,77	0,04	97,25	0,325	
2007 4	mag4T	microlite	core	0,12	11,21	1,48	82,89	0,47	0,78	0,05	97,01	0,324	
2007 4	mag5T	microlite	core	0,05	12,37	1,70	82,07	0,52	0,99	0,03	97,72	0,355	
2007 4	il1	microlite	core	0,00	46,74	0,11	49,07	0,76	1,82	0,00	98,49		0,878
2007 4	il2T	microlite	core	0,02	48,10	0,10	49,65	0,81	1,64	0,00	100,33		0,890
2007 4	il3T	microlite	core	0,05	47,72	0,15	49,71	0,85	1,66	0,03	100,16		0,885
2007 4	il4T	microlite	core	0,02	47,95	0,12	49,62	0,72	1,90	0,02	100,35		0,885
Sample 2005 28													
2005 28	il1	microlite	core	0,04	49,04	0,04	47,39	1,25	2,30	0,00	100,07		0,902
2005 28	il2T	microlite	core	0,02	47,30	0,12	50,27	0,77	1,51	0,02	100,01		0,880
2005 28	mg1	microlite	core	0,06	9,43	1,38	84,02	0,57	0,84	0,04	96,34	0,270	
2005 28	mg2T	microlite	core	0,06	8,91	1,54	84,90	0,62	0,73	0,04	96,81	0,340	
2005 28	mg3	microlite	core	0,08	11,86	1,29	82,35	0,48	0,78	0,03	96,86	0,340	
2005 28	mg4	microlite	core	0,07	11,34	1,39	82,54	0,45	0,78	0,07	96,64	0,320	

Table B.1Continued

Fe-Ti Oxides

Sample		Crystal type	Analysis location	SiO₂	TiO₂	Al₂O₃	FeO (T)	MnO	MgO	Cr₂O₃	Total	X Usp	X Ilm
2006 110	mag2T	microlite	core	0,08	13,57	1,85	77,37	0,56	1,13	0,04	94,59	0,405	
2006 110	mag3T	microlite	core	0,14	11,61	1,57	79,07	0,62	0,88	0,04	93,94	0,347	
2006 110	il1T	microlite	core	0,01	48,44	0,16	47,24	0,87	1,95	0,00	98,67		0,911
2006 110	il2T	microlite	core	0,04	47,91	0,14	47,09	0,82	2,08	0,00	98,09		0,903
2006 110	il3T	microlite	core	0,06	45,57	0,12	48,35	0,95	1,85	0,00	96,90		0,870
Sample 2005 69													
2005 69	il1	microlite	core	0,05	43,98	0,02	52,07	0,72	0,33	0,02	97,19		0,849
2005 69	il2	microlite	core	0,02	43,97	0,31	51,29	0,44	0,26	0,00	96,29		0,859
2005 69	il3	microlite	core	0,01	44,14	0,22	50,45	0,78	0,39	0,03	96,02		0,864
Sample 2005 52													
2005 52	mag2	microlite	core	0,05	4,79	1,23	86,17	1,07	0,21	0,03	93,55	0,140	
2005 52	mag3	microlite	core	0,05	5,11	1,45	84,92	1,13	0,20	0,03	92,90	0,152	
2005 52	il1T	microlite	core	0,07	47,14	0,08	49,11	2,21	0,59	0,01	99,21		0,889
2005 52	il2	microlite	core	0,03	44,40	0,11	48,96	2,68	0,66	0,04	96,87		0,854
2005 52	il3	microlite	core	0,02	45,14	0,08	48,62	1,89	0,65	0,00	96,40		0,874

Table C.1 Electron microprobe analyses of melt inclusions and matrix glasses.

Sample 2005 68 Melt inclusions															
	Host	SiO₂	TiO₂	Al₂O₃	FeO	MnO	MgO	CaO	Na₂O	K₂O	P₂O₅	SO₂	Cl	H₂O	Total
pl3	pl	71,10	1,06	12,90	1,98	0,05	0,30	0,56	5,10	2,75	0,36	0,12	0,05	3,68	100,00
pl5	pl	68,86	0,95	13,28	2,54	0,02	0,06	1,04	5,45	2,72	0,59	0,04	0,06	4,40	100,00
pl6	pl	66,02	0,15	19,71	1,29	0,04	0,05	3,40	2,22	6,99	0,04	0,00	0,02	0,04	99,96
pl7	pl	66,16	3,09	11,06	5,51	0,20	0,22	1,90	4,49	2,42	1,23	0,09	0,03	3,61	100,00
ol1	ol	67,96	1,11	16,30	2,51	0,00	0,23	2,21	2,97	6,68	0,41	0,00	0,07	0,00	100,46
ol2	ol	59,51	1,21	19,67	4,19	0,05	0,78	3,90	2,77	5,25	0,29	0,04	0,04	2,30	100,00
ol3	ol	63,21	1,55	14,94	4,69	0,10	1,85	1,29	5,17	4,97	0,42	0,04	0,02	1,73	100,00
ol3b	ol	67,76	0,74	16,63	1,51	0,06	0,13	1,54	5,79	4,60	0,34	0,01	0,02	0,87	100,00
ol4	ol	68,77	1,24	13,94	2,58	0,02	0,11	0,64	5,56	3,58	0,28	0,02	0,07	3,19	100,00
ol4b	ol	68,48	1,16	14,48	2,17	0,10	0,08	0,52	5,41	3,61	0,27	0,00	0,05	3,66	99,99
ol4c	ol	68,20	1,24	13,99	2,81	0,00	0,16	0,77	5,64	3,91	0,38	0,02	0,03	2,82	99,96
ol6	ol	66,06	0,88	16,51	2,73	0,07	0,41	2,23	3,71	6,27	0,46	0,05	0,05	0,58	100,00
ol7	ol	67,82	1,31	14,15	4,22	0,03	0,47	3,26	2,58	4,87	0,44	0,01	0,04	0,81	100,00
ol7b	ol	67,24	1,29	14,52	3,60	0,02	0,54	3,71	2,91	4,92	0,30	0,00	0,04	0,91	99,99
ol8	ol	64,31	1,38	15,05	4,62	0,06	0,72	4,71	2,52	5,59	0,54	0,03	0,05	0,42	100,00
ol8b	ol	64,53	1,00	14,81	4,76	0,04	0,62	4,27	2,32	6,19	0,52	0,03	0,18	0,73	100,00

(H₂O is estimated assuming that the missing element is H. H₂O is then included in the PAP electron microprobe data correction routine)

Table C.1 Continued

Sample 2005 68 Melt inclusions

	Host	SiO ₂	TiO ₂	Al ₂ O ₃	FeO	MnO	MgO	CaO	Na ₂ O	K ₂ O	P ₂ O ₅	SO ₂	Cl	H ₂ O	Total
	G37	68,43	1,26	14,43	2,78	0,12	0,19	1,20	5,32	4,25	0,23	0,05	0,04	1,70	100,00
	G38	65,19	2,01	13,34	6,48	0,14	0,29	1,88	4,44	4,36	0,68	0,01	0,08	1,09	100,00
	G39	59,09	2,36	9,02	10,96	0,25	1,53	6,11	2,40	3,59	0,38	0,04	0,05	4,22	100,00
	G40	64,16	1,18	12,11	6,41	0,17	0,80	2,80	2,97	4,82	0,31	0,02	0,08	4,19	100,00
	G43	68,35	0,85	14,58	2,97	0,07	0,19	1,11	6,31	3,81	0,32	0,02	0,03	1,38	100,00
	G46	67,90	0,79	16,83	2,34	0,09	0,12	1,52	6,37	3,79	0,13	0,02	0,03	0,07	100,00
	G47	68,71	0,53	14,85	1,52	0,00	0,03	0,39	4,16	5,66	0,20	0,01	0,03	3,89	99,99
	G48	65,97	1,03	17,49	1,88	0,06	0,19	1,62	6,41	3,77	0,24	0,05	0,02	1,28	100,00
	G49	66,77	1,31	15,10	3,81	0,07	0,19	1,86	5,47	3,73	0,47	0,00	0,03	1,18	99,99
	G50	68,58	1,22	14,22	3,50	0,00	0,11	1,21	5,10	4,36	0,42	0,00	0,04	1,21	99,99
	G52	67,14	0,53	16,72	1,63	0,05	0,10	1,54	6,21	3,78	0,13	0,00	0,02	2,15	100,00
	G54	68,81	0,70	15,31	1,81	0,02	0,24	1,30	5,04	4,94	0,34	0,01	0,01	1,48	100,00
	G55	66,75	1,59	13,92	4,54	0,09	0,29	1,37	4,79	4,32	0,36	0,03	0,05	1,90	100,00
	G57	66,07	1,76	13,19	4,07	0,04	0,08	1,34	3,64	5,30	0,60	0,05	0,05	3,81	100,00
	G58	64,61	1,38	13,35	5,99	0,13	0,56	1,92	4,83	3,79	0,51	0,05	0,05	2,84	100,00
	G59	65,28	1,84	11,77	6,98	0,18	0,62	2,10	2,94	4,74	0,41	0,09	0,07	2,97	100,00
	G60	68,40	0,97	14,40	3,01	0,10	0,22	1,24	4,81	4,57	0,41	0,03	0,01	1,84	100,00
	G61	67,05	1,46	13,91	4,05	0,07	0,37	1,59	5,08	4,39	0,54	0,04	0,07	1,38	100,00
	G62	66,97	1,57	14,91	3,53	0,06	0,27	1,46	6,50	3,25	0,60	0,01	0,04	0,84	100,00
	G63	64,64	1,86	14,11	6,19	0,15	0,38	2,43	5,13	3,97	1,05	0,04	0,04	0,03	100,00

Table C.1 Continued

Sample 2006 1 Melt inclusions

	Host	SiO ₂	TiO ₂	Al ₂ O ₃	FeO	MnO	MgO	CaO	Na ₂ O	K ₂ O	P ₂ O ₅	SO ₂	Cl	H ₂ O	Total
6_1	ol	69,28	1,17	15,86	1,29	0,06	0,06	0,33	3,67	6,34	0,09	0,01	0,03	1,78	100,00
6_2	ol	69,15	0,79	15,26	1,30	0,02	0,05	0,31	4,13	6,32	0,06	0,00	0,03	2,58	100,00
6_3	ol	70,87	0,83	16,84	1,40	0,09	0,29	0,46	1,47	5,44	0,24	0,01	0,04	2,01	100,00
6_6	ol	66,66	0,55	17,00	1,64	0,00	0,15	1,03	5,62	6,24	0,58	0,00	0,03	0,49	99,99
6_8	ol	70,42	0,69	16,44	1,42	0,00	0,09	0,97	4,24	4,46	0,38	0,00	0,03	0,83	99,97
6_9	ol	69,97	0,84	16,13	1,18	0,03	0,07	0,46	2,50	6,05	0,29	0,00	0,03	2,44	99,99
6_10	ol	70,53	1,06	16,54	1,36	0,06	0,06	0,47	1,54	5,44	0,19	0,00	0,03	2,73	100,00
6_11	ol	72,07	0,72	15,81	1,26	0,05	0,14	0,46	1,24	5,18	0,29	0,00	0,05	2,74	100,00
6_11	ol	63,00	1,21	15,33	2,12	0,06	0,74	2,68	2,96	5,36	0,23	0,02	0,04	6,25	100,00
6_12	ol	63,07	1,37	15,25	1,21	0,00	0,05	0,82	4,99	5,98	0,36	0,05	0,06	6,74	99,93

Sample 2006 112 Melt inclusions

112_1	ol	64,26	0,29	16,69	3,58	0,07	1,41	2,31	6,64	3,33	0,05	0,05	0,06	1,26	100,00
112_5	ol	65,00	0,18	18,89	1,07	0,02	0,02	0,66	5,69	8,00	0,06	0,02	0,09	0,33	100,00
112_6	ol	65,14	0,14	18,47	1,00	0,00	0,00	0,50	5,34	8,83	0,04	0,01	0,13	0,34	99,93
112_7	ol	66,44	0,10	19,26	1,21	0,00	0,01	0,70	6,11	7,28	0,03	0,00	0,00	0,00	101,14
112_8	ol	63,61	0,75	18,50	2,04	0,00	0,56	3,19	6,80	3,52	0,19	0,01	0,10	0,71	99,98
112_9	ol	65,62	0,53	20,48	1,26	0,00	0,15	0,92	6,78	3,91	0,49	0,05	0,10	0,00	100,29
112_10	ol	65,66	0,51	20,02	1,24	0,02	0,19	0,90	7,10	4,03	0,25	0,00	0,08	0,00	99,99
112_11	ol	65,74	0,48	19,63	1,36	0,06	0,20	1,08	6,91	4,00	0,33	0,07	0,06	0,09	100,00
112_12	ol	64,53	0,60	20,46	1,43	0,00	0,27	1,67	6,66	3,62	0,58	0,01	0,05	0,08	99,96
112_13	ol	64,87	0,61	20,63	1,48	0,05	0,30	1,72	6,64	3,54	0,58	0,00	0,06	0,00	100,48
112_14	ol	64,80	0,61	20,71	1,45	0,05	0,32	1,73	6,84	3,55	0,54	0,01	0,05	0,00	100,66

Table C.1 Continued

Sample 2006 76 Melt inclusions															
	Host	SiO₂	TiO₂	Al₂O₃	FeO	MnO	MgO	CaO	Na₂O	K₂O	P₂O₅	SO₂	Cl	H₂O	Total
76_1	ol	67,79	1,12	16,92	1,48	0,06	0,17	1,24	5,42	4,38	0,42	0,00	0,03	0,95	99,98
76_2	ol	69,62	0,78	17,03	1,56	0,04	0,41	0,38	1,71	4,82	0,15	0,00	0,05	3,45	99,99
76_3	ol	69,30	0,59	17,97	1,37	0,05	0,07	0,82	2,20	5,19	0,28	0,00	0,03	2,13	100,00
76_4	ol	68,07	0,84	17,66	1,35	0,00	0,08	0,70	5,16	5,98	0,22	0,00	0,06	0,00	100,11
76_5	ol	61,48	0,83	17,06	1,40	0,00	0,30	0,42	4,42	6,12	0,42	0,00	0,06	7,46	99,98
76_6	ol	67,74	1,14	15,51	2,09	0,05	0,35	1,44	5,09	4,91	0,37	0,02	0,01	1,26	100,00
76_7	ol	69,49	1,22	15,37	1,33	0,04	0,07	0,91	2,60	5,73	0,23	0,03	0,03	2,96	100,00
76_8	ol	67,60	0,49	17,62	1,90	0,06	0,51	1,35	6,59	3,08	0,35	0,00	0,05	0,41	100,00
76_9	ol	67,10	0,60	18,06	1,38	0,05	0,29	1,86	5,95	4,95	0,38	0,00	0,06	0,00	100,69
76_10	ol	65,61	0,71	15,90	3,13	0,06	1,44	1,74	5,49	3,57	0,52	0,01	0,01	1,80	100,00
76_111	ol	69,08	0,97	18,43	1,92	0,02	0,43	1,73	2,16	3,60	0,43	0,02	0,03	1,16	100,00
76_12	ol	66,56	0,77	16,88	1,25	0,03	0,10	0,86	2,81	5,77	0,56	0,04	0,04	4,33	100,00
76_113	ol	67,66	0,65	16,75	1,14	0,00	0,06	0,72	2,77	5,91	0,43	0,01	0,06	3,84	100,00
76_14	ol	65,83	0,82	13,85	4,25	0,11	0,89	0,79	0,71	4,75	0,64	0,01	0,05	7,31	100,00
76_16	ol	65,58	0,61	17,30	1,90	0,06	0,93	0,59	4,70	6,34	0,41	0,02	0,03	1,52	100,00
76_19	ol	61,96	0,70	20,69	2,04	0,00	0,44	2,93	6,01	3,10	0,51	0,03	0,05	1,55	99,99
76_20	ol	66,24	0,53	17,17	2,11	0,02	1,23	1,03	3,57	5,29	0,42	0,00	0,02	2,35	99,99
76_21	ol	66,51	1,17	16,91	1,59	0,04	0,07	1,04	5,26	6,41	0,53	0,00	0,05	0,41	99,99
76_22	ol	67,27	0,93	17,25	1,59	0,00	0,10	0,72	5,69	6,44	0,34	0,03	0,05	0,00	100,40
Sample 2006 130 Melt inclusions															
130_1	ol	69,71	0,65	16,32	0,01	0,00	0,02	0,35	2,06	6,11	0,12	0,00	0,03	4,58	99,96
130_2	ol	69,80	0,73	16,27	0,00	0,00	0,01	0,35	1,66	6,38	0,02	0,03	0,05	4,67	99,98
130_3	ol	69,51	0,52	16,05	0,00	0,00	0,03	0,34	1,61	6,40	0,02	0,00	0,03	5,46	99,96
130_6	ol	67,14	0,64	17,47	1,71	0,00	0,26	3,66	5,18	3,69	0,37	0,00	0,04	0,00	100,16
130_7	ol	63,81	2,83	15,77	2,23	0,08	0,14	0,33	4,79	5,86	0,26	0,01	0,04	3,85	100,00
130_10	ol	68,60	0,51	13,29	1,86	0,00	0,47	2,26	3,20	6,04	0,03	0,00	0,05	3,50	99,81

Table C.1 Continued**Sample 2006 77 Melt inclusions**

	Host	SiO₂	TiO₂	Al₂O₃	FeO	MnO	MgO	CaO	Na₂O	K₂O	P₂O₅	SO₂	Cl	H₂O	Total
6_77op1	opx	66,60	0,68	16,40	2,00	0,00	0,15	2,62	4,78	4,27	0,16	0,02	0,02	2,26	99,96
6_77op2	opx	64,78	1,04	17,87	2,94	0,02	0,33	2,56	4,58	3,98	0,81	0,04	0,01	1,04	100,00
ol1	ol	68,62	1,19	13,09	3,81	0,18	0,35	1,86	4,29	4,27	0,50	0,01	0,06	1,78	100,00
ol1b	ol	67,38	1,26	13,43	4,28	0,12	0,48	2,70	4,53	3,50	0,26	0,05	0,04	1,95	100,00
ol1c	ol	67,77	1,54	13,33	4,48	0,09	0,57	2,24	4,78	3,38	0,40	0,01	0,05	1,39	100,00
ol2	ol	68,12	0,68	12,14	5,61	0,16	0,40	1,47	3,90	4,62	0,13	0,03	0,03	2,70	100,00
ol2b	ol	68,90	1,14	11,93	5,76	0,14	0,49	1,40	3,51	5,11	0,04	0,00	0,05	1,52	99,99
ol2c	ol	65,74	0,91	16,53	2,80	0,00	0,42	3,41	4,04	3,39	0,33	0,00	0,05	2,36	99,97
ol3	ol	65,42	1,03	16,56	3,09	0,04	0,44	3,14	5,36	3,72	0,32	0,02	0,05	0,81	100,00
pl1	pl	65,05	0,68	16,23	3,24	0,04	0,41	3,42	4,04	3,54	0,33	0,00	0,03	2,99	100,00
pl1b	pl	64,52	0,95	18,03	3,12	0,10	0,24	2,87	5,58	3,88	0,42	0,08	0,12	0,10	100,00

Table C.1 Continued

Sample 2006 77 Matrix glasses

	Host	SiO ₂	TiO ₂	Al ₂ O ₃	FeO	MnO	MgO	CaO	Na ₂ O	K ₂ O	P ₂ O ₅	SO ₂	Cl	H ₂ O	Total
G95		68,16	0,94	13,24	5,05	0,23	0,42	1,54	4,95	4,27	0,11	0,00	0,02	1,05	100,00
G96		67,62	0,70	13,33	4,44	0,11	0,47	1,65	4,92	4,29	0,12	0,00	0,03	2,32	100,00
G97		67,83	0,93	13,44	5,59	0,12	0,51	1,47	4,45	4,48	0,11	0,05	0,04	0,99	100,00
G98		67,26	1,29	13,14	4,87	0,16	0,50	1,63	4,50	4,48	0,14	0,00	0,03	2,01	100,00
G99		67,91	0,76	12,95	4,77	0,10	0,45	1,46	4,29	4,81	0,18	0,00	0,03	2,27	99,99
G100		68,15	0,53	13,32	4,68	0,09	0,46	1,50	4,50	4,53	0,10	0,04	0,03	2,07	100,00
G101		68,05	0,68	12,01	5,24	0,03	0,49	1,61	4,03	4,83	0,12	0,03	0,03	2,86	100,00
G102		68,63	1,03	13,37	4,57	0,08	0,34	1,46	4,99	4,39	0,14	0,01	0,04	0,97	100,00
G103		68,34	0,79	13,54	5,21	0,07	0,46	1,67	4,55	4,15	0,08	0,00	0,02	1,10	99,99
G104		66,76	1,12	13,14	4,51	0,06	0,42	1,36	4,53	4,69	0,19	0,02	0,03	3,18	100,00
G105		67,10	0,79	13,34	4,79	0,15	0,42	1,43	4,85	4,35	0,13	0,00	0,01	2,62	100,00
G106		68,15	0,73	13,37	4,23	0,14	0,32	1,17	4,93	4,80	0,11	0,00	0,04	1,99	100,00
G107		67,60	0,79	13,28	4,94	0,10	0,50	1,59	4,58	4,57	0,11	0,01	0,03	1,90	100,00
G108		67,11	0,53	13,37	4,37	0,11	0,39	1,65	4,82	4,26	0,11	0,00	0,16	3,13	100,00
G110		67,49	0,82	13,42	5,27	0,02	0,52	1,67	5,01	4,04	0,11	0,00	0,02	1,62	99,99
G111		68,00	0,70	13,29	4,92	0,14	0,47	1,61	4,97	4,11	0,13	0,00	0,06	1,59	100,00
G112		68,32	0,82	12,84	4,84	0,12	0,45	1,36	4,90	4,29	0,16	0,00	0,02	1,88	100,00
G113		67,67	0,88	13,03	4,80	0,09	0,43	1,53	4,14	4,83	0,17	0,00	0,03	2,39	100,00
G114		66,78	0,97	12,86	5,04	0,08	0,47	1,39	4,19	4,87	0,15	0,00	0,04	3,15	100,00
G116		67,49	0,82	13,05	5,30	0,11	0,50	1,55	4,56	4,24	0,18	0,00	0,02	2,16	99,98
G117		67,92	0,91	12,86	4,94	0,12	0,52	1,61	4,83	4,14	0,14	0,02	0,05	1,95	100,00
G118		67,88	0,88	13,87	4,64	0,09	0,45	1,51	4,96	4,48	0,09	0,02	0,03	1,09	100,00
G119		67,91	0,70	13,23	5,30	0,14	0,35	1,55	4,79	4,27	0,13	0,02	0,03	1,57	100,00
G120		66,23	1,02	13,30	4,94	0,17	0,49	1,69	5,07	4,39	0,18	0,00	0,03	2,49	99,99

Table C.1 Continued

Sample 2006 86 Melt inclusions

	Host	SiO ₂	TiO ₂	Al ₂ O ₃	FeO	MnO	MgO	CaO	Na ₂ O	K ₂ O	P ₂ O ₅	SO ₂	Cl	H ₂ O	Total
op1	opx	70,57	0,00	14,82	1,55	0,06	0,19	1,31	5,41	2,92	0,21	0,01	0,01	2,90	99,94
op2	opx	70,87	0,54	14,94	1,67	0,03	0,09	1,60	4,31	2,86	0,46	0,02	0,02	2,60	100,00
op3	opx	66,83	1,37	14,82	3,53	0,04	0,30	0,21	7,07	4,51	0,12	0,02	0,03	1,14	100,00
op3b	opx	67,47	1,33	14,39	3,79	0,01	0,31	0,24	5,18	4,57	0,09	0,00	0,01	2,56	99,95
op4	opx	66,78	0,76	15,01	3,63	0,01	0,33	0,15	7,13	4,45	0,19	0,03	0,06	1,46	100,00
op4b	opx	68,53	0,45	15,02	2,82	0,00	0,30	0,14	5,06	4,46	0,19	0,00	0,04	2,95	99,95
op5	opx	68,76	0,47	14,89	3,63	0,16	0,28	0,24	6,60	4,34	0,28	0,05	0,00	0,28	100,00
op6	opx	68,59	1,48	14,21	3,75	0,09	0,25	0,16	4,56	4,70	0,09	0,00	0,03	2,08	99,99
pl1	pl	66,36	0,77	14,26	4,86	0,16	0,77	1,87	5,19	3,91	0,12	0,04	0,03	1,66	100,00
pl2	pl	68,37	0,56	13,23	4,78	0,08	0,85	1,45	5,59	3,50	0,10	0,01	0,05	1,43	100,00
pl2b	pl	68,61	0,74	12,69	4,21	0,12	0,75	1,28	5,28	4,18	0,14	0,00	0,06	1,96	99,99
pl3	pl	67,68	0,92	13,08	4,81	0,06	0,59	1,34	5,80	3,50	0,06	0,01	0,04	2,10	100,00
pl4	pl	68,69	0,59	13,58	4,17	0,08	0,72	1,01	5,14	4,59	0,11	0,01	0,05	1,26	100,00
pl5	pl	67,95	0,89	13,22	4,27	0,05	0,90	1,11	5,17	4,38	0,15	0,00	0,02	1,90	100,00
pl5b	pl	68,64	0,86	13,49	4,17	0,08	0,79	1,11	5,58	3,98	0,18	0,03	0,02	1,07	100,00
pl6	pl	68,17	0,95	13,89	4,11	0,06	0,66	1,12	5,54	4,07	0,06	0,05	0,00	1,32	100,00
pl6b	pl	69,09	0,56	13,39	4,30	0,11	0,76	1,19	5,65	3,86	0,10	0,00	0,03	0,92	99,96
pl7	pl	68,24	0,65	13,00	5,05	0,12	0,96	1,31	5,46	4,12	0,17	0,03	0,04	0,85	100,00
pl8	pl	68,71	0,47	13,68	4,14	0,15	0,67	0,90	5,32	4,39	0,15	0,02	0,04	1,35	100,00
pl9	pl	69,12	0,77	13,47	4,47	0,00	0,81	0,97	5,02	4,75	0,12	0,06	0,06	0,36	99,96
pl10	pl	68,55	0,74	13,23	4,32	0,01	0,75	0,94	4,93	4,80	0,06	0,03	0,05	1,59	100,00

Table C.1 Continued

Sample 2006 86 Matrix glasses

	Host	SiO ₂	TiO ₂	Al ₂ O ₃	FeO	MnO	MgO	CaO	Na ₂ O	K ₂ O	P ₂ O ₅	SO ₂	Cl	H ₂ O	Total
G3		70,48	1,20	13,32	3,63	0,05	0,33	0,82	4,06	5,06	0,24	0,00	0,05	0,75	99,99
G4		71,29	0,82	13,48	3,19	0,03	0,14	0,73	4,91	4,56	0,19	0,02	0,02	0,62	100,00
G7		70,78	1,41	13,04	3,93	0,04	0,21	0,92	5,19	3,55	0,17	0,00	0,04	0,72	99,99
G11		68,36	0,50	15,07	3,82	0,08	0,41	1,28	7,04	2,41	0,08	0,02	0,03	0,91	100,00
G15		71,96	0,82	13,29	2,93	0,03	0,12	0,69	3,66	4,88	0,24	0,00	0,05	1,32	99,99
G17		69,05	0,73	14,33	3,76	0,05	0,94	1,53	4,68	4,09	0,13	0,00	0,02	0,68	99,99
G18		70,66	0,94	13,51	3,18	0,00	0,15	0,71	4,08	4,53	0,23	0,00	0,06	1,92	99,97
G20		71,93	1,34	13,52	2,78	0,01	0,13	0,65	4,41	4,98	0,20	0,00	0,02	0,04	100,00
G21		68,20	0,97	12,40	4,17	0,14	0,73	0,99	3,61	5,05	0,16	0,01	0,05	3,53	100,00
G22		70,76	1,23	12,72	3,49	0,02	0,16	0,79	3,91	4,74	0,17	0,00	0,04	1,97	100,00
G23		71,95	1,31	13,48	3,25	0,16	0,15	0,74	5,01	3,97	0,17	0,00	0,03	0,00	100,22
G24		70,85	1,00	13,44	2,73	0,00	0,09	0,54	4,26	4,97	0,15	0,00	0,01	1,94	99,98
G25		71,43	1,32	13,57	2,85	0,08	0,18	0,68	4,03	5,08	0,17	0,01	0,02	0,58	100,00
G26		71,02	0,62	13,89	2,99	0,10	0,17	0,65	4,18	5,44	0,13	0,03	0,02	0,76	100,00
G27		70,79	0,41	13,70	2,54	0,07	0,26	0,82	4,18	5,38	0,24	0,00	0,03	1,56	99,99
G28		70,77	0,96	13,61	3,18	0,05	0,21	0,73	4,28	5,15	0,15	0,02	0,02	0,87	100,00
G29		72,00	1,02	12,92	2,81	0,04	0,07	0,53	4,12	5,01	0,21	0,02	0,03	1,23	100,00
G33		71,25	0,76	13,39	3,54	0,06	0,26	0,83	5,83	3,68	0,17	0,00	0,03	0,20	99,99

Table C.1 Continued

Sample 2005 10 Melt inclusions

	Host	SiO ₂	TiO ₂	Al ₂ O ₃	FeO	MnO	MgO	CaO	Na ₂ O	K ₂ O	P ₂ O ₅	SO ₂	Cl	H ₂ O	Total
op1	opx	69,46	0,57	14,91	1,53	0,02	0,05	0,47	3,49	5,41	0,02	0,02	0,05	4,00	100,00
op1b	opx	68,82	0,83	15,62	1,60	0,00	0,04	0,46	4,68	5,68	0,09	0,05	0,06	2,06	100,00
op2	opx	68,53	0,51	15,59	1,57	0,01	0,05	0,74	3,44	5,42	0,12	0,00	0,04	3,97	100,00
op3	opx	68,40	0,00	15,51	2,13	0,00	0,07	1,03	4,28	5,66	0,06	0,04	0,04	2,77	99,97
op4	opx	70,16	0,48	15,55	2,68	0,03	0,09	0,38	4,52	3,32	0,20	0,01	0,03	2,54	100,00
op5	opx	71,02	0,47	15,69	1,98	0,12	0,10	1,36	5,28	3,05	0,26	0,00	0,00	0,65	99,98
op6	opx	70,34	0,33	16,08	2,14	0,07	0,09	1,65	4,46	3,25	0,32	0,05	0,01	1,22	100,00
op7	opx	70,21	0,80	16,07	2,20	0,09	0,04	1,37	5,73	3,33	0,11	0,01	0,05	0,00	100,02
op8	opx	72,93	0,74	15,00	1,71	0,09	0,06	1,00	3,92	3,76	0,08	0,03	0,05	0,62	100,00
op10	opx	70,78	0,65	14,71	2,01	0,03	0,11	0,43	4,08	5,62	0,10	0,00	0,03	1,42	99,99
op11	opx	73,19	0,72	11,60	2,57	0,05	0,14	0,44	3,30	4,57	0,15	0,01	0,10	3,16	100,00
op12	opx	70,17	0,68	16,30	2,11	0,05	0,06	1,47	3,92	3,20	0,24	0,05	0,03	1,72	100,00
pl1	pl	74,41	0,39	13,00	2,10	0,00	0,12	0,43	4,17	4,90	0,08	0,03	0,07	0,24	99,94
pl1b	pl	73,81	0,56	12,49	2,09	0,05	0,18	0,41	4,33	5,04	0,10	0,02	0,03	0,89	100,00
pl1c	pl	72,67	0,65	12,32	3,84	0,07	0,21	0,82	4,26	4,73	0,10	0,02	0,04	0,26	100,00
pl2	pl	71,57	0,59	12,75	3,92	0,05	0,31	0,72	4,39	4,59	0,11	0,01	0,09	0,90	100,00
pl2b	pl	73,26	0,65	12,70	3,05	0,03	0,20	0,73	4,35	4,75	0,11	0,03	0,04	0,12	100,00
pl3	pl	71,03	0,60	12,15	3,64	0,14	0,33	1,04	5,05	3,90	0,08	0,01	0,07	1,96	100,00
pl4	pl	74,07	0,53	12,81	2,55	0,07	0,11	0,45	4,35	5,10	0,10	0,04	0,04	0,00	100,22
pl4b	pl	73,46	0,65	12,24	3,13	0,02	0,28	0,76	4,71	4,13	0,09	0,00	0,03	0,49	99,99
pl5	pl	71,00	0,68	12,09	4,36	0,00	0,44	0,83	4,53	4,61	0,24	0,02	0,07	1,14	100,00
pl6	pl	72,88	0,94	12,50	3,33	0,07	0,22	0,83	4,52	4,35	0,12	0,04	0,06	0,14	100,00
pl7	pl	73,28	0,47	12,38	3,41	0,11	0,30	1,01	4,76	3,85	0,10	0,00	0,03	0,29	100,00
pl7b	pl	71,90	0,77	12,51	3,59	0,10	0,34	0,85	4,74	4,47	0,14	0,02	0,08	0,51	100,00
pl8	pl	72,79	0,50	12,39	2,76	0,06	0,21	0,76	4,59	4,17	0,08	0,01	0,09	1,59	100,00
pl8b	pl	73,50	0,50	12,42	3,08	0,11	0,20	0,86	4,99	4,00	0,06	0,00	0,07	0,21	100,00

Table C.1 Continued

Sample 2005 10 Melt inclusions															
	Host	SiO₂	TiO₂	Al₂O₃	FeO	MnO	MgO	CaO	Na₂O	K₂O	P₂O₅	SO₂	Cl	H₂O	Total
pl9	pl	72,09	0,36	12,58	2,87	0,06	0,29	0,89	5,04	3,56	0,11	0,04	0,07	2,04	100,00
pl10	pl	73,53	0,39	12,47	2,92	0,07	0,22	0,68	4,38	4,29	0,09	0,01	0,02	0,92	100,00
pl11	pl	72,07	0,77	11,79	3,50	0,09	0,39	0,70	3,94	4,83	0,14	0,01	0,06	1,71	100,00
pl12	pl	71,54	0,39	12,25	3,57	0,11	0,37	0,71	4,72	4,01	0,14	0,01	0,04	2,14	100,00
pl12b	pl	71,96	0,44	12,50	3,71	0,10	0,38	0,79	4,52	4,34	0,14	0,04	0,05	1,03	100,00
Sample 2005 10 Matrix glasses															
G64		73,09	0,88	12,52	2,15	0,06	0,12	0,32	3,77	5,31	0,04	0,02	0,03	1,69	100,00
G65		74,18	0,41	12,39	2,27	0,09	0,12	0,32	4,51	4,27	0,02	0,02	0,03	1,37	100,00
G66		73,26	0,56	12,29	2,77	0,00	0,10	0,39	4,04	5,31	0,01	0,00	0,06	1,21	99,99
G67		72,26	0,77	12,13	1,99	0,06	0,07	0,30	3,67	5,43	0,04	0,01	0,04	3,24	100,00
G68		74,56	0,82	12,22	2,91	0,08	0,17	0,58	4,96	3,26	0,06	0,01	0,02	0,37	100,00
G69		72,33	0,27	12,35	1,99	0,04	0,06	0,37	3,14	5,58	0,03	0,00	0,06	3,77	99,99
G70		73,38	0,68	11,35	2,28	0,02	0,10	0,40	3,17	5,18	0,08	0,02	0,09	3,25	100,00
G71		73,52	0,24	12,46	2,66	0,02	0,13	0,41	4,02	5,12	0,08	0,00	0,05	1,28	99,98
G74		72,40	0,68	12,39	2,65	0,05	0,13	0,44	3,95	4,95	0,09	0,01	0,03	2,25	100,00
G75		73,19	0,65	12,19	2,36	0,05	0,06	0,42	4,66	5,02	0,10	0,00	0,13	1,16	99,99
G76		73,02	0,76	12,25	3,49	0,09	0,20	0,65	4,29	4,74	0,11	0,00	0,02	0,37	100,00
G78		73,16	0,79	12,47	2,54	0,06	0,07	0,43	4,04	5,24	0,06	0,03	0,07	1,03	100,00
G79		75,39	0,59	11,36	3,60	0,05	0,20	0,73	4,47	3,28	0,06	0,00	0,03	0,24	100,00
G80		73,28	0,53	11,65	1,64	0,10	0,04	0,32	3,54	5,72	0,05	0,01	0,07	3,04	100,00
G81		71,52	0,86	12,56	2,09	0,05	0,05	0,36	3,49	5,43	0,04	0,02	0,02	3,52	100,00
G82		73,43	0,65	12,85	2,51	0,05	0,10	0,85	4,88	3,35	0,10	0,01	0,02	1,20	100,00
G83		73,50	0,65	11,41	2,78	0,08	0,10	0,46	3,93	4,57	0,04	0,02	0,07	2,40	100,00
G84		74,51	0,85	12,35	2,30	0,00	0,08	0,30	4,16	5,09	0,08	0,03	0,03	0,17	99,95
G87		72,69	0,42	12,38	1,77	0,00	0,07	0,27	3,41	5,42	0,05	0,00	0,06	3,47	99,98
G88		73,01	0,80	12,00	1,91	0,10	0,06	0,28	4,02	5,19	0,03	0,02	0,05	2,55	100,00
G89		72,75	0,74	11,34	2,34	0,06	0,15	0,27	2,65	6,08	0,09	0,02	0,07	3,44	100,00
G90		71,43	0,50	11,97	2,64	0,02	0,14	0,53	3,83	5,13	0,04	0,03	0,06	3,68	100,00
G91		71,78	0,71	12,22	2,17	0,06	0,04	0,26	4,02	5,33	0,06	0,02	0,06	3,27	100,00

Table C.1 Continued

Sample 2005 28 Melt inclusions

	Host	SiO ₂	TiO ₂	Al ₂ O ₃	FeO	MnO	MgO	CaO	Na ₂ O	K ₂ O	P ₂ O ₅	SO ₂	Cl	H ₂ O	Total
a1	amp	77,42	0,15	12,85	1,32	0,01	0,18	0,70	1,65	3,93	0,00	0,02	0,06	1,70	99,99
a2	amp	77,10	0,27	13,21	1,17	0,07	0,14	0,75	1,81	4,01	0,00	0,00	0,07	1,39	99,98
a3	amp	77,16	0,18	12,93	1,36	0,09	0,14	0,82	1,51	4,16	0,03	0,00	0,06	1,53	99,99
a4	amp	76,82	0,12	12,42	1,28	0,00	0,20	0,70	1,83	4,16	0,00	0,02	0,07	2,39	99,99
a4b	amp	77,51	0,15	13,11	1,24	0,12	0,19	0,75	1,61	4,29	0,00	0,00	0,07	0,90	99,95
a5	amp	77,86	0,00	13,04	1,15	0,01	0,13	0,62	1,78	4,56	0,03	0,00	0,07	0,70	99,95
a5b	amp	78,39	0,24	12,76	1,32	0,00	0,13	0,63	1,46	4,66	0,00	0,00	0,07	0,27	99,93
a6	amp	77,99	0,00	13,01	1,07	0,05	0,07	0,51	1,44	4,27	0,00	0,00	0,05	1,51	99,96
a7	amp	73,63	0,12	12,29	0,76	0,00	0,02	0,58	2,12	4,67	0,00	0,00	0,05	5,68	99,93
cp1	cpx	74,29	0,09	12,22	0,70	0,03	0,02	0,57	2,36	4,10	0,01	0,00	0,04	5,58	99,99
cp1b	cpx	73,46	0,30	12,37	0,86	0,03	0,01	0,63	3,28	4,58	0,00	0,00	0,06	4,40	99,97
cp2	cpx	73,46	0,21	12,48	1,08	0,00	0,12	0,63	2,43	5,43	0,02	0,02	0,04	4,07	100,00
op1	opx	74,93	0,12	12,31	1,31	0,00	0,03	0,59	2,12	4,92	0,04	0,00	0,06	3,56	99,99
op2	opx	76,93	0,15	11,28	1,47	0,02	0,08	0,22	1,77	4,50	0,00	0,03	0,06	3,48	99,98
op3	opx	74,43	0,35	12,36	2,41	0,09	0,13	0,17	2,92	5,72	0,05	0,00	0,06	1,31	100,00
op3	opx	77,36	0,06	12,37	1,27	0,02	0,11	0,05	3,73	4,42	0,01	0,04	0,06	0,51	100,00
op4	opx	77,47	0,33	12,34	1,44	0,00	0,00	0,59	3,22	4,12	0,00	0,03	0,07	0,36	99,96
op4b	opx	76,41	0,00	12,00	1,27	0,06	0,05	0,64	3,58	4,03	0,00	0,00	0,08	1,76	99,87
op5	opx	76,12	0,00	11,97	1,25	0,06	0,05	0,63	3,10	3,82	0,01	0,00	0,07	2,88	99,96
op6	opx	75,32	0,09	11,68	1,24	0,01	0,07	0,79	3,87	3,56	0,00	0,00	0,06	3,29	99,98

Table C.1 Continued

Sample 2005 28 Matrix glasses

	Host	SiO ₂	TiO ₂	Al ₂ O ₃	FeO	MnO	MgO	CaO	Na ₂ O	K ₂ O	P ₂ O ₅	SO ₂	Cl	H ₂ O	Total
G4		77,28	0,35	11,33	0,66	0,06	0,04	0,26	2,22	4,35	0,00	0,02	0,06	3,37	100,00
G5		77,27	0,34	10,96	0,70	0,02	0,03	0,23	2,78	5,00	0,04	0,01	0,10	2,51	100,00
G6		77,72	0,35	10,77	0,76	0,06	0,01	0,23	1,83	4,31	0,00	0,00	0,09	3,81	99,93
G7		76,44	0,15	11,04	0,80	0,00	0,02	0,27	2,62	5,19	0,00	0,00	0,03	3,38	99,93
G8		79,05	0,00	11,15	0,73	0,00	0,04	0,25	2,19	5,17	0,01	0,00	0,06	1,20	99,85
G10		76,71	0,29	10,65	0,70	0,02	0,02	0,22	2,15	4,77	0,04	0,00	0,07	4,37	100,00
G11		77,79	0,00	12,05	0,66	0,00	0,07	0,27	3,05	5,34	0,04	0,01	0,04	0,60	99,92
G12		77,38	0,43	10,65	0,63	0,02	0,04	0,26	2,20	4,56	0,00	0,02	0,05	3,75	100,00
G13		76,18	0,00	10,75	1,27	0,04	0,18	0,24	2,52	5,00	0,00	0,01	0,03	3,69	99,91
G14		78,80	0,23	11,07	0,72	0,00	0,06	0,27	2,20	4,99	0,03	0,00	0,05	1,52	99,95
G15		76,90	0,30	10,62	0,81	0,00	0,00	0,27	2,56	5,00	0,00	0,00	0,02	3,39	99,88
G16		78,79	0,49	10,93	0,68	0,04	0,00	0,23	2,30	4,75	0,00	0,00	0,04	1,71	99,96
G18		77,95	0,27	10,74	0,66	0,04	0,11	0,23	2,16	4,71	0,02	0,00	0,02	3,07	99,97
G19		77,11	0,33	10,80	0,66	0,03	0,05	0,26	2,72	4,91	0,02	0,01	0,04	3,06	100,00
G20		76,81	0,12	10,41	0,85	0,06	0,03	0,22	1,86	4,84	0,00	0,00	0,06	4,67	99,93
G21		77,04	0,11	11,12	0,65	0,06	0,00	0,24	2,55	5,50	0,01	0,04	0,04	2,64	99,99
G22		76,19	0,06	10,65	0,75	0,05	0,02	0,22	1,80	4,77	0,00	0,01	0,05	5,44	100,00
G23		76,84	0,23	10,90	0,77	0,04	0,05	0,17	2,23	5,35	0,02	0,02	0,04	3,34	100,00
G24		76,60	0,32	10,32	0,70	0,09	0,05	0,30	1,98	4,72	0,01	0,01	0,04	4,86	100,00
G25		75,56	0,17	10,98	0,86	0,00	0,08	0,27	2,80	5,11	0,00	0,01	0,06	4,07	99,98
G26		77,00	0,18	11,01	0,77	0,00	0,02	0,25	2,26	5,02	0,05	0,00	0,09	3,24	99,89
G28		76,63	0,21	10,49	0,81	0,00	0,00	0,26	2,26	4,92	0,05	0,00	0,02	4,29	99,93
G29		73,64	0,20	12,93	0,77	0,02	0,13	0,36	3,61	5,28	0,00	0,04	0,00	3,02	99,99
G30		77,45	0,29	10,58	0,61	0,00	0,00	0,26	2,02	4,67	0,06	0,00	0,14	3,91	99,98

Table C.1 Continued

Sample 2005 52 Melt inclusions

	Host	SiO ₂	TiO ₂	Al ₂ O ₃	FeO	MnO	MgO	CaO	Na ₂ O	K ₂ O	P ₂ O ₅	SO ₂	Cl	H ₂ O	Total
Bio1	bio	76,27	0,12	12,17	0,65	0,03	0,00	0,48	2,46	4,94	0,00	0,00	0,02	2,81	99,97
Bio1b	bio	75,29	0,15	12,33	0,63	0,10	0,03	0,51	2,90	5,22	0,00	0,02	0,02	2,81	100,00
Bio1c	bio	74,70	0,00	12,69	0,67	0,00	0,03	0,48	2,49	5,04	0,00	0,01	0,05	3,78	99,93
Bio2	bio	76,03	0,00	12,38	0,76	0,00	0,02	0,55	2,24	4,59	0,00	0,00	0,04	3,35	99,95
Bio3	bio	76,00	0,09	12,30	0,52	0,02	0,02	0,43	1,76	5,19	0,00	0,00	0,02	3,62	99,96
Bio4	bio	75,52	0,20	12,72	0,72	0,04	0,00	0,59	2,71	5,28	0,00	0,00	0,03	2,18	99,98
Bio5	bio	75,31	0,14	12,96	0,56	0,04	0,00	0,54	2,45	5,15	0,00	0,00	0,04	2,76	99,97
Bio5b	bio	75,35	0,15	13,01	0,60	0,02	0,02	0,56	2,77	5,43	0,02	0,03	0,03	2,00	100,00
Bio6	bio	75,47	0,00	11,93	0,69	0,01	0,05	0,45	1,57	5,21	0,01	0,00	0,05	4,36	99,79
Bio7a	bio	75,06	0,12	12,48	0,74	0,06	0,00	0,45	2,63	5,31	0,04	0,00	0,03	3,08	100,00
Bio7b	bio	75,28	0,09	12,62	0,77	0,00	0,03	0,52	2,51	5,13	0,01	0,01	0,03	2,94	99,95
Bio7c	bio	74,73	0,00	12,61	0,83	0,03	0,00	0,49	2,87	5,25	0,00	0,02	0,05	3,07	99,93
Bio8	bio	74,31	0,18	12,69	0,71	0,04	0,00	0,58	2,77	5,18	0,02	0,01	0,03	3,46	99,99
Bio9	bio	75,11	0,15	12,72	0,76	0,10	0,02	0,54	2,70	5,10	0,00	0,00	0,04	2,75	99,99
Bio9b	bio	75,83	0,09	12,42	0,75	0,05	0,04	0,57	2,53	4,99	0,05	0,00	0,05	2,61	99,98
Bio10	bio	74,31	0,15	12,47	0,85	0,00	0,02	0,71	2,86	5,11	0,00	0,00	0,03	3,47	99,98
Bio11	bio	75,05	0,00	12,56	0,70	0,07	0,05	0,68	2,21	5,07	0,00	0,01	0,06	3,43	99,90
Bio12	bio	75,34	0,09	12,47	0,66	0,03	0,01	0,70	2,64	5,28	0,07	0,03	0,03	2,66	100,00
Bio13	bio	75,01	0,21	12,52	0,69	0,03	0,00	0,59	2,37	5,17	0,02	0,00	0,06	3,30	99,99
Bio14	bio	74,21	0,18	12,64	0,96	0,07	0,05	0,60	2,97	5,07	0,03	0,00	0,04	3,18	99,99
Bio15	bio	74,69	0,37	11,82	0,67	0,01	0,03	0,20	4,10	4,31	0,04	0,00	0,07	3,67	99,99
Bio16	bio	76,17	0,06	12,46	0,61	0,00	0,03	0,37	2,34	5,19	0,00	0,00	0,05	2,68	99,96
Bio17	bio	74,04	0,09	12,85	0,87	0,13	0,02	0,53	2,37	4,97	0,00	0,00	0,04	4,05	99,96
Bio18	bio	78,32	0,06	10,45	0,60	0,13	0,02	0,20	1,62	4,74	0,02	0,00	0,04	3,77	99,97

Table C.1 Continued

Sample 2005 52 Matrix glasses

	Host	SiO ₂	TiO ₂	Al ₂ O ₃	FeO	MnO	MgO	CaO	Na ₂ O	K ₂ O	P ₂ O ₅	SO ₂	Cl	H ₂ O	Total
G1		77,48	0,06	11,19	0,55	0,09	0,00	0,32	1,91	4,46	0,02	0,00	0,04	3,84	99,96
G2		76,49	0,00	11,55	0,51	0,08	0,03	0,34	2,39	4,74	0,00	0,00	0,04	3,62	99,80
G3		76,94	0,14	11,27	0,62	0,11	0,01	0,30	2,02	4,41	0,05	0,02	0,04	4,06	100,00
G5		77,40	0,00	11,23	0,61	0,05	0,03	0,37	2,05	4,67	0,02	0,00	0,03	3,51	99,97
G6		77,77	0,00	11,35	0,57	0,06	0,03	0,32	2,02	5,04	0,00	0,00	0,03	2,70	99,90
G7		76,79	0,06	11,36	0,71	0,06	0,06	0,40	2,12	4,74	0,00	0,00	0,05	3,66	100,00
G8		77,63	0,00	11,39	0,59	0,14	0,04	0,40	2,39	5,09	0,01	0,00	0,03	2,12	99,83
G10		77,26	0,12	11,09	0,60	0,08	0,02	0,30	2,35	5,03	0,00	0,02	0,02	3,08	99,97
G11		76,78	0,00	11,73	0,54	0,08	0,05	0,60	2,65	4,19	0,06	0,00	0,03	3,23	99,96
G13		74,25	0,43	12,48	0,54	0,01	0,00	0,65	3,24	4,15	0,01	0,00	0,03	4,14	99,96
G15		75,36	0,00	10,95	0,62	0,03	0,06	0,32	1,61	5,00	0,04	0,02	0,01	5,92	99,94
G17		77,93	0,00	11,42	0,55	0,06	0,02	0,36	1,94	4,44	0,00	0,00	0,03	3,20	99,96
G18		76,41	0,03	11,41	0,57	0,07	0,00	0,40	2,56	4,84	0,03	0,01	0,04	3,63	99,99
G19		76,77	0,00	11,23	0,55	0,05	0,03	0,34	1,87	4,58	0,00	0,00	0,04	4,31	99,77
G20		76,49	0,15	11,15	0,88	0,02	0,05	0,32	2,47	4,97	0,00	0,00	0,02	3,44	99,97
G22		76,17	0,09	11,29	0,59	0,10	0,01	0,31	2,67	5,09	0,00	0,04	0,03	3,57	99,95
G23		76,94	0,00	11,39	0,63	0,17	0,05	0,33	2,03	4,57	0,04	0,01	0,03	3,81	100,00
G24		76,52	0,03	11,59	0,60	0,10	0,03	0,36	2,29	5,33	0,02	0,03	0,02	3,07	100,00
G25		72,55	0,03	11,49	0,60	0,06	0,00	0,66	2,80	4,05	0,04	0,01	0,04	7,67	99,99
G26		76,57	0,00	11,60	0,58	0,08	0,03	0,31	2,60	4,92	0,05	0,00	0,03	3,22	99,98

Table C.1 Continued

Sample 2007 4 Matrix glasses

	Host	SiO ₂	TiO ₂	Al ₂ O ₃	FeO	MnO	MgO	CaO	Na ₂ O	K ₂ O	P ₂ O ₅	SO ₂	Cl	H ₂ O	Total
G1		76,39	0,31	12,91	0,92	0,00	0,04	0,70	3,26	4,25	0,04	0,00	0,05	1,03	99,90
G2		74,43	0,26	12,27	2,22	0,11	0,43	0,65	3,57	4,46	0,00	0,00	0,05	1,52	99,96
G3		75,25	0,23	12,94	1,03	0,04	0,07	0,64	3,06	4,49	0,00	0,03	0,05	2,17	100,00
G4		74,07	0,31	12,37	2,31	0,05	0,44	0,84	3,42	4,35	0,06	0,02	0,06	1,70	100,00
G5		74,83	0,14	12,70	1,22	0,00	0,08	0,60	2,94	4,53	0,02	0,01	0,04	2,85	99,97
G6		74,14	0,00	13,21	1,79	0,12	0,40	1,03	4,21	3,92	0,01	0,00	0,04	1,10	99,97
G7		75,54	0,12	12,29	0,97	0,00	0,09	0,56	2,86	4,65	0,03	0,03	0,05	2,81	100,00
G8		75,11	0,34	12,11	0,92	0,03	0,07	0,62	3,41	4,55	0,00	0,01	0,05	2,78	100,00
G10		76,28	0,17	12,37	1,04	0,04	0,11	0,58	3,46	4,60	0,01	0,01	0,06	1,29	100,00
G11		74,99	0,17	12,65	1,12	0,10	0,10	0,71	2,77	4,69	0,01	0,02	0,07	2,61	100,00
G12		75,30	0,15	12,82	1,15	0,03	0,09	0,75	3,70	4,63	0,00	0,00	0,07	1,28	99,98
G13		74,93	0,40	12,25	1,04	0,08	0,09	0,65	2,64	4,55	0,01	0,00	0,04	3,32	100,00
G14		76,03	0,23	12,54	1,35	0,04	0,09	0,61	3,74	4,65	0,05	0,01	0,09	0,57	100,00
G16		75,41	0,17	12,95	1,11	0,05	0,07	0,60	3,52	4,60	0,01	0,01	0,05	1,45	100,00
G17		75,90	0,11	12,42	1,01	0,01	0,10	0,68	3,06	4,63	0,02	0,00	0,04	2,01	100,00
G18		75,75	0,26	12,96	1,09	0,03	0,07	0,63	3,57	4,63	0,01	0,00	0,04	0,97	100,00
G19		75,74	0,26	12,14	0,95	0,00	0,11	0,59	2,71	4,71	0,00	0,00	0,06	2,64	99,90
G20		74,25	0,12	13,44	1,20	0,06	0,07	0,83	3,78	4,68	0,03	0,00	0,05	1,47	99,98
G21		75,55	0,26	13,15	1,16	0,07	0,12	0,70	3,10	4,55	0,00	0,00	0,05	1,26	99,98
G22		74,58	0,12	12,09	0,78	0,07	0,08	0,57	3,56	4,56	0,03	0,01	0,01	3,54	100,00
G23		75,29	0,35	12,13	0,97	0,01	0,11	0,52	2,84	4,46	0,02	0,03	0,04	3,24	100,00
G25		76,42	0,17	12,48	1,12	0,00	0,06	0,52	2,80	4,62	0,04	0,05	0,04	1,64	99,96
G26		75,82	0,20	12,79	0,92	0,00	0,00	0,74	3,84	4,46	0,03	0,00	0,03	1,15	99,97
G27		75,79	0,06	12,45	0,95	0,01	0,12	0,56	2,88	4,66	0,00	0,01	0,06	2,43	99,98
G28		75,56	0,12	12,27	0,99	0,10	0,11	0,64	3,48	4,66	0,04	0,00	0,03	2,00	100,00
G29		74,11	0,26	12,20	0,95	0,01	0,12	0,61	2,79	4,68	0,00	0,02	0,03	4,19	99,99

Table C.1 Continued

Sample 2005 69 Matrix glasses

	Host	SiO ₂	TiO ₂	Al ₂ O ₃	FeO	MnO	MgO	CaO	Na ₂ O	K ₂ O	P ₂ O ₅	SO ₂	Cl	H ₂ O	Total
G1		75,98	0,06	13,02	0,25	0,04	0,03	0,49	3,66	4,74	0,00	0,00	0,05	1,64	99,95
G2		76,52	0,14	13,10	0,26	0,00	0,00	0,47	3,21	4,59	0,03	0,00	0,03	1,53	99,90
G3		75,71	0,14	13,27	0,37	0,03	0,04	0,46	4,14	4,64	0,01	0,01	0,00	1,18	100,00
G4		76,93	0,00	13,24	0,48	0,08	0,02	0,51	3,21	4,51	0,00	0,00	0,01	0,96	99,96
G5		74,85	0,21	13,16	0,52	0,08	0,02	0,45	3,85	4,66	0,02	0,00	0,02	2,14	99,99
G6		75,77	0,03	13,08	0,79	0,04	0,00	0,44	3,13	4,53	0,01	0,02	0,01	2,14	100,00
G7		76,60	0,06	13,17	0,16	0,05	0,02	0,47	3,92	4,57	0,00	0,00	0,01	0,94	99,96
G8		76,94	0,03	13,43	0,19	0,04	0,11	0,50	3,25	4,57	0,00	0,00	0,03	0,88	99,96
G9		76,77	0,06	12,67	0,16	0,12	0,00	0,42	3,69	4,63	0,01	0,04	0,01	1,40	99,99
G10		76,20	0,09	13,15	0,08	0,00	0,02	0,42	3,37	4,66	0,05	0,00	0,01	1,93	100,00
G11		77,11	0,17	12,86	0,37	0,05	0,07	0,42	3,57	4,57	0,02	0,00	0,03	0,74	100,00
G12		76,94	0,00	13,28	0,11	0,00	0,03	0,40	3,35	4,59	0,06	0,03	0,01	1,06	99,86
G18		76,03	0,03	12,90	0,16	0,10	0,02	0,44	3,89	4,74	0,00	0,02	0,03	1,63	100,00
G13		76,00	0,00	13,28	0,34	0,07	0,06	0,49	3,57	4,64	0,00	0,00	0,01	1,43	99,90
G14		77,07	0,18	13,56	0,25	0,05	0,06	0,44	4,03	4,58	0,04	0,00	0,01	0,00	100,26
G15		76,86	0,00	13,16	0,32	0,00	0,02	0,47	3,27	4,61	0,00	0,00	0,02	1,20	99,93
G16		76,19	0,03	13,05	1,67	0,10	0,09	0,43	3,55	4,49	0,01	0,02	0,01	0,37	100,00
G17		75,65	0,09	12,95	0,50	0,07	0,00	0,48	3,46	4,66	0,01	0,02	0,01	2,11	100,00
G19		76,11	0,20	13,18	0,62	0,00	0,06	0,46	4,06	4,77	0,01	0,00	0,02	0,50	99,99
G20		76,25	0,06	13,53	0,58	0,11	0,09	0,49	3,53	4,59	0,04	0,02	0,03	0,69	100,00
G21		76,50	0,09	13,18	0,55	0,00	0,04	0,53	3,95	4,64	0,05	0,00	0,00	0,42	99,96
G22		76,09	0,00	13,02	0,53	0,00	0,03	0,43	3,28	4,47	0,00	0,02	0,02	1,97	99,86
G23		75,27	0,09	13,09	0,47	0,07	0,01	0,46	3,93	4,70	0,02	0,00	0,02	1,86	99,99
G24		76,11	0,00	13,15	0,54	0,07	0,01	0,47	3,18	4,43	0,03	0,03	0,03	1,97	100,00
G25		77,08	0,09	13,12	0,53	0,00	0,02	0,52	3,91	4,54	0,02	0,01	0,04	0,08	99,96
G26		76,25	0,09	13,31	0,62	0,05	0,08	0,49	3,07	4,51	0,03	0,01	0,01	1,48	100,00

Compositions of experimental glasses for trachyandesite (A)
and basalt (B) (Luhr, 1990)**Table D. 1** Compositons of experimental glasses for trachyandesite (A) and basalt (B) (Luhr, 1990)

Phase	T (C)	P (bar)	H ₂ O	O ₂ buffer	St. Comp.	SiO ₂	TiO ₂	Al ₂ O ₃	Fe ₂ O ₃	FeO	MnO	MgO	CaO	Na ₂ O	K ₂ O	Total
153	800	2000	6,02	FMQ	A	69,31	0,21	16,16	0,38	1,56	0,12	0,16	1,7	4,84	5,51	99,95
149	850	2000	5,98	MNH	A	70,35	0,26	15,86	0,81	0,45	0,13	0,25	1,61	4,61	5,61	99,94
105	850	2000	5,95	MTH	A	70,59	0,19	16,1	0,84	0,35	0,15	0,24	1,64	4,07	5,79	99,96
218	850	4000	8,25	FMQ	A	66,1	0,21	18,35	0,4	1,52	0,17	0,29	3,25	4,9	4,78	99,97
203	850	4000	8,24	MNH	A	67,31	0,19	17,89	0,87	0,45	0,13	0,38	2,71	5,31	4,63	99,87
193	800	4000	8,3	MTH	A	67,24	0,1	17,74	0,92	0,35	0,16	0,38	2,7	5,66	4,62	99,87
144	850	2000	6,04	FMQ	A	65,19	0,29	17,6	0,69	2,88	0,18	0,42	2,88	5,06	4,74	99,93
165	850	2000	5,99	MNH	A	67,37	0,48	17,22	1,08	0,6	0,16	0,46	2,62	4,72	5,2	99,91
139	850	2000	5,99	MTH	A	67,87	0,25	17,32	1,13	0,45	0,17	0,8	2,37	4,65	4,9	99,91
228	850	4000	8,24	FMQ	A	62,43	0,3	19,65	0,64	2,56	0,18	0,47	5,25	4,85	3,67	100
213	850	4000	8,19	MNH	A	64,47	0,28	19,26	1,25	0,66	0,18	0,65	4,18	4,89	3,99	99,81
208	850	4000	8,22	MTH	A	64,47	0,24	19,2	1,28	0,5	0,19	0,69	4,23	5,03	3,98	99,81
185	900	2000	6,08	FMQ	A	59,67	0,48	19,37	1,03	4,5	0,18	0,99	5,35	4,86	3,44	99,87
169	900	2000	6,05	MNH	A	64,14	0,54	18,46	1,51	0,83	0,2	0,96	3,96	5,01	4,17	99,78
114	900	2000	6,05	MTH	A	64,84	0,48	18,27	1,52	0,57	0,19	0,96	3,71	4,97	4,32	99,83
223	900	4000	8,19	FMQ	A	59,3	0,52	19,72	0,99	4,09	0,19	1,05	6,3	4,48	3,29	99,93
189	900	4000	8,21	MNH	A	60,77	0,52	20,22	1,65	0,86	0,19	0,97	6,39	4,86	3,18	99,61
181	900	4000	8,12	MTH	A	61,98	0,29	19,99	1,66	0,65	0,19	0,83	6,45	4,52	3,04	99,6
198	950	2000	6,06	FMQ	A	57,44	0,63	18,96	1,13	4,93	0,21	1,93	6,86	4,75	3,03	99,87
104	950	2000	5,98	MNH	A	60,83	0,61	19,13	2,03	1,13	0,24	1,43	6,41	4,48	3,29	99,58
119	950	4000	5,98	MTH	A	60,74	0,65	19,05	2,36	0,88	0,23	1,42	6,54	4,56	3,19	99,62
233	950	4000	8,03	MNH	A	59,84	0,63	18,93	1,91	0,95	0,21	0,3	9,65	4,63	2,08	99,13
243	950	4000	8,09	MTH	A	59,82	0,44	19,62	2,05	0,73	0,19	0,44	8,92	4,76	2,28	99,25
161	1000	2000	5,95	FMQ	A	57,95	0,66	18,89	1,06	5,03	0,21	1,45	8,32	4,15	2,17	99,89
93	1000	2000	5,94	MNH	A	57,55	0,64	18,69	3,19	1,74	0,31	1,99	8,45	4,13	2,51	99,2
110	1000	2000	5,97	MTH	A	57,62	0,66	18,75	3,38	1,2	0,21	2,09	8,46	4,15	2,76	99,28
248	1000	4000	7,99	MNH	A	58,63	0,57	19,67	2,09	1,04	0,22	0,32	10,15	4,36	2,01	99,06
238	1000	4000	8,02	MTH	A	57,98	0,55	18,76	3,15	1,06	0,21	0,79	9,52	4,51	2,26	98,79

Table D.1 Continued

Phase	T (C)	P(bar)	H2O	O2 buffer	St. Comp.	SiO ₂	TiO ₂	Al ₂ O ₃	Fe ₂ O ₃	FeO	MnO	MgO	CaO	Na ₂ O	K ₂ O	Total
155	800	2000	5,95	FMQ	B	72,18	0,12	15,5	0,24	1,1	0,03	0,45	1,45	5,53	3,33	99,93
152	800	2000	5,81	MNH	B	73,46	0,22	14,94	0,74	0,51	0,08	0,93	2,35	4,32	2,4	99,95
108	800	2000	5,81	MTH	B	74,42	0,15	15,25	0,73	0,38	0,07	0,9	1,96	4,02	2,05	99,93
220	800	4000	8,04	FMQ	B	70,07	0,1	17,3	0,32	1,47	0,09	0,65	2,99	4,99	1,98	99,96
205	800	4000	8,12	MNH	B	69,98	0,17	17,71	0,77	0,48	0,1	0,82	2,82	5,23	1,8	99,88
195	800	4000	8,12	MTH	B	70,45	0,13	18,31	0,75	0,39	0,11	0,75	2,91	4,42	1,65	99,87
146	850	2000	6,01	FMQ	B	69,44	0,13	17,36	0,29	1,4	0,05	0,57	2,17	5,45	3,08	99,94
168	850	2000	5,91	MNH	B	71,8	0,22	16,61	0,87	0,6	0,07	0,69	2,16	4,74	2,16	99,92
141	850	2000	5,88	MTH	B	72,34	0,17	16,66	0,91	0,45	0,06	0,65	2,27	4,28	2,12	99,91
230	850	4000	8,1	FMQ	B	67,39	0,12	19	0,37	1,77	0,08	0,64	4	5,04	1,56	99,97
215	850	4000	8,13	MNH	B	67,51	0,22	19,45	0,94	0,6	0,1	0,7	4,04	4,93	1,31	99,8
210	850	4000	8,07	MTH	B	67,94	0,19	19,33	1,04	0,51	0,09	0,78	4,22	4,43	1,3	99,83
187	900	2000	6,02	FMQ	B	67,14	0,24	18,71	0,39	1,94	0,09	0,39	3,47	5,5	2,05	99,92
171	900	2000	5,96	MNH	B	68,47	0,21	18,24	1,13	0,77	0,1	0,89	3,58	4,73	1,67	99,79
116	900	2000	5,91	MTH	B	65,04	0,24	17,88	1,28	0,61	0,1	3,98	5,3	3,97	1,47	99,87
225	900	4000	8,16	FMQ	B	65,26	0,11	20,81	0,35	1,83	0,09	0,6	4,93	4,64	1,33	99,95
183	900	4000	7,95	MTH	B	65,59	0,28	19,49	1,36	0,63	0,1	1	5,68	4,48	1,05	99,66
200	950	2000	6,08	FMQ	B	63,59	0,62	21,38	0,31	1,62	0,1	0,28	4,97	5,5	1,57	99,94
103	950	2000	5,93	MNH	B	64,6	0,27	19,59	1,48	1,01	0,13	1,59	5,29	4,41	1,22	99,59
121	950	2000	5,89	MTH	B	64,29	0,28	18,97	1,81	0,8	0,1	2	5,56	4,54	1,27	99,62
275	950	4000	8,05	FMQ	B	64,64	0,2	21,55	0,24	1,3	0,12	0,37	6,11	4,2	1,23	99,96
235	950	4000	8	MNH	B	63,05	0,38	20,31	1,41	0,86	0,16	0,8	6,38	4,69	1,06	99,1
245	950	4000	8,02	MTH	B	63,65	0,36	20,49	1,28	0,55	0,13	0,57	6,2	4,87	1,19	99,29
163	1000	2000	6,05	FMQ	B	60,25	0,45	22,41	0,48	2,48	0,09	0,34	6,8	5,38	1,22	99,9
95	1000	2000	5,96	MNH	B	59,71	0,62	21,54	1,62	1,04	0,22	0,9	7,7	4,34	1,07	98,76
112	1000	2000	5,99	MTH	B	60,67	0,67	21,11	1,72	0,73	0,1	1,11	7,06	4,61	1,07	98,85
260	1000	4000	8,07	FMQ	B	61,34	0,44	22,2	0,33	1,63	0,12	0,36	7,45	5,09	0,99	99,95
250	1000	4000	7,99	MNH	B	60,66	0,42	20,49	1,25	0,7	0,12	0,36	8,42	4,77	1,12	98,31

**Compositions of experimental glasses for alkali basalt
(OB93-190) and tholeiitic basalt (35R2) (Freise et al, 2009)**

Table E.1 Compositons of experimental glasses for alkali basalt (OB93-190) and tholeiitic basalt (35R2) (Freise et al, 2009).

Phase	T (C)	P (Mpa)	H ₂ O	O ₂ buffer	St. Comp.	SiO ₂	TiO ₂	Al ₂ O ₃	FeO	MnO	MgO	CaO	Na ₂ O	K ₂ O	Total
48	1050	500	9,52	QFM+4	OB93-190	51,82	2,42	16,57	9,12	0,18	5,78	10,03	2,87	1,21	100
49	1050	500	6,24	QFM+4	OB93-190	51,46	2,49	16,52	9,09	0,18	5,86	10,17	3,07	1,15	100
50	1050	500	3,05	QFM+4	OB93-190	54,82	1,89	18,93	6,02	0,19	4,23	8,39	3,93	1,61	100
51	1000	500	9,31	QFM+4	OB93-190	55,12	1,56	19,06	5,73	0,18	4,75	9,34	2,94	1,33	100
52	1000	500	5,76	QFM+4	OB93-190	57,08	1,23	19,35	5,03	0,12	3,43	8,3	4,01	1,45	100
53	1000	500	2,52	QFM+4	OB93-190	60,09	1,04	19,07	4,57	0,17	2,59	6,36	4,16	1,96	100
54	950	500	9,19	QFM+4	OB93-190	59,11	0,86	19,77	4,09	0,17	2,54	8,31	3,61	1,53	100
55	950	500	6,56	QFM+4	OB93-190	62,67	0,71	18,64	3,65	0,16	1,87	6,06	4,22	2,02	100
56	950	500	3,42	QFM+4	OB93-190	65,1	0,64	17,19	3,96	0,13	1,95	4,56	3,56	2,91	100
57	1050	500	1,32	QFM+4	OB93-190	57,53	1,62	18,16	5,78	0,15	3,63	6,61	4,33	2,21	100
58	1000	500	1,96	QFM+4	OB93-190	60,25	1,04	19,5	3,92	0,06	1,9	5,62	4,38	3,34	100
59	950	500	2,2	QFM+4	OB93-190	59,68	0,64	21,22	2,15	0,01	1,15	10,05	4,28	0,82	100
60	900	500	9,19	QFM+4	OB93-190	63,39	0,59	19,43	2,79	0,22	1,4	6,6	3,74	1,83	100
61	900	500	5,36	QFM+4	OB93-190	66,47	0,61	17,7	2,95	0,08	1,34	4,89	3,45	2,51	100
62	1100	500	3,51	QFM+4	OB93-190	51,82	2,63	16,62	8,56	0,2	5,61	10,23	3,12	1,2	100
63	1100	500	2,61	QFM+4	OB93-190	52,8	2,64	17,56	8,09	0,13	4,8	9,27	3,41	1,29	100
148	1150	500	9,54	QFM+4	OB93-190	49,68	2,83	16,33	11,03	0,17	5,67	9,98	3,11	1,19	100
149	1150	500	6,47	QFM+4	OB93-190	49,45	2,85	16,21	11,58	0,14	5,73	9,82	3,04	1,17	100
150	1150	500	3,39	QFM+4	OB93-190	48,84	2,86	16,11	11,9	0,18	5,64	10,08	3,23	1,17	100
151	1150	495,3	2,51	QFM+4	OB93-190	49,47	2,76	16,22	11,69	0,17	5,66	9,87	2,99	1,16	100
80	1040	495,3	9,28	QFM	OB93-190	49,12	3,28	16,25	11,31	0,18	5,73	9,94	2,99	1,2	100
81	1040	495,3	7,3	QFM	OB93-190	48,85	3,26	16,57	11,55	0,19	5,41	9,83	3,14	1,19	100
82	1040	495,3	4,32	QFM	OB93-190	48,85	3,14	17,26	11,79	0,2	5,12	9,17	3,24	1,23	100

Table E.1 Continued

Phase	T (C)	P (Mpa)	H2O	O2 buffer	St. Comp.	SiO ₂	TiO ₂	Al ₂ O ₃	FeO	MnO	MgO	CaO	Na ₂ O	K ₂ O	Total
83	1040	499,6	2,84	QFM	OB93-190	50,25	2,88	17,79	11,29	0,14	4,38	7,77	3,9	1,6	100
85	1000	499,6	6,75	QFM	OB93-190	50,64	2,6	17,68	11,17	0,3	4,19	9,02	3,03	1,35	100
86	1000	499,6	5,03	QFM	OB93-190	52,63	2,37	18,62	9,56	0,09	3,39	8,4	3,37	1,57	100
87	1000	499,6	4,1	QFM	OB93-190	53,28	1,98	18,1	10,78	0,17	2,82	7,24	3,73	1,9	100
88	1080	515,2	9,27	QFM	OB93-190	49,47	2,84	16,3	11,28	0,13	5,9	9,76	3,18	1,13	100
89	1080	515,2	7,75	QFM	OB93-190	49,78	2,91	16,24	10,99	0,16	5,9	9,85	3,03	1,13	100
90	1080	515,2	4,82	QFM	OB93-190	50,45	2,92	16,54	10	0,17	6	9,71	3,07	1,13	100
91	1080	515,2	2,91	QFM	OB93-190	52,63	2,99	16,95	9,78	0,06	3,58	9,55	3,34	1,12	100
92	1120	513	9,4	QFM	OB93-190	49,57	2,84	16	11,15	0,13	5,86	9,85	3,45	1,14	100
93	1120	513	6,36	QFM	OB93-190	49,87	2,93	16,36	10,74	0,19	5,91	9,87	3,02	1,11	100
94	1120	513	4,79	QFM	OB93-190	50,61	2,95	16,27	10,29	0,18	5,94	9,67	2,91	1,18	100
95	1120	513	2,21	QFM	OB93-190	51,13	2,96	16,72	8,85	0,19	6,09	9,91	3,01	1,13	100
96	1000	492,9	9,18	QFM	OB93-190	49,67	2,91	16,73	11,39	0,13	5,23	9,96	2,87	1,11	100
97	960	500,3	9,32	QFM	OB93-190	52,93	1,91	17,79	10,78	0,17	3,34	9,03	2,89	1,16	100
98	960	500,3	6,93	QFM	OB93-190	55,65	1,48	18,11	9,88	0,2	2,38	8,67	2,4	1,22	100
99	960	500,3	3,82	QFM	OB93-190	57,36	1,19	17,65	9,72	0,15	1,99	7,07	3,1	1,76	100
100	960	500,3	2,4	QFM	OB93-190	57,09	0,98	19,01	6,93	0,04	1,76	7,8	4,33	2,06	100
101	1000	492,9	3,92	QFM	OB93-190	54,62	1,78	17,58	10,36	0,18	2,61	6,72	3,92	2,24	100
102	1000	492,9	2,04	QFM	OB93-190	55,31	1,66	17,73	10,16	0,19	2,44	6	3,74	2,75	100
103	1040	489,3	1,65	QFM	OB93-190	51,5	2,66	17,46	11,45	0,08	3,25	8,26	3,59	1,75	100
104	1040	489,3	0,92	QFM	OB93-190	51,82	2,55	17,09	11,35	0,15	3,11	8,12	3,71	2,09	100
108	1000	500	9,59	QFM+4	35R2	63,68	0,6	22,73	1,08	0,11	0,34	7,4	3,88	0,18	100
109	1000	500	7,74	QFM+4	35R2	64,86	0,67	22,26	1,3	0,04	0,48	6,51	3,68	0,2	100
110	1000	500	3,52	QFM+4	35R2	65,46	0,78	18,81	1,6	0,02	0,42	6,17	5,29	0,06	100
112	1040	500	9,67	QFM+4	35R2	52,63	1,63	16,03	8,38	0,18	6,07	12,35	2,59	0,13	100
113	1040	500	5,83	QFM+4	35R2	54,44	1,58	17,8	7,66	0,15	4,67	10,52	3,05	0,13	100
114	1040	500	4,44	QFM+4	35R2	57,47	1,63	17,74	6,55	0,12	4,07	8,48	3,74	0,19	100
115	1040	500	0,62	QFM+4	35R2	59,1	1,13	18,65	5,78	0,27	2,86	7,98	3,99	0,24	100

Table E.1 Continued

Phase	T (C)	P (Mpa)	H ₂ O	O ₂ buffer	St. Comp.	SiO ₂	TiO ₂	Al ₂ O ₃	FeO	MnO	MgO	CaO	Na ₂ O	K ₂ O	Total
116	1080	500	9,55	QFM+4	35R2	51,51	1,53	14,9	9,64	0,14	6,78	12,78	2,59	0,13	100
117	1080	500	7,58	QFM+4	35R2	52,3	1,62	16,19	8,62	0,09	6,14	12,17	2,77	0,11	100
118	1080	500	2,11	QFM+4	35R2	54,29	1,66	17,62	7,85	0,14	4,83	10,2	3,27	0,13	100
119	1080	500	1,17	QFM+4	35R2	56,66	2,05	16,59	7,65	0,22	4,32	8,5	3,82	0,2	100
120	1120	500	9,27	QFM+4	35R2	50,35	1,51	14,72	10,86	0,17	6,81	12,8	2,59	0,18	100
121	1120	500	6,01	QFM+4	35R2	50,58	1,55	14,76	10,08	0,17	7,02	13,21	2,52	0,12	100
122	1120	500	2,95	QFM+4	35R2	50,29	1,48	14,75	11,2	0,18	6,58	12,79	2,62	0,1	100
123	1120	500	0,46	QFM+4	35R2	51,38	1,79	16,09	11,35	0,16	5,53	10,45	3,12	0,12	100
124	1160	500	4,22	QFM+4	35R2	50,23	1,5	14,99	11	0,14	6,8	12,51	2,7	0,12	100
125	1160	500	3,12	QFM+4	35R2	50,13	1,51	15,12	11,04	0,18	6,79	12,42	2,71	0,1	100
126	960	500	9,48	QFM+4	35R2	63,3	0,62	15,61	4,52	0,1	5,2	7,8	2,69	0,16	100
127	960	500	7,82	QFM+4	35R2	64,87	0,57	16,02	3,82	0,04	2,54	7,89	3,71	0,56	100
128	1000	495,3	9,11	QFM	35R2	50,37	1,65	17,57	11,47	0,21	5,11	10,55	2,94	0,14	100
129	1000	495,3	6,4	QFM	35R2	51,51	1,59	18,41	10,96	0,16	4,36	9,39	3,49	0,13	100
130	1000	495,3	5,08	QFM	35R2	53,33	1,63	17,83	11,34	0,2	3,19	8,77	3,51	0,18	100
131	1000	495,3	3,45	QFM	35R2	54,11	1,9	16,91	12,17	0,26	2,76	7,81	3,8	0,29	100
132	1040	499,6	9,18	QFM	35R2	51,03	1,62	15,67	10,77	0,08	6,06	12,07	2,58	0,12	100
133	1040	499,6	6,01	QFM	35R2	50,69	1,64	17,09	10,96	0,21	5,42	10,81	3,05	0,15	100
134	1040	499,6	4,8	QFM	35R2	51,15	1,64	18,01	10,77	0,14	4,56	10,19	3,4	0,14	100
135	1040	499,6	2,28	QFM	35R2	51,96	2,02	17,58	11,7	0,16	3,72	9,17	3,51	0,18	100
136	1080	515,2	9,29	QFM	35R2	50,75	1,52	15,02	10,3	0,19	6,89	12,68	2,54	0,11	100
137	1080	515,2	5,63	QFM	35R2	50,77	1,6	15,9	10,23	0,19	6,32	12,06	2,8	0,13	100
138	1080	515,2	4,32	QFM	35R2	51,28	1,67	17,14	9,83	0,17	5,45	11,17	3,14	0,16	100
139	1080	515,2	3,16	QFM	35R2	51,06	1,71	17,65	10,31	0,18	4,92	10,75	3,27	0,17	100

CURRICULUM VITAE

PERSONAL INFORMATION

Surname, Name : Yavuz ÖZDEMİR

Nationality : Turkish (T.C.)

Date and Place of Birth : 10 October 1974, Van

Marital Status : Married

Phone : +90 312 210 57 12

Fax : +90 312 210 57 50

E-mail : yozdemir@metu.edu.tr

EDUCATION

Degree	Institution	Year of Graduation
M.Sc	Yüzüncüyil University, Geological Engineering	2003
B.Sc	Dokuz Eylül University, Geological Engineering	1998
High School	Lake Van Anatolian High School	1993

WORK EXPERIENCES

Year	Place	Enrollment
2004-present	METU, Dept. of Geol. Eng.	Research Assistant
2009	Dept. of Earth Sciences,	Academic Visitor
March-December	University of Bristol	
2000-2003	Yüzüncü Yıl University	Research Assistant

FOREIGN LANGUAGES

English

PUBLICATIONS

Articles published in periodicals recognized by SCI

ÖZDEMİR, Y., BLUNDY, J.D., GÜLEÇ, N., 2011. The importance of fractional crystallization and magma mixing in controlling chemical differentiation at Süphan Stratovolcano, Eastern Anatolia, Turkey. Contributions to Mineralogy and Petrology, in press.

ÖZDEMİR, Y., KARAOĞLU, Ö., TOLLUOĞLU, A.Ü., GÜLEÇ, N., 2007. Reply to discussion by Evren Çubukçu, Erkan Aydar and Alain Gourgaud of ;Volcanostratigraphy and petrogenesis of the Nemrut stratovolcano (East Anatolian High Plateau): The most recent post-collisional volcanism 2 in Turkey ; by Y. Özdemir, Ö. Karaoğlu, A.Ü. Tolluoğlu and N. Güleç. Chemical Geology, 245, 130-134.

ÖZDEMİR, Y., KARAOĞLU, Ö., TOLLUOĞLU, A.Ü., GÜLEÇ, N., 2006. Volcanostratigraphy and Petrogenesis of the Nemrut Stratovolcano (East Anatolian High Plateau): The Most Recent Post-Collisional Volcanism in Turkey. Chemical Geology, 226, 189-211.

KARAOĞLU, Ö., ÖZDEMİR, Y., TOLLUOĞLU, A.Ü., KARABIYIKOĞLU, M., KÖSE, O., FROGER, J.L., 2005 Stratigraphy of the volcanic products around Nemrut Caldera: implications for reconstruction of the Caldera Formation. Turkish Journal of Earth Sciences, 14, 123-143.

Conference Papers

ÖZDEMİR, Y., GÜLEÇ, N., TOLLUOĞLU, A.Ü. 2007. Süphan Stratovolkanının bazaltik trakiandezitik lavlarının mineralojik-petrografik ve jeokimyasal özellikleri: Çukurova Üniversitesi, Jeoloji Müh. Bölümü 30.Yıl Sempozyumu, Bildiri Özleri Kitabı, 25-27 Ekim, 75, Adana.

KARAOĞLU, Ö., ÖZDEMİR, Y. & TOLLUOĞLU, A.Ü. 2004. Physical Evolution, emplacement of Ignimbrite and characteristic eruption types of Nemrut Stratovolcano: a caldera system at Eastern Anatolia-Turkey: In proceedings of 5th International Symposium on Eastern Mediterranean Geology, 1287- 1290, Greece.

KARAOĞLU, Ö., ÖZDEMİR, Y., TOLLUOĞLU, A.Ü., 2004. Nemrut Stratovolkanının patlama dinamikleri ve tipleri: 57. Türkiye Jeoloji Kurultayı Bildiri Özleri Kitabı, 08-14 Mart, 228-230, Ankara.

OYAN, V., TOLLUOĞLU, A.Ü., ÖZDEMİR, Y., 2004. Van (Timar) çevresindeki bazik volkanizmanın mineralojik-petrografik özellikleri: 57.Jeoloji Kurultayı Bildiri Özleri kitabı, 310-312, Ankara.

KARAOĞLU, Ö., ÖZDEMİR, Y., TOLLUOĞLU, A.Ü., 2003. Nemrut Stratovolkanı Kuzeyinde Yüzeyleyen Farklı Bazalt Akıntılarının Mineralojik-Petrografik Karakteristikleri: 56. Türkiye Jeoloji Kurultayı Bildiri Özleri Kitabı, 14-20 Nisan, 26-27, 2003, Ankara.

KARAOĞLU, Ö., ÖZDEMİR, Y., TOLLUOĞLU, A.Ü., 2003. Nemrut açılma Çatlağı'nın Etkinliğine ait bulgular: ATAG-7 Bildiri Özleri Kitabı, 01-03 Ekim, 32, Van.

ÖZDEMİR, Y., TOLLUOĞLU, A.Ü., KARAOĞLU, Ö., 2003. Nemrut İgnimbiritinin Fiziksel ve Mineralojik-Petrografik Karakteristikleri: Mersin

Üniversitesi, Mühendislik Fak.Jeoloji Müh. Bölümü 10.Yıl Sempozyumu, Bildiri Özleri Kitabı, 15-18 Ekim, 64, Mersin.

KARAOĞLU, Ö., TOLLUOĞLU, A.Ü., ÖZDEMİR, Y., 2003. Nemrut Stratovolkanı Lavlarının Mineralojik-Petrografik değişimi ve dinamiği: Mersin Üniversitesi, Mühendislik Fak.Jeoloji Müh. Bölümü 10.Yıl Sempozyumu, Bildiri Özleri Kitabı, 15-18 Ekim, 48, Mersin.

ÖZDEMİR, Y., KARAOĞLU, Ö., OYAN, V., TOLLUOĞLU, A.Ü.,2003. Nemrut volkanizmasına bağlı olarak gelişen pomza geri düşme ürünleri: Doğu Anadolu Endüstriyel Hammadde Çalıştayı Bildiriler Kitabı, 117-124, Van.

ÖZDEMİR, Y., KARAOĞLU, Ö., TOLLUOĞLU, A.Ü., 2002. Nemrut volkanı kaldera duvarlarında gözlenen postkaldera lamprofir(?) dayklarının mineralojik-petrografik karakteristikleri: Doğu Anadolu Jeoloji Çalıştayı Bildiri Özleri Kitapçığı. 02-06 Eylül, 46-47, Van.

HOBBIES

Swimming, Football, Travelling